IMPROVED PREDICTIONS OF CONTAMINANT DEGRADATION IN WATER TREATMENT REACTORS

Alexander Sean Gorzalski

A dissertation submitted to the faculty at the University of North Carolina at Chapel Hill in partial fulfillment of the requirements for the degree of Doctor of Philosophy in the Department of Environmental Sciences and Engineering in the Gillings School of Global Public Health.

Chapel Hill

2019

Approved by:

Orlando Coronell

Gregory Harrington

Michael Aitken

Gregory Characklis

Will Vizuete

ABSTRACT

Alexander Sean Gorzalski: Improved Predictions of
Contaminant Degradation in Water Treatment Reactors
(Under the direction of Orlando Coronell and Gregory Harrington)

The efficacy of fundamental water treatment processes depends on reactor hydraulics. Despite the importance of reactor hydraulics, oversimplified hydraulic models have been used for the design, operation, and regulation of water treatment reactors. The most commonly used model assumes plug flow reactor (PFR) behavior with residence time equal to the time for the first 10 percent of flow to leave the reactor (PFR t_{10}). This simplification is overly conservative when targeting low log reductions of contaminants, and may also overestimate treatment efficacy when targeting higher log reductions, such as in water reuse applications.

The overall goal of this dissertation was to improve the prediction of contaminant degradation in water treatment reactors by accurately modeling reactor hydraulics. This goal was met through the following three objectives: (i) development of accurate models for residence time distribution (RTD) (i.e., macromixing); (ii) assessment of flow segregation and earliness of mixing (i.e., micromixing) in full-scale water treatment reactors; and (iii) quantitative evaluation of the effect of RTD model selection on predictions of contaminant degradation.

This work generated a number of major conclusions and contributions to the modeling of contaminant degradation. (i) Reactor network (RN) models accurately represented observed RTD using fewer fitting parameters than alternative models and (ii) an open-source tool was created to fit RN models to tracer data. (iii) Micromixing was observed to be prevalent in full-scale

reactors, and (iv) the tanks-in-series (TIS) and certain RN models most accurately represented micromixing. (v) Micromixing had the greatest impact on predictions of pathogen disinfection when specific lethality coefficient and disinfectant decay rate were high. (vi) The PFR t_{10} model may cease to be conservative when predicting contaminant reductions >2-log. (vi) Designing reactors for 1-log reduction using the PFR t_{10} model may increase capital costs by 10-80% relative to an accurate RTD model like the RN model; (vii) at 6-log reduction, properly sizing oxidation processes using the RN model may increase costs by over 100% relative to the PFR t_{10} model.

Overall, this work provides a fundamental basis for the rational design, operation, and regulation of water treatment processes using the TIS or RN models.

ACKNOWLEDGEMENTS

This work has been possible thanks to numerous individuals whose mentorship and guidance have opened doors throughout my academic and professional careers. I am immensely grateful to Greg Harrington, who provided my first research opportunity over a decade ago. From selecting a graduate school to helping me identify a range of potential career paths, his counsel has been invaluable. I thank Orlando Coronell for his openness to a non-traditional research approach. I am deeply appreciative of his guidance and support throughout my master's and PhD research, as well as the quality of his teachings and insights into the field. My pursuit of a PhD originated with Anne Spiesman and Mel Tesema at the Washington Aqueduct. They encouraged and supported my research, provided countless opportunities for professional growth, and are exemplary public servants who I hold in the highest regard.

I would also like to acknowledge to my committee: Mike Aitken, Greg Characklis, and Will Vizuete. Their guidance improved the quality and cohesiveness of this dissertation. To the past and present members of the Coronell research group, serving as a sounding board for each other's ideas was one of my favorite experiences as a graduate student. Your feedback on presentations was especially appreciated. This work also depended on the generous financial support of the US Department of Defense and the American Water Works Association.

Most importantly, I would like to thank my family. My parents, Patty and Sean, taught me the importance of hard work and demonstrated it each day. Their sacrifice and support ensured that I had every opportunity to succeed in my education. Finally, I will be forever

grateful to my wife, Rhea, for her endless patience, encouragement, and support. I am blessed to have her as a partner for the journeys we have completed together and all those yet to come.

TABLE OF CONTENTS

LIST OF TABLES

LIST OF FIGURES

LIST OF ABBREVIATIONS

CFD	Computational fluid dynamics
$Comb Cl_2$	Combined chlorine
CSTR	Continuous-flow stirred tank reactor
CT	Produce of oxidant concentration and contact time
CW	Clearwells
DBP	Disinfection by-product
DPD	N,N-diethyl-p-phenylenediamine
$Free Cl_2$	Free chlorine
IDDF	Integrated disinfection design framework
LRV	Log reduction value
MIB	2-methylisoborneol
MGD	Million gallons per day
MM	Maximum Mixedness
MSE	Mean squared error
NDMA	N-nitrosodimethylamine
NRMSE	Normalized root-mean-square error
PFR	Plug flow reactor
RTD	Residence time distribution
RSE	Residual standard error
SF	Segregated flow
TIS	Tanks-in-series
$Total Cl_2$	Total chlorine

LIST OF SYMBOLS

B_F	Baffle factor
C	Concentration of a tracer or oxidant
D	Dispersion number
k	Reaction rate constant
$\dot{m}$	Mass flow rate
n	Number of tanks in a tanks-in-series reactor
N	Concentration of a contaminant
Q	Volumetric flow rate
R^2	Coefficient of determination
t	Time
t_X	Time for the first X% of flow to leave a reactor (e.g., $t_{0.1}$, t_1, t_5, t_{10}, t_{50}, t_{90})
V	Volume
τ	Hydraulic residence time
Θ	Tracer run time divided by hydraulic residence time (t/τ)

CHAPTER 1 - INTRODUCTION

1.1 Background and Motivation

1.1.1 Applications of Reactor Modeling in Water Treatment

1.1.1.1 Water Treatment Reactors

The largest flow-through reactors in existence are used in water treatment (Crittenden et al. 2012). Water treatment reactors include clearwells, ozone contactors, sedimentation basins, and filters; reactions can occur in any unit process, and these reactions can be engineered or unintentional. Deviation from ideal performance increases with increasing reactor size, and thus, reactor design depends on understanding non-ideal reactor performance (Crittenden et al. 2012).

1.1.1.2 Disinfection

With the exception of a small number of high-quality groundwaters, public water systems in the United States are required to disinfect drinking water, and criteria for meeting disinfection requirements are based on reactor modeling (USEPA 1991, USEPA 2009, USEPA 2010). Waterborne pathogens present the greatest public health risk of any class of contaminants in drinking water. Even in the United States, which has greatly reduced the number of waterborne disease outbreaks through treatment and regulatory developments, microbial contaminants still present the greatest health risk (Seidel et al. 2014). The disinfection of pathogens is typically achieved using chemical disinfectants, although the use of ultraviolet light is a notable exception. Disinfection in the United States is most commonly performed using free chlorine; in a recent survey, 71% of systems used free chlorine, 21% used chloramines. Chlorine dioxide, ozone, and

ultraviolet light were each used by 7% of systems (AWWA 2018)[1]. Thus, disinfection in the United States is still predominantly performed with free chlorine, and models are used to determine what concentration and contact time is required to achieve adequate pathogen inactivation.

1.1.1.3 Oxidation of Reactive Contaminants

Another use of water treatment reactors is the degradation or transformation of chemical contaminants by oxidation. This includes the treatment of hydrogen sulfide, iron and manganese, color, as well as taste and odor compounds such as 2-methylisoborneol (MIB) and geosmin (Crittenden et al. 2012). Oxidation can be used to treat disinfection by-product (DBP) precursors, such as organic nitrogen that can form N-nitrosodimethylamine (NDMA) (Krasner et al. 2013). The use of water treatment oxidants is also a common treatment strategy for the control of algal toxins (Rodriguez et al. 2007) and degradation of certain endocrine disrupting compounds, pharmaceuticals, and personal care products (Westerhoff et al. 2005).

1.1.2 Reactor Models

1.1.2.1 Fundamentals of Reactor Modeling

Reactor performance for a single fluid is a function of four factors: reaction kinetics, residence time distribution (RTD), degree of segregation, and earliness of mixing (Levenspiel 1999). RTD is commonly referred to as macromixing, while degree of segregation and earliness of mixing are collectively referred to as micromixing. Predicting or modeling reactor

[1]Note that the sum of disinfection technologies used exceeds 100% as some systems used multiple disinfection technologies.

performance depends on determining, or assuming, these four factors.

Degree of segregation and earliness of mixing become important when a reaction is not first order or pseudo-first order, RTD deviates from plug flow, conversion (or reduction) of a constituent is high, or multiple reactions occur simultaneously (Levenspiel 1999). However, degree of segregation and earliness of mixing (i.e., micromixing) are not important where there is no reaction, such as tracer studies performed with a conservative tracer. Also, reactions that are first order or pseudo-first order are not affected by micromixing (Levenspiel 1999).

1.1.2.2 Ideal Reactor Models

Batch Reactor

Reaction rates are typically determined at laboratory scale in batch reactors, including disinfection studies (Crittenden et al. 2012). Reactants are initially added to a vessel, well mixed, and allowed to react before being discharged (Levenspiel 1999). Depictions of a batch reactor and other ideal reactors are shown in Figure 1.1. The batch reactor is operated in a non-steady state manner because concentrations of reactants and products change over time (Levenspiel 1999).

Plug Flow Reactor (PFR)

The plug flow reactor (PFR) is an ideal, steady-state, flow-through reactor with no mixing or dispersion in the direction of flow (Levenspiel 1999). Mixing may occur transverse to the direction of flow, however the presence or absence of transverse mixing does not affect the definition of plug flow. The absence of longitudinal mixing and dispersion results in all flow elements having equal residence time in the reactor. The effluent concentrations of a PFR will be equal to the effluent concentrations of a batch reactor with equal residence time. Similarly,

concentrations in a batch reactor at any given time will be equivalent to the effluent of a PFR with the same residence time.

Continuous-Flow Stirred Tank Reactor (CSTR)

The continuous-flow stirred tank reactor (CSTR) is a steady state, flow-through reactor. It differs from the PFR in that perfect mixing is assumed in all directions, resulting in uniform conditions throughout the reactor (Levenspiel 1999). The concentration of reactants and products leaving the reactor at any time are thus equal to the concentration within the reactor.

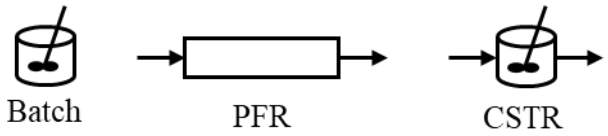

Figure 1.1. Schematic representation of the three ideal reactor types: batch reactor, plug flow reactor (PFR), and continuous-flow stirred tank reactor (CSTR).

1.1.2.3 Non-Ideal Reactor Models and their use in Water Treatment

Although reactors are typically designed so that their flows approach the ideal conditions described above (Levenspiel 1999), water treatment reactors commonly exhibit non-ideal flow (Crittenden et al. 2012). This section will describe reactor models used in the literature and in practice to describe non-ideal flow in water treatment reactors.

PFR t_{10}

To account for short-circuiting through reactors, U.S. EPA credits the time for the first 10% of flow to exit a reactor (t_{10}) (USEPA 1991, USEPA 2010). The value of t_{10} should be determined via tracer study, although methods are available to estimate t_{10} from qualitative assessments of internal baffling (USEPA 1991). Dividing t_{10} by the nominal hydraulic residence

time, τ, produces the reactor baffle factor (B_F). The PFR t_{10} model will behave the same as the PFR, except that the credited residence time is shorter. A schematic representation of PFR t_{10} and other non-ideal reactors is shown in Figure 1.2.

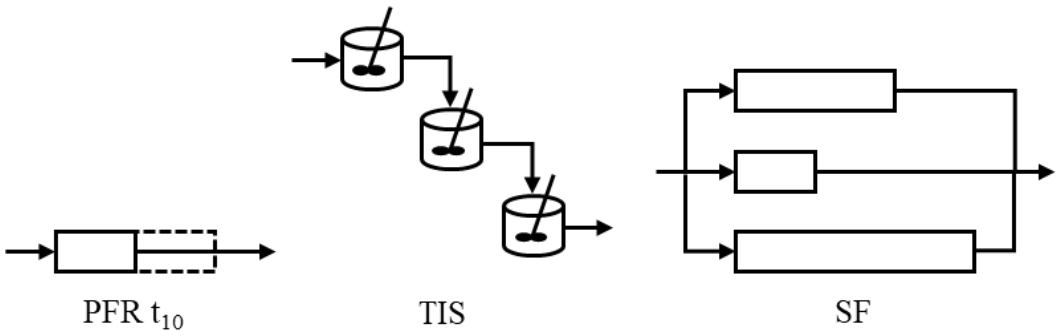

Figure 1.2. Schematic representation of three non-ideal reactor types: t_{10} plug flow reactor (PFR), tanks-in-series (TIS), segregated flow (SF).

Modeling RTD using t_{10} was demonstrated to be overly simplistic, requiring excessive contact time to receive credit for relatively low log reductions and, conversely, underestimating the contact time necessary to achieve higher log reductions (Lawler and Singer, 1993).

Tanks-in-Series (TIS) and Axial Dispersion

More accurate representations of hydraulic residence time distribution (RTD) can be provided by the tanks-in-series (TIS) or axial dispersion models (Teefy and Singer 1990, Lawler and Singer 1993, Crozes et al. 1999, Ducoste et al. 2001). These models have one parameter, number of tanks (n) or dispersion number (D), that can be fit to tracer data. The TIS and axial dispersion models produce similar results when dispersion in a reactor is low (Crittenden et al. 2012). Although this is not true of all water treatment reactors, most disinfection reactors are designed to reduce dispersion. For this reason, only the TIS model is used here to avoid duplication of model results.

The TIS model divides the reactor into *n* equal-volume CSTRs arranged in series (see Figure 1.2). As *n* approaches infinity, TIS reactor performance will approach that of a PFR; as *n* approaches unity, TIS reactor performance will approach that of a CSTR. Any value of *n* where $1 < n < \infty$ will produce performance between that of a CSTR and a PFR.

Bellamy et al. (1998) coupled one parameter models with the Hom model for pathogen inactivation and first-order oxidant decay to develop the integrated disinfection design framework (IDDF). The stated purpose of the IDDF was to balance pathogen disinfection with DBP formation by developing site-specific disinfection models. IDDF models were intended to provide disinfection treatment credit with lower oxidant concentrations or contact times than PFR t_{10}. Limitations of the original IDDF were its reliance on complex integrals and that it could only be used when deviations from plug flow were small (i.e., $B_F > 0.5$) (Carlson et al. 2001). Although efforts were undertaken to standardize the implementation of the IDDF so that it would be recognized by utility, academic, consulting, and regulatory communities (Carlson et al. 2001), the PFR t_{10} still remains the standard approach to disinfection some 18 years later.

Segregated Flow (SF)

The segregated flow (SF) model represents RTD as a number of PFRs arranged in parallel, each having different residence times (see Figure 1.2). The SF model assumes that fluid elements do not mix or interact with each other. Concentrations in reactor effluent can be calculated by estimating the reaction for each fluid element, and summing (i.e., mixing) all fluid elements at the point that flow leaves the reactor (Crittenden et al. 2012). Detailed descriptions of the SF model are available in chemical engineering (Levenspiel 1999) and water treatment engineering textbooks (Crittenden et al. 2012).

The SF model consists of only PFRs, and contaminant degradation in PFRs is equivalent to degradation in batch reactors with equal residence times (as discussed earlier). Therefore, contaminant degradation in SF can be calculated directly from laboratory batch experiments. By making the conservative assumption that disinfectant concentration throughout the reactor is equal to the observed effluent concentration, contaminant removal can be calculated for each hypothetical PFR based on observation in a batch reactor with the same exposure duration (Crittenden et al. 2012).

The SWTR Guidance Manual describes the use of SF for *Giardia* and virus disinfection calculations (USEPA 1991). However, discussion of SF is limited to ozone disinfection, and was described in limited detail, hindering its implementation by utilities and state regulatory agencies (Najm et al. 2009). The use of SF is not a permissible method for calculating *Cryptosporidium* inactivation under the Long Term 2 Enhanced SWTR (LT2) (USEPA 2010); EPA requested comment in the draft guidance manual on whether SF should be included (USEPA 2003) and ultimately excluded SF from the final guidance due to questions about SF accuracy and lack of supporting experimental data (Najm et al. 2009).

Limitations of SF include that it will overestimate contaminant degradation for reaction orders greater than 1.0 (Crittenden et al. 2012), which could present a risk to public health. SF also assumes that there is no mixing within a reactor; this assumption may not be accurate for many water treatment reactors.

Part of U.S. EPA's concern about the use of SF for disinfection credit in LT2 was that SF might overestimate pathogen inactivation (USEPA 2003). As discussed later, SF produces significantly higher estimates of inactivation than models that include mixing when

incorporating decaying oxidant concentrations (i.e., not assuming concentration throughout the reactor is equal to reactor effluent concentration) (Craik 2005, Pfeiffer and Barbeau 2014). Therefore, it would benefit the field to understand the extent to which mixing occurs within water treatment reactors. If reactor mixing is indeed significant, other models should be sought to accurately represent both RTD and internal mixing.

Maximum Mixedness (MM)

While the SF model assumes that flow entering the reactor does not mix with the reactor contents, the maximum mixedness (MM) model assumes the opposite: that flow entering the reactor perfectly mixes with reactor contents (Fogler 2005). The SF and MM models present opposite extremes of mixing assumptions for a reactor with a given RTD. For a single first-order reaction, the MM model and SF model produce equivalent predictions of contaminant degradation (Fogler 2005), such as Chick-Watson disinfection when oxidant concentration is constant (Craik 2005, Pfeiffer and Barbeau 2014). However, for a multi-reaction system such as disinfection with a decaying oxidant, SF and MM will produce different predictions of contaminant degradation (Craik 2005, Pfeiffer and Barbeau 2014).

Computational Fluid Dynamics (CFD)

Computational fluid dynamics (CFD) models have been used to predict pathogen inactivation, disinfectant residual, and disinfection by-product formation spatially throughout reactors (Greene et al. 2004, Greene et al. 2006, Angeloudis et al. 2014). A benefit of CFD over methods that rely on tracer data is that CFD can predict reactor performance prior to construction, estimate the effects of reactor design modifications, and simulate a range of flow conditions with relatively little additional effort.

However, CFD modeling remains too computationally resource-intensive for every day reactor design and operation (Laurent et al. 2014) at steady state, and simulations for dynamic conditions require even greater computing power (Wicklein et al. 2015). Further, modern CFD codes still generally perform poorly at estimating RTD (Naumann 2008). For these reasons CFD was not used in this dissertation.

1.1.2.4 Equations for Step Dose Tracer RTD and Contaminant Removal

Although tracer studies can be either pulse dose or step dose (Fogler 2005), this dissertation will be limited to the use of step dose tracers. This type is more commonly used in water treatment, and a guide on performing tracer studies can be found elsewhere (Teefy 1996). Figure 1.3 shows the cumulative distribution curve produced by a step dose tracer. Equations for tracer effluent predicted by ideal and non-ideal reactor types are shown in 1.1.

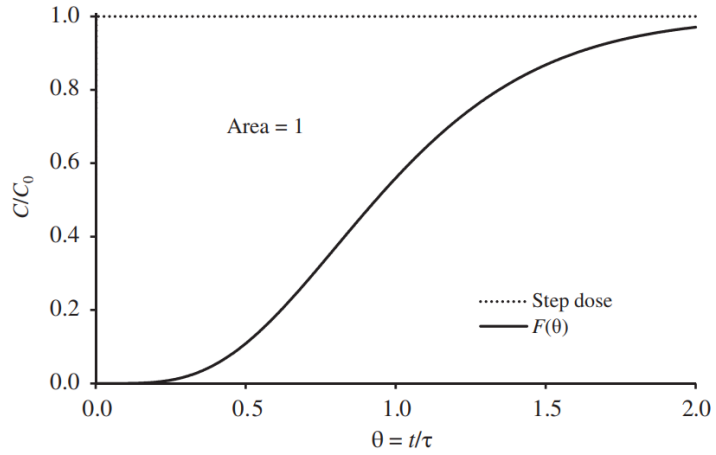

Figure 1.3. Cumulative distribution curve for a step-dose tracer.

For the tracer shown in Figure 1.3, C is the observed concentration of a conservative tracer over time, and C_0 is the initial step dose concentration. The normalized residence time, Θ, is equal to time (t) divided by τ. Dividing reactor volume (V) by flow rate (Q) yields τ.

Contaminant oxidation in water treatment reactors may be a function of numerous independent variables, including pH, temperature, flow rate, reactor volume, oxidant concentration, and contaminant concentration. These variables can be expressed as a single number: the Damköhler number (*Da*). *Da* is a unitless number defined by Fogler (2005) as

$$Da = \frac{reaction\ rate}{mass\ transport\ rate} = \frac{-rV}{\dot{m}}, \tag{1.1}$$

where *r* is the reaction rate (mg/L-min), and $\dot{m}$ is the mass flow rate (mg/min). Higher *Da* indicates more reaction (e.g., contaminant removal) and is generalizable to reactions of any order in flow through reactors (Fogler 2005, Howe et al. 2012). Consider an example reaction that is second order overall and first order with respect to each of two reactants [e.g., an oxidant (*C*) and a contaminant (*N*, mg/L), which could be microbial or chemical]. The *Da* for contaminant with concentration *N* in this case would be

$$Da = \frac{-\mathrm{rV}}{\dot{\mathrm{m}}} = \frac{-\mathrm{k'CNV}}{\mathrm{QN}} = -\mathrm{k'C}\tau\ , \tag{1.2}$$

as used by Lawler and Singer (1993). Contaminant removal equations for the type of reaction described above are shown for ideal and non-ideal reactors in Table 1.1.

Table 1.1. Normalized step dose tracer concentration and contaminant remaining for ideal and non-ideal reactor models currently used in water treatment. Contaminant remaining equations are for reactions that are second order overall, first-order with respect to the contaminant and oxidant. Contaminant remaining equations are shown as a function of the Damköler number (Da). Modified from Chapter 2, Table 2.7 (Gorzalski et al. 2018).

Reactor	**Reactor Effluent Tracer Concentration, C/C_0**	**Contaminant Remaining N/N_0**
Batch	N/A	$\frac{N}{N_0} = \mathrm{e}^{-Da}$
PFR	For $\theta < 1 \quad F(\theta) = 0$ For $\theta \geq 1 \quad F(\theta) = 1$	$\frac{N}{N_0} = \mathrm{e}^{-Da}$
PFR t_{10}	For $\theta < B_F \quad F(\theta) = 0$ For $\theta \geq B_F \quad F(\theta) = 1$	$\frac{N}{N_0} = \mathrm{e}^{-B_F Da}$
CSTR	$F(\theta) = 1 - \mathrm{e}^{-\theta}$	$\frac{N}{N_0} = \frac{1}{1+Da}$
TIS	$F(\theta) = \int_0^\theta \frac{n(n\theta)^{n-1}}{\Gamma(n)} \mathrm{e}^{-n\theta} \mathrm{d}\theta$ where $\Gamma(n) = \int_0^\infty \mathrm{e}^{-x} x^{n-1} \mathrm{d}x$	$\frac{N}{N_0} = \frac{1}{\left(1+\frac{Da}{\mathrm{n}}\right)^{\mathrm{n}}}$
SF	N/A	$\frac{N}{N_0} = \sum \left[\left(\frac{C}{C_0}\right)_2 - \left(\frac{C}{C_0}\right)_1\right] e^{-Da\frac{\theta_1+\theta_2}{2}} + \cdots + \left[\left(\frac{C}{C_0}\right)_z - \left(\frac{C}{C_0}\right)_{z-1}\right] e^{-Da\frac{\theta_z+\theta_{z-1}}{2}}$

1.1.3 Needs and Knowledge Gaps for Hydraulic Models of Water Treatment Reactors

1.1.3.1 Accurate, Simple Models to Simulate RTD and Predict Contaminant Degradation

As discussed in the previous section, there are numerous ideal and non-ideal reactor models that can be used to model water treatment reactors. However, very few of these models closely represent the observed RTD as determined by tracer study (see Figure 1.4). The PFR and PFR t_{10} models are unable to accurately represent RTD. The TIS model provides considerable improvement in fit accuracy compared to the PFR and PFR t_{10} models. However, the TIS model is limited in its ability to fit the observed RTD due to having only one fitting parameter. SF uses tracer data directly[2], and thus can represent any observed tracer data. However, the equation to

[2] For each tracer data point, the observed Θ represents normalized residence time, and $\Delta C/C_0$ represents the fraction of flow that passes through the PFR.

describe contaminant degradation using SF is long and complex. For the tracer data shown in Figure 1.4, SF would require 72 PFRs and 146 unique inputs to predict contaminant degradation. This expression is considerably longer than the expressions for other reactor models as shown in Table 1.1.

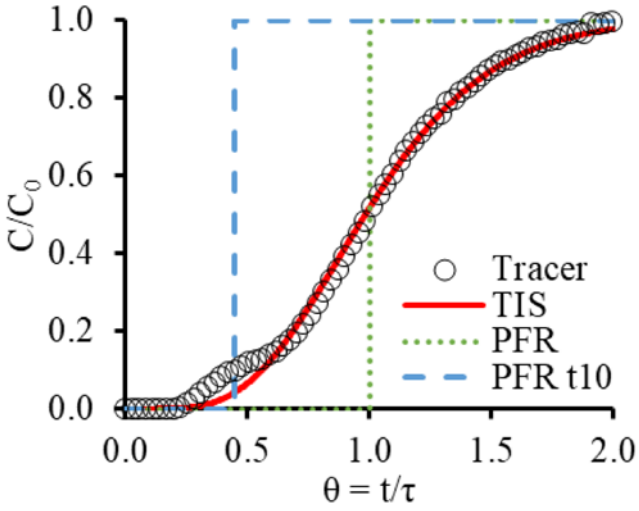

Figure 1.4. RTD as observed by a step dose tracer and predicted by PFR, PFR t10, and TIS models.

Thus, the water treatment field would benefit from reactor models that can accurately represent RTD with less complexity than SF.

1.1.3.2 Understanding Flow Segregation and Earliness of Mixing in Water Treatment Reactors

As discussed in Section 1.1.2.1 above, reactor performance is a function of reaction kinetics, RTD, flow segregation, and earliness of mixing; these concepts are depicted in Figure 1.5. However, reactor models commonly used in water treatment, including IDDF and SF, have considered only reaction kinetics and RTD, and make implicit assumptions about flow segregation and mixing. SF assumes perfect segregation throughout, with all flows mixing at the end of the reactor similar to a zero residence time CSTR. The MM model uses the same RTD as

SF, but assumes perfect mixing when flows enter the reactor. IDDF with TIS reactors assume perfect mixing in the reactor in a discrete series of CSTRs. Previous studies have shown that in the presence of a decaying oxidant, pathogen log inactivation would be predicted to increase with increasing flow segregation (i.e., MM < TIS < SF) (Craik 2005, Pfeiffer and Barbeau 2014).

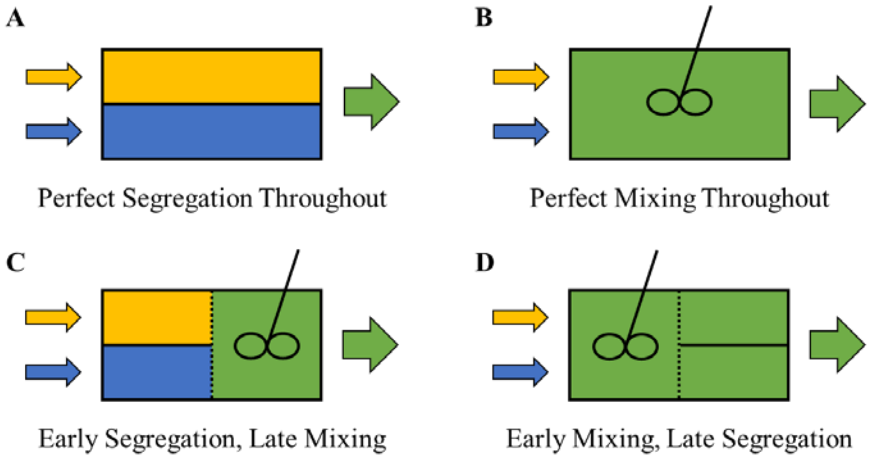

Figure 1.5. Visual representation of reactor segregation and mixing. Blue and yellow solutions, when mixed together, form a green solution. Solid lines represent boundaries through which flow cannot pass, while dashed lines represent boundaries through which flow can pass.

Although differences in segregation and mixing can have important impacts on predicted contaminant degradation under certain conditions (i.e., reaction not 1st order, RTD deviates from plug flow, target reduction is high, multiple reactions), these concepts have not been investigated in drinking water treatment reactors. There is a gap in the existing literature regarding whether flow in full-scale reactors is perfectly segregated, perfectly mixed, or somewhere in between. A previous study (Gresch et al. 2011) successfully investigated these conditions using ammonia as a reactive tracer in an actively mixed nitrification reactor treating wastewater. A similar study could be performed in drinking water reactors if a suitable reactive tracer could be used at full scale. These findings would inform decisions about model selection (e.g., perfect segregation versus assumed mixing).

1.1.3.3 Effects of Model Selection on Contaminant Degradation Predictions

Despite its shortcomings, the PFR t_{10} is still used for disinfection credit in the United States (USEPA 1991, USEPA 2010), as well as for predicting the degradation of emerging contaminants such as cyanotoxins (Stanford et al. 2016). Although the IDDF and SF provide more accurate predictions of reactor performance, the PFR t_{10} is generally considered to be a conservative lower bound of contaminant degradation (Crittenden et al. 2012). As a result, California allows up to 6-log reduction of pathogens in water reuse projects to be credited based on t_{10} (CDPH 2014). The pathogen risk assessment for a 1 MGD demonstration-scale facility in San Diego (Pecson et al. 2017) credited 6-log *Giardia* and virus credit for an ozone contactor based on t_{10}.

Crediting 6-log pathogen removal based on t_{10} raises questions about whether a parameter that specifies a minimum residence time for only 90% of flow can be used to credit 99.9999% degradation. The water treatment field would benefit from a study of the reductions at which the PFR t_{10} model typically ceases to be conservative for estimating disinfection in water treatment reactors.

Further, the field would also benefit from a better understanding of the effect that flow segregation and earliness of mixing in different reactor hydraulic models have on estimates of contaminant degradation.

1.1.3.4 Reactor Network Models in Water Treatment

Reactor network (RN) models consist of different reactor types and sizes arranged in parallel and series combinations. Chemical engineering textbooks describe basic RNs, such as PFRs and CSTRs arranged in series (Levenspiel 1999, Fogler 2005). Reactor networks

consisting of three to five TIS reactors have been used to model RTD in high-dispersion, chemical engineering applications, such as a packed bed reactor, an internally recirculating CSTR, and a simulated cuboid with multi-port inlet manifold (Martin 2000). The RN models used by Martin (2000) were able to represent RTD accurately using fewer total reactors than networks using only PFRs and CSTRs.

Reactor network models have the potential to improve modeling accuracy in water treatment reactors. However, reactor network models have not been used in the water treatment field to date. Numerous questions remain about their application. Whether they can more accurately represent RTD than models currently used in the field, what network arrangements should be used, and their relative effort and complexity compared to current models (i.e., PFR t_{10}, TIS, SF) have yet to be investigated.

1.1.3.5 Summary of Knowledge Gaps

In summary, important knowledge gaps in water treatment reactor modeling include:

1. Lack of accurate, simple models for representing reactor RTD.
2. Limited understanding of the degree of flow segregation and earliness of mixing in water treatment reactors.
3. Lack of guidance on the use of different RTD models when designing systems for different ranges of contaminant degradation (i.e., log reduction).

1.2 Objectives

1.2.1 Overall Dissertation Goal

The overall goal of this dissertation was to identify and recommend accurate methods for the calculation of contaminant degradation in water treatment reactors.

1.2.2 Specific Objectives

To accomplish this overall goal, I pursued the following specific objectives:

1. Develop reactor network models for water treatment reactors.
2. Assess the degree of full-scale reactor segregation and mixing using reactive tracers.
3. Quantitative evaluation of how RTD model selection impacts predicted contaminant degradation.

1.3 Dissertation Organization

This dissertation consists of six chapters. Chapter 1 provides background and motivation for the research performed, including a discussion of applications of reactor modeling, description of individual reactor models, and summary of needs and knowledge gaps. Chapters 2-4 consist of research project descriptions to address the specific objectives described in the previous section. Each chapter contains introduction, methods, results and discussion, and conclusion sections. A brief description of Chapters 2-4 is provided below:

Chapter 2: Specific Objective 1 is addressed in this chapter. This chapter identified a short list of reactor network models that were broadly effective in modeling the RTD of tracer studies from literature. A process for selecting a single reactor network model for a given set of tracer data based on goodness of fit and model simplicity is also described. Tutorial videos were created and code for fitting reactor network models to tracer data were made publicly available on a website created for this purpose. Reactor network models are then used in Chapters 3 and 4.

Chapter 3: Specific Objective 2 is addressed in this chapter. Flow segregation and earliness of mixing were investigated using reactive tracers generated from the seasonal conversion of residual disinfectant from chloramine to free chlorine. Reactor models used to

represent RTD in Chapter 2, each with differing assumptions about flow segregation and mixing, were used to predict concentrations of reactive tracers. Model predictions were compared to observation to indirectly assess flow segregation and mixing in water treatment reactors.

Chapter 4: Specific Objective 3 is addressed in this chapter. For 35 reactors from literature, the effect of model selection on predicted contaminant degradation was studied in four ways. First, the *Da* required to achieve different target log reductions is computed for using different RTD models. Second, the range of log reduction at which the PFR t_{10} model can be considered conservative is calculated. Third, the impact of reactor model selection on capital costs of reactor construction is estimated. Finally, quantitative guidance is provided on the range of *Da* at which reactor modeling is necessary.

Chapter 5 summarizes conclusions that were reached from the collective findings in Chapters 2-4. Conclusions reached from an individual chapter are contained within the conclusions section of each chapter. Chapter 6 provides additional research questions, along with why answering those question is important to the field and potential technical approaches to address each research question.

REFERENCES

American Water Works Association (AWWA). 2018. 2017 Water Utility Disinfection Survey Report.

Angeloudis, A., Stoesser, T., Falconer, R. A. 2014. Predicting the disinfection efficiency range in chlorine contact tanks through a CFD-based approach. *Water Research*, 60: 118-129.

Bellamy, W.D.; Haas, C.; Finch, G. 1998. Integrated Disinfection Design Framework. AWWA Research Foundation. Denver, CO.

California Department of Public Health (CDPH). 2014. Regulations Related to Recycled Water. California Code of Regulations Titles 22 and 17.

Craik, S.A. 2005. Effect of micro-mixing conditions on predictions of Cryptosporidium inactivation in an ozone contactor. *Ozone Sci. Eng.*, 27 (6): 487–494.

Crittenden, J. C., Trussell, R. R., Hand, D. W., Howe, K. J., & Tchobanoglous, G. 2012. MWH's water treatment: principles and design. 2nd Ed. Hoboken, NJ: John Wiley & Sons.

Carlson, K.; Pier, D.; Bellamy, W.; Carlson, M.; Ducoste, J.; Amy, G.; Rakness, K. 2001. Implementation of the Integrated Disinfection Design Framework. AWWA Research Foundation. Denver, CO.

Crozes, G.F.; Hagstrom, J.P.; Clark, M.M.; Ducoste, J.; Burns, C. 1999. Improving Clearwell Design for CT Compliance. AWWA Research Foundation. Denver, CO.

Ducoste, J.; Carlson, K.; Bellamy, W. 2001. The integrated disinfection design framework approach to reactor hydraulics characterization. *Journal of Water Supply: Research and Technology – AQUA*, 50 (4): 245-261.

Fogler, H.S. 2005. *Elements of Chemical Reaction Engineering*. 4th ed. Boston, MA: Pearson Education.

Gorzalski, A.S., Harrington, G.W., Coronell, O. 2018. Modeling water treatment reactor hydraulics using reactor networks. *Journal AWWA*, 110 (8): 13-29.

Greene, D.J., Farouk, B., Haas, C.N. 2004. CFD Design Approach for Chlorine Disinfection Processes. *Journal AWWA*, 96 (8): 138-150.

Greene, D. J., Haas, C. N., Farouk, B. 2006. Computational fluid dynamics analysis of the effects of reactor configuration on disinfection efficiency. *Water Environment Research*, 78 (9): 909-919.

Gresch, M., Braun, D., Gujer, W. 2011. Using reactive tracers to detect flow field anomalies in water treatment reactors. *Water Research*, 45 (5): 1984-1994.

Krasner, S. W.; Mitch, W. A.; McCurry, D. L.; Hanigan, D.; Westerhoff, P. 2013. Formation, precursors, control, and occurrence of nitrosamines in drinking water: a review. *Water Research*, 47 (13), 4433-4450.

Laurent, J., Samstag, R. W., Ducoste, J. M., Griborio, A., Nopens, I., Batstone, D. J., Wiks, J. D., Saunders, S., Potier, O. 2014. A protocol for the use of computational fluid dynamics as a supportive tool for wastewater treatment plant modelling. *Water Science and Technology*, 70 (10): 1575-1584.

Lawler, D.F., Singer, P.C. 1993. Analyzing Disinfection Kinetics and Reactor Design: A Conceptual Approach Versus the SWTR. *Journal AWWA*, 85 (11): 67-76.

Levenspiel, O. 1999. *Chemical Reaction Engineering*. 3rd ed. New York: Wiley and Sons.

Martin, A.D. 2000. Interpretation of residence time distribution data. *Chemical Engineering Science*, 55 (23): 5907-5917.

Mitch, W. A., & Sedlak, D. L. 2004. Characterization and fate of N-nitrosodimethylamine precursors in municipal wastewater treatment plants. *ES&T*, 38 (5): 1445-1454.

Najm, I., Brown, N.P., Gramith, K., Hargy, T. 2009. Validating Disinfection in Ozone Contactors. Water Research Foundation. Denver, CO.

Nauman, B.E. 2008. Residence Time Theory. *Ind. Eng. Chem. Res.*, 47 (10): 4752-3766.

Pfeiffer, V., Barbeau, B., 2014. Validation of a simple method for predicting the disinfection performance in a flow-through contactor. *Water Res.*, 49 144–156.

Rodriguez, E., Onstad, G., Kull, T., Metcalf, J., Acero, J., von Gunten, U. 2007. Oxidative Elimination of Cyanotoxins: Comparison of Ozone, Chlorine, Chlorine Dioxide and Permanganate. *Water Research*, 41 (15): 3381-3393.

Seidel, C., Ghosh, A., Tang, G., Hubbs, S. A., Raucher, R., Crawford-Brown, D. 2014. Identifying Meaningful Opportunities for Drinking Water Health Risk Reduction in the United States [Project# 4310]. *Water Research Foundation*.

Stanford, B. D., Adams, C., Rosenfeldt, E. J., Arevalo, E., Reinert, A. 2016. CyanoTOX: Tools for Managing Cyanotoxins in Drinking Water Treatment With Chemical Oxidants. *Journal AWWA*, 108 (12): 41-46.

Teefy, S., 1996. Tracer Studies in Water Treatment Facilities: A Protocol and Case Studies. Water Research Foundation, Denver

Teefy, S.M.; Singer, P.C. 1990. Performance and Analysis of Tracer Tests to Determine Compliance of a Disinfection Scheme with the SWTR. *Journal AWWA*, 82 (12): 88-98.

United States Environmental Protection Agency (USEPA). 1991. Guidance Manual for Compliance with the Filtration and Disinfection Requirements for Public Water Systems using Surface Water Sources. Washington, DC.

United States Environmental Protection Agency (USEPA). 2003. Long Term 2 Enhanced Surface Water Treatment Rule Toolbox Guidance Manual (Draft). Washington, DC. EPA 815-R-03-009.

United States Environmental Protection Agency (USEPA). 2009. The Ground Water Rule (GWR) Implementation Guidance. Washington, DC. EPA 816-R-09-004.

United States Environmental Protection Agency (USEPA). 2010. Long Term 2 Enhanced Surface Water Treatment Rule Toolbox Guidance Manual. Washington, DC. EPA 815-R-09-016.

Wicklein, E., Batstone, D. J., Ducoste, J., Laurent, J., Griborio, A., Wicks, J., Saunders, S., Samstag, R., Potier, O., Nopens, I. 2015. Good modelling practice in applying computational fluid dynamics for WWTP modelling. *Water Science and Technology*, 73 (5): 969-982.

CHAPTER 2 - MODELING WATER TREATMENT REACTOR HYDRAULICS USING REACTOR NETWORKS[3]

2.1 Introduction

Improved design and operation of water treatment reactors through a more detailed understanding of reactor hydraulics has been the subject of education and research for over four decades (Weber 1972, Trussell and Chao 1977). In addition to improving reactor design and operation, this understanding of reactor hydraulics has served as a foundation for regulating the performance of water treatment reactors (USEPA 1991, Harrington et al. 1993).

Reactor hydraulics are also fundamental to more recent developments in the drinking water field, including treating contaminants of emerging concern and planned wastewater reuse. Accurate modeling of reactor residence time is necessary to construct models of treatment efficacy for balancing disinfection with disinfection by-product formation and for oxidative degradation of emerging contaminants such as algal toxins (Rodriguez et al. 2007), N-nitrosodimethylamine (NDMA) precursors (Krasner et al. 2013), and certain endocrine disrupting compounds, pharmaceuticals, and personal care products (Westerhoff et al. 2005). Planned reuse applications may also require improved hydraulic modeling compared to

[3]This chapter previously appeared as an article in *Journal AWWA*. The original citation is as follows: Published in Gorzalski, A.S., Harrington, G.W., Coronell, O. 2018. Modeling water treatment reactor hydraulics using reactor networks. *Journal AWWA* (2018), 110 (8): 13-29.

conventional surface water treatment due to vastly different regulatory requirements for pathogen barriers. For example, the state of California requires 10^7 times more reduction credit (i.e., 10-log versus 3-log) for *Giardia* and *Cryptosporidium* in groundwater replenishment projects than in surface water treatment (CDPH 2014).

Real-world, continuous flow reactors exhibit hydraulic behavior that falls between two ideal reactor types: the continuous flow stirred-tank reactor (CSTR) and the plug flow reactor (PFR). The CSTR is assumed to have infinite dispersion in all directions, giving rise to complete mixing throughout the reactor. The PFR is assumed to have zero dispersion parallel to the direction of flow, but infinite dispersion perpendicular to the direction of flow, and is mathematically equivalent to an infinite number of infinitesimal CSTRs connected in series. When a finite number of equally sized CSTRs (e.g., 2-100) are arranged in series, the resulting tanks-in-series (TIS) reactor exhibits dispersion between the CSTR and PFR.

The Surface Water Treatment Rule (SWTR, USEPA 1991) addresses reactor dispersion in disinfection calculations by crediting only the time for the first 10 percent of flow to exit the reactor (t_{10}). A reactor baffle factor is calculated by dividing t_{10} by the nominal hydraulic residence time (τ). Log reduction credit is calculated as the ratio of achieved CT (residual oxidant concentration, *C*, times t_{10}) to required CT. The current regulatory approach was demonstrated to be overly simplistic, requiring excessively high chlorine CT values (i.e., the product of chorine residual multiplied by contact time, USEPA 1991) for low log reductions and, conversely, underestimating the CT necessary for higher log reductions (Lawler and Singer 1993).

Reactor models with one fitting parameter, including the axial dispersion and the TIS models (Teefy and Singer 1990, Lawler and Singer 1993, Crozes et al. 1999, Ducoste et al.

2001), more accurately represent hydraulic conditions than t_{10}/τ baffle factors. The axial dispersion and TIS models are roughly equivalent and perform well when deviations from plug flow are small (Levenspiel 1999). However, a single fitting parameter constrains model flexibility and thus accuracy, particularly for higher dispersion reactors.

Computational fluid dynamics (CFD) presents the opposite end of the spectrum, producing flexible models with a large number of input parameters. Improvements in CFD modeling have enabled prediction of residence time indices (e.g., t_{10}/τ) within ~10% (Templeton et al. 2006, Zhang et al. 2016). While CFD has utility in estimating performance before reactors are constructed or modified, tracer tests provide greater accuracy for existing reactors at lower cost using more transparent methods. In a review of residence time theory, Naumann (2008) commented that modern CFD codes generally perform poorly at estimating residence time distribution and expressed concern over the potential for CFD to be used improperly.

Previous efforts have succeeded in modeling residence time distribution with greater accuracy than either single parameter or CFD models by modeling one reactor as a combination of multiple reactors. Najm et al. (2009) were able to accurately predict spore inactivation through an ozone contactor using segregated flow (SF). The SF model treated a single contactor as 26 parallel PFRs. This approach accurately fit tracer data and predicted disinfection performance (Najm et al. 2009), but yielded a large number of reactors. In chemical engineering applications, Martin (2000) noted that combinations having only ideal PFRs and CSTRs can lead to large and cumbersome models. Martin was able to reduce the number of reactors by using TIS reactors arranged in various parallel and series combinations.

In chemical reactor design, reactors arranged in parallel and series combinations,

typically of varying types and sizes, are known as reactor networks. Basic reactor networks using CSTRs and PFRs are described in chemical engineering textbooks (Levenspiel 1999, Fogler 2005). Martin (2000) developed networks of three to five TIS reactors to describe high-dispersion chemical engineering reactors, which included a packed bed reactor, an internally recirculating CSTR, and a simulated cuboid with multi-port inlet manifold. Reactor networks were shown to accurately represent non-ideal flow with relatively simple models. Water treatment plants operate the largest continuous flow reactors in existence, considerably larger than most chemical engineering reactors (Howe et al. 2012). Departure from ideal flow increases with reactor size, and therefore the design of water treatment reactors depends on understanding this nonideality (Howe et al. 2012). Thus, reactor networks could have utility in modeling drinking water reactors. However, to the authors' knowledge, reactor networks have not yet been applied to water treatment reactors (e.g., clearwells and ozone contactors), nor have their benefits and drawbacks in terms of accuracy, broad applicability, modeling effort, and model complexity been compared to existing approaches (i.e., t_{10}/τ baffle factors, TIS models, and SF).

This work identifies a small number of reactor networks that accurately model residence time distributions across a wide range of water treatment reactors and describes the process for fitting these models to user-supplied data sets with open source software. In addition, this work provides the first application of reactor networks to water treatment reactors and compares reactor networks to existing approaches with a discussion of balancing goodness of fit with model complexity.

2.2 Modeling Methods

2.2.1 Tracer Studies

A total of 19 tracer data sets from 14 reactors, including clearwells, ozone contactors,

clarifiers, and filters (see Table 2.1), were obtained both from literature and previously unpublished data. The unpublished tracer data corresponds to clearwell tracer studies, 1A and 1B, conducted at full-scale using step-dose fluoride ($\Delta C \approx 0.7$ mg/L) experiments.

2.2.2 Normalized F vs. θ curve

There are two common types of tracer studies: the pulse dose and the step dose (Fogler 2005). A detailed guide on conducting tracer studies was provided by Teefy (1996) and thus is not provided here. All tracer data were converted to the normalized step dose $F(\theta)$ curve as described elsewhere (Levenspiel 1999). As shown in Figure 2.1, F is the tracer concentration leaving the reactor divided by the step dose concentration (C/C_0), and θ is the normalized run time, where $\theta = t/\tau$. The nominal hydraulic residence time, τ, is defined as $\tau = V/Q$ where V is the reactor volume and Q is the volumetric flow rate.

2.2.3 Reactor Network Hydraulic Models

Hydraulic models for reactor networks were constructed from various combinations of PFR, CSTR, and TIS reactors. These included reactors arranged in parallel, series, or some combination thereof. All models contained four or fewer reactors. Twenty-nine models were developed with and without dead space for a total of 58 separate hydraulic models.

Table 2.1. Summary of tracer data used for testing various hydraulic models.

ID	Plant Type	Contactor Type	Tracer Type	Replicates	t_{10}/τ	Reference
1A	Water	Clearwell	Step Dose	1	0.45	This Chapter
1B	Water	Clearwell	Step Dose	4	0.45	This Chapter
2A	Water	Clearwell	Step Dose	1	0.39 *	Teefy and Singer 1990
3A	Water	Filters (6)	Pulse Input	1	0.50 *	Teefy 1996
3B	Water	Clearwell	Step Dose	2	0.72-0.80	Teefy 1996
3C	Water	Clearwell	Step Dose	1	0.67	Teefy 1996
3D	Water	Ozone Contactor	Step Dose	2	0.61	Teefy 1996
3E	Wastewater	Secondary Clarifier	Pulse Input	1	0.19	Teefy 1996
3F	Wastewater	Chlorine Contact Chamber	Pulse Input	1	0.43	Teefy 1996
3G	Water	Clearwell	Step Dose	1	0.67	Teefy 1996
3H	Water	Clearwell (Circular)	Step Dose	1	0.57	Teefy 1996
4A	NR	NR	Step Dose	1	0.31 *	Carlson et al. 2001
5A	Water	Ozone Contactor	Step Dose	1	0.69 *	Najm et al. 2009
5B	Water	Ozone Contactor	Pulse Input	1	0.70 *	Najm et al. 2009

NR - not reported

* Not reported, but calculated via linear interpolation from reported data

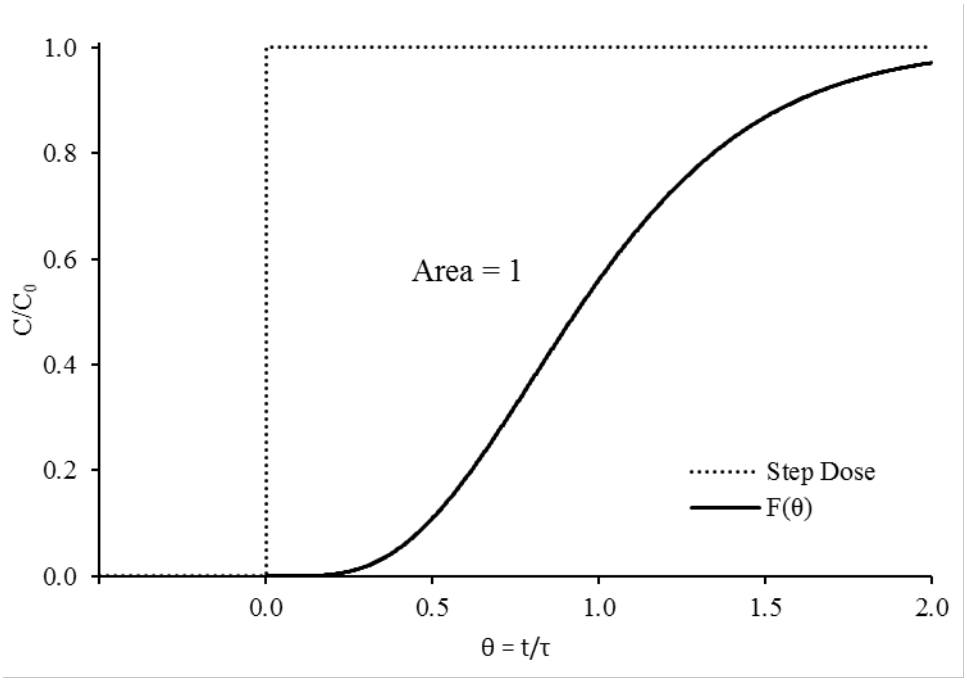

Figure 2.1. The F(θ) cumulative distribution curve as shown for a step dose tracer.

2.2.4 Screening for Well-Performing Hydraulic Models

The process for selecting a shortlist of hydraulic models from the initial list of 58 candidate hydraulic models is shown in the left half of Figure 2.2. Each of the 19 tracer data sets were fit with all 58 hydraulic models. For models with zero fitting parameters (i.e., PFR and CSTR), no fitting was performed but residuals (i.e., observed minus predicted values of C/C_0) were calculated. For models with one or more fitting parameters, model regression was performed by minimizing the sum of squared residuals. Model regression was done in R (R Core Team 2016) using the *optim* and *nlminb* functions for single parameter and multiple parameter models, respectively, where sum of squared residuals was the objective function to be minimized. These optimization functions were used in place of regression functions (e.g., *nls*) because the optimization functions were less sensitive to initial conditions. To begin the iteration process used by the optimization function, initial parameter estimates for any given network model assumed equal proportioning of reactor volume and flow fraction between all reactors,

and n = 2 for TIS models. Once all of the 58 model regressions were completed for each data set, a subset of nine models was selected based on goodness of fit and number of successful fits. Metrics for goodness of fit are described in the following section.

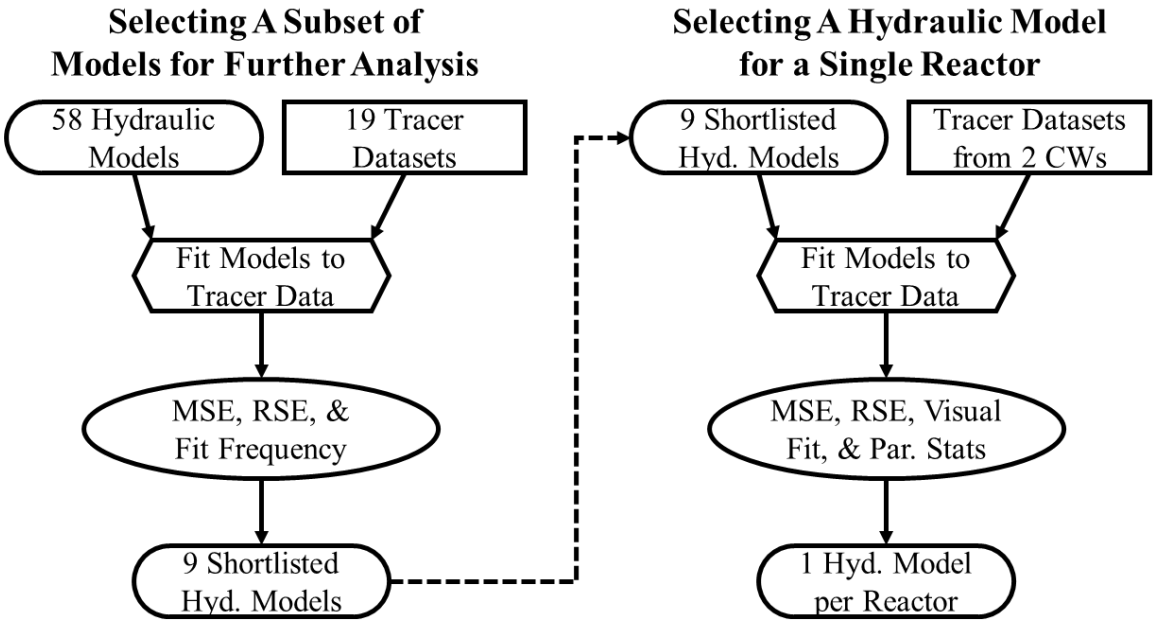

Figure 2.2. Process for selecting a reactor hydraulic model. Parameter statistics used in evaluating models include total number of parameters as well as p-value and confidence intervals for each parameter.
MSE – mean squared error
RSE – residual standard error

2.2.5 Determining goodness of fit: MSE and RSE

The goodness of fit for each model was determined using two statistical parameters: mean squared error (MSE) and residual standard error (RSE). MSE describes the goodness of fit without respect to the number of fitting parameters and was calculated as

$$MSE = \frac{\Sigma_1^j \left(\left[\frac{C}{C_0}\right]_{modeled,j} - \left[\frac{C}{C_0}\right]_{observed,j} \right)^2}{j}, \quad 2.1$$

where *j* is the number of data points in the tracer study. RSE is similar to MSE, but penalizes

goodness of fit based on the number of fitting parameters used. RSE was calculated as

$$RSE = \sqrt{\frac{\sum_1^j \left(\left[\frac{C}{C_0}\right]_{modeled,j} - \left[\frac{C}{C_0}\right]_{observed,j} \right)^2}{j-p}}, \quad 2.2$$

where *p* is the number of fitting parameters. Fitting parameters include reactor volume fractions, volume fraction of dead space, flow fractions for parallel trains, and number of tanks in a TIS reactor. RSE is defined in the *stats* base package in R (R Core Team 2016).

2.2.6 Process for Selecting a Model for a Given Data Set

The process of selecting a single hydraulic model for clearwells (CW) 1A and 1B is presented in detail in the results and discussion section, along with the selected models for the other 12 reactors. A visual representation of this process is shown in the right half of Figure 2.2. Regression was performed to fit the nine shortlisted models to each data set using nls, a function in R for estimating parameters in nonlinear models using least-squares. The *nls* function is more sensitive to initial values and consumes more computational resources than the *nlminb* optimization function. However, it provides additional information regarding the goodness of fit and fitting parameter statistics. Goodness of fit, visual inspection of fits, and statistics of fitting parameters were then used to select a single hydraulic model for each clearwell.

2.2.7 Monte Carlo Analysis for Fit Confidence Limits

A Monte Carlo analysis was performed to estimate the confidence limits of the overall fits for CW 1A and CW 1B. These limits represented the fit as a whole rather than for a single fitting parameter. The sum of squared error at the confidence limits was determined using the “F” statistical distribution used by Bellamy et al. (1998), not to be confused with the $F(\theta)$ curves discussed earlier. Using parameter estimates and standard deviations, 100,000 random

combinations of normally distributed fitting parameters were tested. Those that yielded the largest sum of squared error within the allowable sum of squared residuals constituted the confidence limits.

2.2.8 Evaluating Reactor Models across Uniform Conditions

Comparing hydraulic models requires a consistent set of reaction conditions. Lawler and Singer (1993) used $k'C\tau$ (unitless) for disinfection, where k' is the inactivation rate constant (at a given temperature, pH, and chlorine concentration) and C is the disinfectant concentration. This unitless term is a disinfection-specific example of a more generalized term called the Damköhler number (*Da*). *Da* is a unitless number comparing the rate of reaction to the rate of transport, and is defined by Fogler (2005) as

$$Da = \frac{reaction\ rate}{mass\ transport\ rate} = \frac{-rV}{\dot{m}}, \tag{2.3}$$

where r is the reaction rate (mg/L-min), and $\dot{m}$ is the mass flow rate (mg/min). If a reaction rate is second order overall and first order with respect to each of two reactants [e.g., an oxidant (C) and a contaminant (N, mg/L), which could be microbial or chemical], then Equation 2.3 becomes

$$Da = \frac{-rV}{\dot{m}} = \frac{-k'CNV}{QN} = -k'C\tau, \tag{2.4}$$

as used by Lawler and Singer (1993). *Da* is used in this study because it is generalizable to reactions of any order in flow through reactors (Fogler 2005, Howe et al. 2012). This allows a comparison of the reactor models themselves, independent of water quality or flow conditions, and is generalizable to any oxidant (e.g., ozone, permanganate). Predicted log reduction versus *Da* for different reactor models are presented in the results and discussion section to illustrate the importance of selecting an accurate hydraulic model.

2.2.9 Code for Fitting RN Models to Tracer Data

The code used for fitting RN models to tracer data is shown in APPENDIX A. This code, along with tutorial videos describing its use, are shown in www.tools4water.com.

2.3 Results and Discussion

2.3.1 Screening Hydraulic Models

The 58 candidate hydraulic models (29 with and without dead space) were fit to 19 tracer data sets. Models were then evaluated on how well they fit the data sets. Desirable qualities in a model include good fit (e.g., low MSE and RSE, normally distributed residuals), ability to fit a large number of data sets, small number of fitting parameters, and ability to yield parameter estimates having a reasonably small p-value (i.e., $p \leq 0.1$). Nine shortlisted models were identified and are shown in Figure 2.3, labeled Models A through I. The selection process for these nine models is described in this section.

Table 2.2 is provided as an example of the MSE and RSE ranking process for different reactor network model fits to data set 1A. The short-listed models produced MSE and RSE 1-3 orders of magnitude lower than poorly performing models (e.g., PFR, PFR and CSTR in series with PFR in parallel, and 3 CSTRs in parallel). Some models failed to converge on a fit, including Model C with dead space and Model F without dead space. The PFR & TIS in series repeated in parallel with dead space (Model I) had the lowest MSE, while the PFR & TIS in series with a TIS in parallel with dead space (Model E) had the lowest RSE. Model I is equivalent to Model F with the addition of a PFR in front of the second TIS; the additional PFR produced negligible improvement in the overall fit (MSE decreased 0.20%), not enough to offset the additional fitting parameter (RSE increased 0.65%). In all cases the addition of a dead space reactor improved the fit of the model compared to the same model without dead space.

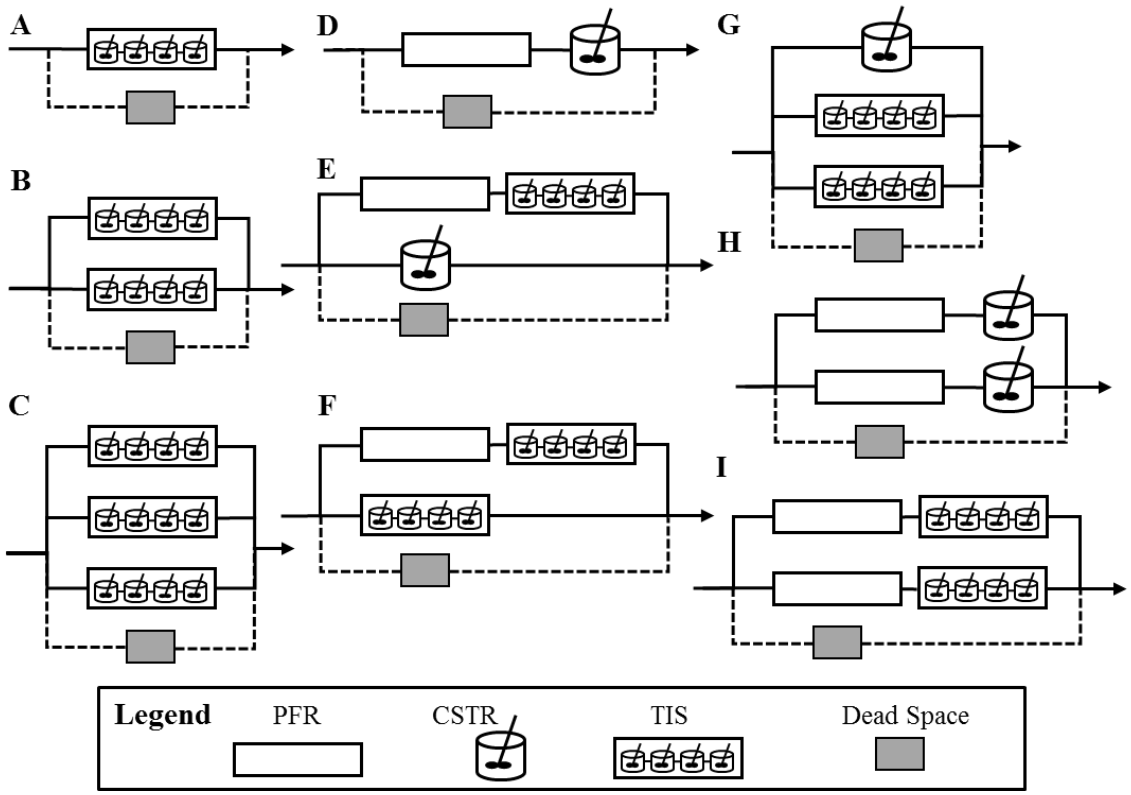

Figure 2.3. Schematics of nine shortlisted reactor network models: (A) TIS, (B) 2 TIS in parallel, (C) 3 TIS in parallel, (D) PFR and CSTR in series, (E) PFR and TIS in series and CSTR in parallel, (F) PFR and TIS in series and TIS in parallel, (G) CSTR and 2 TIS in parallel, (H) PFR and CSTR in series with a parallel PFR and CSTR in series, (I) PFR and TIS in series with a parallel PFR and TIS in series.

Table 2.2. Example of goodness of fit for the nine short-listed hydraulic models, with and without dead space, using data set 1A. Three poor performing hydraulic models are also provided as examples.

Model	Hydraulic Model	Dead Space	Fitting Parameters	Successful Fit?	MSE		RSE	
					Value	Rank	Value	Rank
A	TIS	N	1	Yes	8.96E-04	21	3.01E-02	21
		Y	2	Yes	4.67E-04	18	2.19E-02	17
B	2 TIS in Parallel	N	4	Yes	1.37E-04	8	1.20E-02	8
		Y	5	Yes	1.12E-04	4	1.10E-02	4
C	3 TIS in Parallel	N	7	Yes	1.31E-04	6	1.20E-02	7
		Y	8	No	-		-	
D	PFR & CSTR in Series	N	1	Yes	5.03E-03	26	7.14E-02	26
		Y	2	Yes	2.96E-03	25	5.52E-02	25
E	PFR & TIS in Series, CSTR in Parallel	N	4	Yes	2.38E-04	15	1.59E-02	14
		Y	5	Yes	1.69E-04	10	1.35E-02	10
F	PFR & TIS in Series, TIS in Parallel	N	5	No	-		-	
		Y	6	Yes	3.58E-05	2	6.25E-03	1
G	CSTR and 2 TIS in Parallel	N	6	Yes	1.31E-04	5	1.19E-02	5
		Y	7	Yes	6.00E-05	3	8.14E-03	3
H	PFR & CSTR in Series, Repeated in Parallel	N	4	Yes	7.03E-04	20	2.73E-02	20
		Y	5	Yes	4.08E-04	16	2.09E-02	16
I	PFR & TIS in Series, Repeated in Parallel	N	6	Yes	1.32E-04	7	1.20E-02	6
		Y	7	Yes	3.58E-05	1	6.29E-03	2
Not Selected	PFR	N	0	Yes	4.37E-02	46	2.09E-01	46
		Y	1	Yes	4.37E-02	46	2.10E-01	47
	PFR & CSTR in Series, PFR in Parallel	N	3	Yes	1.70E-02	38	1.33E-01	37
		Y	4	Yes	1.70E-02	37	1.34E-01	38
	3 CSTRs in Parallel	N	4	Yes	3.12E-02	43	1.82E-01	45
		Y	5	Yes	2.75E-02	42	1.72E-01	42

MSE – mean squared error, RSE – residual standard error

Table 2.2 also shows how parallel flows produced better model fits. Having two TIS reactors in parallel (Model B) reduced MSE by 76% compared to a single TIS reactor (Model A); MSE was also reduced by 86% when the PFR and CSTR in series (Model C) was repeated in parallel (Model H). In addition to the number of parallel reactors, the reactor type also significantly impacts goodness of fit. For example, 2 TIS reactors in parallel reduced MSE 400 fold compared to 2 PFRs in parallel (MSE = 0.00012 versus MSE = 0.044, data not shown).

The identification of models with broad applicability in water treatment required testing models for tracer data from different reactors and reactor types. The remaining 18 data sets were fit with the 58 models and both MSE and RSE were calculated accordingly. A summary of how the nine shortlisted models performed for all 19 data sets is shown in Figure 2.3, along with examples from three poorly performing reactor networks. Average MSE and RSE rank across 19 data set fits is shown (e.g., 2.3 and 2.4 for Model F, 44 and 43.5 for PFR), along with relative index of the average (e.g., 1^{st} and 1^{st} for Model F, 58^{th} and 56^{th} for PFR).

As shown in Table 2.3, models with dead space had lower MSE and RSE than those without dead space. This is because reactors without dead space are constrained to a normalized reactor volume (V_{norm}), or area to the left of the tracer curve, equal to one (see Figure 2.1). As discussed in detail in a subsequent section, reactor dead zones and metering issues can produce $V_{norm} \neq 1$. Only models containing dead space were selected for further analysis to ensure they would be applicable to data sets with $V_{norm} \neq 1$.

Table 2.3. Relative performance of the nine short-listed hydraulic models, with and without dead space, for all 19 data sets. Three poor performing hydraulic models are also provided as examples. The relative performance of each model (e.g., see Figure 2.2 rank) was averaged for all 19 data sets to produce average mean squared error (MSE) and residual standard error (RSE) rank. The order of that average rank compared to the other 58 hydraulic models is shown in parenthesis.

Model	Hydraulic Model	Dead Space	Fitting Parameters	Successful Fits	MSE Rank	RSE Rank			Further Analysis
					Average	Average	Worst	Best	
A	TIS	N	1	19	23.2 (31)	20.8 (26)	26	9	No
		Y	2	19	13.3 (17)	12.5 (15)	17	5	Yes
B	2 TIS in Parallel	N	4	15	18.7 (23)	19.3 (24)	30	5	No
		Y	5	12	5.6 (6)	4.8 (3)	8	3	Yes
C	3 TIS in Parallel	N	7	13	11.8 (16)	13.5 (18)	27	1	No
		Y	8	10	3.7 (3)	5.3 (4)	14	1	Yes
D	PFR & CSTR in Series	N	1	19	24.7 (32)	24.1 (32)	32	15	No
		Y	2	19	14.3 (19)	13.3 (17)	28	1	Yes
E	PFR & TIS in Series, CSTR in Parallel	N	4	18	9.7 (12)	9.2 (10)	22	1	No
		Y	5	19	5.3 (5)	5.9 (7)	16	1	Yes
F	PFR & TIS in Series, TIS in Parallel	N	5	5	7.2 (8)	8.6 (8)	24	3	No
		Y	6	9	2.3 (1)	2.4 (1)	5	1	Yes
G	CSTR and 2 TIS in Parallel	N	6	8	13.6 (18)	16 (19)	24	5	No
		Y	7	14	4.3 (4)	5.5 (5)	22	1	Yes
H	PFR & CSTR in Series, Repeated in Parallel	N	4	19	18.6 (22)	18.9 (23)	28	6	No
		Y	5	19	9.3 (10)	9.6 (12)	30	1	Yes
I	PFR & TIS in Series, Repeated in Parallel	N	6	12	11.3 (14)	13.3 (16)	27	4	No
		Y	7	14	2.9 (2)	3.7 (2)	11	1	Yes

Model	Hydraulic Model	Dead Space	Fitting Parameters	Successful Fits	MSE Rank	RSE Rank			Further Analysis
					Average	Average	Worst	Best	
Not Selected	PFR	N	0	19	44 (58)	43.5 (56)	52	35	No
		Y	1	19	41.4 (54)	40.5 (53)	51	23	No
	PFR & CSTR in Series, PFR in Parallel	N	3	19	27.2 (35)	27.4 (34)	46	6	No
		Y	4	19	28.1 (39)	29.5 (40)	41	9	No
	3 CSTRs in Parallel	N	4	19	38.7 (52)	40.9 (54)	54	24	No
		Y	5	19	31.9 (45)	34.2 (48)	50	16	No

The first set of models added to the shortlist were those that fit tracer data with the lowest residual error, defined as an average MSE or RSE ranked in the top five. These included 2 TIS in parallel (Model B), 3 TIS in parallel (Model C), PFR and TIS in series with CSTR in parallel (Model E), PFR and TIS in series with another TIS in parallel (Model F), CSTR and 2 TIS in parallel (Model G), and PFR and TIS in series repeated in parallel (Model I). Although these six models fit data well, all six had a relatively high number of fitting parameters (5-8), and only one (Model E) was able to successfully fit all of the 19 data sets. By contrast, most of the worse performing models produced successful fits for all 19 data sets and had fewer fitting parameters (e.g., see Table 2.3, models not selected). The best fitting models were generally more complex, as indicated by the large number of fitting parameters and five of six having at least two parallel TIS reactors. Failure to converge on a solution for all 19 datasets also indicated that the best fitting models tended to be more sensitive to initial conditions than simpler models. For example, 20 of 22 models with 3 or fewer fitting parameters fit at least 17 of 19 datasets, whereas 0 of 11 models with 6 or more fitting parameters fit at least 15 of 19 datasets (data not shown).

Additional models were selected for further analysis which had low residual error, successfully fit all 19 data sets, and were dissimilar from the six models described in the previous paragraph. The TIS reactor (Model A) was selected for its frequent use in literature and textbooks, and also its successful fitting of all 19 data sets with only two fitting parameters. Two parallel sets of PFR and CSTR in series (Model H) fit all 19 data sets and had the lowest MSE and RSE for a model that did not include a TIS reactor and was therefore also selected. The PFR and CSTR in series (Model D) was selected as the ninth and final model for detailed analysis because it had a number of desirable characteristics: it fit all 19 data sets, had only two fitting parameters, did not include a TIS reactor, and produced a good fit for CW 1B. Also known as the

‘fractional tubularity model,’ Model D was used in what was possibly the first fitting of reactor network models to tracer data (Naumann 2008).

All of these shortlisted models contained between one and four reactors, not counting dead space as a reactor.

2.3.2 Selecting a Single Hydraulic Model for a Reactor

The next step was to use the nine short-listed models to determine the best reactor model for each tracer data set listed in Table 2.1. An appropriate hydraulic model should fit the tracer data well (i.e., low MSE) and have an appropriate number of parameters as indicated by RSE, number of fitting parameters, and parameter p-values < 0.1. This section describes in detail how models were selected for two primary disinfection clearwells: CW 1A and CW 1B. Model selections for the other 12 reactors are also provided.

Fits of the nine short-listed models are shown for CW 1A and CW 1B in Figure 2.4 and Figure 2.5, respectively. For CW 1A, it is relatively clear which models fit the data better than others. Two or three TIS reactors in parallel (Models B and C) fit CW 1A data better than one (Model A). A PFR and CSTR in series did not fit well as a single train (Model D) or as a parallel reactor set (Model H). However, amongst Models B, C, F, G, and I, it was difficult to visually determine which model fit CW 1A data the best. For CW 1B, differences in fit are apparent amongst some of the models, but greater uncertainty in the observed data (which represent four separate step-dose tracer experiments at different flow rates) made it difficult to visually evaluate which models provided a better fit. Thus, metrics such as MSE and RSE were needed to supplement the information provided by visual inspection.

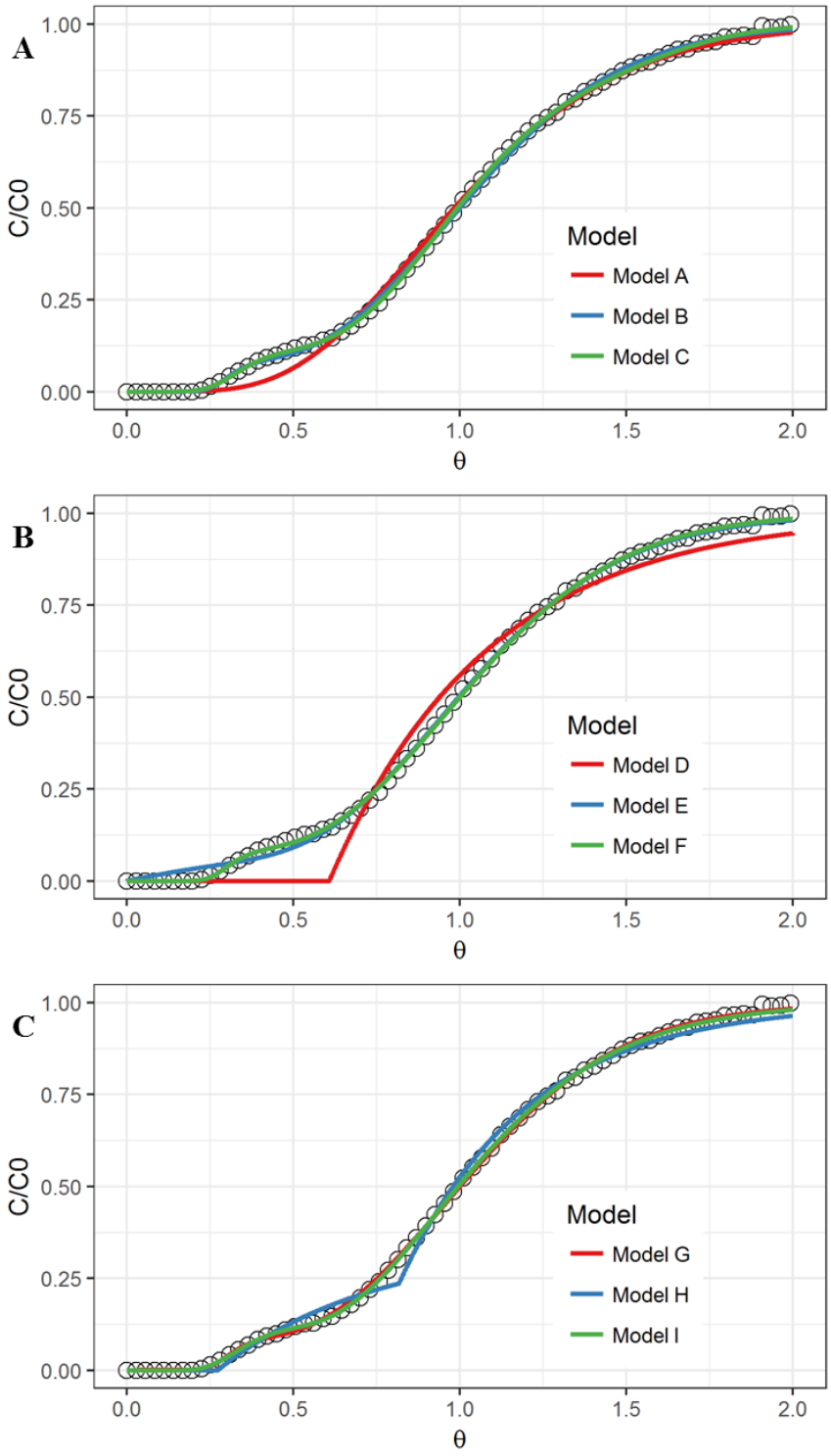

Figure 2.4. Results of fitting shortlisted models A-I to CW 1A tracer data. The schematic of each reactor model A-I is presented in Figure 2.3. MSE and RSE values from model fit are presented in Table 2.4.

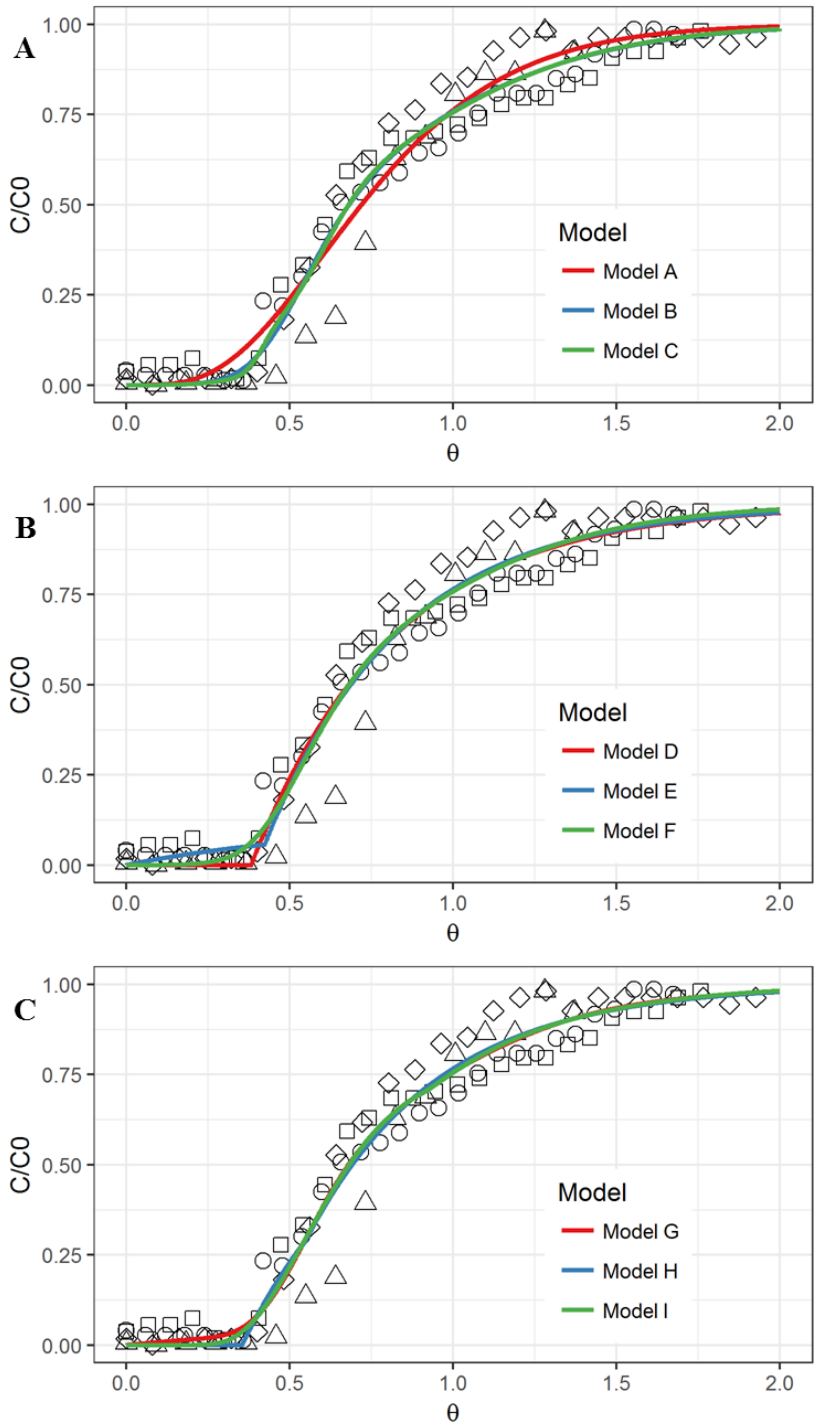

Figure 2.5. Results of fitting shortlisted models A-I to CW 1B tracer data. The schematic of each reactor model A-I is presented in Figure 2.3. MSE and RSE values from model fit are presented in Table 2.4. Data were collected at four different flow rates, with circles (○) from 68 MGD, squares (□) from 77 MGD, diamonds (◊) from 94 MGD, and triangles (Δ) from 104 MGD.

MSE and RSE produced by the fits are shown in Table 2.4. Models for CW 1A generally fitted better than those for CW 1B, as evidenced both visually and by MSE values on the order of 10^{-5}-10^{-4} for CW 1A and 10^{-3} for CW 1B. This is primarily attributable to the use of four separate tracer studies in CW 1B compared to one in CW 1A.

Table 2.4. Mean squared error (MSE) and residual standard error (RSE) for fits of 9 shortlisted hydraulic models.

Model	Hydraulic Model	CW 1A		CW 1B	
		MSE	RSE	MSE	RSE
A	TIS	4.67E-04	2.19E-02	4.62E-03	6.87E-02
B	2 TIS in Parallel	6.03E-05	8.05E-03	3.87E-03	6.39E-02
C	3 TIS in Parallel	1.39E-05	3.96E-03	3.84E-03	6.47E-02
D	PFR & CSTR in Series	2.94E-03	5.50E-02	3.97E-03	6.36E-02
E	PFR & TIS in Series, CSTR in Parallel	1.69E-04	1.35E-02	3.97E-03	6.47E-02
F	PFR & TIS in Series, TIS in Parallel	6.06E-05	8.13E-03	3.88E-03	6.43E-02
G	CSTR and 2 TIS in Parallel	5.98E-05	8.13E-03	3.84E-03	6.43E-02
H	PFR & CSTR in Series, Repeated in Parallel	4.08E-04	2.09E-02	3.87E-03	6.38E-02
I	PFR & TIS in Series, Repeated in Parallel	3.58E-05	6.29E-03	3.87E-03	6.46E-02

As was observed for the visual fits in Figure 2.5, all models for CW 1B achieved similar goodness of fit as measured by MSE and RSE; MSE and RSE values were within 20% and 7.9%, respectively, inclusive of TIS (Model A) and within 3.5% and 1.7% excluding the TIS model. Because most of the models achieved similar goodness of fit, the choices were narrowed to the models with the fewest fitting parameters. The TIS (Model A) and the PFR and CSTR in series (Model D) models had 2 fitting parameters each, including dead space volume, which was significant for CW 1B. The other seven models had between 5 and 8 fitting parameters. The first model with two fitting parameters, the TIS model, was the worst fitting (i.e., highest MSE and RSE) out of the original nine (see Table 2.4) and predicted $t_{10}/\tau = 0.36$; all other models predicted t_{10}/τ of 0.41 to 0.44 (see Figure 2.4). Conversely, the PFR and CSTR in series model was the best fitting (i.e., lowest RSE) of the original nine models and both fitting parameter p-

values were << 0.0001. The PFR and CSTR in series model (Model D) was thus selected for CW 1B.

Based on RSE, the five best fitting models for CW 1A were 3 TIS in parallel (Model C), PFR and TIS in series repeated in parallel (Model I), 2 TIS in parallel (Model B), CSTR and 2 TIS in parallel (Model G), and PFR and TIS in series with a TIS in parallel (Model F). Further analysis was needed to select one of these five models. A summary of fitting information is provided in Table 2.5. All five models produced fits with low RSE (RSE < 0.0081), and the t_{10}/τ, t_{50}/τ, and t_{90}/τ ratios from all five model fits were within 7% of those observed in the tracer data.

Table 2.5. Residual standard error (RSE), flow indices, fitting parameter estimates, and p-values for best performing CW 1A hydraulic models. The t_{10}/τ, t_{50}/τ, and t_{90}/τ from tracer data were 0.45, 0.99, and 1.57, respectively.

Model	Model	RSE	t_{10}/τ	t_{50}/τ	t_{90}/τ	# Par	Parameters	Estimate	P-Value
B	2 TIS in Parallel	0.0080	0.48	1.00	1.54	5	VF_TIS1	0.024	0.000
							VF_TIS2	0.993	-
							VF_dead	-0.017	0.000
							Q1	0.079	0.000
							Q2	0.921	-
							n1	32.288	0.025
							n2	8.784	0.000
C	3 TIS in Parallel	0.0040	0.44	0.99	1.57	8	VF_TIS1	0.781	0.000
							VF_TIS2	0.036	0.000
							VF_TIS3	0.198	-
							VF_dead	-0.016	0.000
							Q1	0.773	0.000
							Q2	0.107	0.000
							Q3	0.120	-
							n1	13.551	0.000
							n2	18.175	0.000
							n3	53.210	0.000
F	PFR & TIS in Series, TIS in Parallel	0.0081	0.48	1.00	1.54	6	VF_PFR1	0.010	0.744
							VF_TIS2	0.015	0.620
							VF_TIS3	0.992	-
							VF_dead	-0.017	0.000
							Q1	0.079	0.000
							Q2	0.921	-
							n2	11.579	0.818
							n3	8.786	0.000

G	CSTR and 2 TIS in Parallel	0.0081	0.48	1.00	1.54	7	VF_CSTR1	0.018	0.370
							VF_TIS2	0.025	0.000
							VF_TIS3	0.980	-
							VF_dead	-0.023	0.156
							Q1	0.010	0.700
							Q2	0.079	0.000
							Q3	0.911	-
							n2	32.928	0.075
							n3	8.992	0.000
I	PFR & TIS in Series, Repeated in Parallel	0.0063	0.44	0.99	1.55	7	VF_PFR1	0.384	0.000
							VF_TIS2	0.591	0.000
							VF_PFR3	0.016	0.548
							VF_TIS4	0.030	-
							VF_dead	-0.020	0.000
							Q1	0.875	0.000
							Q2	0.125	-
							n2	3.616	0.000
							n4	5.770	0.619

Parameter estimates and p-values were used to eliminate Models F, G, and I. Multiple fitting parameters in each of these models had p-values > 0.35, far greater than commonly-used benchmarks of 0.05 or 0.10 for determining if a fitting parameter adds value. Volume fractions for one PFR or CSTR in each of these models were also near 0.01 (i.e., the lower bound allowed for fitting), which indicated that a better fit could possibly have been achieved in the absence of these fitting parameters. In fact, the two parallel PFR and TIS in series (Model I) becomes the PFR and TIS in series with TIS in parallel (Model F) when one of the PFR volumes approaches zero. Similarly, the PFR and TIS in series with TIS in parallel (Model F) becomes the 2 TIS in parallel (Model B) when the volume fraction of the only PFR approaches zero. This suggests that a multiple TIS in parallel construct is capable of explaining most of the variation in CW 1A.

Having eliminated Models F, G, and I in Table 2.5, the model options left were the 2 TIS in parallel (Model B, RSE = 0.0080, five fitting parameters) and 3 TIS in parallel (Model C, RSE = 0.004, eight fitting parameters). As indicated by their low and similar RSE values (0.0081 vs 0.0040), the two models fit the tracer data well, and achieved effectively the same goodness of fit. Also, the two models had similar t_{10}/τ, t_{50}/τ, and t_{90}/τ ratios (i.e., within 9.4%, 1.0%, and 1.9%, respectively). Parameter estimates were all greater than the lower bound of 0.01 and had p-values $\leq$ 0.025. It was determined that the incremental improvement in RSE of 3 TIS in parallel over 2 TIS in parallel did not justify increasing the number of fitting parameters from five to eight, and therefore the 2 TIS in parallel (Model B) was selected to represent CW 1A.

Dead space fitting parameters were statistically significant for all five models (p-value < 0.001) despite only representing an additional 1.6-2.3% of reactor volume. This supports the decision to use only models which contained dead space.

A Monte Carlo analysis was performed to determine confidence limits for overall fits, rather than for individual fitting parameters (data not shown). For CW 1A, which achieved low residual error from least squares regression fit (i.e., MSE < 10^{-3}), the 95% confidence limits were visually indistinguishable from the best fit line. The 95% confidence limits for CW 1B were also similar to the best fit line. This is because the large number of observations, 73 for CW 1A and 97 for CW 1B, resulted in allowable error that was less than 20% larger than the best fit error. These findings give greater confidence in the accuracy of the fits found by regression.

The model selection process was repeated for the remaining 12 reactors. Selected models for each reactor are shown in Table 2.6. The most common best fitting reactor model was the 2 TIS in parallel model (Model B), which was selected for 6 of the 14 reactors. Single or parallel sets of a PFR and CSTR in series (Models D or H, respectively) were each selected for 2 of the 14 reactors. The remaining four reactors were best fit with Models A (TIS), C (3 parallel TIS), G (CSTR and 2 TIS in parallel), and E (PFR and TIS in series, CSTR in parallel). These represent 7 of the 9 shortlisted models. Models F (PFR and TIS in series with TIS in parallel) and I (PFR and TIS repeated in parallel) were not selected as the best fit for any of the 14 reactors.

Table 2.6. Selected hydraulic model and normalized reactor volume, V_{norm}, for all data sets.

Reactor ID	t_{10}/τ	Selected Hydraulic Model	Model	Normalized Volume, V_{norm}
1A	0.45	2 TIS in Parallel	B	1.02
1B	0.45	PFR and CSTR in Series	D	0.81
2A	0.39 *	TIS	A	1.00
3A	0.50 *,a	3 TIS in Parallel	C	1.12
3B	0.72-0.80	PFR and CSTR in Series, Repeated in Parallel	H	1.22
3C	0.67	2 TIS in Parallel	B	1.25
3D	0.61	PFR and CSTR in Series, Repeated in Parallel	H	1.24
3E	0.19	CSTR and 2 TIS in Parallel	G	0.84
3F	0.43	PFR and TIS in Series, CSTR in Parallel	E	1.19
3G	0.67	2 TIS in Parallel	B	1.27
3H	0.57	2 TIS in Parallel	B	1.12
4A	0.31 *	PFR and CSTR in Series	D	1.12
5A	0.69 *	2 TIS in Parallel	B	1.26
5B	0.70 *	2 TIS in Parallel	B	1.23

* Not reported, but calculated via linear interpolation from reported data

a Truncated at C/C0 = 0.80, recovery < 0.95 at $\theta > 4$ requires $V_{norm} \sim 3.0$

2.3.3 Normalized Reactor Volume

A simple and prudent check on the feasibility of a reactor model, and validity of the tracer study, is to look at the normalized reactor volume, V_{norm}. V_{norm} is the area to the left of the tracer output curve in Figure 2.1, which can be conceptualized as the volume needed to fit a model to tracer data divided by the available volume of the reactor.

Table 2.6 shows the V_{norm} values produced by best fit models for all 14 reactors. Two reactors had V_{norm} within 2% of unity (1A and 2A) and two reactors had V_{norm} 16 to 19% lower than unity (1B and 3E). The fitting process assumes that $V_{norm} < 1$ is due to the presence of dead volume in the reactor, but the difference could also be due to a reactor volume smaller, or a flow rate larger, than estimated during the tracer test. Steps should be taken to identify the underlying

causes when V_{norm} is significantly less than unity because short-circuiting may not be the only cause. There may have been issues with metering volume or flow (i.e., tracer study validity) as well.

Ten reactors produced $V_{norm} > 1.1$, six of which exceeded 1.2. $V_{norm} > 1$ is impossible in a reactor with steady flow, steady volume, and a conservative tracer that neither reacts nor adheres to reactor surfaces. $V_{norm} > 1$ could be caused by either a flow rate smaller than originally estimated and/or a reactor volume greater than originally estimated. A result of $V_{norm} > 1$ should prompt further investigation of volume and flow estimates, because one or both were determined erroneously.

Reactor flow metering at many plants may be imprecise or inaccurate. Typical drivers for accurate metering, including accounting (e.g., billing) or critical chemical pacing (e.g., ammonia for chloramination), may not apply to many reactors. A recent study of 33 systems in the state of Washington found that 58% did not directly measure flows for disinfection calculations (Deem and Feagin 2016); 85% of systems also did not calibrate or verify the peak hourly flow or the plant effluent flow meter. A reactor where influent flow exceeds effluent flow (i.e., volume accumulation in a reactor used for both storage and disinfection) could also produce $V_{norm} > 1$.

Reactor volume estimates may have accuracy limitations as well. These limitations may stem from incorrectly estimating reactor geometry (i.e., water level versus volume) or incorrectly estimating how water level changes over time. Deem and Feagin (2016) found that 55% of systems did not verify contact chamber volume and that dimensions of contact chambers in five of 11 systems measured did not match the dimensions used for contact volumes. They also observed that half of systems using tanks or clearwells for disinfection contact did not record

tank levels. Their findings suggest widespread issues with clearwell volume estimates, which could in part explain the observed deviation of V_{norm} from unity in tracer data from literature. Non-negligible residence time may also be introduced by reactor influent channels, effluent channels, and sample lines, leading to an underestimation of volume.

Systems are likely to overestimate disinfection or other reactor performance metrics if $V_{norm} > 1$. For example, one case study of a chlorine contact basin (reactor 3B in Table 2.1 and Table 2.6) produced $t_{10}/\tau = 0.72$ and 0.80 (Teefy 1996). The author commented that they were surprised at the high t_{10}/τ given contact basin geometry. Fitting Model H to these two data sets produced $V_{norm} = 1.16$ and 1.32, respectively, or 1.22 when fit to both data sets simultaneously. Dividing t_{10}/τ by V_{norm} would produce $t_{10}/\tau = 0.62$ and 0.60, respectively, for the two tracer tests. Thus, t_{10}/τ may be overestimated when $V_{norm} > 1$.

These results should not be misinterpreted as questioning the utility of previous tracer tests in protecting public health through assurance of adequate disinfection. There are numerous conservative factors in the SWTR that protect public health, such as basing 3-log *Giardia* credit on the 99% upper confidence limit for 4-log observed inactivation (SWTR 1991). Also, the value of t_{10} would not be affected by $V_{norm} > 1$, except due to residence time in a sample line. If tracers were conducted under conditions representative of routine operation, then CT achieved (i.e., C^*t_{10}) should be representative as well. Problems with metering flow and assessing volume would instead manifest in potentially inaccurate determinations of τ, and subsequently the t_{10}/τ baffle factor. Water systems should consider the importance of flow metering and reactor volume determination when conducting future tracer tests on new or modified reactors.

One benefit of the reactor network models over the t_{10}/τ baffle factor calculation and

segregated flow (SF) models is that reactor networks yield V_{norm}. The t_{10}/τ baffle factor and SF methods can be completed without any check on the validity of the tracer study and, hence, the reactor volume or flow, thereby potentially allowing overestimation of reactor residence time. Regardless of the method used to interpret tracer study results, practitioners should verify that $V_{norm} \leq 1$. This is equivalent to verifying that the calculated average residence time is less than or equal to τ.

2.3.4 Log Reduction Calculations by Reactor Networks, SF, and SWTR

Results presented prior to this section have focused on how different hydraulic models represent reactor residence time distributions as determined by tracer studies. This section discusses how hydraulic model selection impacts predicted reactor performance (e.g., contaminant removal). Specific topics include the value of hydraulic models that accurately represent tracer data, an illustration that t_{10}/τ baffle factors are not universally conservative, and a comparison of reactor networks with SF, which accurately predicted disinfection in an ozone contactor (Najm et al. 2009).

An important application of hydraulic models is the assessment of disinfection adequacy. Lawler and Singer (1993) demonstrated that the SWTR's t_{10}/τ approach would overestimate the necessary CT for low log inactivations and underestimate the necessary CT for high log inactivations in a CSTR, an ideal reactor with infinite dispersion. Their analysis was expanded from an ideal CSTR to a real-world clearwell, and added SF and reactor network models.

Predicted contaminant reduction in CW 1A, a real-world clearwell used for primary disinfection, is shown in Figure 2.6A. Modeled log reduction vs. *Da* is reported for ideal PFRs and CSTRs, along with SF, the 2 TIS reactor network selected for CW 1A, and the credit

provided by the SWTR (PFR t_{10}, where $t_{10}/\tau = 0.45$). For PFR t_{10}, residence time is equal to 0.45τ, whereas for all other models residence time is equal to τ. The blue and gray lines show predicted log reduction versus *Da* in plug flow and perfectly mixed flow, respectively. Real-world reactors behave between these two extremes, which the SWTR accounts for by crediting t_{10} (green line). However, none of these three models accurately represents residence time distribution.

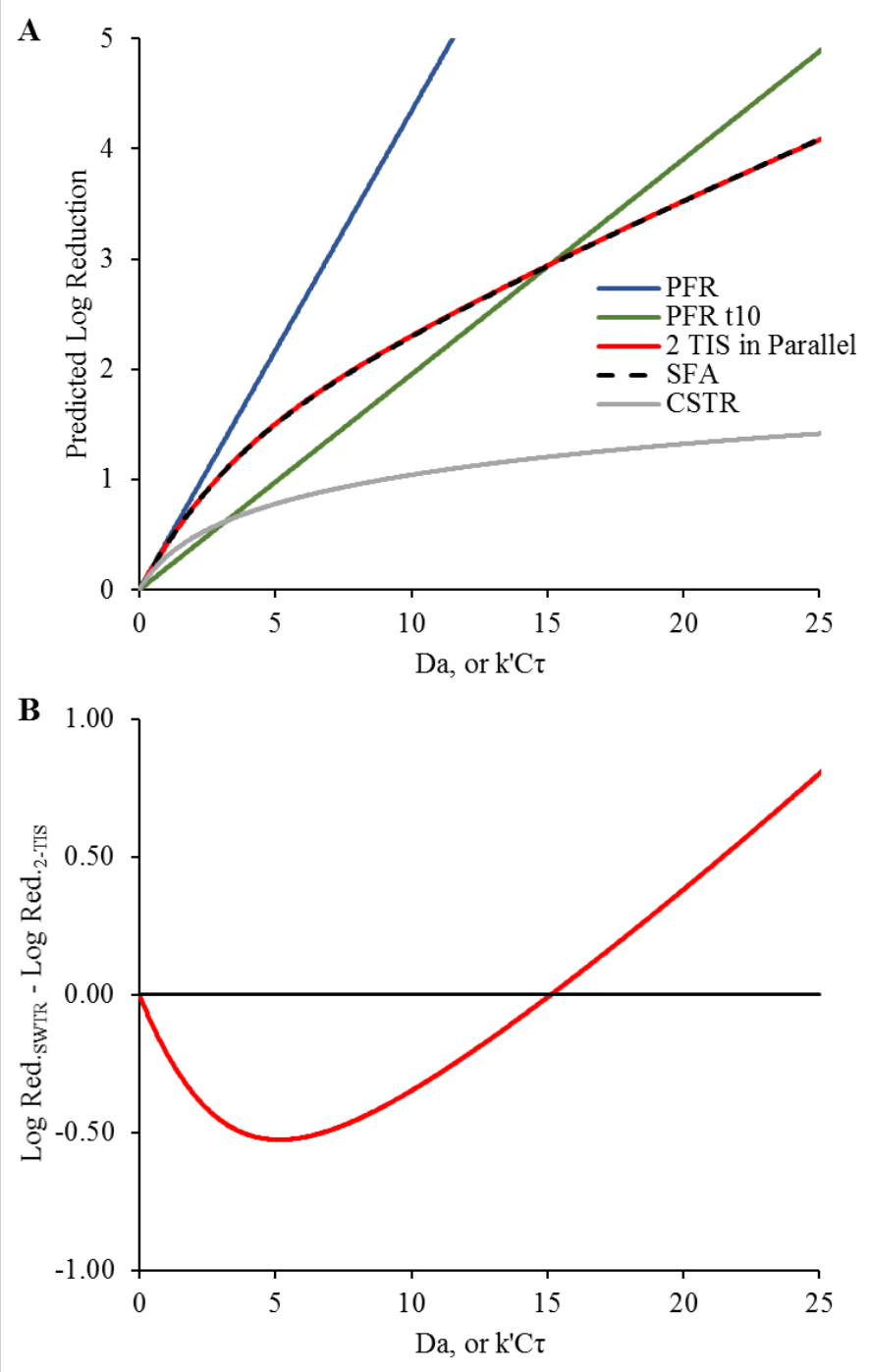

Figure 2.6. Effect of reactor model selection on predicted log reduction for CW 1A. (A) Comparison of predicted log reduction versus *Da* for CW 1A using different models: PFR, PFR t_{10}, 2 TIS in parallel, SF, and CSTR. (B) Difference in predicted log reduction between SWTR procedures and the selected reactor network model for CW 1A (2 TIS in parallel).Results shown are for reactions that are second order overall, first-order with respect to the contaminant and oxidant (see Equation 2.4).

Reactor network and SF models both represent residence time distribution more accurately than the models used to show compliance with the SWTR. These are shown by the red and black dashed lines, respectively. Figure 2.6A shows that the SWTR calculation method (PFR t_{10}) overestimates the necessary *Da* (e.g., CT) for CW 1A at reductions less than 2.95-log, and underestimates necessary *Da* at higher log reductions. The difference in log reduction between the SWTR calculation method and the 2-TIS reactor network model (found to be the optimum model for CW 1A in the sections above) is shown in Figure 2.6B.

The SWTR requires 3.0-log reduction of *Giardia,* with conventional treatment and direct filtration receiving 2.5 and 2.0-log credit, respectively, and the remaining 0.5 or 1.0-log credit required through disinfection. Under the reaction conditions (i.e., *Da*) that would achieve 0.5 and 1.0-log disinfection credit in CW 1A by either the reactor network or SF model, SWTR would credit only 0.25 and 0.56-log, respectively, as shown in Figure 2.6A. At SWTR credit of 0.5 and 1.0-log, the reactor network and SF models predict 0.92 and 1.52-log, respectively. This indicates that at relatively low log reduction credits, the SWTR overestimates CT necessary for *Giardia* disinfection in CW 1A. This overestimation has implications for simultaneous compliance with both disinfection and disinfection by-product requirements. The SWTR approach may result in feeding twice as much chlorine or having contact times twice as long as necessary, consuming more chlorine and producing higher concentrations of disinfection by-products.

Conversely, the t_{10}/τ baffle factor approach in the SWTR underestimates the necessary CT at > 2.95-log reduction in CW 1A. Current regulations do not require > 2.95-log reduction in CW 1A, but higher reductions are necessary for reactors in water reuse applications. California requires a 12-log virus, 10-log *Giardia*, and 10-log *Cryptosporidium* reduction for groundwater replenishment projects, with up to 6-log credit being issued for a single treatment process

(CDPH 2014). Texas requires a baseline removal of 8-log virus, 6-log *Giardia*, 5.5-log *Cryptosporidium*, which can be increased depending on wastewater effluent quality (TWDB 2015). Assuming PFR hydraulics with t_{10}/τ baffle factors may overestimate treatment efficacy at these higher log reductions. The design of ozone contactors for 6-log *Giardia* and virus reduction credit in potable reuse applications based on t_{10}/τ baffle factors (Calvet et al. 2017) raises questions about the expansion of SWTR disinfection modeling to reuse regulations. Modeling treatment efficacy for high log reductions could be improved by more accurate representations of residence time distribution, which can be provided by reactor network models or SF.

Reactor network models and SF were compared for their ability to model reactor performance. As shown in Figure 2.6A, both reactor networks and SF modeled log reduction versus reaction conditions (i.e., *Da*) similarly: within 0.14% up to 4-log reduction.

Results in this section demonstrate that the t_{10}/τ baffle factor may be conservative for the purpose it was originally implemented under the SWTR, i.e., calculating disinfection credit at low log reductions. However, the t_{10}/τ baffle factor may not be conservative for current and future needs in water treatment, including simultaneous compliance, water reuse, and removal of emerging contaminants. The t_{10}/τ baffle factor accurately represents reactor performance at a single, reactor-specific log reduction: 1.54-log in a CSTR (Lawler and Singer, 1993), 2.95-log in CW 1A. Reactor networks and SF more accurately represent reactor performance at a range of log reduction targets. Future regulatory revisions should consider SFA, beyond the discussion in the SWTR of its use for calculating ozone disinfection credit, and the reactor network approach to hydraulic modeling at the national level.

2.3.5 Reactor Network Modeling vs Segregated Flow

In the previous section, reactor networks and SF were shown to produce nearly equivalent predictions of contaminant removal. However, reactor networks having some advantages relative to SF, including concise equations, ability to fit multiple tracer data sets, and a built-in check on V_{norm}.

With regard to tracer data sources, two benefits of reactor networks over SF are that i) a single network can be fit to multiple tracer data sets and ii) fitting reactor networks yields V_{norm}. A single representative tracer data set needs to be selected to perform SF, while regression in reactor network fitting provides flexibility in the number of tracer data sets used. This allowed the reactor network model for CW 1B to use data from all four tracer data sets, while SF would require selecting a single representative tracer data set. Reactor networks, which yield V_{norm}, provide a check on tracer data that SF does not. Najm et al. (2009) used a pilot-scale ozone contactor to validate disinfection predicted by SF modeling; however, tracer data the authors provided for a full-scale contactor had $V_{norm} \geq 1$ (1.23-1.26, see Table 2.6 ID's 5A and 5B). Reactor networks highlight potential tracer data issues more clearly than SF.

Reactor networks and SF vary in the number of reactors used as well as reactor type. SF uses only PFRs, consistent with the SWTR t_{10}/τ approach. However, SF requires a large number of reactors, one less than the number of data points in a tracer test. For example, the SF equation for a reaction in CW 1A with 72 reactors is given by

$$\frac{N}{N_0} = \sum\left[\left(\frac{C}{C_0}\right)_2 - \left(\frac{C}{C_0}\right)_1\right] e^{-Da\frac{\theta_1+\theta_2}{2}} + \left[\left(\frac{C}{C_0}\right)_3 - \left(\frac{C}{C_0}\right)_2\right] e^{-Da\frac{\theta_2+\theta_3}{2}} + \cdots + \left[\left(\frac{C}{C_0}\right)_{73} - \left(\frac{C}{C_0}\right)_{72}\right] e^{-Da\frac{\theta_{72}+\theta_{73}}{2}}. \quad 2.5$$

While this works well in a spreadsheet, the written equation is cumbersome. Conversely, the reactor network models use far fewer reactors. The equation for the 2 TIS in parallel reactor (Model B) takes the form

$$\frac{N}{N_0} = = Q_1 \frac{1}{\left(1+\frac{DaV_{TIS,1}}{n_1 Q_1}\right)^{n_1}} + Q_2 \frac{1}{\left(1+\frac{DaV_{TIS,2}}{n_2 Q_2}\right)^{n_2}} = \frac{Q_1}{\left(1+\frac{DaV_{TIS,1}}{n_1 Q_1}\right)^{n_1}} + \frac{1-Q_1}{\left(1+\frac{Da(1-V_{TIS,1}-V_{dead})}{n_2(1-Q_1)}\right)^{n_2}} \quad 2.6$$

where $V_{TIS,1}$ and $V_{TIS,2}$ are the volume fractions ($0 \leq V \leq 1$) of the two reactors, n_1 and n_2 are the number of CSTRs in each TIS reactor, and Q_1 and Q_2 are the flow fractions ($0 \leq Q \leq 1$) for each of the two reactors (see Table 2.5 for volume and flow fraction examples). This example reactor network model uses 2 reactors and 5 fitting parameters for CW 1A, while SF used 72 reactors and 146 inputs for the same clearwell, demonstrating the advantage of the reactor network approach in terms of simplicity. Substituting parameter estimates from Table 2.5 into 2.6 yields Equation 2.7, which is simpler than the SF equation.

$$\frac{N}{N_0} = 0.079 \frac{1}{\left(1+\frac{0.024Da}{32.29*0.079}\right)^{32.29}} + 0.921 \frac{1}{\left(1+\frac{0.993Da}{8.78*0.921}\right)^{8.78}}. \quad 2.7$$

The equation for CW 1B can be described even more concisely as

$$\frac{N}{N_0} = \frac{e^{-DaV_{PFR,1}}}{1+DaV_{CSTR,2}} = \frac{e^{-DaV_{PFR,1}}}{1+Da(1-V_{PFR,1}-V_{dead})} = \frac{e^{-0.381Da}}{1+0.432Da}, \quad 2.8$$

where $V_{PFR,1}$ and $V_{CSTR,2}$ are the volume fractions of the PFR and CSTR, respectively. These equations are provided in Table 2.7, along with those for PFR, CSTR, and TIS (with *Vnorm* = 1,

which differs from Model A). This table also shows the equations for effluent tracer concentrations from step dose tracer studies.

Table 2.7. Equations for reactor effluent tracer concentration and remaining contaminant for different reactor types: PFR, CSTR, TIS, Model B, and Model D. It should be noted that in the TIS shown, V_{norm} is constrained to unity, unlike Model A.

Reactor	Reactor Effluent Tracer Concentration, C/C_0	Contaminant Remaining N/N_0
PFR	For $\theta < 1 \quad F(\theta) = 0$ For $\theta \geq 1 \quad F(\theta) = 1$	$\frac{N}{N_0} = \mathrm{e}^{-\mathrm{Da}}$
CSTR	$F(\theta) = 1 - \mathrm{e}^{-\theta}$	$\frac{N}{N_0} = \frac{1}{1+Da}$
TIS	$F(\theta) = \int_0^{\theta} \frac{n(n\theta)^{n-1}}{\Gamma(n)} \mathrm{e}^{-n\theta} \mathrm{d}\theta$ where $\Gamma(n) = \int_0^{\infty} \mathrm{e}^{-x} x^{n-1} \mathrm{d}x$	$\frac{N}{N_0} = \frac{1}{\left(1+\frac{Da}{\mathrm{n}}\right)^{\mathrm{n}}}$
Model B (CW 1A)	$F(\theta) = \mathrm{Q}_1 \left[\int_0^{\theta} \frac{n_1 \left(n_1 \frac{\theta Q_1}{V_{TIS,1}}\right)^{n_1-1}}{\Gamma(n_1)} \mathrm{e}^{-n_1 \frac{\theta Q_1}{V_{TIS,1}}} \mathrm{d}\theta \right] + \mathrm{Q}_2 \left[\int_0^{\theta} \frac{n_2 \left(n_2 \frac{\theta Q_2}{V_{TIS,2}}\right)^{n_2-1}}{\Gamma(n_2)} \mathrm{e}^{-n_2 \frac{\theta Q_2}{V_{TIS,2}}} \mathrm{d}\theta \right]$ where $\Gamma(n) = \int_0^{\infty} \mathrm{e}^{-x} x^{n-1} \mathrm{d}x$	$\frac{N}{N_0} = Q_1 \frac{1}{\left(1+\frac{DaV_{TIS,1}}{n_1 Q_1}\right)^{n_1}} + Q_2 \frac{1}{\left(1+\frac{DaV_{TIS,2}}{n_2 Q_2}\right)^{n_2}}$
Model D (CW1B)	For $\theta < V_{PFR,1}, \; F(\theta) = 0$ For $\theta \geq V_{PFR,1}, F(\theta) = 1 - \mathrm{e}^{-\frac{\theta - V_{PFR,1}}{V_{CSTR,2}}}$	$\frac{N}{N_0} = \frac{\mathrm{e}^{-DaV_{PFR,1}}}{1+DaV_{CSTR,2}}$

Note: Contaminant remaining equations are for reactions that are second order overall, first-order with respect to the contaminant and oxidant (see Equation 2.4).

2.3.6 Benefits and Drawbacks of Modeling Approaches

Although the t_{10}/τ baffle factor approach used in the SWTR overestimates necessary CT for low log reductions and underestimates the CT necessary for higher log reductions, it still presents numerous benefits. The SWTR approach is understood by regulators and water systems alike, and enables operators to quickly calculate disinfection credit by hand. It also uses the simplest hydraulics: those of a PFR. Further, t_{10}/τ can be estimated in the absence of tracer data using knowledge about reactor geometry (e.g., length:width ratio, Crozes et al. 1999).

Similarly, the number of tanks in a single TIS reactor can be estimated from a reactor's

length:width ratio inclusive of baffling (Crozes et al. 1999). The TIS reactor provides significant accuracy improvement over the t_{10}/τ baffle factor (see Figure 2.4A and Figure 2.5A); however, it should still be fit to tracer data, preferably using a least-squares regression. The TIS reaction equation is also more complicated than those of a PFR or CSTR. Although it was beyond the purpose of this study, accounting for a decaying oxidant in a TIS introduces further complexity.

SF can accurately predict disinfection efficacy as demonstrated by Najm et al. (2009) at pilot scale and also uses simple PFR hydraulics. However, SF requires a large number of reactors to fit tracer data, which makes the reaction equations cumbersome. It also cannot account for multiple tracer data sets without creating multiple models.

Reactor networks are able to account for multiple tracer data sets and can approximate residence time with a much smaller number of reactors than SF. However, they require non-linear least squares regression to fit the models to data sets; although this process is described in detail in this work and can be automated using open source software, this process is nontrivial. Users also need to select from a set of broadly applicable models, which requires the application of engineering judgment.

With these factors in mind, it appears that there is no single “best” modeling approach, and that users should choose which model to use based on the resources at their disposal and the end goal of the modeling effort. PFRs with t_{10}/τ baffle factors are best suited to situations where low log reductions are necessary and overdesign does not have adverse consequences. SF and reactor networks should be used for modeling higher log reductions or where reactor overdesign is undesirable. SF is appropriate for spreadsheet-based analyses, and reactor networks are better suited to situations where a compact equation or dynamic (i.e., real-time) calculation is needed.

Finally, the TIS (or axial dispersion) model is appropriate for moderate log reductions.

2.3.7 Implications and Future Work

Water treatment plants are preparing to address currently unregulated contaminants which can be treated by oxidation processes, including NDMA precursors and algal toxins. Quantifying treatment for these contaminants will likely require a more advanced understanding of reactor hydraulics than t_{10}/τ baffle factors. Reactor networks can provide that advanced understanding. Moving forward, reactor networks could be used in predicting treatment efficacy for unregulated contaminants.

The important subject of reactor mixing was beyond the scope of this study. According to Levenspiel (1999), there are two overlapping aspects to mixing: degree of segregation and earliness of mixing. Segregation describes whether a fluid is mixed at the microscopic or macroscopic level, and earliness of mixing describes whether the mixing of fluids occurs early or late within a reactor. SF and reactor network models make very different assumptions about mixing. The following chapter will test how multiple reactor models perform in explaining water quality changes where mixing is important, using seasonal conversion from chloramines to free chlorine as a reactive tracer.

2.4 Conclusions and Recommendations

Based on the results and discussion presented in this work, the following conclusions were reached:

1. Some systems may overestimate reactor performance based on volume and flow metering inaccuracies. Regardless of what reactor modeling method is used, it is advised that V_{norm} be calculated as a verification of tracer data quality.

2. Nine reactor network models with broad applicability to water treatment reactors were identified. The best fitting models most often had two parallel TIS reactors.
3. Reactor networks and SF both approximate reactor hydraulics well, while reactor networks use far fewer reactors and can accommodate replicate tracer tests conducted at different flow rates.
4. The SWTR t_{10}/τ approach underestimates treatment efficacy at low log reductions, and overestimates treatment efficacy at higher log reductions. For one of the clearwells studied (CW 1A), the SWTR would credit only 0.25-log reduction for disinfection but both reactor network and SF models would credit 0.5-log reduction.
5. Different hydraulic modeling approaches each have their respective benefits and drawbacks. Reactor networks and SF are more complicated than the SWTR approach for *Giardia* disinfection. However, potential revisions to disinfection treatment techniques should consider adding more accurate modeling methods (e.g., reactor networks and SF) as options for compliance calculations. Doing so would assist the balancing of disinfection with disinfection by-product formation, as well as other simultaneous compliance considerations.

ACKNOWLEDGMENTS

The authors appreciate generous support from the Richard Hazen Fellowship, Herman G. Baity Bicentennial Fellowship, and National Defense Science and Engineering Graduate Fellowship in supporting Alexander Gorzalski's tuition.

REFERENCES

Bellamy, W.D.; Haas, C.; Finch, G. 1998. Integrated Disinfection Design Framework. AWWA Research Foundation. Denver, CO.

California Department of Public Health (CDPH). 2014. Regulations Related to Recycled Water. California Code of Regulations Titles 22 and 17.

Carlson, K.; Pier, D.; Bellamy, W.; Carlson, M.; Ducoste, J.; Amy, G.; Rakness, K. 2001. Implementation of the Integrated Disinfection Design Framework. AWWA Research Foundation. Denver, CO.

Calvet, S.; Hadaceck, T.; Bartels, J.; Priest, M.; Borchardt, J.; Gerringer, F.; Trussell, R. 2017. Limited Footpring and CFD-Based Design of High Ozone Dose Contactor for Potable Resuse. 2017 IOA World Congress, Washington, DC.

Crozes, G.F.; Hagstrom, J.P.; Clark, M.M.; Ducoste, J.; Burns, C. 1999. Improving Clearwell Design for CT Compliance. AWWA Research Foundation. Denver, CO.

Deem, S.; Feagin, N. 2016. Disinfection Data Integrity in Washington State. *Journal AWWA*, 108 (10): 24-30.

Ducoste, J.; Carlson, K.; Bellamy, W. 2001. The integrated disinfection design framework approach to reactor hydraulics characterization. *Journal of Water Supply: Research and Technology – AQUA*, 50 (4): 245-261.

Lawler, D.F.; Singer, P.C. 1993. Analyzing Disinfection Kinetics and Reactor Design: A Conceptual Approach Versus the SWTR. *Journal AWWA*, 85 (11): 67-76.

Fogler, H.S. 2005. *Elements of Chemical Reaction Engineering*. 4th ed. Boston, MA: Pearson Education.

Harrington, G.W.; Chowdhury, Z.K.; Owen, D.M. 1992. Developing a Computer Model to Simulate DBP Formation During Water Treatment. *Journal AWWA*, 84 (11): 78-87.

Howe, K. J.; Crittenden, J. C.; Hand, D. W.; Trussell, R. R.; Tchobanoglous, G. 2012. *Principles of water treatment*. John Wiley & Sons, Hoboken, NJ.

Krasner, S. W.; Mitch, W. A.; McCurry, D. L.; Hanigan, D.; Westerhoff, P. 2013. Formation, precursors, control, and occurrence of nitrosamines in drinking water: a review. *Water Research*, 47 (13), 4433-4450.

Levenspiel, O. 1999. *Chemical Reaction Engineering*. 3rd ed. New York: Wiley and Sons.

Martin, A.D. 2000. Interpretation of residence time distribution data. *Chemical Engineering Science*, 55 (23): 5907-5917.

Najm, I.; Brown, N.P.; Gramith, K.; Hargy, T. Validating Disinfection in Ozone Contactors. Water Research Foundation. Denver, CO.

Nauman, B.E. 2008. Residence Time Theory. *Ind. Eng. Chem. Res.,* 47 (10): 4752-3766.

R Core Team. 2016. R: A language and environment for statistical computing. R Foundation for Statistical Computing, Vienna, Austria. URL https://www.R-project.org/.

Rodríguez, E; Onstad, G.D.; Kull, T.P.; Metcalf, J.S.; Acero, J.L.; von Gunten, U. 2007. Oxidative elimination of cyanotoxins: Comparison of ozone, chlorine, chlorine dioxide and permanganate. *Water Research*, (41) 15: 3381-3393.

Teefy, S.M.; Singer, P.C. 1990. Performance and Analysis of Tracer Tests to Determine Compliance of a Disinfection Scheme with the SWTR. *Journal AWWA*, 82 (12): 88-98.

Teefy, S. 1996. Tracer Studies in Water Treatment Facilities: A Protocol and Case Studies. AWWA Research Foundation. Denver, CO.

Templeton, M.R.; Hofmann, R.; Andrews, R.C. 2006. Case Study Comparisons of Computational Fluid Dynamics (CFD) Modeling Versus Tracer Testing for Determining Clearwell Residence Times in Drinking Water Treatment. *Journal of Environmental Engineering and Science*, 5(6): 529-536.

Texas Water Development Board (TWDB). 2015. Direct Potable Reuse Resource Document: Final Report.

Trussell, R.R. and Chao, J-L. 1977. Rational design of chlorine contact facilities. *Journal WPCF*, 49 (4): 659-667.

United States Environmental Protection Agency (USEPA). 1991. Guidance manual for compliance with the filtration and disinfection requirements for public water systems using surface water sources. Washington, DC.

Weber, W.J. 1972. Physicochemical Processes for Water Quality Control. Wiley & Sons. New York, NY.

Westerhoff, P.; Yoon, Y.; Snyder, S.; Wert, E. 2005. Fate of endocrine-disruptor, pharmaceutical, and personal care product chemicals during simulated drinking water treatment processes. *Envir. Sci. & Tech.,* 39 (17), 6649-6663.

Zhang, J.; Tejada- Martinez, A.E.; Zhang, Q. 2016. Rapid Analysis of Disinfection

Efficiency Through Computational Fluid Dynamics. *Journal AWWA*, 108 (1): E50-59.

CHAPTER 3 - ASSESSING FLOW SEGREGATION AND MIXING BY MODELING RESIDUAL DISINFECTANT CONVERSION

3.1 Introduction

Diverse applications of reactors in environmental engineering include catalytic converters in automobiles (Oh and Cavendish 1985), production and transport of gas and heat in landfills (El-Fadel et al. 1996), scrubbers in power plants (Kiil et al. 1998), activated sludge tanks in wastewater treatment (Henze et al. 2000), and chlorinated clearwells in water treatment (Clark 1998). This work focuses on water treatment reactors, which may include ozone contactors, clearwells, filters, or raw water pipelines. Regardless of the reactor, performance is a function of the same four factors: reaction kinetics, residence time distribution (RTD), degree of segregation, and earliness of mixing (Levenspiel 1999). Modeling reactor performance requires either experimentally determining or assuming these four factors.

Reaction kinetics can be determined by experimentation in controlled laboratory environments. RTDs are known for ideal reactors, such as the plug-flow reactor (PFR) and continuous flow stirred-tank reactor (CSTR), and can be determined for real-world reactors via tracer studies (Teefy 1996, Crittenden et al. 2005). RTD describes the macromixing of a reactor, capturing conditions such as short-circuiting and stagnation zones (Fogler 2006, Pfeiffer and Barbeau 2014). Modeling a single first-order or pseudo first order reaction in a reactor requires knowing only the reaction kinetics and macromixing (i.e., RTD) (Fogler 2006). Such reactions are common in disinfection regulation, including prediction of pathogen inactivation using

Chick-Watson kinetics and residual oxidant concentration (Crittenden et al. 2005).

Modeling reactions that are not first order overall requires understanding micromixing within the reactor (Levenspiel 1999, Fogler 2006). Micromixing encompasses both degree of segregation and earliness of mixing. Micromixing describes how flow entering the reactor encounters water that is already in the reactor (Fogler 2006). If flow elements of differing ages do not mix at all, then flow is considered to be perfectly segregated and can be represented by the segregated flow (SF) model (Fogler 2006) (see Key Concepts below and APPENDIX B for additional explanation). If flow entering a reactor is assumed to be immediately mixed with all of the reactor contents, it is represented by the maximum mixedness (MM) model (Fogler 2006). Reactions that require understanding micromixing conditions include pathogen inactivation according to Chick-Watson kinetics in the presence of a decaying oxidant (Pfeiffer and Barbeau 2014, Craik 2005).

Micromixing is also important for other reactions that are not first order or pseudo-first order and for multiple reactions that occur simultaneously (Levenspiel 1999). Many microorganisms do not follow first-order Chick-Watson kinetics (Crittenden et al. 2005), and oxidation reactions for cyanotoxins such as microcystin follow second-order kinetics, only becoming pseudo-first order when the oxidant concentration is assumed to be constant (Acero et al. 2005). Multiple, simultaneous, and non-first-order reactions occur in water treatment reactors for processes such as the formation of bromate (von Gunten 2003), ammonia breakpoint and chloramination (Jafvert and Valentine 1992), and the formation of chlorinated disinfection byproducts (DBPs) (Deborde and von Gunten 2008). Thus, there are many situations where micromixing (i.e., segregation and earliness of mixing) affects reactions of interest in water treatment.

However, most water treatment reactor models, including those used in regulation, do not account for micromixing. The CT method, which is based on the product of disinfectant residual and time for the first 10% of flow to leave the reactor (t_{10}), accounts only for reaction kinetics and macromixing (USEPA 1991, USEPA 2010). The extended t_{10} and extended CSTR methods for ozone contactors credit greater CT by incorporating oxidant decay (USEPA 2010), but do not account for micromixing. Alternative reactor models more accurately represent macromixing, including the axial dispersion, tanks-in-series (TIS), segregated flow (SF), and reactor network (RN) models (Teefy and Singer 1990, Ducoste et al. 2001, Najm et al. 2009, Crittenden et al. 2005, Chapter 2). The TIS, SF, and RN models, which are described in detail in APPENDIX B, vary significantly in their assumptions about micromixing (see Table 3.1). It would be valuable to assess which models accurately represent micromixing in water treatment reactors.

Table 3.1. Assumptions about degree of segregation and earliness of mixing for five different reactor models. Mixing in TIS reactors occurs in stages, where mixing is immediate in the first CSTR, and then occurs in successive stages in subsequent CSTRs. Degree of segregation and earliness of mixing in RN models varies depending on the type, number, and arrangement of simplified reactor types.

Model Type	Degree of Segregation	Earliness of Mixing
Plug flow reactor (PFR)	None	None
Continuous flow stirred-tank reactor (CSTR)	None	Immediate
Tanks-in-series (TIS)	None	Staged
Segregated flow (SF)	Perfect	Latest possible
Maximum mixedness (MM)	None	Immediate
Reactor network (RN)	Varies	Varies

Previous work has studied the effect of micromixing assumptions on predictions of contaminant decay in water treatment reactors. Computer simulations by Craik (2005) in the presence of a decaying oxidant predicted degree of inactivation as follows: PFR > SF > TIS > MM. The SF, TIS, and MM models produced similar predictions when disinfectant decay was negligible. Craik (2005) studied a range of micromixing (i.e., PFR, SF, TIS, MM) and

macromixing (i.e., TIS with 2-100 CSTRs) conditions, but did not compare predictions to experimental data. Pfeiffer and Barbeau (2014) compared predictions from SF, TIS, MM, and regulatory models with observed *E. coli* inactivation in a pilot-scale chlorine contactor. They found that the CT, extended t_{10}, and SF models overestimated inactivation, and recommended the TIS model for its relative accuracy and simplicity. MM was not recommended because it was the most complicated to be implemented at a water utility.

As noted by Pfeiffer and Barbeau (2014), validation of disinfection reactor models has rarely been achieved. Efforts have been made to explore micromixing through computational fluid dynamics (CFD), scale modeling, and the use of reactive tracers. Specifically, CFD models have been used to provide spatially-resolved predictions of pathogen inactivation, disinfectant residual, and disinfection by-product formation (Greene et al. 2004, Greene et al. 2006, Angeloudis et al. 2014); 3D laser-induced fluorescence was used to directly observe mixing in bench-scale ozone contactors (Kim et al. 2010a, Kim et al. 2010b) and UV reactors (Gandhi et al. 2011, Gandhi et al. 2012); and a reactive tracer (i.e., ammonia) was used to observe mixing in a wastewater nitrification reactor equipped with axial mixers (Gresch et al. 2011). However, CFD modeling remains too computationally intensive for every day reactor design and operation (Laurent et al. 2014), particularly for unsteady flows (Wicklein et al. 2015); 3D laser-induced fluorescence is not applicable to full-scale reactors (Kim et al. 2010a); and most drinking water treatment reactors (e.g., ozone contactors, clearwells) are unlike the nitrification reactor studied in some important ways (e.g., reactors are often baffled to encourage plug flow rather than actively mixed, and target contaminants do not lend themselves to real-time measurement).

However, a reactive tracer could provide a mechanism to study micromixing in drinking water treatment reactors if it were detectable using common online monitoring equipment and

safe to apply at detectable concentrations. Such a reactive tracer experiment occurs in systems that periodically convert between free chlorine and monochloramine as a residual disinfectant. This conversion is known as temporal disinfectant switching, and may be performed to meet state requirements or control nitrification (Vikesland et al. 2006), as well as facilitate distribution system flushing or maintenance activities. Temporal disinfectant switching has been used to estimate residence time in distribution storage tanks (Vikesland et al. 2006) and validate water age models (Deason et al. 2017). However, to the authors' knowledge, temporal disinfectant switching has not been used to assess the degree of micromixing in water treatment reactors.

The primary objective of this study was to investigate the nature of micromixing in full-scale water treatment reactors. Different reactor models (i.e., SF, TIS, RN, and MM), with differing implicit assumptions about degree of segregation and earliness of mixing (see Table 3.1), were tested for their accuracy in predicting observed free and combined chlorine species during temporal disinfectant switching. The effect of model assumptions regarding micromixing on predictions of microbial inactivation are discussed as well.

A secondary objective of this work was to assess whether accepted chloramine reaction kinetics (i.e., Jafvert and Valentine 1992, Vikesland et al. 2001) could be coupled with an appropriate reactor model to predict breakpoint in full-scale flow-through reactors. The 2017 AWWA disinfection survey found that 9% of respondents blended chlorinated and chloraminated water in their distribution systems, and that 44% of respondents using chloramines as a residual disinfectant periodically converted to free chlorine (AWWA 2018). Both practices would result in breakpoint reactions in the distribution system, yielding time periods with little to no disinfectant residual. Breakpoint reactions have long been of interest, and have been investigated at bench (Barrett et al. 1985) and pilot scale (Saunier and Selleck 1985). To the authors' knowledge, there

has been no demonstration coupling accepted reaction kinetics with an appropriate reactor model to predict breakpoint at full scale. This work provides such a demonstration, which is expected to benefit the field by informing operations of distribution systems where chlorinated and chloraminated waters are blended and for systems that conduct temporal disinfectant switching.

3.2 Modeling Methods

3.2.1 Description of Reactor Systems

Two full-scale clearwells were studied at water treatment plants with production capacities of 225 and 120 million gallons per day (MGD). For the time periods used in this study, both plants had two clearwells operated in series. A free chlorine residual was maintained through the first clearwell for primary disinfection, with ammonia added prior the second clearwell to form chloramines. Ammonia was added in the form of liquid ammonium hydroxide (19% as ammonia), injected at full strength without the use of upstream carry water or dilution water at the point of injection. There was no mechanical mixing at the point of injection; however, flow conditions were turbulent at the point of injection and downstream as detailed in APPENDIX B, indicating that ammonia was likely well mixed with the bulk flow. The clearwells containing chloramine are referred to as A and B and had volumes of 32.4 and 20.3 million gallons, respectively. Plan views of Clearwells A and B are shown in Figure B.1 and Figure B.2 of APPENDIX B. Figure B.3 in APPENDIX B shows a detail of a submerged overflow structure in Clearwell A near the end of the clearwell where intermittent chlorine and ammonia feeds are located. These feed locations can be used if the primary disinfection clearwell is out of service. Photographs from each clearwell are shown in Figure B.4 and Figure B.5 of APPENDIX B.

3.2.2 Observation of Reactor Effluent

Concentrations of reactive tracers were measured using online process monitoring equipment. Total and free chlorine were measured using CL17 chlorine analyzers (Hach Company, Loveland, CO). CL17 analyzers use N,N-diethyl-p-phenylenediamine (DPD) for colorimetric analysis of chlorine concentrations and provide readings every 2.5 minutes. Online chlorine readings were checked hourly using amperometric titrations according to Standard Method 4500-Cl Part D (APHA 1992). Total ammonia and monochloramine were measured using a ChemScan UV-2150/S (ASA Analytics, Waukesha, WI) with readings taken every 10 minutes.

3.2.3 Modeling of Reactor Effluent

Modeling concentrations of reactive tracer species in Clearwells A and B required a chemical reaction model, different hydraulic models, operations data for model inputs, and a method for calculating concentrations of reactive species.

The chemical reaction model is summarized in Table 3.2 and is based on an accepted chloramine model developed by others (i.e., Jafvert and Valentine 1992, Vikesland et al. 2001). This model assumes the absence of other chloramine-consuming reactions with clearwell surfaces and substances such as natural organic matter and reduced iron. Reactions involving bromide were neglected because annual maximum source water bromide concentrations were < 0.1 milligrams per liter (mg/L) (Luh and Mariñas 2014, Vikesland et al. 2001). Both reactors had upstream free chlorine contact of > 700 mg-min/L, and reductions in total chlorine residual across Clearwells A and B were less than 0.1 mg/L during normal operation. Therefore, free chlorine demand and decay were neglected during modeling.

Table 3.2. Model predicting the reaction of chloramine species with free chlorine. Adapted from monochloramine decay models developed by Jafvert and Valentine (1992) and Vikesland et al. 2001.

Reaction Stoichiometry		Rate Expression	Rate Constant
(1)	$HOCl + NH_3 \rightarrow NH_2Cl + H_2O$	$k_1[HOCl][NH_3]$	$k_1 = 2.37 \times 10^{12} e^{-1510/T}$ L/mol-h
(2)	$NH_2Cl + H_2O \rightarrow HOCl + NH_3$	$k_2[NH_2Cl]$	$k_2 = 6.7 \times 10^{11} e^{-8800/T}$ 1/ h
(3)	$HOCl + NH_2Cl \rightarrow NHCl_2 + H_2O$	$k_3[HOCl][NH_2Cl]$	$k_3 = 1.08 \times 10^{9} e^{-2010/T}$ L/mol-h
(4)	$NHCl_2 + H_2O \rightarrow HOCl + NH_2Cl$	$k_4[NHCl_2]$	$k_4 = 2.3 \times 10^{-3}$ 1/ h
(5)	$NH_2Cl + NH_2Cl \rightarrow NHCl_2 + NH_3$	$k_5[NH_2Cl]^2$	$k_5 = k_{H^+}[H^+] + k_{HCO_3^-}[HCO_3^-] + k_{H_2CO_3}[H_2CO_3]$ $k_{H^+} = 3.78 \times 10^{10} e^{-2169/T}$ L^2/mol^2-h $k_{HCO_3^-} = 1.5 \times 10^{35} e^{-22144/T}$ L^2/mol^2-h $k_{H_2CO_3} = 2.95 \times 10^{10} e^{-4026/T}$ L^2/mol^2-h
(6)	$NHCl_2 + NH_3 \rightarrow NH_2Cl + NH_2Cl$	$k_6[NHCl_2][NH_3][H^+]$	$k_6 = 2.2 \times 10^{8}$ L^2/mol^2-h
(7)	$NHCl_2 + H_2O \rightarrow I$	$k_7[NHCl_2][OH^-]$	$k_7 = 4.0 \times 10^{5}$ L/mol-h
(8)	$I + NHCl_2 \rightarrow HOCl + products$	$k_8[I][NHCl_2]$	$k_8 = 1.0 \times 10^{8}$ L/mol-h
(9)	$I + NH_2Cl \rightarrow products$	$k_9[I][NH_2Cl]$	$k_9 = 3.0 \times 10^{7}$ L/mol-h
(10)	$NH_2Cl + NHCl_2 \rightarrow products$	$k_{10}[NH_2Cl][NHCl_2]$	$k_{10} = 55$ L/mol-h
(11)	$HOCl + NHCl_2 \rightarrow NCl_3 + H_2O$	$k_{11}[HOCl][NHCl_2]$	$k_{11} = k_{HPO_4^{2-}}[HPO_4^{2-}] + k_{OCl^-}[OCl^-] + k_{OH^-}[OH^-]$ $k_{HPO_4^{2-}} = 5.72 \times 10^{7}$ L^2/mol^2-h $k_{OCl^-} = 3.14 \times 10^{8}$ L^2/mol^2-h $k_{OH^-} = 1.18 \times 10^{13}$ L^2/mol^2-h
(12)	$NHCl_2 + NCl_3 + 2H_2O \rightarrow 2HOCl + products$	$k_{12}[NHCl_2][NCl_3][OH^-]$	$k_{12} = 2.0 \times 10^{14}$ L^2/mol^2-h
(13)	$NH_2Cl + NCl_3 + H_2O \rightarrow HOCl + products$	$k_{13}[NH_2Cl][NCl_3][OH^-]$	$k_{13} = 5.0 \times 10^{12}$ L^2/mol^2-h
(14)	$NHCl_2 + 2HOCl + H_2O \rightarrow NO_3^- + 5H^+ + 4Cl^-$	$k_{14}[NHCl_2][OCl^-]$	$k_{14} = 8.3 \times 10^{5}$ L/mol-h
(E1)	$HOCl \leftrightarrow OCl^- + H^+$	N/A	$pk_a = 1.18 \times 10^{-4}T^2 - 7.86 \times 10^{-2}T + 20.5$
(E2)	$NH_4^+ \leftrightarrow NH_3 + H^+$	N/A	$pk_a = 1.03 \times 10^{-4}T^2 - 9.21 \times 10^{-2}T + 27.6$
(E3)	$H_2CO_3 \leftrightarrow HCO_3^- + H^+$	N/A	$pk_a = 1.48 \times 10^{-4}T^2 - 9.39 \times 10^{-2}T + 21.2$
(E4)	$HCO_3^- \leftrightarrow CO_3^{2-} + H^+$	N/A	$pk_a = 1.19 \times 10^{-4}T^2 - 7.99 \times 10^{-2}T + 23.6$
where temperature, T, is in degrees Kelvin			

Commonly used chemical species are abbreviated, including combined chlorine ($CombCl_2$), free chlorine ($FreeCl_2$), and total chlorine ($TotalCl_2$). Abbreviations for frequently referenced chemical species, groups of species, and temporal disinfectant switching are included in Table 3.3.

Table 3.3. Abbreviations for common chemical species, groups of species, and temporal disinfectant switching.

Abbreviation	Description
NH_3, NH_4^+	Ammonia, ammonium
Free ammonia	Sum of NH_3, NH_4^+
HOCl, OCl^-	Hypochlorous acid, hypochlorite
$FreeCl_2$	Free chlorine, equal to sum of HOCl and OCl^-
NH_2Cl, $NHCl_2$, NCl_3	Monochloramine, dichloramine, trichloramine
$CombCl_2$	Combined chlorine, equal to sum of NH_2Cl, $NHCl_2$, and NCl_3
$TotalCl_2$	Total chlorine, equal to sum of $FreeCl_2$ and $CombCl_2$
Total ammonia	Sum of free ammonia, $CombCl_2$
$CombCl_2 \rightarrow FreeCl_2$	Temporal disinfectant switching from $CombCl_2$ to $FreeCl_2$
$FreeCl_2 \rightarrow CombCl_2$	Temporal disinfectant switching from $FreeCl_2$ to $CombCl_2$

Reactor models for the two clearwells included SF, MM, TIS, and RN models, which are discussed in detail in APPENDIX B. Description of these models can also be found in Chapter 2, as well as reference textbooks and the literature (Crittenden et al. 2005, Fogler 2006, Levenspiel 1999, Najm et al. 2009, Craik 2005, Pfeiffer and Barbeau 2014). Models were developed from the tracer data in Figure 3.1, which shows the normalized tracer concentration (C/C_0) versus θ (normalized run time, $\theta = t/\tau$). The nominal hydraulic residence time, τ, is equal to V/Q where V is the reactor volume and Q is the volumetric flow rate. The number of tanks, n, for TIS models representing Clearwells A and B were found to be 5 and 3, respectively, via least squares regression. RN models were selected based on fits to non-reactive tracer data using a process described in Chapter 2. The parallel TIS RN model was selected for Clearwell A (see diagram on Figure 3.1A for fitting parameters). The RN model selected for Clearwell B was PFR and CSTR in series, repeated in parallel (see diagram on Figure 3.1B for fitting parameters). SF and MM

models for Clearwells A and B were developed from RN model fits shown in Figure 3.1 using steps of 0.05θ from 0 to 3θ. This was done to eliminate errors that may result from noise in tracer data.

All inputs for modeling full-scale reactors were either observed, or calculated from, online flow meters or online analyzers. Figure 3.2A shows an example of how model inputs change over time. Effluent flow varied from 24 to 90 MGD. This range of flow occurred in less than a three-hour period, and flow changes caused τ to vary 4.7 to 18.9 hours. Thus, reactor operation was typically not at steady state, and neither were the reactor models used. Model input data were collected at five-minute increments, which is consistent with response time of the ChemScan instrument (ChemsScan Inc. 1998). Five-minute increments were also used for predicted outputs from different reactor models. Downscaling five-minute data to one-minute data using linear interpolation and rerunning models did not have a noticeable effect on model outputs (data not shown). Influent chlorine concentration and ammonia dose were relatively steady prior to a conversion from chloramines to free chlorine (i.e., $CombCl_2 \rightarrow FreeCl_2$) (Figure 3.2Figure 3.2B). Chlorine feed rates were adjusted to target an effluent residual of 3.7 mg/L-Cl_2 when $CombCl_2$ was used a residual disinfectant, and 3.0 mg/L when $FreeCl_2$ was used. To convert from $CombCl_2 \rightarrow FreeCl_2$, ammonia feed was ceased and dose became zero.

Model initial conditions were set equal to reactor effluent conditions at a time no less than 48 hours prior to change in disinfectant. For example, if a disinfectant change occurred on March 15 at 6:00am, the model was initialized no later than March 13 at 6:00am. Observed time-dependent model inputs (e.g., process flow rate, clearwell volume, chlorine concentration, ammonia dose) without any averaging were then used to model reactor outputs before, during, and after breakpoint for comparison with observed reactor effluent.

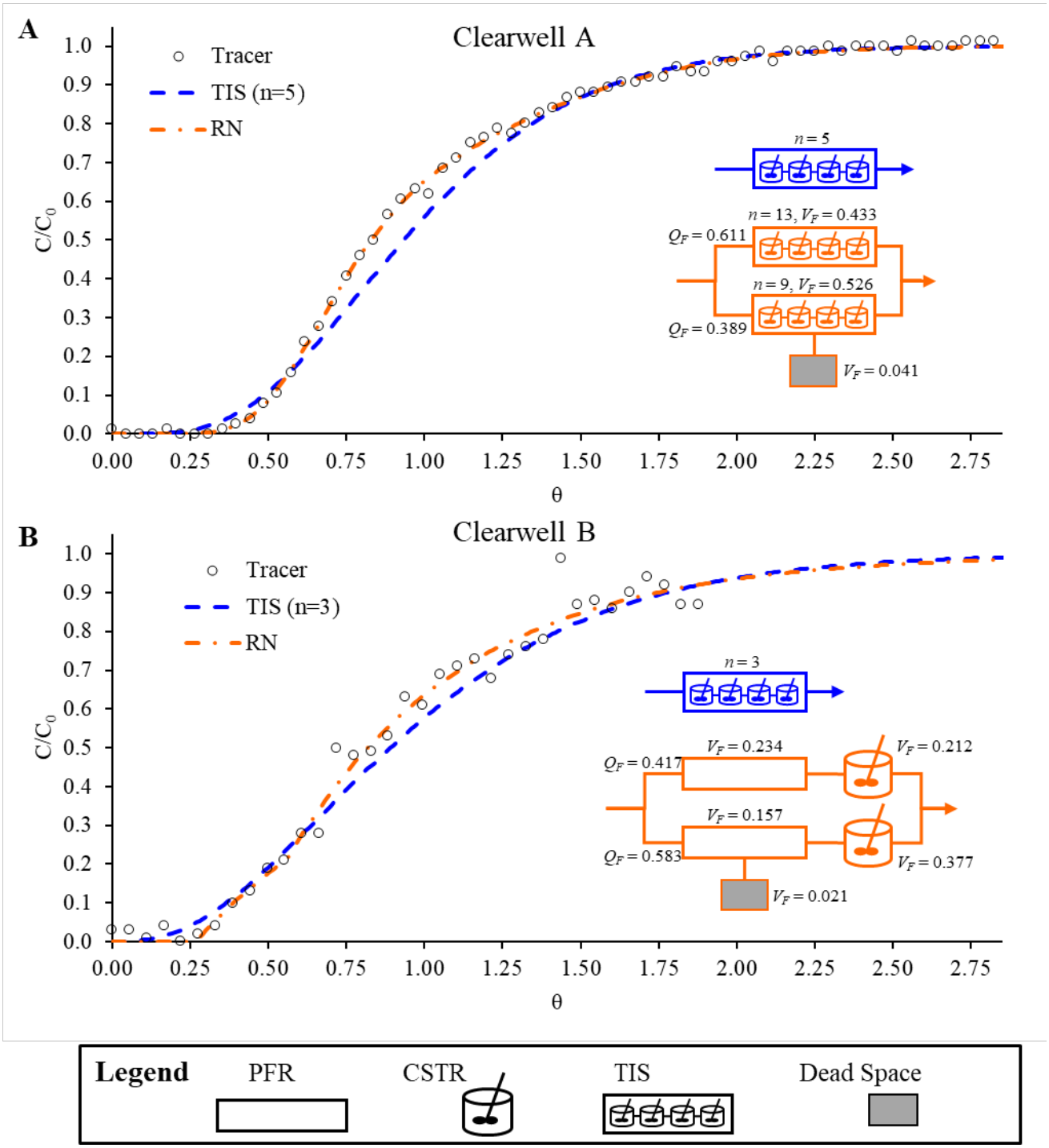

Figure 3.1. Tracer data for (A) Clearwell A and (B) Clearwell B fit with TIS and RN models. The SF model uses tracer data directly and therefore is not shown in the figure. Normalized run time, $\Theta = t/\tau$.

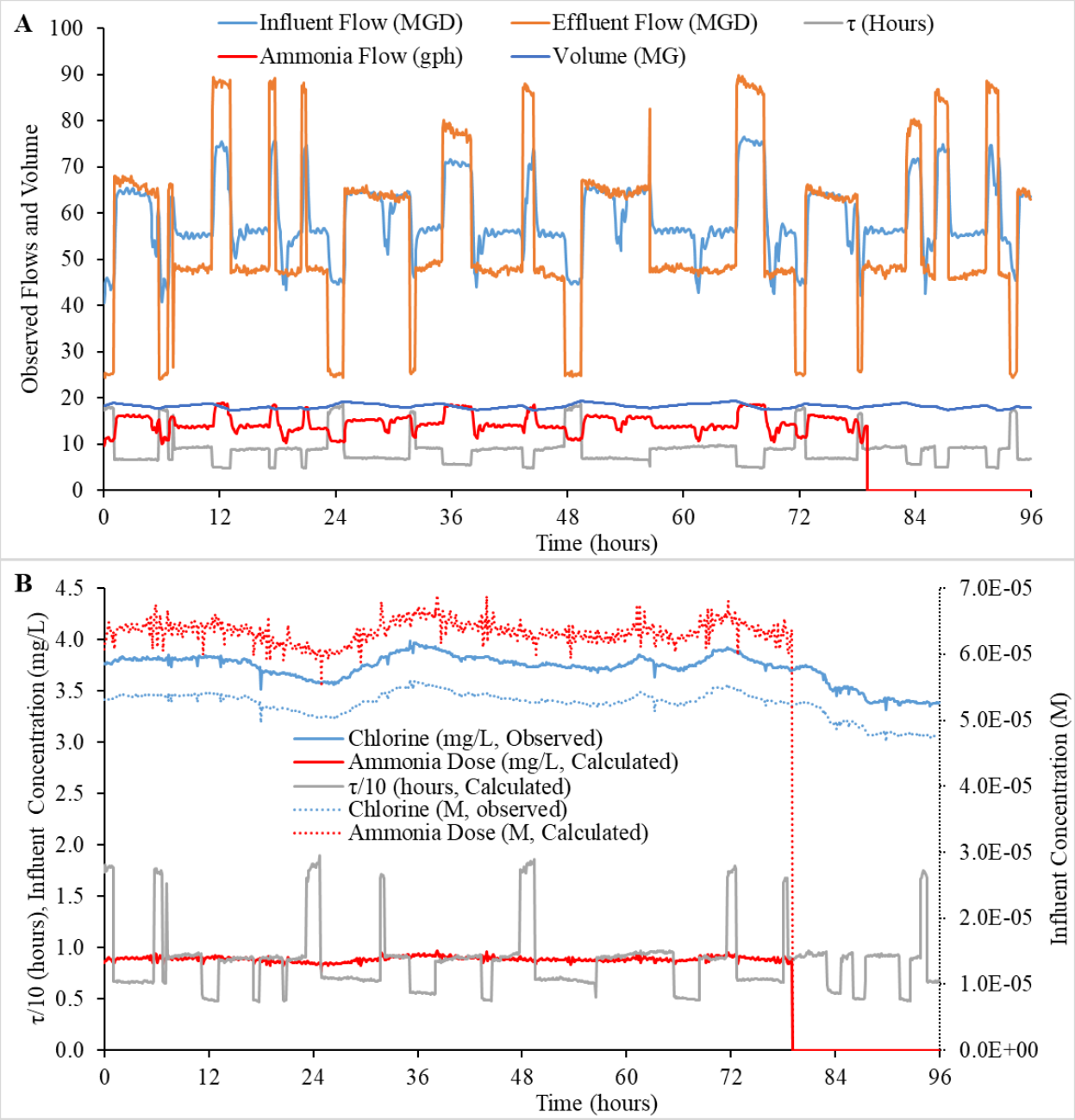

Figure 3.2. Example online, full-scale data used as model inputs. These include (A) reactor influent and effluent flows, calculated clearwell volumes (from online level indicators), metered bulk ammonia influent flow, and τ. The three model inputs that varied over time were (B) chlorine concentration, influent ammonia concentration, and τ.

Clearwell effluent concentrations of the chemical species in Table 3.2 were predicted using SF, MM, TIS, and RN models. The process for calculating the effluent species concentrations is described in detail for each model in APPENDIX B. All models involve setting

up a series of differential equations from the chemical reactions shown in Table 3.2 and solving them using the *deSolve* package (Soetaert et al. 2010) in R (R Core Team 2016). Example code for solving the SF, MM, TIS, and RN models is shown in APPENDIX B.

3.2.4 Quantifying Model Error

The difference between modeled and observed concentrations over a given range of time was quantified using normalized root-mean-square error (NRMSE). NRMSE was calculated as follows

$$NRMSE = \frac{1}{\overline{C}_{Obs}}\sqrt{\frac{\sum_1^Z (C_{Mod,i} - C_{Obs,i})^2}{Z}}, \quad 3.1$$

where C_{Mod} is the modeled concentration, C_{Obs} is the observed concentration, $\overline{C}_{Obs}$ is average observed concentration, and Z is the total number of observations, individually denoted as i.

3.2.5 Reactions in Reactor Effluent

Model outputs indicated that breakpoint reactions may be incomplete in clearwell effluent near the time of observed minimum disinfectant residual, and therefore the ability of different reactor models to predict residual disinfectant stability was also studied. Samples of Clearwell A effluent were collected both before and after the minimum observed effluent chlorine residual during $CombCl_2 \rightarrow FreeCl_2$. Sample collection times included 55 minutes before, 15 minutes before, and 25 minutes after the minimum chlorine residual. Minimum chlorine residual was observed nine hours and 20 minutes after ammonia feed was ceased. Total residual chlorine in each collected sample was measured over time using a DPD pocket colorimeter (Hach Co., Loveland, CO). These results were compared to predicted decay in modeled SF, TIS, and RN effluent following holding time in a hypothetical batch reactor (i.e., predicted concentrations

downstream).

3.2.6 Microbial Inactivation Using Segregated and Mixed Models

The effects of flow segregation and earliness of mixing (i.e., micromixing) on predicted microbial inactivation were investigated. Microbial inactivation was calculated for two models with equivalent kinetic parameters and RTD, but with different assumptions micromixing: SF and TIS models.

A hypothetical disinfection contactor was used for this analysis instead of Clearwells A or B. Clearwells A and B had relatively low rates of observed oxidant decay, and therefore flow segregation and mixing would be relatively unimportant. The hypothetical disinfection contactor was assumed to have τ = 10 minutes and RTD described by TIS with n = 5. Initial oxidant concentration was assumed to be 1 mg/L. First-order oxidant decay was assumed such that

$$\frac{dC}{dt} = -k_d C, \qquad 3.2$$

where C is the oxidant concentration (mg/L) and k_d is the rate constant for first-order decay (min^{-1}). Microbial inactivation was assumed to follow Chick-Watson kinetics (Crittenden et al. 2005)

$$\frac{dN}{dt} = -k_i C N, \qquad 3.3$$

where k_i is the coefficient of specific lethality (L/mg-min) and N is the microbial concentration (i.e., concentration of viable microbes). This expression becomes pseudo-first order when C is constant, although for this study oxidant decay was assumed. For the TIS reactor, oxidant and microbial concentrations in each CSTR were calculated according to

$$\frac{C}{C_0} = \frac{1}{1+k_d\tau/n}, \quad 3.4$$

and

$$\frac{N}{N_0} = \frac{1}{1+k_i C\tau/n}, \quad 3.5$$

where C_0 and N_0 are the influent concentrations of disinfectant and microbial contaminants, respectively (Levenspiel 1999). For the SF model, concentrations of disinfectant and microbial contaminants were calculated using Equations 3.2 and 3.3 in the *deSolve* package. The SF model used one PFR for every 0.01θ up to 3θ, or 300 PFRs.

Microbial inactivation was predicted over a range of oxidant decay constant and specific lethality constant values. The oxidant decay constant was varied from 0 to 0.5 min^{-1} and the specific lethality coefficient from 0 to 5 L/mg-min (Crittenden et al. 2005).

3.3 Key Concepts – Summary

A detailed discussion of flow segregation and mixing (i.e., micromixing), reactor model types, and how different model types respond to temporal disinfectant switching is provided in APPENDIX B. A brief summary of these 'Key Concepts' is included in this section. These conceptual investigations are important for framing the predicted full-scale results that follow.

Visual representations of perfect segregation, perfect mixing, early segregation, and late segregation are shown in Figure 3.3. Assumptions about flow segregation and mixing have important consequences when mixing reactants (e.g., free and combined chlorine). Temporal disinfectant switching in a CSTR produces breakpoint (see Figure B.6 in APPENDIX B), while breakpoint would not occur in a PFR due to lack of longitudinal mixing (see Figure B.7 in

APPENDIX B). CSTRs and PFRs are the building blocks of more complex models, including the TIS and SF models. The TIS model predicts breakpoint (see Figure B.8 in APPENDIX B). However, breakpoint reactions may not have progressed to completion, even with residence times on the order of hours (see Figure B.9 in APPENDIX B). This phenomenon is more pronounced for SF models as shown in Figure B.10 in APPENDIX B. Loss of chlorine residual is predicted after flow leaves the SF reactor because there is no internal mixing, so free and combined chlorine are first assumed to mix leaving the reactor.

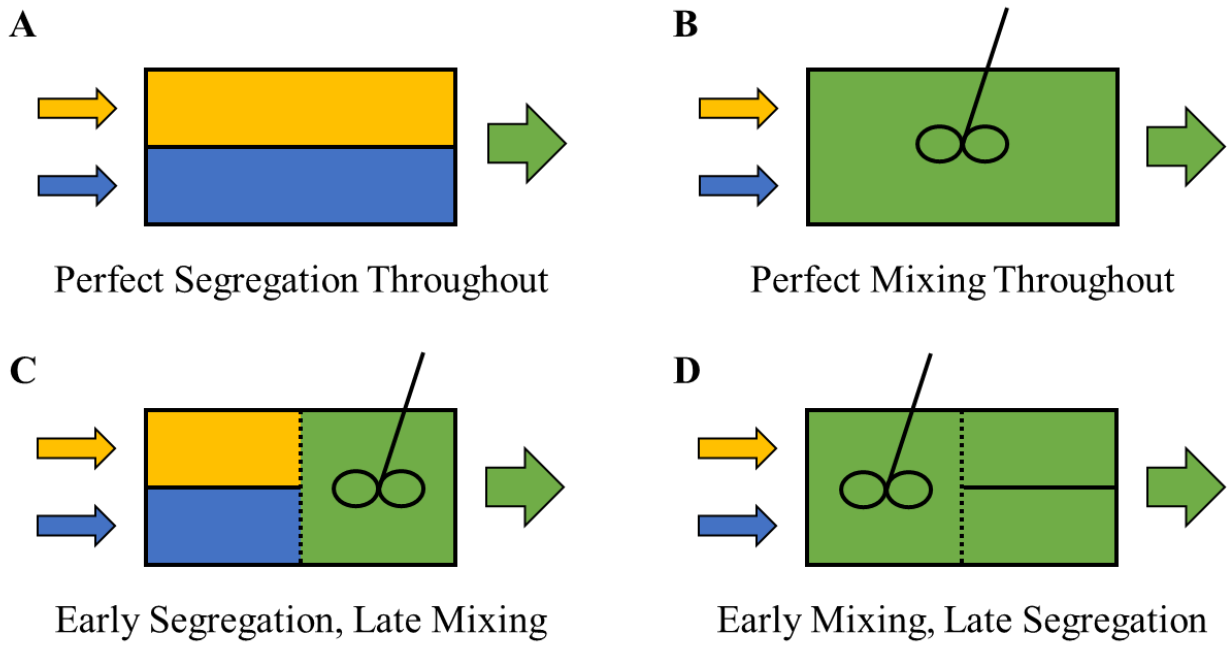

Figure 3.3. Visual representation of reactor segregation and mixing. Blue and yellow solutions, when mixed together, form a green solution. Solid lines represent boundaries where flow cannot pass between, while dashed lines represent boundaries through which flow can pass.

3.4 Results and Discussion

3.4.1 Full-Scale Results: Observed and Modeled

Figure 3.4 shows ammonia dose along with observed and modeled TotalCl_2 residual in Clearwell A for CombCl_2→FreeCl_2, including the preceding 79 hours since model initialization.

Prior to the switch from chloramines to free chlorine, NRMSE values between modeled and observed $TotalCl_2$ concentrations were 8.3, 2.8, 15.6, and 1.1% for SF, TIS, MM, and RN models, respectively. The SF model tended to underestimate effluent $TotalCl_2$ due to NH_2Cl decay in PFRs with long residence time. Over the period shown in which ammonia was added, average τ was 11.5 hours. This long residence time, coupled with tracer data showing 38% of flow spending longer than τ in the reactor (see Figure 3.1A), was likely the cause of the SF model underestimating effluent $TotalCl_2$ concentrations. The MM model underestimated effluent $TotalCl_2$ due to the model assumption that both $FreeCl_2$ and ammonia (rather than NH_2Cl) are injected throughout the length of the reactor. This resulted in partial breakpoint before NH_2Cl could be formed. TIS and RN model predictions were substantially closer to the observed concentrations.

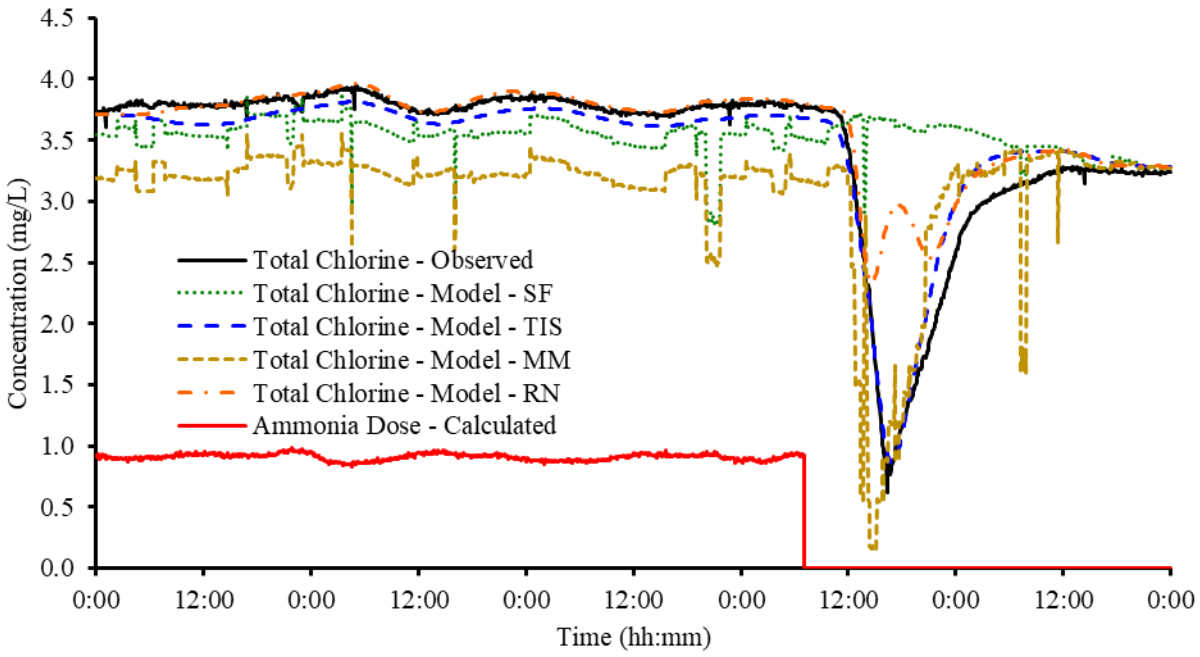

Figure 3.4. Observed and modeled TotalCl2 for CombCl2→FreeCl2 in Clearwell A.

For the period after ammonia feed was ceased, breakpoint chemistry was observed and Figure 3.4 shows significant differences among reactor model predictions of $TotalCl_2$. The SF model predicted no reduction in $TotalCl_2$ because flows from individual PFRs mix at the reactor effluent with zero time for breakpoint reactions to occur (see Figure B.10 and Key Concepts in APPENDIX B). The SF model prediction differed significantly from observation, with NRMSE of 36%. The TIS model performed well (NRMSE of 7%) except for a period after breakpoint where $TotalCl_2$ was overestimated by 4 to 22% relative to observed concentrations, before later converging to similar concentrations after complete conversion to free chlorine. The MM model predicted breakpoint earlier than was observed, and predicted free chlorine concentrations would increase more quickly than was observed (NRMSE = 20%). The RN model performed similarly to the TIS model toward the beginning and end of breakpoint. However, the RN model predicted a local maximum in $TotalCl_2$ in between two local minima. This resulted from two segregated flows with differing residence times mixing together with zero time for breakpoint reactions (see Figure 3.1A for parallel TIS RN model). NRMSE for the RN model in the period after ammonia feed was ceased was 22%.

Model outputs were compared to observation for total ammonia, NH_2Cl, and $FreeCl_2$ in addition to $TotalCl_2$. This comparison was performed for both the baffled Clearwell A and unbaffled Clearwell B. $CombCl_2 \rightarrow FreeCl_2$ and $FreeCl_2 \rightarrow CombCl_2$ conversions are shown in Figure 3.5 and Figure 3.6 for Clearwell A and in Figure 3.7 and Figure 3.8 for Clearwell B. Data are shown specifically for a 24-hour period in which breakpoint occurs. Results shown in Figure 3.5A are similar to Figure 3.4, but for a different year.

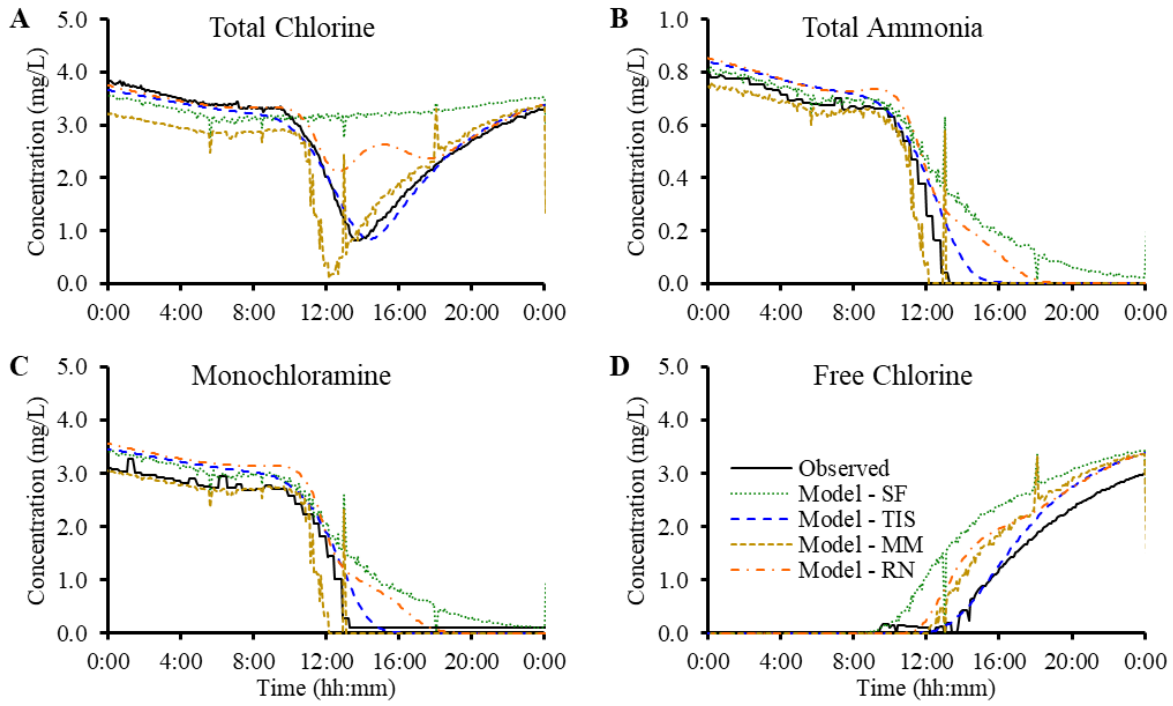

Figure 3.5. Observed and modeled species concentrations for $CombCl_2 \rightarrow FreeCl_2$ in Clearwell A. Results shown in panel A are similar to those in Figure 3.4 but for a different year.

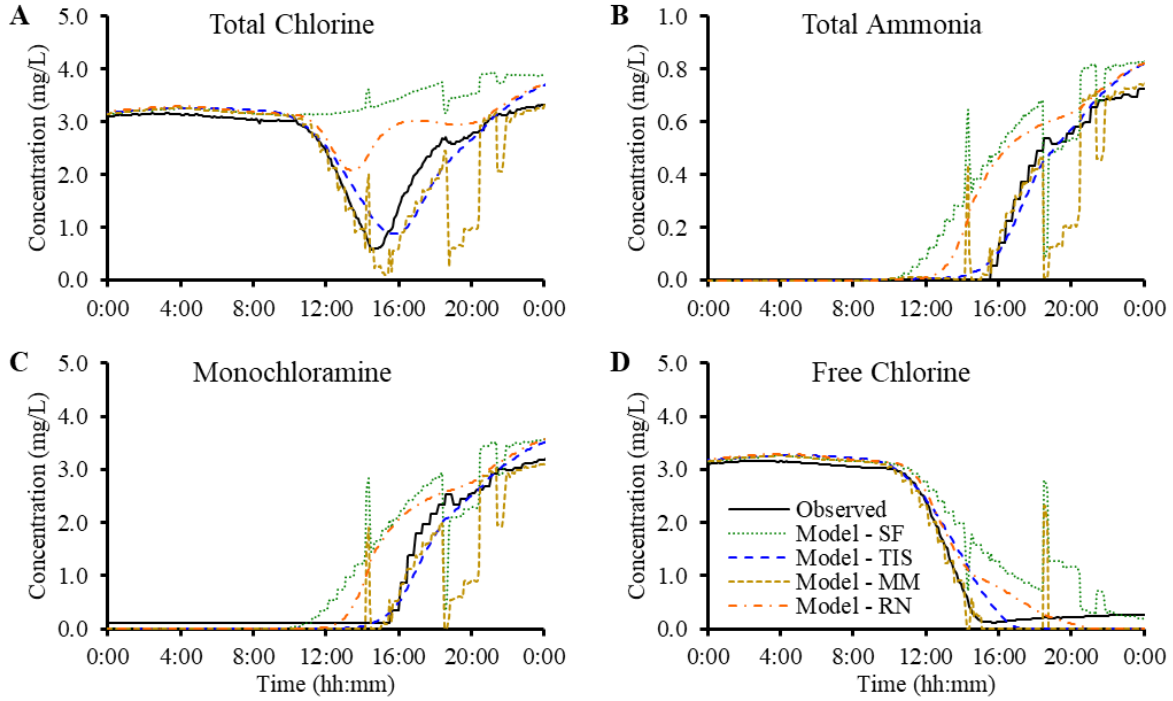

Figure 3.6. Observed and modeled species concentrations for $FreeCl_2 \rightarrow CombCl_2$ in Clearwell A.

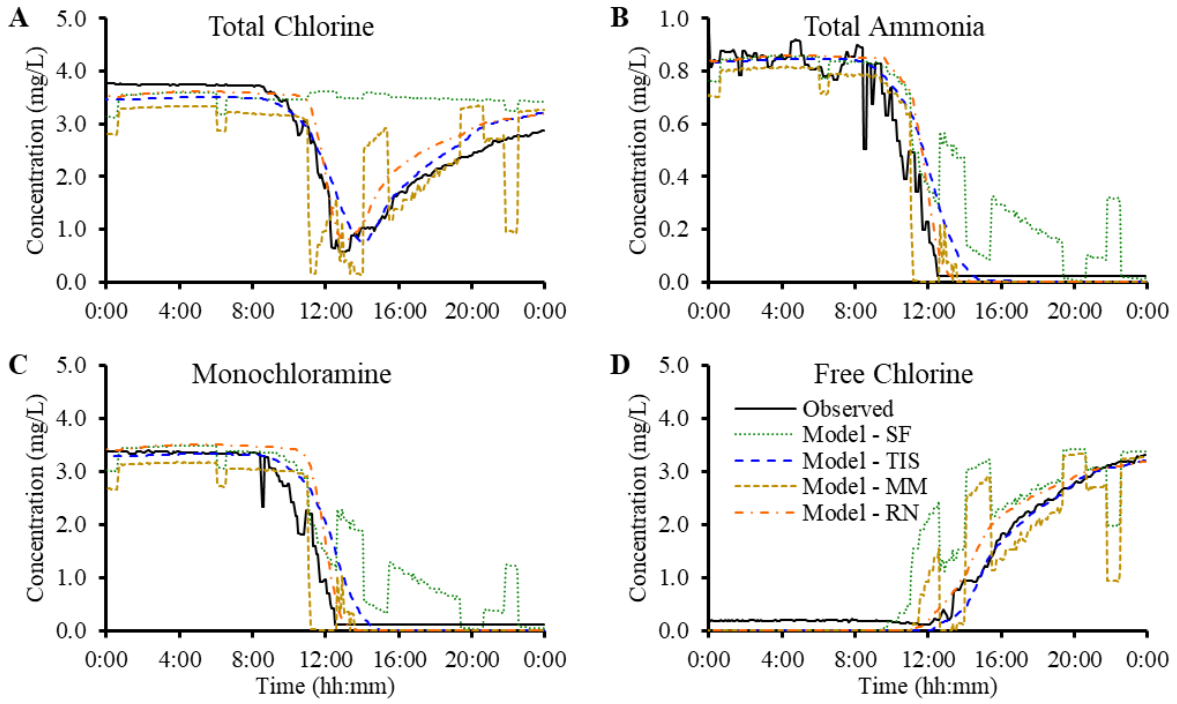

Figure 3.7. Observed and modeled species concentrations for $CombCl_2 \rightarrow FreeCl_2$ in Clearwell B.

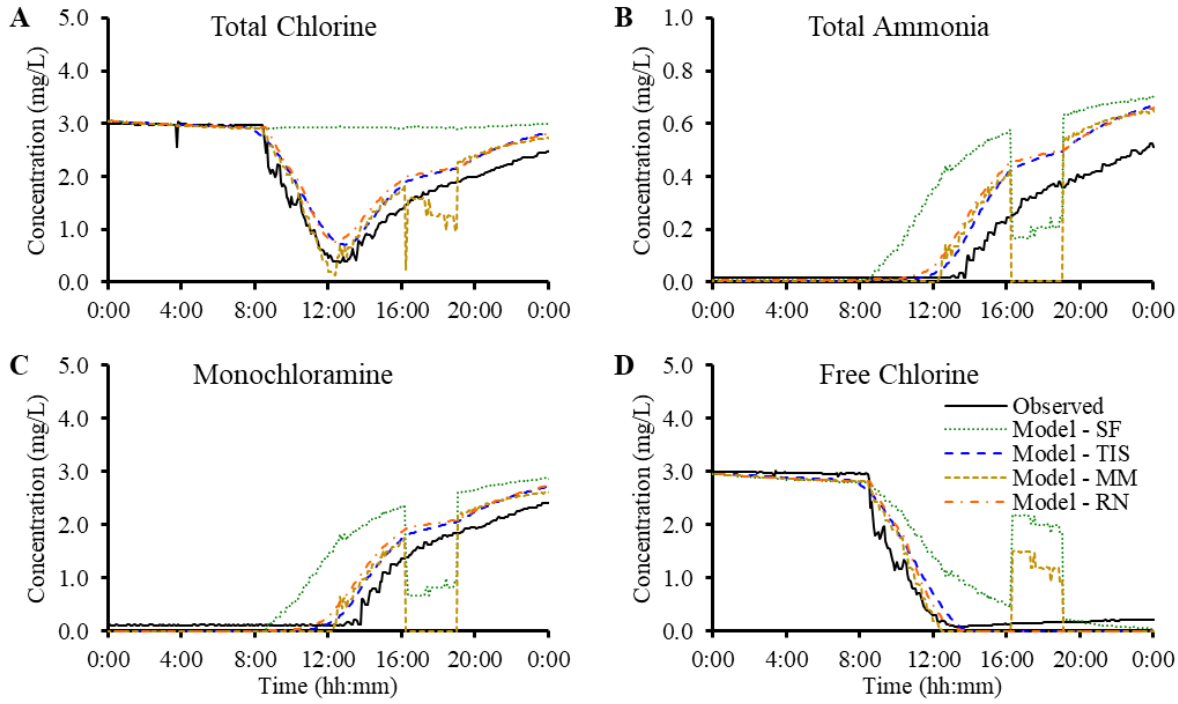

Figure 3.8. Observed and modeled species concentrations for $FreeCl_2 \rightarrow CombCl_2$ in Clearwell B.

SF model predictions generally differed from observation, with TotalCl_2 NRMSE of 35, 40, 46, and 58% over the 24-hour periods shown in Figure 3.5 - Figure 3.8. The SF model did a poor job of predicting breakpoint reactions, indicating that SF is also a poor predictor of micromixing in the reactors studied. The SF model predicted numerous step changes in species concentrations, particularly for Clearwell B (Figure 3.7, Figure 3.8). Similar step changes in concentrations were observed for the MM model that coincided in time with those for the SF model. To investigate a potential explanation, model prediction was compared with τ as shown in Figure 3.9. Large changes in predicted concentration corresponded to changes in τ, which resulted from finished water pumps being turned on and off (i.e., effluent flow changes). This in turn effected how far back in time ($\tau^*\Theta_i$) the models looked for inputs due to unsteady operation (see Figure B.11). When flow decreased, τ increased and with it the proportion of model inflows containing ammonia as the SF and MM models referenced inflows that occurred farther back in time. This led to higher predicted concentrations of NH_2Cl. As flow increased, τ decreased and with it the proportion of model inflows containing ammonia as the models referenced more recent inflows. This led to higher predicted concentrations of FreeCl_2. Susceptibility to unsteady flow rates likely explain the concentration step changes predicted by the SF and MM models. The TIS and RN models did not predict step changes, indicating that these models are less sensitive to unsteady flows than the SF and MM models.

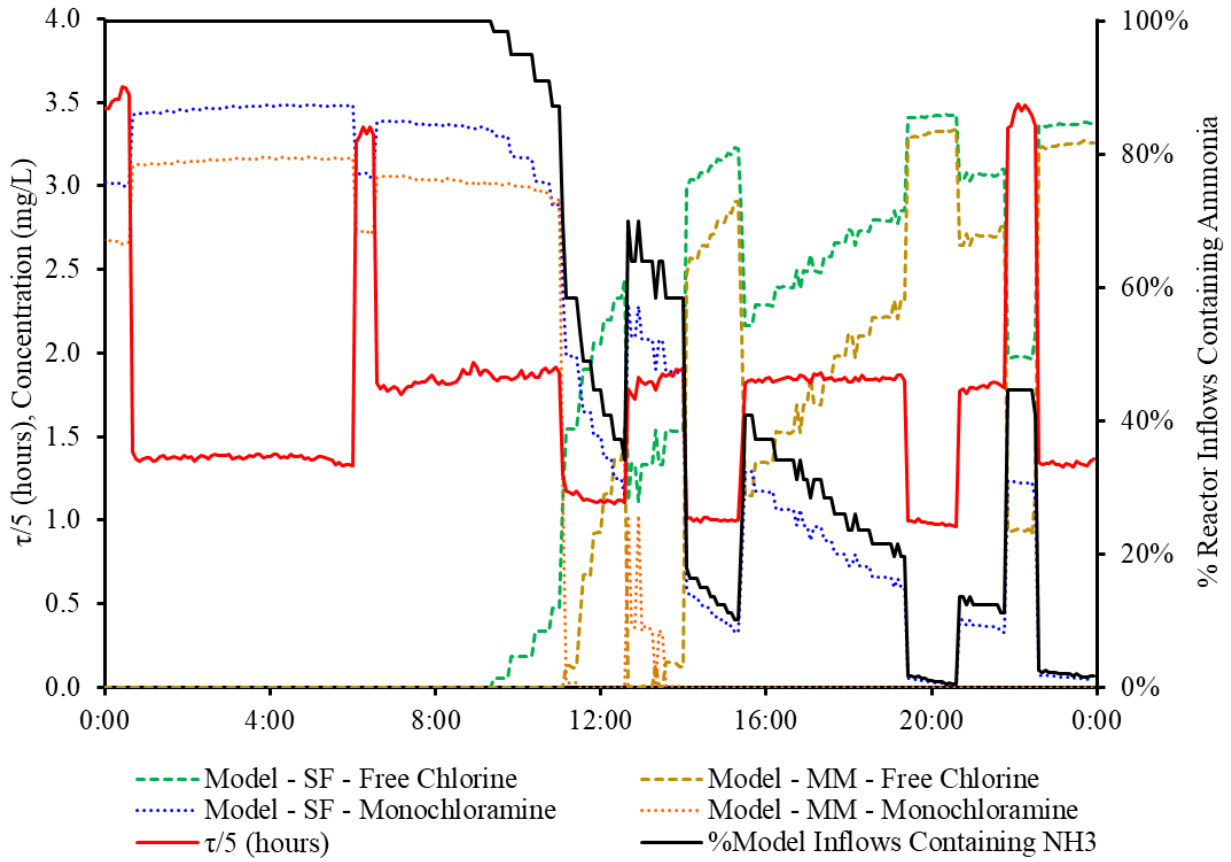

Figure 3.9. SF and MM model predictions for free chlorine and monochloramine compared with τ and percentage modeled inflows containing ammonia. The period represented is equivalent to that shown in Figure 3.7.

To eliminate the effect of unsteady flows, the SF and MM models were also run using a constant τ. The value of τ used was the average over the period shown in Figure 3.7 and Figure 3.9 (i.e., 8.5 hours). Results of the constant and variable τ model runs are shown in Figure 3.10. The step changes in predicted concentrations did not occur when the average τ was used. The SF model poorly predicted observed species concentrations even when using average τ. MM model predictions improved significantly in accuracy when using average τ; NRMSE was reduced from 28, 58, 27, and 25% to 14, 17, 23, and 20% for $TotalCl_2$, $FreeCl_2$, NH_2Cl, and total ammonia, respectively. These findings indicate that average τ improves the accuracy of MM predictions.

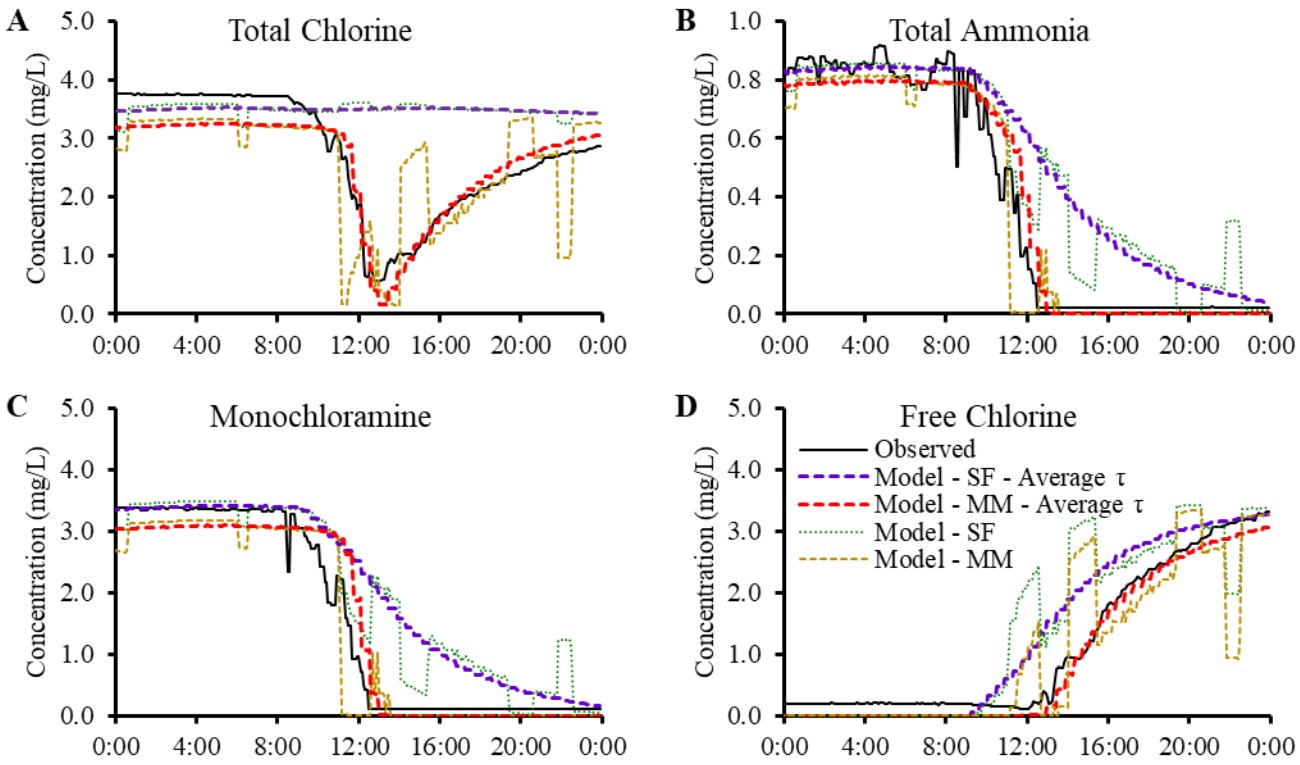

Figure 3.10. SF and MM model predictions from Figure 3.7 along with model predictions calculated using the average τ over the time period shown.

Even at steady flows, the MM model tended to predict lower minimum $TotalCl_2$ concentrations at breakpoint than were observed. This was particularly pronounced in Figure 3.5 and Figure 3.6, where the MM model predicted minimum $TotalCl_2$ concentrations of <0.1 mg/L, compared with observed minima of 0.81 and 0.58 mg/L. The NRMSE for MM $TotalCl_2$ in Figure 3.5 - Figure 3.8 was 20, 22, 28, and 14%. The $FreeCl_2 \rightarrow CombCl_2$ conversion shown in Figure 3.8 had relatively steady τ, with only one flow change (data not shown) which is evident in the predicted species concentrations. Except during the period of τ change, the MM model predictions shown in Figure 3.8 matched observation more closely than in Figure 3.4 – Figure 3.7. This finding suggests that the MM model performs reasonably well in predicting micromixing when there is no or poor baffling and reactor operation is steady (i.e., steady τ resulting from steady volume and flow).

The TIS model performed well in both Clearwell A (n = 5) and Clearwell B (n = 3). TotalCl_2 NRMSE was 5, 11, 12, and 14% in Figure 3.5 – Figure 3.8 respectively, which was lower than for all other models. This also held true for other species, such as FreeCl_2 and NH_2Cl. The TIS model's predicted timing of breakpoint and species (i.e., TotalCl_2, TotalNH_3, NH_2Cl, FreeCl_2) concentrations were all consistent with observation. However, TIS often predicted that the oxidant initially present (i.e., NH_2Cl, FreeCl_2) would persist longer, and that the influent oxidant (i.e., FreeCl_2, NH_2Cl) would appear sooner after breakpoint, than was observed. Predictions of TotalCl_2 were generally not improved by changing the number of n tanks found by tracer fitting, although for Clearwell B n-1 produced lower NRMSE (see Figure B.12 in APPENDIX B). Overall, TIS model predictions closely matched observation, indicating that the TIS model also likely provides an accurate representation of micromixing in the reactors studied.

For the RN model, predictions matched observation more closely for Clearwell B than for Clearwell A. TotalCl_2 NRMSE values for CombCl_2→FreeCl_2 and FreeCl_2→ CombCl_2 in Clearwell B were 13 and 16% (see Figure 3.7, Figure 3.8), similar to the 12 and 14% for TIS. However, the RN model did not perform as well for Clearwell A. TotalCl_2 NRMSE values for CombCl_2→FreeCl_2 and FreeCl_2→ CombCl_2 were 20 and 25% (see Figure 3.5 and Figure 3.6), worse than the 5 and 11% for TIS. The RN model for Clearwell A significantly overestimated all species near observed minimum TotalCl_2, although the RN model for Clearwell B produced estimates closer to observed concentrations. Further investigation into model outputs suggests that more accurate prediction by the RN model for Clearwell B than Clearwell A appear to be related to residence times in segregated (i.e., parallel) flows as discussed next.

RN models achieve better fits to nonreactive tracer data as the number of parallel flows increases from one to two, and from two to three (see Chapter 2). This can be seen in Figure

3.1A, where the parallel TIS RN model achieved a better fit than a single TIS reactor. Better fits result, in part, from parallel flows having different residence times. In the Clearwell A RN model, 61.1% of the flow passed through 43.3% of the volume (exiting 41.1% faster than the overall τ), while 38.9% of the flow passed through 52.6% of the volume (exiting 26.0% slower than the overall τ) (see fitting parameters in Figure 3.1). For the Clearwell B RN model, 58.3% of the flow passed through 53.4% of the volume (exiting 9.2% faster than the overall τ) while 41.7% of the flow passed through 44.6% of the volume (exiting 6.5% slower than the overall τ). Differences in residence times between the parallel flows in Clearwell A (41.1% faster, 26.0% slower than τ) result in the prediction of two TotalCl_2 minima that are seen in Figure 3.4 – Figure 3.6. By contrast, the two parallel flows for Clearwell B have relatively similar residence times: only 9.2% faster and 6.5% slower than τ. As a result, the Clearwell B RN model predicts a single TotalCl_2 minimum (see Figure 3.7 and Figure 3.8). This finding suggests that parallel (i.e., segregated) flows in reactor networks improve the prediction of macromixing conditions, but do not necessarily improve the prediction of micromixing conditions.

In summary, the TIS models performed well in predicting reactor effluent species for both baffled and unbaffled clearwells (TotalCl_2 NRMSE 5-14%). The SF model did not perform well, predicting concentrations that varied significantly from observed results (TotalCl_2 NRMSE 34-53%). RN models performed similarly to TIS for Clearwell B (TotalCl_2 NRMSE 13-16%) but worse for Clearwell A (TotalCl_2 NRMSE 20-25%); this can be explained by the difference in τ for parallel flows in each model. The MM model accurately predicted species concentrations in unbaffled Clearwell B when flows were steady (TotalCl_2 NRMSE 14%), but was less accurate for the baffled Clearwell A or when flows were unsteady (TotalCl_2 NRMSE 20-28%). These results indicate that TIS model most accurately and consistently represented micromixing

conditions in the reactors studied.

This work also demonstrated that when combined with an appropriate reactor model (e.g., TIS), the generally accepted kinetic model of Jafvert and Valentine (1992) and Vikesland et al. (2001) was capable of predicting breakpoint reactions in full-scale, flow through reactors.

3.4.2 Reactions in Reactor Effluent

The previous section highlighted that SF models, along with RN models for Clearwell A, predicted TotalCl_2 residuals that were significantly greater than observed values. For these models, CombCl_2 and FreeCl_2 were predicted to co-occur in reactor effluent due to the late mixing of segregated flows. Co-occurrence of CombCl_2 and FreeCl_2 would be expected to result in breakpoint reactions. Figure 3.11 compares observed TotalCl_2 effluent concentrations to modeled concentrations leaving Clearwell A before and after 60 minutes in a PFR (or batch reactor). Observed results from grab samples were allowed to react in batch reactors for 60 minutes prior to TotalCl_2 measurement. Modeled values are presented for a PFR receiving effluent from SF, TIS, MM, and RN models. Differences in model outputs before and after a 60-minute hold time result from breakpoint reactions (i.e., kinetic model in Table 3.2).

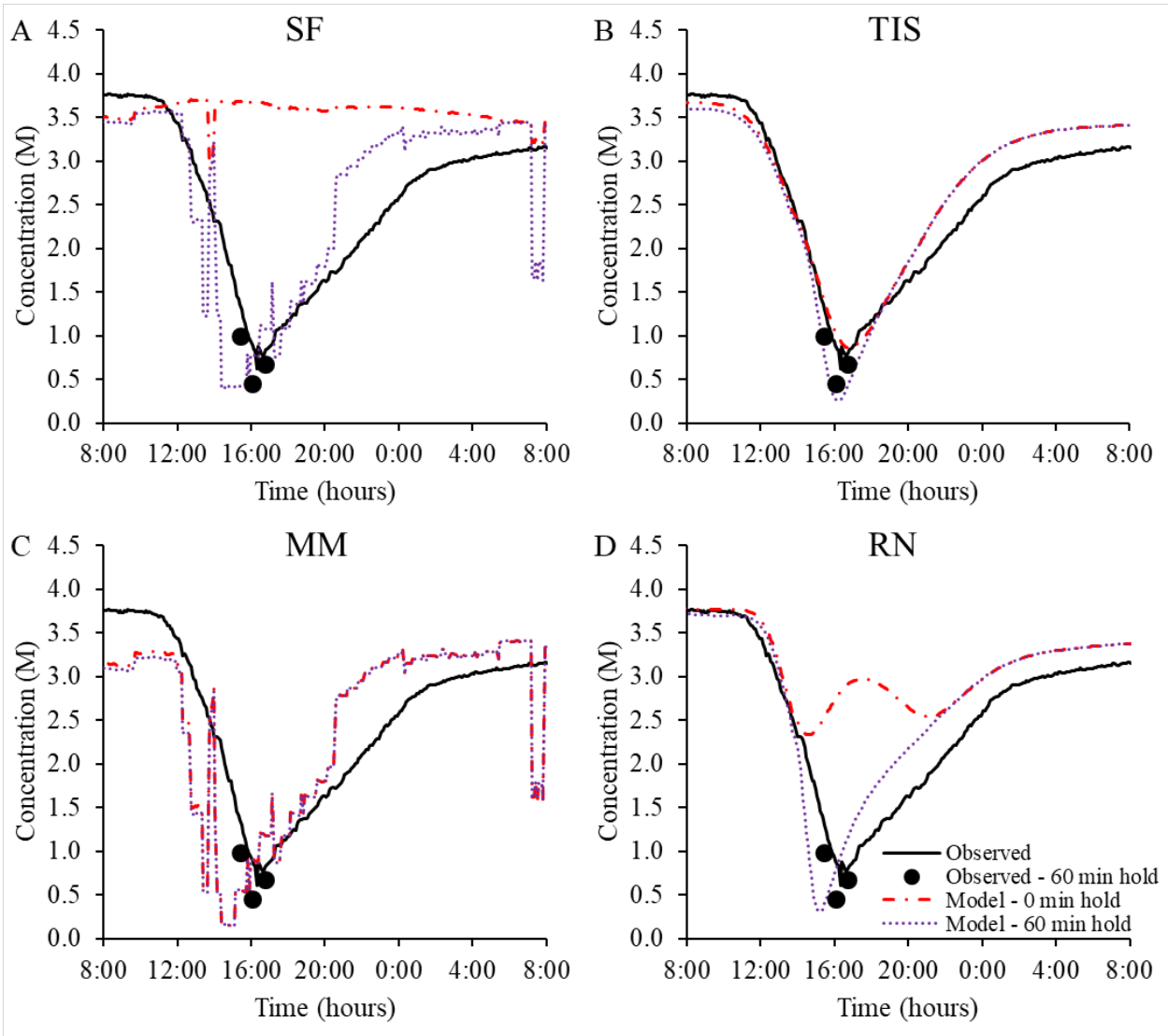

Figure 3.11. Observed and predicted TotalCl_2 concentrations in Clearwell A effluent before and after a 60-minute hold during CombCl_2→FreeCl_2 shown in Figure 3.4.

As shown in Figure 3.11, continued loss of Total Cl_2 was observed when clearwell effluent samples were held in a batch reactor for 60 minutes. Thus, even though Clearwell A had residence time on the order of nine hours during CombCl_2→FreeCl_2 (see Figure 3.2), breakpoint reactions were incomplete in the reactor effluent and are expected to continue as water enters the distribution system. Following a modeled 60-minute reaction period, SF and RN results for Clearwell A were much closer to observed concentrations. The MM model predictions were

largely unchanged after the 60 minute reaction time, and were similar to the SF model predictions after a 60 minute reaction time. The TIS model effectively predicted breakpoint reactions in both reactor effluent and in the held samples. These results indicate the importance of representing micromixing in reactive systems. Internal micromixing was prevalent in the reactors studied as evidenced by observed loss of TotalCl_2. This is likely the case for many water treatment reactors, with flow segregation in RN and SF models possibly being an artifact of the inability to perfectly simulate micromixing using combinations of PFRs, CSTRs, and TIS reactors to model RTD (i.e., macromixing).

3.4.3 Modeled Microbial Inactivation in Reactors with and without Mixing

A common application of water treatment reactors is to degrade chemical or microbial contaminants. The purpose of this section is to investigate how predictions of microbial inactivation might be affected by model selection when the models make different assumptions about degree of segregation and earliness of mixing, specifically TIS and SF models.

Results of this analysis are shown in Figure 3.12. Panels A and B show log reduction calculated by SF and TIS, respectively, and Panel C shows the difference in the two calculations. Note that SF and TIS are modeling the same RTD. For both models, as expected, higher log reductions are calculated when specific lethality coefficient, k_i, is large and oxidant decay rate, k_d, is small (i.e., rapid disinfection, persistent disinfectant). Fast disinfectant decay and/or a resistant microorganism results in lower calculated log reductions. Although the overall trends are the same for TIS and SF, the magnitude of calculated log reduction differs considerably between the two models.

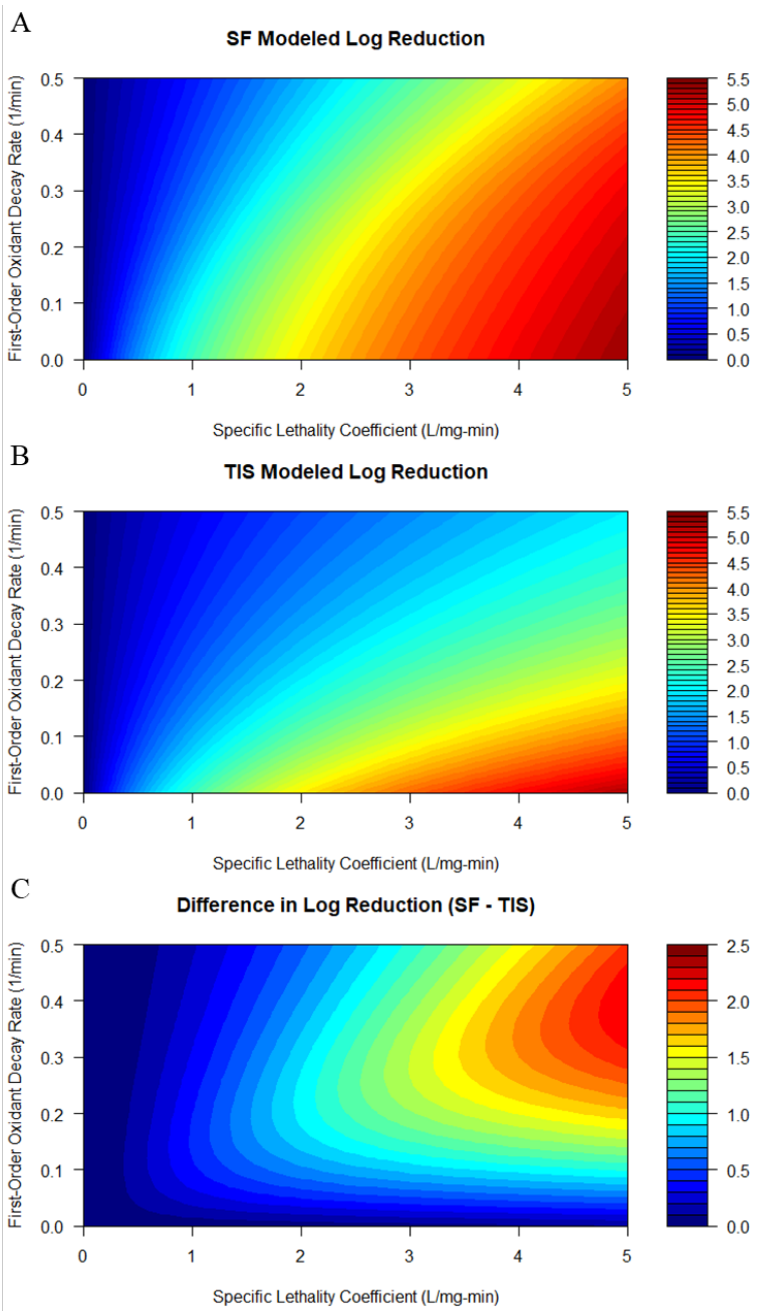

Figure 3.12. Influence of hydraulic model selection on predicted contaminant reduction. Assumed reaction conditions include 1 mg/L initial oxidant concentration, τ = 10 min, first-order contaminant degradation (e.g., Chick-Watson), and first-order oxidant decay. (A) Predicted log reduction in a SF reactor with RTD equivalent to TIS with n = 5, (B) predicted log reduction in a TIS reactor with n = 5, and (C) the difference in predicted log reduction between SF and TIS. Example specific lethality coefficients for microorganisms with various oxidants include: 0.0327 L/mg-min – E. coli with monochloramine, 0.83 L/mg-min – Cryptosporidium with ozone, 1.9 L/mg-min – Giardia with Ozone, 3.4 L/mg-min – MS-2 with chlorine (Crittenden et al. 2005).

The SF model predicted significantly higher log reduction than the TIS model despite using the same RTD. SF predicted more than 100 times more removal than TIS (i.e., >2-log difference) for some conditions shown. The SF model assumes that the high initial oxidant concentration is in contact with the high initial microorganism concentration, whereas the TIS model assumes that both are immediately diluted in the first of a series of CSTRs. A hypothetical microorganism that short circuits (i.e., low residence time) would be in contact with much lower oxidant concentrations in each CSTR of a TIS reactor than a microorganism passing through a PFR with low residence time in SF. These differences in model assumptions likely explain the difference in predicted log inactivation shown in Figure 3.12C. Results presented earlier in this work demonstrate that the TIS model was more effective in describing internal reactor segregation and mixing conditions than the SF model for the clearwells studied. Thus, the SF may overestimate disinfection efficacy in reactors like Clearwells A and B. This is consistent previously-reported model predictions (Craik 2005, Pfeiffer and Barbeau 2014)

However, it is important to differentiate the situations where model selection has significant influence on predicted log reductions from the situations where model selection is less important. Model selection is clearly important where specific lethality and oxidant decay are high (upper right corner of Figure 3.12C). Such an example includes the use of ozone for virus inactivation in wastewater reuse where decaying, not residual, ozone is used to determine treatment credit. Model selection would be less important where specific lethality is low (left area of Figure 3.12C) or residual oxidant is used (bottom area of Figure 3.12C). Such examples include the use of monochloramine for *Giardia* or virus inactivation or when residual disinfectant is used in calculating CT (USEPA 1991). This is consistent with a study by Craik (2005), who predicted similar inactivation using the SF, TIS, and MM models when oxidant

decay rate approached zero. If residual oxidant is used, then selecting from PFR t_{10}, TIS, SF, or RN model will be governed by the resources available to the modeler, the ultimate use of the model, and potential detrimental consequences of reactor overdesign (see Chapter 2).

These results demonstrate that two models using the same RTD will produce differing estimates of microbial inactivation based on assumptions about micromixing. Micromixing does not affect model predictions for a single first-order reaction (Levenspiel 1999). However, when multiple reactions occur simultaneously, micromixing is important. The reactor with mixing and without segregation (i.e., TIS) predicted disinfection to be less effective than the reactor without mixing and with segregation (i.e., SF model). When calculating microbial inactivation in reactors with a decaying oxidant, micromixing can have important implications, particularly when high log reductions are required. Micromixing should thus be considered when developing models for multiple reactions or pathogen inactivation by a decaying oxidant.

Model results can also inform the design and modification of disinfection contactors. Although segregated flows are expected to achieve more disinfection than mixed flows, it is not readily apparent how traditional baffling or inlet/outlet modifications could encourage flow segregation. Random packing has recently been proposed as a method to reduce dispersion in water treatment reactors (Barnett et al. 2014, Kattnig and Venayagamoorthy 2015). A similar concept could be employed using structured, tubular packing. Tubular packing could be similar to tube settlers, which have a long history of use in sedimentation (Willis 1978). Packing would likely be made of plastic with zero degrees of inclination. Retrofit or initial design of such packing into disinfection reactors could encourage SF behavior, potentially improving disinfection.

The conclusions for microbial inactivation can also be applied more broadly to other reactive contaminants. This includes predicting the degradation of contaminants such as cyanotoxins and disinfection by-product precursors.

3.5 Conclusions and Recommendations

In this study, temporal disinfectant switching was used to investigate flow segregation and earliness of mixing (i.e., micromixing) in full-scale water treatment reactors. Results presented herein demonstrate that micromixing was significant in the two full-scale clearwells studied, and that assuming flow segregation produced inaccurate predictions of reactive tracer concentrations in some models. Specific findings include:

1. When combined with an accepted kinetic model, hydraulic models that accurately represented micromixing were capable of predicting breakpoint reactions in flow-through reactors at full scale with an acceptable level of accuracy.
2. The TIS model satisfactorily predicted free and combined chlorine species concentrations for both the baffled Clearwell A and the unbaffled Clearwell B. The SF model was the worst performing model. The RN model performed similarly to the TIS model for Clearwell B, but did not perform as well for Clearwell A. This can be attributed primarily to the two segregated flows having significantly different residence times in the RN model for Clearwell A. The MM model provided similar accuracy to the TIS model for an unbaffled clearwell when flow through the reactor was steady, but otherwise produced inaccurate predictions.
3. SF models for both clearwells and the RN model for Clearwell A produced predictions that were closer to observation when segregated flows were modeled to react for 60 minutes following the mixing of segregated flows, but not as close as the TIS model.

4. For a given RTD, reactor models without micromixing (e.g., SF) predicted greater microbial inactivation than reactors with micromixing (e.g., TIS) under the conditions tested: Chick-Watson disinfection kinetics and first-order oxidant decay. Given that significant internal mixing existed in Clearwells A and B, contaminant removal may be overestimated if models do not account for internal mixing. Although microbial inactivation was the focus of this study, these findings are also generalizable to reactive contaminants and precursors.
5. If a slowly-decaying or residual oxidant concentration was used, all models (e.g., TIS, SF, RN) would yield similar predictions of microbial inactivation provided that they similarly represent observed RTD.

ACKNOWLEDGEMENTS

This work was supported by the Larson Aquatic Research Support Scholarship from AWWA, the Abel Wolman Fellowship from AWWA, and the National Defense Science and Engineering Graduate Fellowship.

REFERENCES

Acero, J. L., Rodriguez, E., Meriluoto, J. 2005. Kinetics of reactions between chlorine and the cyanobacterial toxins microcystins. *Water Research*, 39 (8): 1628-1638.

American Public Health Association (APHA). 1992. Standard Methods for the Examination of Water and Wastewater, 18th edition. American Public Health Association, Washington, D.C.

American Water Works Association (AWWA). 2018. 2017 Water Utility Disnfection Survey Report.

Angeloudis, A., Stoesser, T., Falconer, R. A. 2014. Predicting the disinfection efficiency range in chlorine contact tanks through a CFD-based approach. *Water Research*, 60: 118-129.

ChemScan Inc. 1998. ChemScan UV-2150 Series Technical Specification.

Barnett, T. C., Kattnig, J. J., Venayagamoorthy, S. K., Whittaker, G. 2014. Improving the hydraulics of drinking water contact tanks using random packing material. *Journal AWWA*, 106 (2): E98-E104.

Barrett, S. E., Davis, M. K., McGuire, M. J. 1985. Blending chloraminated and chlorinated waters. *Journal AWWA*, 77(1): 50-61.

Clark, R. M. 1998. Chlorine demand and TTHM formation kinetics: a second-order model. *Journal of Environmental Engineering*, 124 (1): 16-24.

Craik, S.A. 2005. Effect of micro-mixing conditions on predictions of *Cryptosporidium* inactivation in an ozone contactor. *Ozone: Science and Engineering*, 27:6: 487-494.

Crittenden, J. C., Trussell, R. R., Hand, D. W., Howe, K. J., & Tchobanoglous, G. 2005. MWH's water treatment: principles and design. 2nd Ed. Hoboken, NJ: John Wiley & Sons.

Deason, R. D., Civardi, J., Woldemariam, E. 2017. Development and Performance of Tracer Study to Improve Water Distribution Operations. 2017 WQTC: Portland, OR.

Deborde, M., Von Gunten, U. 2008. Reactions of chlorine with inorganic and organic compounds during water treatment – kinetics and mechanisms: a critical review. *Water Research*, 42 (1-2): 13-51.

Ducoste, J., Carlson, K., Bellamy, W. 2001. The integrated disinfection design framework approach to reactor hydraulics characterization. *Journal of Water Supply: Research and Technology – AQUA*, 50 (4): 245-261.

El-Fadel, M., Findikakis, A. N., Leckie, J. O. 1996. Numerical modelling of generation and transport of gas and heat in landfills I. Model formulation. *Waste Management & Research*, 14 (5): 483-504.

Fogler, H. S. 2006. *Elements of Chemical Reaction Engineering*. 4th ed. Pearson Education: Boston, MA.

Gandhi, V., Roberts, P. J., Stoesser, T., Wright, H., Kim, J. H. 2011. UV reactor flow visualization and mixing quantification using three-dimensional laser-induced fluorescence. *Water Research*, 45 (13): 3855-3862.

Gandhi, V. N., Roberts, P. J., Kim, J. H. 2012. Visualizing and quantifying dose distribution in a UV reactor using three-dimensional laser-induced fluorescence. *Environmental Science & Technology*, 46 (24): 13220-13226.

Gorzalski, A.S., Harrington, G.W., Coronell, O. 2018. Modeling water treatment reactor hydraulics using reactor networks. *Journal AWWA*, 110 (8): 13-29.

Greene, D.J., Farouk, B., Haas, C.N. 2004. CFD Design Approach for Chlorine Disinfection Processes. *Journal AWWA*, 96 (8): 138-150.

Greene, D. J., Haas, C. N., Farouk, B. 2006. Computational fluid dynamics analysis of the effects of reactor configuration on disinfection efficiency. *Water Environment Research*, 78 (9): 909-919.

Gresch, M., Braun, D., Gujer, W. 2011. Using reactive tracers to detect flow field anomalies in water treatment reactors. *Water Research*, 45 (5): 1984-1994.

Henze, M., Gujer, W., Mino, T., van Loosdrecht, M. C. M. 2000. Activated sludge models ASM1, ASM2, ASM2d and ASM3. IWA Publishing.

Jafvert, C. T., Valentine, R. L. 1992. Reaction scheme for the chlorination of ammoniacal water. *Environmental Science & Technology*, 26 (3): 577-586.

Kattnig, J. J., and Venayagamoorthy, S. K. 2015. A Hybrid Approach for Increasing Baffling Factors in Contact Tanks. *Journal AWWA*, 107 (12): E702-E711.

Kiil, S., Michelsen, M. L., Dam-Johansen, K. 1998. Experimental investigation and modeling of a wet flue gas desulfurization pilot plant. *Industrial & Engineering Chemistry Research*, 37 (7): 2792-2806.

Kim, D., Nemlioglu, S., Roberts, P. J., Kim, J. H. 2010a. Ozone-contactor flow visualization and quantification using three-dimensional laser-induced fluorescence. *Journal AWWA*, 102 (1): 90-99.

Kim, D., Elovitz, M., Roberts, P. J., Kim, J. H. 2010b. Using 3D LIF to investigate and improve performance of a multichamber ozone contactor. *Journal AWWA*, 102 (10): 61-70.

Laurent, J., Samstag, R. W., Ducoste, J. M., Griborio, A., Nopens, I., Batstone, D. J., Wiks, J. D., Saunders, S., Potier, O. 2014. A protocol for the use of computational fluid dynamics as a supportive tool for wastewater treatment plant modelling. *Water Science and Technology*, 70 (10): 1575-1584.

Levenspiel, O. 1999. *Chemical Reaction Engineering*. 3rd ed. New York: Wiley and Sons.

Oh, S. H., Cavendish, J. C. 1985. Mathematical modeling of catalytic converter lightoff. Part III: Prediction of vehicle exhaust emissions and parametric analysis. *AIChE Journal*, 31 (6): 943-949.

Luh, J., Mariñas, B. J. (2014). Kinetics of bromochloramine formation and decomposition. *ES&T*, 48 (5): 2843-2852.

Najm, I.; Brown, N.P.; Gramith, K.; Hargy, T. 2009. Validating Disinfection in Ozone Contactors. Water Research Foundation. Denver, CO.

Pfeiffer, V., Barbeau, B. 2014. Validation of a simple method for predicting the disinfection performance in a flow-through contactor. *Water Research*, 49: 144-156.

R Core Team. 2016. R: A language and environment for statistical computing. R Foundation for Statistical Computing, Vienna, Austria. URL https://www.R-project.org/.

Saunier, B. M., Selleck, R. E. 1979. The kinetics of breakpoint chlorination in continuous flow systems. *Journal AWWA*, 71(3): 164-172.

Soetaert, K., Petzoldt, T., Setzer, R. W. 2010. Solving differential equations in R: package deSolve. *Journal of Statistical Software*, 33 (9): 1-25.

Teefy, S.M., Singer, P.C. 1990. Performance and Analysis of Tracer Tests to Determine Compliance of a Disinfection Scheme with the SWTR. *Journal AWWA*, 82 (12): 88-98.

Teefy, S. 1996. Tracer Studies in Water Treatment Facilities: A Protocol and Case Studies. AWWA Research Foundation. Denver, CO.

United States Environmental Protection Agency (USEPA). 1991. Guidance manual for compliance with the filtration and disinfection requirements for public water systems using surface water sources. Washington, DC.

United States Environmental Protection Agency (USEPA). 2010. Long Term 2 Enhanced Surface Water Treatment Rule Toolbox Guidance Manual. Washington, DC.

Von Gunten, U. 2003. Ozonation of drinking water: Part II. Disinfection and by-product formation in presence of bromide, iodide or chlorine. *Water Research*, 37 (7): 1469-1487.

Vikesland, P. J., Ozekin, K., & Valentine, R. L. 2001. Monochloramine decay in model and distribution system waters. *Water Research*, 35 (7): 1766-1776.

Vikesland, P. J., Love, N. G., Chandran, K., Fiss, E. M., Rebodos, R., Zaklikowski, A.E., DiGiano, F.A., Ferguson, B. 2006. Seasonal Chlorination Practices and Impacts to Chloraminating Utilities. AWWA Research Foundation. Denver, CO.

Wicklein, E., Batstone, D. J., Ducoste, J., Laurent, J., Griborio, A., Wicks, J., Saunders, S., Samstag, R., Potier, O., Nopens, I. 2015. Good modelling practice in applying computational fluid dynamics for WWTP modelling. *Water Science and Technology*, 73 (5): 969-982.

Willis, R. M. 1978. Tubular settlers—A technical review. *Journal AWWA*, 70 (6): 331-335.

CHAPTER 4 - IMPACT OF MODEL SELECTION ON PREDICTED CONTAMINANT DEGRADATION IN FULL-SCALE WATER TREATMENT REACTORS

4.1 Introduction

The modeling of contaminant removal is fundamental to the design, operation, and regulation of reactive contaminants in water treatment processes. The concentrations of microbial contaminants in finished drinking water are typically too low to be reliably measured (USEPA 1992). For this reason, regulations for enteric viruses, *Giardia*, and *Cryptosporidium* are not based on observed finished water concentrations. Instead, treatment (i.e., log reduction value, LRV) requirements are based on risk assessment, and treatment credits are provided based on pathogen inactivation models (USEPA 2010, USEPA 2008, USEPA 1991). The acceptable level of risk in surface water systems has been defined as one case of illness per 10,000 people per year (USEPA 1992), and water reuse requirements typically have targeted this same population health risk (Amoueyan et al. 2017, WateReuse Colorado 2018, TWDB 2015, USEPA 2017).

Modeling of contaminant oxidation has also proven to be useful for contaminants of emerging concern (CECs), such as cyanotoxins (Gorzalski et al. 2017, Stanford et al. 2016). Cyanotoxins can occur in the absence of a visible cyanobacterial bloom (Westrick and Szlag 2018), complicating attempts to develop triggered monitoring strategies based on bloom observation. Current analytical methods for cyanotoxins also have limitations in terms of sensitivity and specificity (Guo et al. 2017, Westrick and Szlag 2018), providing further motivation for the development of models to assess the efficacy of oxidative treatment barriers.

Contaminant degradation is a function of four factors: reaction kinetics, residence time distribution (RTD), degree of segregation, and earliness of mixing (Levenspiel 1999). If reaction kinetics are assumed to be first order, such as for Chick-Watson inactivation kinetics used in disinfection regulations (USEPA 2010, 1991) or cyanotoxin degradation when oxidant concentration is constant (Acero et al. 2005, Rodríguez et al. 2007b), degree of segregation and earliness of mixing can be ignored (Fogler 2005, Levenspiel 1999, Chapter 3). Reaction modeling is then only a function of reaction kinetics and RTD. For pathogen regulations, reaction kinetics are typically provided in the form of CT tables (USEPA 2010, 1991), where CT is the product of disinfectant concentration (C) and contact time (T). For cyanotoxins, extensive studies of reaction kinetics are available in the literature (Acero et al. 2008, Acero et al. 2005, Onstad et al. 2007, Rodríguez et al. 2007a, Rodríguez et al. 2007b, Rodríguez et al. 2007c). As demonstrated in Chapter 2, RTD information can be gained through tracer studies (Crittenden et al. 2012, Gorzalski et al. 2018, Teefy 1996), empirical models relating RTD to reactor geometry (Crozes et al. 1999, Porter et al. 2018), or computational fluid dynamics (Wols et al. 2010, Zhang et al. 2014).

For over 25 years, the plug flow reactor (PFR) t_{10} model for RTD has been the standard reactor model used in pathogen inactivation regulations (USEPA 2010, USEPA 1991). Limitations of the PFR t_{10} model have been well-documented, including how it tends to underestimate pathogen inactivation at low LRVs and overestimate pathogen inactivation at high LRVs as discussed in Chapter 2 (Gorzalski et al. 2018, Lawler and Singer 1993, Pfeiffer and Barbeau 2014). Alternative frameworks for calculating disinfection efficacy were developed, which used reactor models such as the axial dispersion, tanks-in-series (TIS), segregated flow (SF), and reactor network (RN) models (Bellamy et al. 1998, Carlson et al. 2001, Najm et al.

2009, Chapter 2). The maximum mixedness model yields equivalent predictions to the SF model when oxidant concentration is constant (Craik 2005, Pfeiffer and Barbeau 2014), and therefore is not discussed here. Despite the plethora of models developed, validating models with observed data has proven difficult, even at pilot scale (Pfeiffer and Barbeau 2014). The models that most closely represent observed results also tend to vary between studies (Haas et al. 1998, Najm et al. 2009, Pfeiffer and Barbeau 2014, Smeets et al. 2006, Tang et al. 2005). In the absence of a consistently verifiable alternative, the PFR t_{10} model has continued to be applied not just for the disinfection of surface water (USEPA 2010, USEPA 1991), but water reuse as well (Olivieri et al. 2016, Pecson et al. 2017).

Water reuse requires greater pathogen LRVs, both in overall treatment trains and individual unit processes, due to elevated pathogen concentrations in wastewater effluent. California requires 12/10/10-log reduction of viruses, *Cryptosporidium*, and *Giardia* (CA SWRCB 2018, WateReuse Colorado 2018), while Texas requires a minimum of 8/5.5/6-log for these pathogens which can be increased based on source concentrations (WateReuse Colorado 2018, TWDB 2015). Both states target one illness per 10,000 people per year (WateReuse Colorado 2018, USEPA 2017), but LRV requirements differ due to assumed starting points for treatment (i.e., raw wastewater in California, treated wastewater effluent in Texas (WateReuse Colorado 2018)). These higher overall reductions are also accompanied by higher LRVs in unit process. California allows for up to 6-log reduction in each treatment barrier (CA SWRCB 2018), while Texas allows 5-log reduction for ozone disinfection of viruses, with greater reductions potentially being approved on a site-specific basis (TWDB 2015). At these higher LRVs, it is unclear whether the PFR t_{10} model would underestimate or overestimate treatment performance.

The potential for short-circuiting to compromise disinfection efficacy at high LRVs (e.g., 6-log) has been recognized in recent studies (Olivieri et al. 2016, Pecson et al. 2017). It has been advised that evidence of reactor hydraulics be provided when crediting high LRVs (Olivieri et al. 2016). However, the PFR t_{10} model is still being used in risk assessments crediting 6-log reduction through oxidation processes (Pecson et al. 2017). There is a lack of quantitative guidance regarding LRVs at which PFR t_{10} should be used, and limited examples of how LRV prediction is affected by reactor model selection (e.g., PFR t_{10} versus TIS, SF, RN).

Reactor model selection is not only important for predicting pathogen inactivation, but also for CECs that are susceptible to oxidation. CECs such as NDMA precursors (Krasner et al. 2013), numerous endocrine disrupting compounds (Westerhoff et al. 2005), and cyanotoxins (Rodríguez et al. 2007b) are susceptible to oxidation. Cyanotoxins are of particular interest because they have resulted in ‘do not use’ orders in multiple US cities as well as drinking water advisories internationally (Davis et al. 2019), have well-studied degradation kinetics (Acero et al. 2008, Acero et al. 2005, Onstad et al. 2007, Rodríguez et al. 2007a, Rodríguez et al. 2007b, Rodríguez et al. 2007c), and have reaction rates that vary over orders of magnitude depending on the toxin and oxidant of interest. Given increased interest in predictive modeling for cyanotoxin oxidation (Gorzalski et al. 2017, Stanford et al. 2016), the effect of reactor model selection on predicted degradation warrants further investigation.

The objective of this work was to perform a quantitative evaluation of how reactor model selection affects prediction of contaminant degradation across a range of different reactor types and sizes, and to use this knowledge to provide guidance on reactor model selection for different LRVs. Results are presented here to:

i) quantify the level of treatment (e.g., CT) that would be required using different reactor models,
ii) calculate the log reductions at which the PFR t_{10} model is conservative,
iii) estimate the impacts of reactor model selection on reactor capital costs, and
iv) provide quantitative guidance on conditions where predictions of treatment efficacy are sensitive to reactor model selection.

The conclusions from this analysis are intended to inform the design, operation, and regulation of water treatment reactors.

4.2 Modeling Methods

4.2.1 Reactor Models

Five different reactor models were used in this work: PFR, PFR t_{10}, TIS, SF, and RN. The PFR model assumes all water spends the same amount of time in the reactor. That time is equal to the average hydraulic residence time, τ [min], which is defined as V/Q where V is the reactor volume [gal] and Q [gal·min^{-1}] is the volumetric flow rate. The PFR t_{10} model similarly assumes that all water spends the same amount of time in the reactor, but that time is assumed to be equal to the time it takes the first ten percent of flow to exit the reactor, t_{10}, rather than τ. The baffle factor (B_F), calculated as t_{10}/τ, was obtained from tracer data and t_{10} was obtained from the product of B_F and τ. The TIS reactor consists of a finite number of continuous flow stirred tank reactors (CSTRs) arranged in series (Levenspiel 1999). Although a wide variety of RN models can be constructed, a single RN model was used in this study. The RN model used consisted of two TIS reactors in parallel (one TIS reactor on each parallel flow path), which was shown in Chapter 2 to accurately fit tracer data from numerous water treatment reactors. TIS and RN models were fit to tracer data using nonlinear least squares regression as described elsewhere

(Chapter 2). The SF model consists of PFRs with differing τ arranged in parallel; details on the SF model are provided elsewhere (Chapter 2, Najm et al. 2009).

The maximum mixedness model was excluded because it yields equivalent predictions to the SF model when oxidant concentration is constant (Craik 2005, Pfeiffer and Barbeau 2014).

4.2.2 Tracer Studies and Data Correction

Data sets from tracer studies using conservative, non-reactive tracers for 35 water treatment reactors were gathered from the literature (see Table C.1 in APPENDIX C). Reactor types included clearwells, chlorine contactors, ozone contactors, filters, and clarifiers. For reactors with multiple tracer data sets, a single representative tracer was selected. All tracer data were converted to normalized step dose tracer plots of F/F_0 versus Θ, where F/F_0 is the observed tracer concentration divided by step dose tracer concentration and $\Theta = t/\tau$. It was assumed that all reactors had closed boundary conditions, meaning that flow elements can only enter and exit the reactor one time (i.e., plug flow upstream and downstream). As was discussed in detail in Chapter 2 (see also Figure C.1 and corresponding discussion in the APPENDIX C), fitting of RN models to tracer data indicated that overestimation of flow and/or underestimation of volume potentially occurred in a majority of tracer studies reported in the literature. Such tracer studies had normalized reactor volume (V_{norm}), conceptualized as the volume needed to fit a model to tracer data divided by the actual total volume of the reactor, that exceeded unity. For any tracer study where fitting with the RN model produced $V_{norm} > 1.05$, Θ was divided by V_{norm} to correct the data set.

4.2.3 Calculating Contaminant Removal Using the Damköhler Number

This work is limited to reactions that are first order with respect to the contaminant of

interest and the oxidant concentration is constant. Many reactions in water treatment can be described as being second order overall, first order with respect to a contaminant N (mg·L^{-1} or organisms·L^{-1}) and first order with respect to an oxidant C (mg·L^{-1}) as given by

$$\frac{dN}{dt} = -kCN, \quad 4.1$$

where k (L·mg^{-1}·min^{-1}) is the second-order rate constant. Note that Equation 4.1 applies only to batch reactors. Common reactions described by this rate law include organisms that are disinfected according to Chick-Watson kinetics (Crittenden et al. 2012) and the oxidation of cyanotoxins (Acero et al. 2005, Onstad et al. 2007, Rodríguez et al. 2007c, 2007b).

Assuming oxidant concentration does not vary with time, integrating Equation 4.1 for a batch reactor produces

$$\ln\left(\frac{N}{N_0}\right) = -kCt, \quad 4.2$$

where t is reaction time (min). To calculate pathogen removal in a PFR, the batch reaction time (t) is replaced with the reactor residence time (τ). Lawler and Singer (1993) used the dimensionless parameter $kC\tau$ to describe the extent of disinfection in PFR, CSTR, and TIS reactors. $kC\tau$ can be calculated easily for any treatment plant or operating conditions (Lawler and Singer 1993).

The parameter $kC\tau$ is analogous to the Damköhler number (Da), a generalized term used to compare the rate of reaction to the rate of transport in flow-through reactors (Fogler 2005). The Damköhler number is calculated as

$$Da = \frac{\text{reaction rate}}{\text{mass transport rate}} = \frac{-rV}{\dot{m}}, \quad 4.3$$

where r is the reaction rate (mg·min·L^{-1}), and $\dot{m}$ is the mass flow rate (mg·min^{-1}). For the first-order reaction with constant oxidant concentration described above, *Da* becomes

$$Da = \frac{-rV}{\dot{m}} = \frac{-kCNV}{QN} = -kC\tau, \quad 4.4$$

When *C* is constant, the rate constant becomes pseudo first order such that

$$k' = -kC, \quad 4.5$$

where *k'* (min^{-1}) is the pseudo first-order rate constant, and the expression for *Da* becomes

$$Da = \frac{-rV}{\dot{m}} = \frac{-k'NV}{QN} = -k'\tau, \quad 4.6$$

From Equation 4.2, the equation for contaminant removal in a batch reactor would become

$$\ln\left(\frac{N}{N_0}\right) = -k't. \quad 4.7$$

Both $kC\tau$ and $k'\tau$ yield the same unitless parameter (i.e., *Da*), thus yielding equivalent results.

Table 4.1 shows contaminant degradation equations as a function of *Da* for both ideal (e.g., PFR, CSTR) and non-ideal (e.g., TIS, SF, RN) reactor models. These equations apply only

to conditions where the oxidant concentration is constant and reaction kinetics are first order with respect to the contaminant of interest.

Table 4.1. Contaminant degradation equations for PFR, PFR t_{10}, TIS, SF, and RN models. These equations assume that the reaction is first-order with respect to the contaminant of interest.

Reactor Model	**Constant Oxidant** $\frac{N}{N_0} =$
PFR	e^{-Da}
PFR t_{10} [a]	$e^{-B_F Da}$
TIS [b]	$\frac{1}{\left(1+\frac{V_{TIS} Da}{n}\right)^n}$
SF [c]	$\sum\left[\left(\frac{F}{F_0}\right)_2 - \left(\frac{F}{F_0}\right)_1\right] e^{-Da\frac{\theta_1+\theta_2}{2}} + \left[\left(\frac{F}{F_0}\right)_3 - \left(\frac{F}{F_0}\right)_2\right] e^{-Da\frac{\theta_2+\theta_3}{2}} + \cdots$
RN (parallel TIS)	$Q_1 \frac{1}{\left(1+\frac{Da V_{TIS,1}}{n_1 Q_1}\right)^{n_1}} + Q_2 \frac{1}{\left(1+\frac{Da V_{TIS,2}}{n_2 Q_2}\right)^{n_2}}$

[a] Baffle factor (B_F) equal to t_{10}/τ. [b] V_{TIS} indicates volume fraction(s) found through non-linear regression. [c] F and F_0 indicate observed output and input step dose tracer concentrations, respectively.

4.2.4 Cyanotoxin Oxidation

The *Da* for the oxidation of microcystin, cylindrospermopsin, and anatoxin-a by free chlorine was calculated from Clearwell 1A operations data. Operations data were collected on an hourly basis over a three-year period and included parameters such as clearwell volume, flow rate, pH, temperature, and chlorine residual. The reaction rate constant *k* was calculated as a function of temperature and pH according to kinetic models from the literature for microcystin (MC) (Acero et al. 2005) and cylindrospermopsin (CYL) (Rodríguez et al. 2007c). Microcystin was assumed to be in the form of the MC-LR congener. The rate constant for anatoxin-a (ANA) was set equal to a value obtained from the literature at pH 7 and 25°C (Rodríguez et al. 2007c); adjustments for pH and temperature were not available from the literature (Stanford et al. 2016).

4.2.5 Disinfection Kinetics

To use the *Da* concept for disinfection, *k* was calculated from CT tables provided by USEPA. This calculation was performed as (Lawler and Singer 1993)

$$k = \frac{-\ln\left(\frac{N}{N_0}\right)}{Ct} = \frac{-\ln(10)\times\log_{10}\left(\frac{N}{N_0}\right)}{Ct}. \quad 4.8$$

For example, USEPA uses the Chick-Watson model to describe the inactivation of microorganisms by chlorine (USEPA 1991) and ozone (Clark et al. 2002, USEPA 2010, 1991). Alternative kinetic models have been tested (Driedger et al. 2001, Li et al. 2003, Oppenheimer et al. 2000), including the Hom model, but were not found to result in significant improvement in model fit (Clark et al. 2002), and thus the Chick-Watson model was used in this study. The inactivation of *Cryptosporidium*, *Giardia*, and virus by ozone can be modeled according to (USEPA 2010)

$$Log\ Credit_{Cryptosporidium} = 0.0397 \times (1.09757)^{Temp} \times CT, \quad 4.9$$

$$Log\ Credit_{Giardia} = 1.0380 \times (1.0741)^{Temp} \times CT, \quad 4.10$$

and

$$Log\ Credit_{virus} = 2.1744 \times (1.0726)^{Temp} \times CT, \quad 4.11$$

where *C* is ozone concentration (mg·L^{-1}), *Temp* is temperature (˚C), and *T* is contact time (min) (USEPA 2010). From Equations 4.9 – 4.11, the expression for *k* for each pathogen can be expressed as

$$k_{Cryptosporidium} = \ln(10) \times 0.0397 \times (1.09757)^{Temp}, \quad 4.12$$

$$k_{Giardia} = \ln(10) \times 1.0380 \times (1.0741)^{Temp}, \quad 4.13$$

and

$$k_{virus} = \ln(10) \times 2.1744 \times (1.0726)^{Temp}. \quad 4.14$$

For pathogens that follow Chick-Watson kinetics, *k* has units of $L \cdot mg^{-1} \cdot min^{-1}$ and is referred to as the specific lethality coefficient.

4.2.6 Model Accuracy

This work compares predictions from different reactor models but does not provide physical validation. Contaminant degradation was assumed to occur according to kinetics shown in Equation 4.1, as indicated in published literature and required by regulation as described above. Analyses have been restricted to first-order and pseudo-first-order reactions, and therefore the accuracy of model predictions is assumed to be a function only of the hydraulic model's accuracy in representing observed RTD. Model accuracy in representing RTD increases as follows: PFR t_{10} < TIS < SF ≈ RN (Chapter 2). Therefore, any discussion of model accuracy in this study pertains to the model's accuracy in representing RTD rather than physical validation.

4.2.7 Cost Analysis

An analysis was conducted to determine how model selection would affect capital costs of constructing water treatment facilities. Models of capital costs for water treatment unit processes are available in the literature (Clark and Dorsey 1982, McGivney and Kawamura 2008, Sethi and Clark 1998). This work used the cost estimating manual from McGivney and

Kawamura (2008). Their cost models were indexed to September 2007 in Los Angeles, CA (Engineering News Record Construction Cost Index = 8889). No attempt was made to update costs for the current year or to make location-specific adjustments. Instead, changes in capital costs were calculated on a percentage basis (rather than absolute dollars) depending on the change in required *Da*.

The three capital costs studied were ozone generation equipment, ozone contactor construction, and clearwell construction (below ground). Ozone generation and contactor construction costs were both reported to be power functions with respect to generator capacity and contactor volume, respectively, while the cost of clearwell construction was linear with respect to volume (McGivney and Kawamura 2008). The design parameters were assumed to fall in the middle of the range of data from which the cost functions in the manual (McGivney and Kawamura 2008) were developed: 1755 lb/day of ozone generation capacity, 0.21 million gallon ozone contactor, and 4 million gallon clearwell. Differences in cost were compared between the PFR t_{10} model, which is commonly used in disinfection regulation (USEPA 2010, USEPA 1991), and the RN model, which accurately represents observed RTD (see Chapter 2).

Required *Da* to achieve 1-log and 6-log reduction were calculated using the PFR t_{10} and RN models. Because *Da* increases linearly with increasing C and τ (see Equation 4.4), percent difference in required *Da* between the PFR t_{10} and RN models corresponds to the same percent difference in either C (e.g., ozone generation) or τ (e.g., contactor or clearwell volume) under a given set of reaction conditions (i.e., k) and flow rates (i.e., $Q = V/\tau$). Percent change in cost was calculated from the change in C or τ (i.e., change in *Da*) using the cost curves described above (McGivney and Kawamura 2008). This allowed comparison of cost between the PFR t_{10} and RN models.

Percent changes in ozone generation and contactor costs were similar for a given change in required *Da* because the two cost curves are power functions to a similar exponent (difference of 0.5%) (McGivney and Kawamura 2008). For this reason, percent change in costs were reported as an average of the two percent changes (i.e., ozonation).

All 35 tracer data sets were used for both the ozone cost analysis and the clearwell cost analysis regardless of reactor type. All tracer data was used to maximize the number of data points available and capture the widest range of RTDs.

4.3 Results and Discussion

Results are presented in a progression from applied case studies to analyses inclusive of all 35 reactors. Case studies are provided for cyanotoxin oxidation and pathogen inactivation using different RTD models. Effect of model selection is then discussed in more generalizable terms, using *Da* in place of specific contaminants. Analyses are presented to define the conservative range of the PFR t_{10} model, followed by the impact of model selection on the sizing of oxidation facilities and associated capital costs. Finally, guidance is presented on the ranges of *Da* in which reactor selection is important; outside of these ranges *Da* is either too low to achieve the target log reduction or sufficiently high that the target log reduction is likely to be predicted by all reactor models.

4.3.1 Cyanotoxin Oxidation – Clearwell 1A Case Study

The impact of model selection on predicted contaminant degradation was investigated using cyanotoxins as illustrative contaminants of interest. A chlorinated clearwell (i.e., Clearwell 1A) was used as an illustrative treatment barrier. Clearwell 1A was selected for this case study because the authors had access to operations data, while for most reactors only tracer data were

available from the literature. The analysis involved calculating *Da* across three years of varying operating conditions, comparing *Da* for three toxins that had chlorine reaction rates which varied by over three orders of magnitude, and comparing predictions of log degradation with the levels needed for public health protection.

Figure 4.1 shows the cumulative distribution of *Da* values for microcystin, cylindrospermopsin, and anatoxin-a over a three-year period and Figure 4.2 shows predicted log reduction versus *Da* using different model types. The range of *Da* observed in Figure 4.1 for each individual cyanotoxin can be explained by variability in operating conditions (e.g., temperature, pH, residence time, chlorine concentration), while the differences between cyanotoxins is a result of different reactivities with chlorine (i.e., *k*). For a given *Da*, different models yield different predictions of LRV. At *Da* <14.3 and LRV <2.7, the PFR t_{10} model underestimates LRV relative to the TIS, SF, and RN models. At higher *Da* and LRV, the PFR t_{10} model overestimates LRV relative to the TIS, SF, and RN models. Observed *Da* (Figure 4.1) can be combined with predictions of contaminant degradation (Table 4.1, Figure 4.2) to draw conclusions about the efficacy of treatment and importance of reactor model selection.

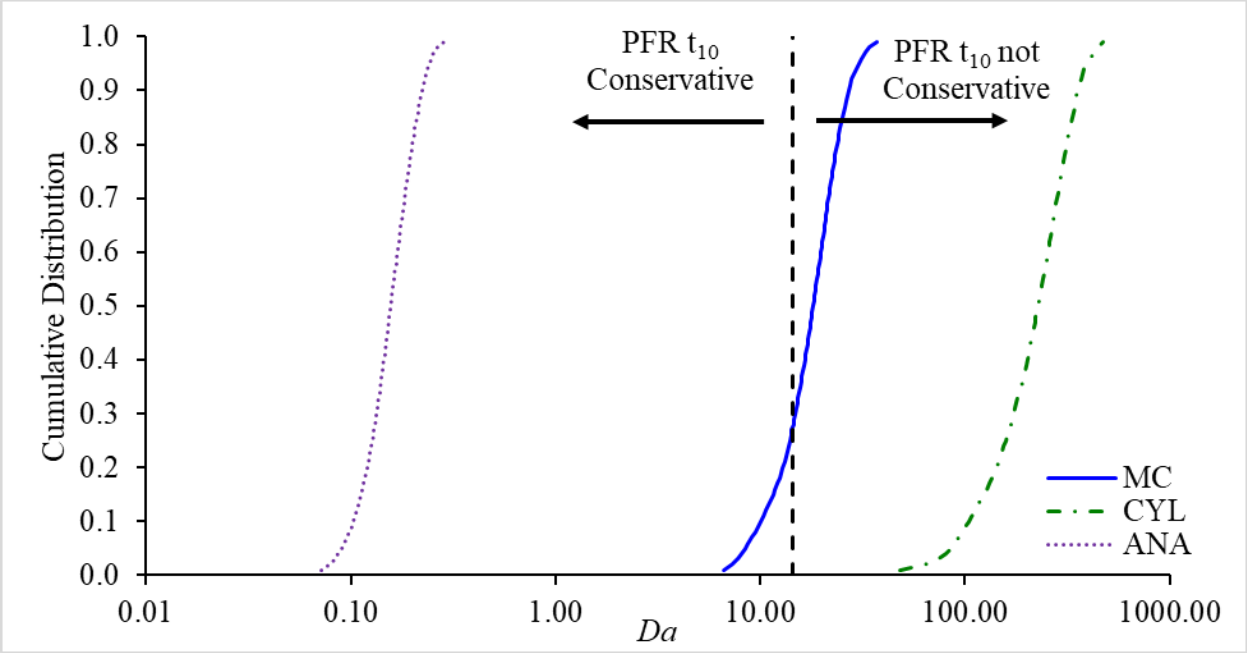

Figure 4.1. Cumulative distribution of values of *Da* in Clearwell 1A over a 3-year period for microcystin (MC), cylindrospermopsin (CYL), and anatoxin (ANA).

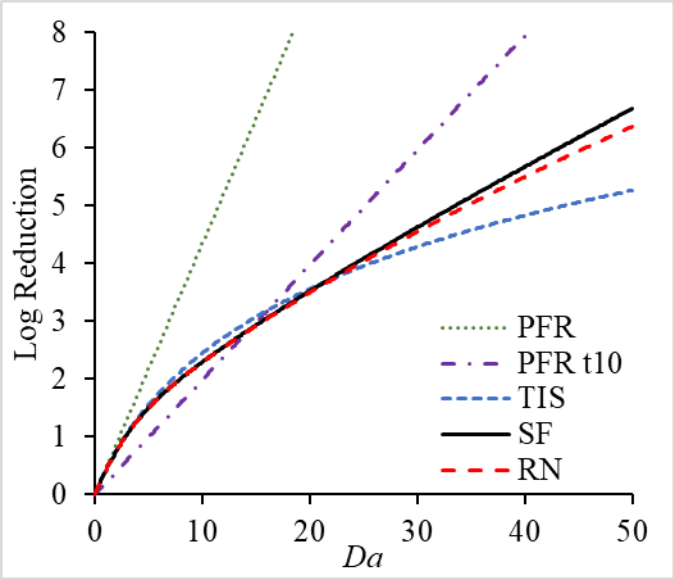

Figure 4.2. Predicted log reduction in Clearwell 1A versus *Da* for different reactor models.

Anatoxin-a is not particularly susceptible to degradation by free chlorine, and had a median *Da* of 0.16, for which no model would predict more than a 15% reduction in this clearwell (data not shown, see equations in Table 4.1). Thus, because chlorine was not an

effective barrier to anatoxin-a, the selection of model was not particularly important for predicting anatoxin-a oxidation in Clearwell 1A (see *Da* = 0.16 in Figure 4.2). This is an example of how low reactivity can render model selection unimportant.

Compare this to cylindrospermopsin, which is more susceptible to chlorine oxidation and had a median *Da* of 227.2. At this level of treatment all models would predict >8-log removal in this clearwell. Reducing the highest observed concentration (4.4 µg/L) in the National Lake Assessment to below the 0.7 µg/L health advisory level for children less than 6 years of age (USEPA 2015) would require only 0.8-log reduction. Therefore, the selection of hydraulic model was not particularly important for predicting the oxidation of cylindrospermopsin in Clearwell 1A. This is an example of how high reactivity (coupled with a low required LRV) can render model selection unimportant.

Microcystin-LR was a cyanotoxin for which the selection of reactor model was important. The PFR t_{10} model ceases to be conservative relative to other reactor models at a *Da* of 14.3, which is within the observed operating range of Clearwell 1A for microcystin-LR. Table 4.2 shows the predicted log removal of microcystin at typical and design flows (see caption for description of flow conditions) using the PFR t_{10} and TIS models. At typical flows, reductions in microcystin-LR were predicted to be ≥ 3.27-log (99.95%) for all models. Results were similar for all models except the PFR (see Figure 4.2) and also indicate a robust treatment barrier for the toxin. At design flows, the five models yielded differing predictions. The PFR t_{10} model predicted 0.57-log (73%) reduction, while the TIS, SF, and RN models predicted approximately 1-log (90%) reduction. These differences increased further when the rate constant was reduced by 50%, as might occur at higher pH or lower temperature (Acero et al. 2005), or if contaminant removal is measured using the enzyme-linked immunosorbent assay (ELISA) method rather than

liquid chromatography with tandem mass spectrometry (He et al. 2017). Under these conditions, the PFR t_{10} model would have predicted a 0.29-log (48%) reduction in toxin concentration, while the TIS, SF, and RN models would have predicted 0.57-log (73%) reduction.

Table 4.2. Predicted log removal of microcystin-LR by chlorine in Clearwell 1A using five reactor models under typical flows, design flows, and design flows with *k* reduced by 50%.

Model	Typical Flows	Design Flows	Design Flows, 0.5**k*
PFR	7.79	1.26	0.63
PFR t_{10}	3.57	0.57	0.29
TIS	3.38	1.03	0.57
SF	3.29	1.01	0.57
RN	3.27	1.01	0.57

Note: All three conditions were assumed to operate at 20˚C and pH 7.5 with effluent chlorine residual was assumed to be 4 $mg \cdot L^{-1}$. Typical flows were considered to be 100 MGD with the clearwell containing 5.5 MG. At typical flows the *Da* equal to 17.94 was approximately equal to median value from Figure 4.1. Plant design capacity is 225 MGD, and the clearwell was assumed to contain 2 MG due to high demands under the design flows condition (*Da* = 2.90). The third column uses *Da* = 1.45 which uses the same design flows, but reduces *k* by 50% as might occur at higher pH, lower temperatures, or the use of a different analytical method (i.e., enzyme-linked immunosorbent assay) from that used to establish reaction kinetics (i.e., liquid chromatography with tandem mass spectrometry)(He et al. 2017).

4.3.2 Disinfection with Ozone – Contactor 5A Residual Oxidant

The previous section focused on evaluating the effect of model selection on predictions of the degradation of cyanotoxins (as case study contaminants) based on observed *Da*. This analysis was complemented by investigating the effect of model selection on predictions of the CT (i.e., *Da*) required to inactivate pathogens. An ozone contactor was selected because ozone is effective for *Cryptosporidium*, *Giardia*, and viruses, while chlorination is not effective for *Cryptosporidium* (USEPA 2010) . Ozone Contactor 5A was specifically chosen because it was used in a study focused on validating disinfection models (Najm et al. 2009). Predicted log reduction was first calculated based on *Da* using the equations in Table 4.1, and then required CT to achieve a given LRV was calculated using different reactor models (Equations 4.4 and 4.9 – 4.11).

Log reductions predicted by the PFR, PFR t_{10}, TIS, SF, and RN models as a function of *Da* are shown in Figure 4.3. The TIS, SF, and RN models produced similar predictions up to approximately 3-log reduction. At higher LRVs, greater discrepancies are observed, with the RN model being the most conservative. The PFR model was the least conservative, and the PFR t_{10} model ceased to be conservative at higher LRVs.

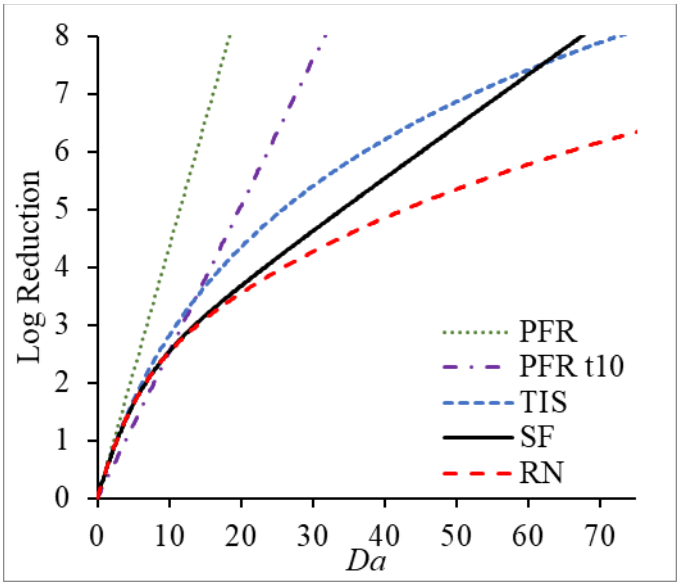

Figure 4.3. Predicted log reduction in Ozone Contactor 5A versus *Da* for different reactor models.

Table 4.3 shows the *Da* that would be required for ozone contactor 5A to achieve different LRVs using the PFR t_{10} and RN models, as well as the corresponding CT values, at 20˚C. To achieve a given LRV, the PFR t_{10} model requires greater *Da* and CT up to LRV = 2.53-log (*Da* = 10), above which the RN model requires greater *Da* and CT (Figure 4.3).

Table 4.3. Required CT to achieve different target log reductions for *Cryptosporidium*, *Giardia*, and virus in ozone contactor 5A at 20˚C. Required *Da* was determined from Figure 4.3 and CT required was calculated by dividing *Da* by the *k* shown in Equations 4.12 – 4.14.

			CT Required (mg·min·L^{-1})					
Log Reduction	***Da* Required**		***Cryptosporidium***		***Giardia***		**Virus**	
	PFR t10	**RN**	**PFR t10**	**RN**	**PFR t10**	**RN**	**PFR t10**	**RN**
0.5	2.0	1.3	3.4	2.2	0.2	0.1	0.1	0.1
1.0	4.0	2.8	6.8	4.8	0.4	0.3	0.2	0.1
2.0	8.0	6.8	13.6	11.6	0.8	0.7	0.4	0.3
3.0	11.9	14.0	20.2	23.8	1.2	1.4	0.6	0.7
4.0	15.9	26.0	27.0	44.2	1.6	2.6	0.8	1.3
5.0	19.8	42.9	33.7	72.9	2.0	4.3	1.0	2.1
6.0	23.8	65.7	40.5	111.7	2.4	6.6	1.2	3.2

This has important implications for how disinfection systems are designed. For example, consider the assigning of disinfection credit in a water reuse system. A recent quantitative microbial risk assessment by Pecson et al. (2017) credited 6 logs of *Giardia* and virus removal when adequate ozone CT was achieved for 1-log *Cryptosporidium* credit. This is consistent with regulatory requirements, and appears conservative using the PFR t_{10} model. The PFR t_{10} model would require a CT of 6.8 mg·min·L^{-1} for 1-log *Cryptosporidium*, which is much higher than the 2.4 and 1.2 mg·min·L^{-1} required for 6-log *Giardia* and virus credit.

However, the PFR t_{10} model provides false confidence in the factor of safety for 6-log *Giardia* and virus credit compared to the RN model. The PFR t_{10} model CT value for 1-log *Cryptosporidium* corresponds to factors of safety of 2.9 and 5.8 for 6-log *Giardia* and virus, respectively. However, these factors of safety are reduced to 1.0 and 2.1 for *Giardia* and virus, respectively, when considering the CT required for 6-log credit using the RN model: 6.6 and 3.2 mg·min·L^{-1}. Therefore, design, operation, or regulation of 6-log *Giardia* or virus inactivation

based on 1-log *Cryptosporidium* credit is not recommended for this reactor.

If disinfection credit is not sought for *Cryptosporidium*, systems practicing water reuse may still target 6-log credit for *Giardia* and virus. In order to get this credit by using the PFR t_{10} model for Ozone Contactor 5A, a CT of 2.4 mg·min·L^{-1} would be needed. However, if the RN model were used to get this credit, a CT of 6.6 mg·min·L^{-1} would be required, 2.76 times higher CT for the same LRV. The RN model is assumed to be more accurate than the PFR t_{10} model as described in Chapter 2 and Section 4.2.6 above. Therefore, the use of the PFR t_{10} model may result in significant underdesign of *Da* for disinfection (or operation at insufficient CT), potentially providing insufficient public health protection. Use of the PFR t_{10} model for designing, operating, or crediting 6-log pathogen reduction is not recommended for this reactor.

The discrepancy between the PFR t_{10} and RN models is not limited to water reuse and may also impact conventional and direct filtration systems. Consider that conventional systems are required to achieve 0.5-log *Giardia* and 2.0-log virus credit by disinfection, while direct filtration systems must achieve 1.0-log *Giardia* and 3.0-log virus credit. For Ozone Contactor 5A, the RN model would require 35% and 30% lower CT for 0.5- and 1.0-log *Giardia* credit compared with the PFR t_{10} model. For virus credit, required CT would be 15% lower for 2.0-log credit, but 18% higher for 3.0-log credit using the RN model compared to the PFR t_{10} model. Thus, the RN model could allow systems to operate at lower CT when required LRV is low, but would require systems to operate at higher CT when target LRV is high. Regulators should consider the use of a more accurate RTD model, such as the RN model, when approving designs for new processes or reevaluating treatment efficacy for existing processes (i.e., required CT for a target LRV).

4.3.3 Relationship Between Log Reduction and *Da* for Various Reactor Models

The preceding sections provided examples of how predicted LRV for a given *Da* and required *Da* for a target LRV are dependent on the reactor model used to represent the RTD. A similar analysis was performed for all 35 reactors, and this section discusses the corresponding results. Figure 4.4 shows plots of log reduction versus *Da* for the PFR, PFR t_{10}, TIS, SF, and RN models for three example reactors. Plots for all 35 reactors are included in Figure C.2 through Figure C.6 of APPENDIX C. As expected, the PFR model predicts the highest log reduction for any given *Da*. PFR t_{10} predicts the lowest log reduction up to a given *Da* that varies from reactor to reactor. At higher *Da*, the PFR t_{10} model predicts more removal than the TIS, SF, and RN models.

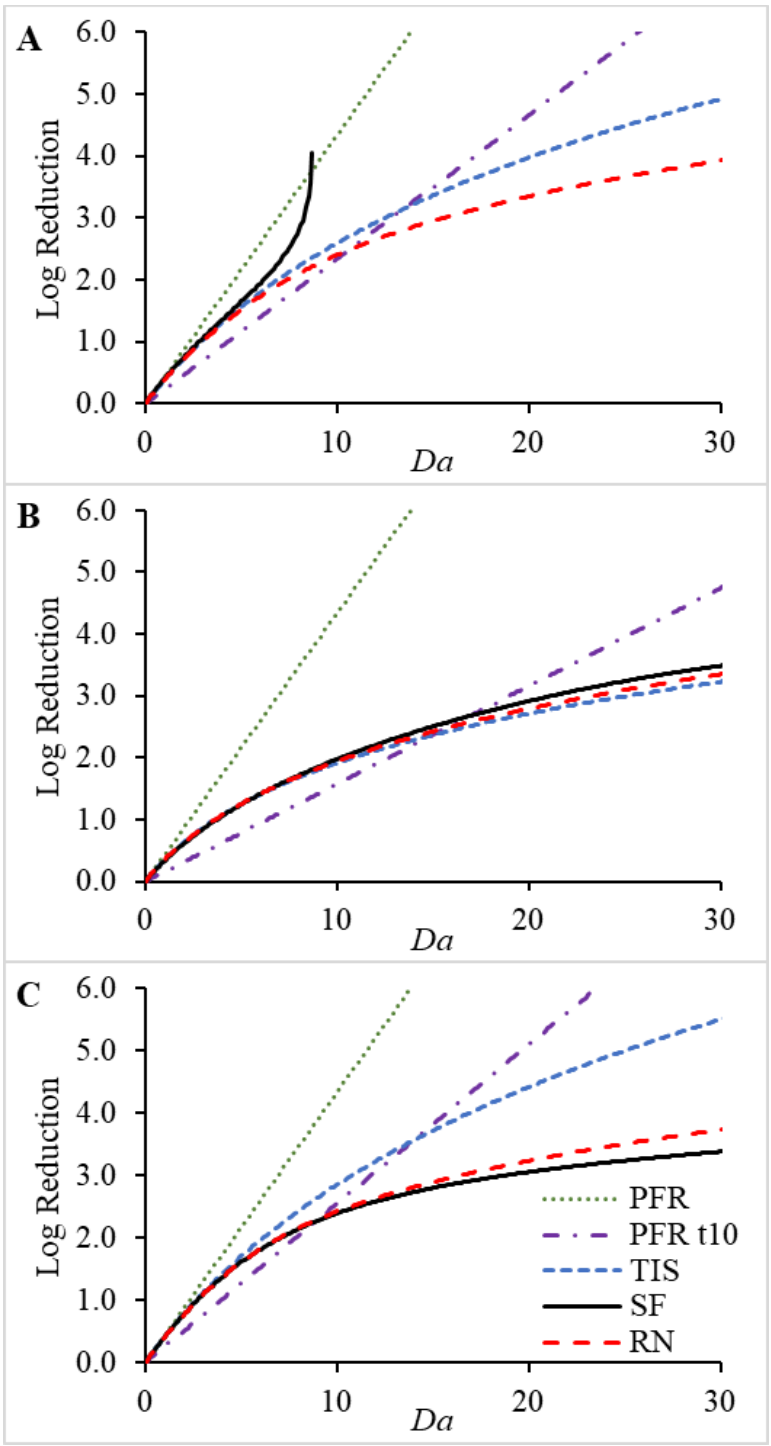

Figure 4.4. Log reduction versus *Da* plots for three example reactors. Selected reactors provide examples where (A) SF model produces errant predictions due to nonmonotonic tracer data, (B) TIS, SF, and RN models yield similar predictions, and (C) TIS model predictions differ significantly from SF and RN models. APPENDIX C contains these plots for all 35 reactors, and panels (A), (B), and (C) correspond to reactors 3H, 3F, and 5B shown in Figure C.3 in APPENDIX C.

For some reactors, the LRV predicted by the SF approached infinity when *Da* exceeded a certain threshold (e.g., Figure 4.4A). This is an artifact resulting from nonmonotonic tracer data. When the observed tracer concentration decreases, particularly early in the tracer run, the SF model predicts negative contaminant concentrations for that particular PFR, which when summed with the other hypothetical PFRs produces an errantly high prediction of log reduction. Nonmonotonic tracer curves could result from fluctuating background concentrations of the tracer or from inaccuracies in measuring tracer concentrations. This should be considered a limitation of the SF model: it should not be used for nonmonotonic tracer data due to erroneous predictions that become increasingly significant above a threshold *Da* or log reduction.

Predictions of log reduction for TIS, SF, and RN models were similar at lower log reductions, with differences in predictions occurring at higher log reductions. This indicates that the higher the target LRV, the more important the selection of reactor model. Depending on the observed RTD and the corresponding fit of reactor models, the TIS may yield similar predictions to the more complex RN and SF models as shown in Figure 4.4B. However, there were also reactors where the TIS model did not have the same flexibility to represent the observed RTD, resulting in predictions that differed significantly from the SF and RN models (e.g., Figure 4.4C).

Box and whisker plots were created to visualize the range of *Da* required for the 35 reactors to achieve a target log reduction using different models. These results, shown in Figure 4.5, excluded the PFR and SF models. The PFR model was excluded because it underestimates required *Da* (see Figure 4.2 through Figure 4.4), and the SF model was excluded due to the issue with nonmonotonic tracer data discussed earlier (Figure 4.4A and corresponding discussion). The results shown in Figure 4.5 are applicable to any first-order reaction where oxidant concentration

is constant. At low log reductions such as 0.5-log, higher *Da* would be required if the PFR t_{10} model was used than if the TIS or RN models were used. This supports the use of the PFR t_{10} model in disinfection regulation when conservative reactor design and operation is desirable for LRVs of 0.5.

At higher log reductions, the TIS and RN models require higher *Da* than the PFR t_{10} model. For example, the median values of *Da* for the TIS and RN models were approximately twice as high as for the PFR t_{10} model when targeting 6-log reduction. Because the TIS and RN models more accurately represent RTD than the PFR t_{10} model, especially at the lower residence time portions of the RTD curve (Chapter 2), the TIS and RN models are more appropriate for processes targeting 6-log reduction. This finding should inform the selection of RTD model in the design and regulation of disinfection, particularly in water reuse applications where higher log reductions are required.

The PFR t_{10}, TIS, and RN models required similar *Da* at 3.0-log, but significantly different *Da* at 0.5-log or 6.0-log (see Figure 4.5). The log reduction versus *Da* figures in APPENDIX C show that predictions from the PFR t_{10}, TIS, and RN models often intersect around 2.0- to 4.0-log. The PFR t_{10} model predictions are likely most accurate in this range. The following section will examine at what log reduction the PFR t_{10} model ceases to be conservative, which is also the point at which it is most accurate (i.e., produces the same prediction as the RN model).

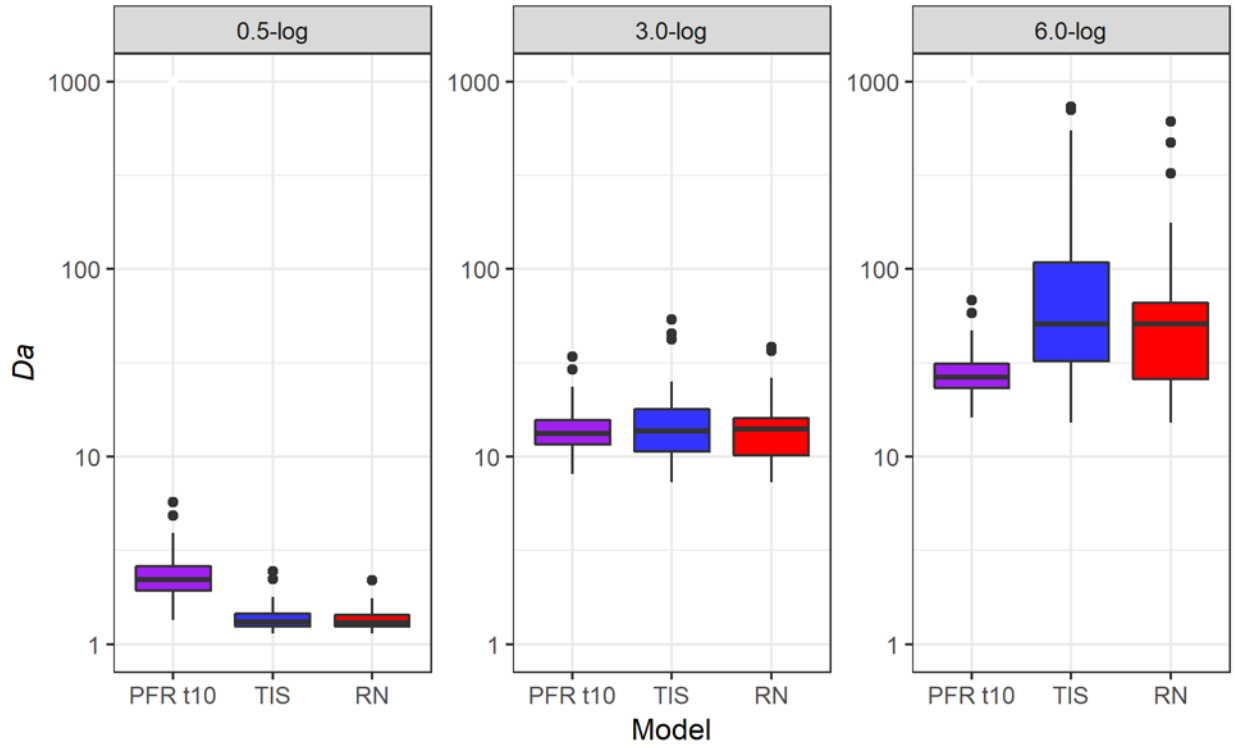

Figure 4.5. Required *Da* to achieve different log reductions using PFR t_{10}, TIS and RN models. Note that of 35 reactors, one at the 6-log treatment target would require values of *Da* greater than 1000 using the RN model, and thus is not shown on the plot. This box and whiskers plot provides the 25th percentile, median, and 75th percentile as horizontal lines. The vertical lines represent observations that are within 1.5 times the interquartile range. Individual data points are outliers that are outside the range represented by the vertical lines.

4.3.4 Conservative Range of PFR t_{10}

The LRV where PFR t_{10} ceased to be conservative was defined as the point at which the PFR t_{10} and RN models yield the same predictions. At lower LRVs, the PFR t_{10} model would predict less degradation than the RN model, and at higher LRVs, PFR t_{10} would predict more degradation. The RN model was used as a reference for accuracy given that it can accurately represent RTD observed by tracer studies as demonstrated in Chapter 2. Four example reactors and their log reduction intersections are shown in Figure 4.6. All four have similar t_{10}/τ baffle factors (0.55-0.58) but different log reduction intersections (2.5- to 4.6-log). Tracer data and fitted RN models are shown in Figure 4.6A – Figure 4.6D, along with log reduction versus *Da*

for both PFR t_{10} and RN models in Figure 4.6E– Figure 4.6H. When the tracer was observed to leave the reactor earlier in the tracer run (e.g., Figure 4.6D, Figure 4.6H), PFR t_{10} ceased to be conservative at lower LRVs (i.e., 2.5-log). In contrast, reactors where tracer concentration was not observed in the effluent until later in the tracer run (e.g., Figure 4.6B, Figure 4.6F), PFR t_{10} ceased to be conservative at relatively high LRVs (i.e., 4.6-log). These results illustrate that the higher the target LRV, the more important a small percentage of flow breakthrough becomes.

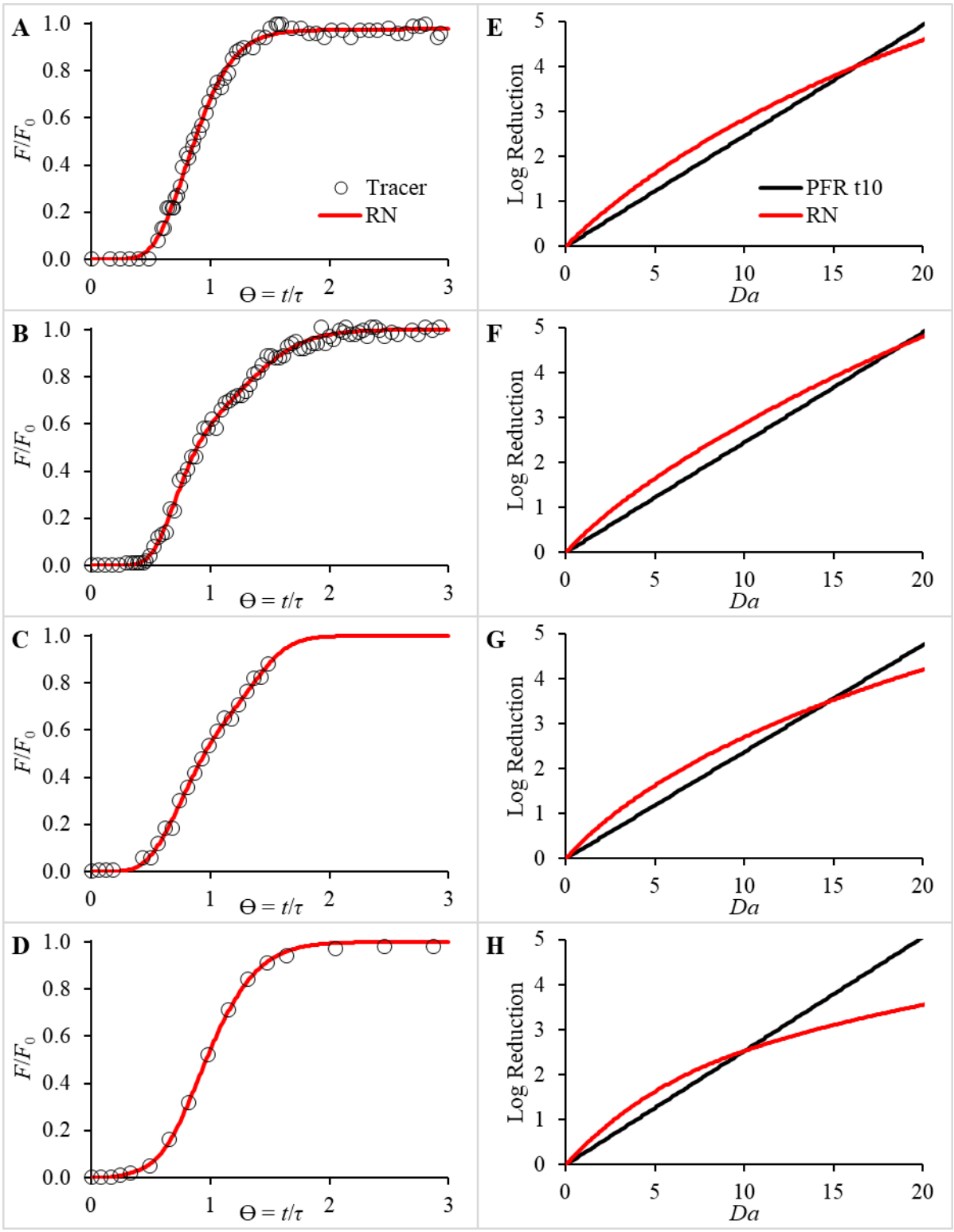

Figure 4.6. Tracer data and log reduction intersection. Tracer data and RNM model fit (A-D) with log reductions predicted by PFR t_{10} and RN models (E-H).

Figure 4.7 shows the log reduction intersection for 35 reactors versus different metrics for earliness of tracer breakthrough (t_{10}/τ, t_5/τ, t_1/τ, $t_{0.1}/\tau$). Log reduction intersection varied significantly, between 2.1- and 11.4-log. Ninety percent of reactors had log reduction intersections less than 5.5-log, and 30% had log reduction intersections less than or equal to 3.0-log. This indicates significant variability in the range of contaminant degradation at which PFR t_{10} ceases to be conservative. Despite this variability, none of the 35 reactors analyzed had a log reduction intersection less than 2.0-log. Thus, the PFR t_{10} model can be assumed to be conservative up to 2.0-log, and it is advisable to test an additional reactor model when designing or calculating higher log reductions.

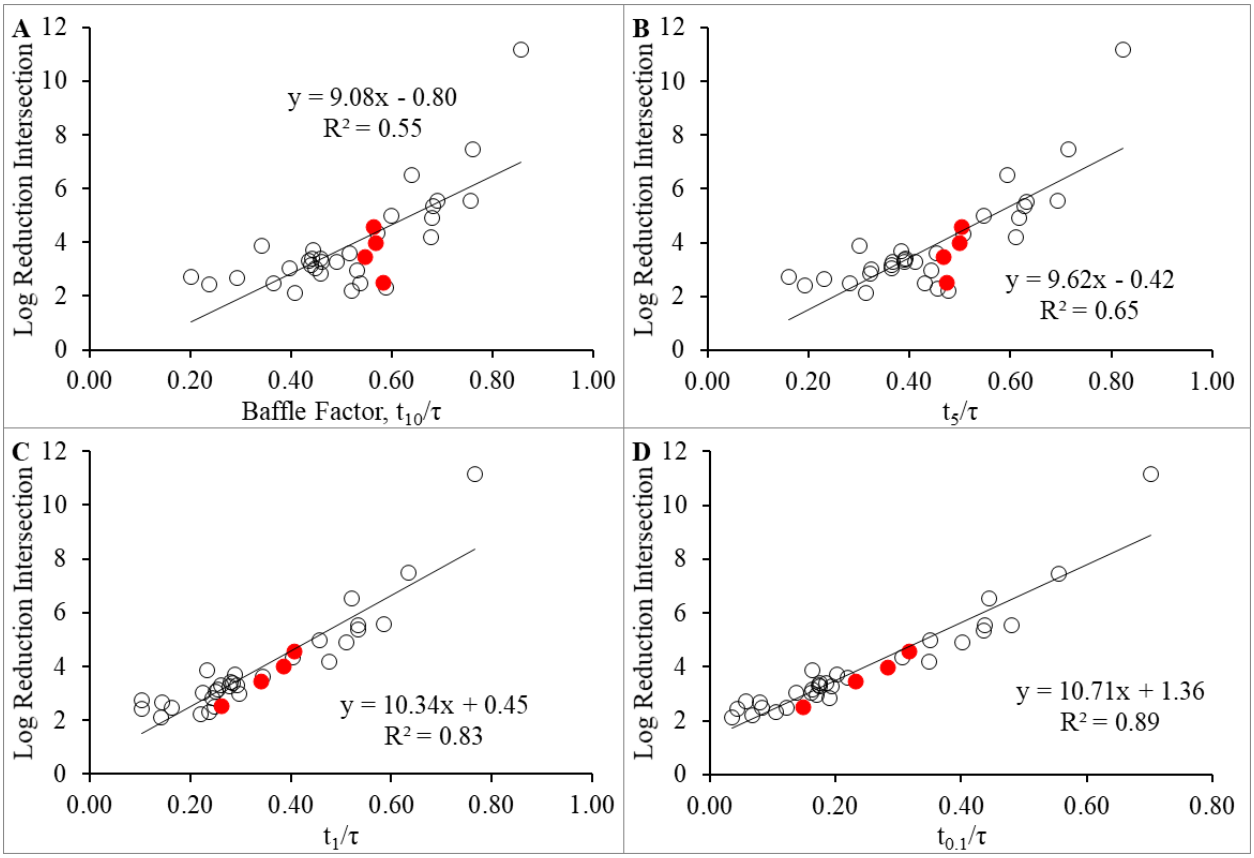

Figure 4.7. Correlation between log reduction intersection and t_{10}/τ (A), t_5/τ (B), t_1/τ (C), and $t_{0.1}/\tau$ (D). Filled red circles indicate the reactors shown in Figure 4.6 and open circles represent the other 31 reactors.

Figure 4.7 also shows that the strength of correlation between log reduction intersection and flow parameter increased with decreasing fractions of flow (i.e., $t_{0.1}/\tau$ had the strongest correlation). The four example reactors in Figure 4.6 are represented by filled red circles in Figure 4.7. For these example reactors, it was observed that log reduction intersection was poorly correlated with t_{10}/τ and t_5/τ, but correlated well with t_1/τ and $t_{0.1}/\tau$. This is consistent with the finding for the 35 reactors overall, where 10%, 5%, 1%, and 0.1% of tracer breakthrough can explain 55%, 65%, 83%, and 89% of the observed variation (see R^2 values in Figure 4.8).

The relatively high correlation observed between log reduction intersection and $t_{0.1}/\tau$ suggests that when targeting high log reductions, $t_{0.1}$ is more important in characterizing reactor performance than t_{10}. This may add complexity to conducting tracer studies, as differentiating a 0.1% increase in common tracer substances (e.g., fluoride) from background concentrations is much more difficult than differentiating 10% of step dose tracer concentration. For this reason, accounting for low residence time portions of flow in disinfection calculations would likely require fitting an appropriate RTD model to tracer data.

Findings in this section have important implications for the regulation, and subsequently design and operation, of water treatment reactors. When targeting LRVs >2-log, the use of alternative RTD models such as TIS, SF, or RN should be considered. The use of the PFR t_{10} model may overestimate reactor performance at higher LRVs.

4.3.5 Cost Analysis

The previous section showed how the use of TIS and RN models in place of the PFR t_{10} model would result in lower *Da* requirements at low LRVs, but higher *Da* requirements at higher LRVs. The purpose of this section is to estimate how facility capital costs might be affected by

model selection. Specifically, the PFR t_{10} and RN models are compared for contaminant reductions of 1-log and 6-log.

Figure 4.8 shows how capital costs would increase using the PFR t_{10} model relative to the RN model when designing for 1-log degradation. This can also be conceptualized as the cost of using a conservative model (i.e., PFR t_{10}) rather than an accurate model (i.e., RN). Cost increases are plotted versus t_5/τ because t_5/τ had the strongest correlation to cost increases of any of the flow parameters tested in the previous section (i.e., t_{10}/τ, t_5/τ, t_1/τ, and $t_{0.1}/\tau$). For 1-log degradation, ozonation capital costs are estimated to be 9% to 73% higher with a median of 35% using the PFR t_{10} model rather than the RN model, while clearwell costs would be estimated to be 12% to 80% higher with a median of 45%. This finding is consistent with the conclusion reached by Lawler and Singer (1993) that the PFR t_{10} model used in the SWTR may be unnecessarily costly for many water treatment plants.

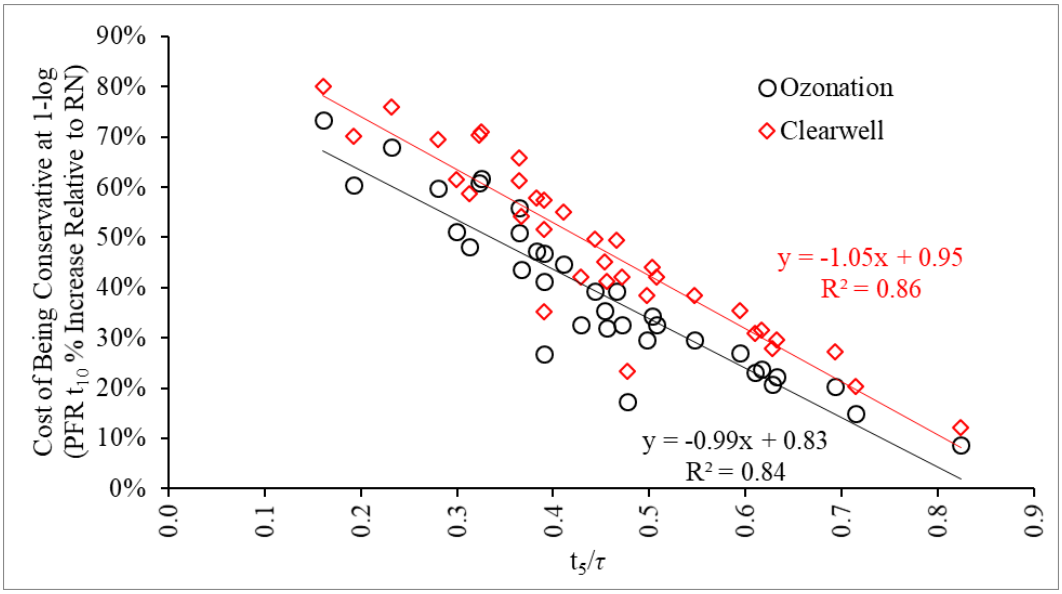

Figure 4.8. Additional capital cost that would result from using the PFR t_{10} model relative to the RN model when designing for 1-log reduction, plotted versus t_5/τ. The PFR t_{10} model is conservative at 1-log reduction, and thus the additional cost of using the PFR t_{10} model relative to the RN model represents the cost of using a conservative model.

The cost of being conservative had an inverse linear relationship with t_5/τ where the t_5/τ parameter can explain 84%-86% of the variability in cost increase. This indicates that using the PFR t_{10} model is most costly in reactors with the greatest short-circuiting (i.e., closer to CSTR than PFR behavior). In other words, the use of the RN model in place of the PFR t_{10} model could result in the greatest cost savings for reactors that have generally poor baffling. Even if the overall size of the reactor were not reduced (e.g., clearwell storage requirements dictate design volume rather than disinfection), use of the RN model could reduce the number of baffle walls required, thereby reducing cost.

Using the PFR t_{10} model is more costly than the RN model at low LRVs, but using the PFR t_{10} is less costly than the RN model at higher LRVs. This is because the PFR t_{10} model predicts greater log reductions for a given *Da* than the TIS, SF, and RN models when LRV is high as demonstrated earlier. Accurately modeling RTD with a RN model would increase the cost of clearwells and ozone contactors as shown in Figure 4.9. For 6-log degradation, using a RN model in place of the PFR t_{10} model would increase the cost of ozonation processes by as much as 254%, with a median of 37%. For clearwells, the cost would be expected to increase by as much as 557%, with a median of 57%. Caution should be used in interpreting cost increases >100%, as these values were extrapolated outside the range of observed cost data used by McGivney and Kawamura (2008) to develop cost curves. Note that for the three reactors with log reduction intersections >6-log, RN models would reduce the cost by 2%-6%.

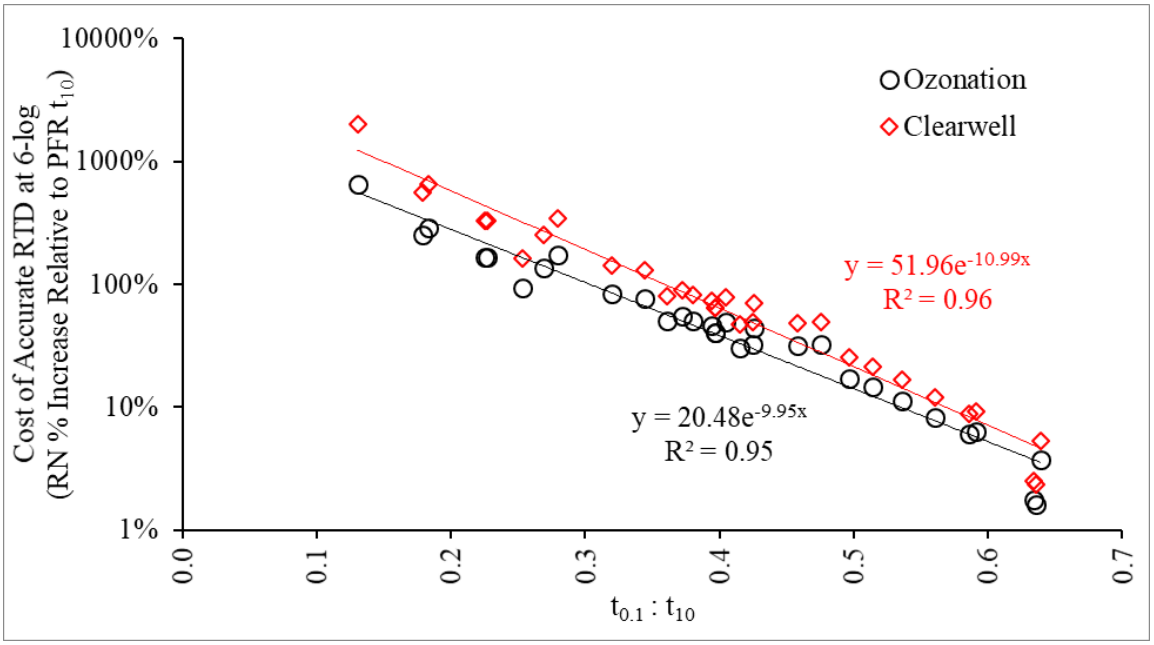

Figure 4.9. Additional capital cost that would result from using the RN model in place of the PFR t_{10} model when designing for 6-log reduction, plotted versus the ratio of $t_{0.1}$:t_{10}. The PFR t_{10} model is generally not conservative at 6-log reduction, and using an accurate RTD model like the RN model would increase capital cost. Note that data are only included for 31 of 35 reactors. Three reactors had log reduction intersections >6-logs and they produced negative cost increases (i.e., cost decrease), and one reactor required *Da* > 1,000 to achieve 6-log reduction which was outside the range tested. Caution should be used in interpreting cost increases >100%, as these values were extrapolated outside the range of observed data used by McGivney and Kawamura (2008) to develop cost curves.

For some reactors with early tracer breakthrough, the increase in cost would be large enough to potentially make the treatment process impractical. For example, increased contactor and clearwell sizes might exceed available site footprint, or push process design toward UV disinfection for chlorine-resistant pathogens like *Giardia* and *Cryptosporidium*. The use of an accurate RTD model such as the RN model may limit the feasible LRV in any individual reactor unless reactor hydraulics can be improved (e.g., achieve $t_{0.1}$ similar to t_{10}).

When target LRV is high and RTD differs significantly from plug flow, it may be more cost-effective to arrange reactors in series. Consider a target 4-log reduction for the reactor shown in Figure 4.4C. A *Da* of 37 would be required in a single reactor. However, 2-log

reduction requires only a *Da* of 7. Arranging two 2-log reactors in series would provide 4-log reduction with a total *Da* of 14, which is 62% lower than a *Da* of 37 that would be required if 4-log reduction was sought in a single reactor.

The increase in cost that would result from using the RN model is log linear with respect to the ratio of $t_{0.1}$:t_{10} (Figure 4.9). The ratio of $t_{0.1}$:t_{10} can explain 95%-96% of the observed variability in cost increase. The cost increase is expected to be less than 10% when the ratio of $t_{0.1}$:t_{10} is greater than or equal to 0.6. Likewise, the cost increase is expected to be greater than or equal to 100% when the ratio of $t_{0.1}$:t_{10} is less than or equal to 0.3. This supports the finding from the previous section that when designing reactors for high log reductions (e.g., 6-log), lower residence time portions of the RTD become increasingly important.

4.3.6 Guidance on the Range of *Da* at which Model Selection is Important

An objective of this work was to define a range of *Da* at which model selection is important for assessing treatment efficacy. For each reactor, the maximum *Da* required between the PFR t_{10}, TIS, and RN models to achieve a given LRV is shown in Figure 4.10. This was considered a reasonable representation of the range of reactors used in water treatment given the number (35) and variety of reactors studied. Outliers were identified using the box and whisker plots shown in Figure C.7 in APPENDIX C. The estimated bounds for the importance of *Da* are also show in Figure 4.10. The lower bound is equal to ideal PFR performance. The upper bound is equal to the maximum non-outlier observation. *Da* can be calculated for any first order reaction and compared to Figure 4.10. If a reactor has a *Da* below the lower bound, it will fail to meet the target log reduction regardless of the reactor model used. Similarly, for any of the non-outlier reactors studied, if the reactor has a *Da* above the upper bound it will be predicted to achieve the target log reduction regardless of the reactor model used. Only *Da* within these

ranges requires modeling for most reactors.

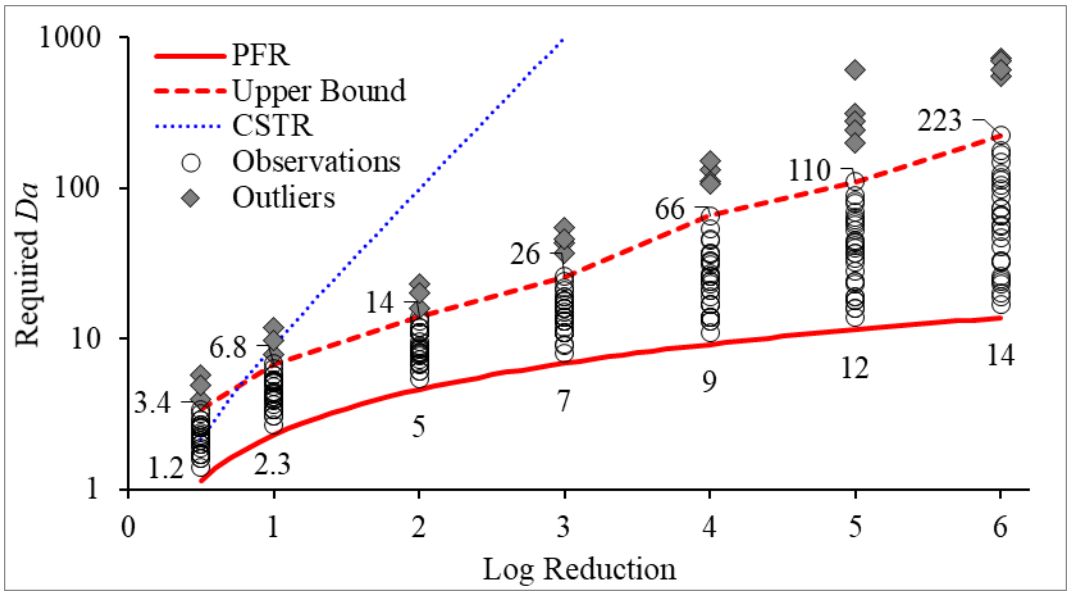

Figure 4.10. Range of *Da* in which model selection is important. Outliers were identified using the box and whisker plots shown in Figure C.7 in APPENDIX C. Black circles indicate observations of the worst-case *Da* (i.e., maximum *Da* required between the PFR t10, TIS, and RN models) for each of 35 reactors that were not outliers. Estimated bounds at which model selection is important are shown by the solid and dashed red lines. Lower bound is equal to the required *Da* for an ideal PFR, and upper bound indicates the highest observed *Da* for non-outlier reactors. Below the lower bound of *Da*, target log inactivation will not be achieved regardless of the model selected. Above the upper bound *Da*, target log reduction would be achieved in all non-outlier reactors. Note that one observation for 6-log reduction is not included due to required *Da* > 1,000.

Consider the *Da* results from the Clearwell 1A case study. The median *Da* was 0.16 for anatoxin-a, too low to achieve 0.5-log reduction even in a PFR. The median *Da* of 227.2 for cylindrospermopsin would be sufficient to obtain > 6-log reduction in the reactors studied. For these two cyanotoxins, the potential for contaminant removal could be quickly assessed without performing reactor modeling.

Another example is virus disinfection with free chlorine. For a groundwater at 10˚C and pH 6-9, the specific lethality coefficient (i.e., *k* of disinfection) is equal to 1.5 $L \cdot mg^{-1} \cdot min^{-1}$. If 4-log disinfection were desired for compliance with the Groundwater Rule (USEPA 2008), the

required CT in a pipeline (assumed by regulation to be a PFR) would be only Da / k = 9.2 / 1.5 $L \cdot mg^{-1} \cdot min^{-1}$ = 6.1 $mg \cdot min \cdot L^{-1}$. However, if that disinfection occurred in a tank with a RTD differing from the ideal PFR, the required CT may be as high as Da/k = 66 / 1.5 $L \cdot mg^{-1} \cdot min^{-1}$ = 44 $mg \cdot min \cdot L^{-1}$ depending on the observed RTD and reactor model used.

This analysis also demonstrates that deviation from plug flow becomes increasingly important at higher log reductions. The ratio of upper bound to lower bound is approximately 3.0 at log reductions of 0.5-, 1,0-, and 2.0-log. This indicates that even for high-dispersion reactors, the CT required would be only 3.0 times higher than for a PFR. However, at 4.0-, 5.0-, and 6.0-log reduction, the ratio of upper bound to lower bound is 7, 10, and 16, respectively. Thus, designing reactors to achieve RTD similar to a PFR is more important at high log reductions than low log reductions.

This guidance may allow for rapid screening of treatment efficacy without performing reactor modeling. For contaminants with known k and processes with known CT, Da can be calculated and compared to Figure 4.10.

4.4 Conclusions and Recommendations

The results and analyses presented in this work support the following conclusions and recommendations:

1. When designing for log reductions >2-log, hydraulic models that more accurately represent RTD should be considered, including TIS, SF, or RN models.
2. Metrics of earliness of tracer breakthrough such as t_1 and $t_{0.1}$ better characterize reactor performance than the commonly used t_{10} when targeting high log reductions.

3. This work estimated the ranges of *Da* at which reactor modeling is important for target log reductions between 0.5-log and 6.0-log reduction. Below these *Da* ranges, reactors will not achieve the target performance. Above these *Da* ranges, the reactor will achieve the target performance with a high degree of confidence, regardless of the reactor model used.
4. The use of a more accurate model such as the RN model may reduce capital costs compared to the PFR t_{10} model when designing for low log reductions (e.g., 1-log). However, using the RN model may result in significantly higher costs at higher log reductions (e.g., 6-log), particularly if the ratio of $t_{0.1}$:t_{10} is small.

ACKNOWLEDGEMENTS

This work was supported by the Abel Wolman Fellowship from AWWA and the National Defense Science and Engineering Graduate Fellowship. The authors thank Keith Stewart for sharing tracer data from an extensive study conducted by the Washington State Department of Health.

REFERENCES

Acero, J.L., Rodríguez, E., Majado, M.E., Sordo, A., Meriluoto, J. 2008. Oxidation of microcystin-LR with chlorine and permanganate during drinking water treatment. *J. Water Supply Res. Technol. - AQUA*, 57 (6): 371–380.

Acero, J.L., Rodriguez, E., Meriluoto, J. 2005. Kinetics of reactions between chlorine and the cyanobacterial toxins microcystins. *Water Research*, 39 (8): 1628–1638.

Amoueyan, E., Ahmad, S., Eisenberg, J.N.S., Pecson, B., Gerrity, D. 2017. Quantifying pathogen risks associated with potable reuse: A risk assessment case study for Cryptosporidium. *Water Research*, 119: 252–266.

Bellamy, W.D., Finch, G.R., Haas, C.N. 1998. Integrated Disinfection Design Framework. Water Research Foundation, Denver, CO.

CA SWRCB. 2018. Regulations Related to Recycled Water.

Carlson, K., Pier, D., Bellamy, W., Carlson, M., Ducoste, J., Amy, G., Rakness, K. 2001. Implementation of the Integrated Disinfection Design Framework. Water Research Foundation, Denver, CO.

Clark, R.M., Dorsey, P. 1982. A model of costs for treating drinking water. *Journal AWWA*, 74 (12): 618–627.

Clark, R.M., Sivaganesan, M., Rice, E.W., Chen, J. 2002. Development of a Ct equation for the inactivation of Cryptosporidium oocysts with ozone. *Water Research*, 36 (12): 3141–3149.

Craik, S.A. 2005. Effect of micro-mixing conditions on predictions of Cryptosporidium inactivation in an ozone contactor. *Ozone Sci. Eng.*, 27 (6): 487–494.

Crittenden, J.C., Trussell, R.R., Hand, D.W., Howe, K.J., Tchobanoglous, G. 2012. Water Treatment: Principles and Design, 3rd ed. John Wiley & Sons, Inc., Hoboken, NJ.

Crozes, G.F., Hagstrom, J.P., Clark, M.M., Ducoste, J., Burns, C. 1999. Improving Clearwell Design for CT Compliance. AWWA Research Foundation, Denver, CO.

Davis, T.W., Stumpf, R., Bullerjahn, G.S., McKay, R.M.L., Chaffin, J.D., Bridgeman, T.B., Winslow, C. 2019. Science meets policy: A framework for determining impairment designation criteria for large waterbodies affected by cyanobacterial harmful algal blooms. *Harmful Algae*, 81 (8): 59–64.

Driedger, A.M., Rennecker, J.L., Mariñas, B.J. 2001. Inactivation of Cryptosporidium parvum oocysts with ozone and monochloramine at low temperature. *Water Research*, 35 (1): 41–48.

Fogler, H.S. 2005. Elements of Chemical Reaction Engineering, 4th ed. Pearson Education, Boston, MA.

Gorzalski, A.S., Harrington, G.W., Coronell, O. 2018. Modeling Water Treatment Reactor Hydraulics Using Reactor Networks. *Journal AWWA*, 110 (8): 13–29.

Gorzalski, A.S., Harrington, G.W., Hayden, A.L., Spiesman, A.L., Coronell, O. 2017. Real-Time Modeling of Cyanotoxin Oxidation in Clearwells, in: AWWA Water Quality Technology Conference. Portland, OR.

Guo, Y.C., Lee, A.K., Yates, R.S., Liang, S., Rochelle, P.A. 2017. Analysis of microcystins in drinking water by ELISA and LC/MS/MS. *Journal AWWA*, 109 (3): 13–25.

Haas, C.N., Joffe, J., Heath, M., Jacangelo, J., Anmangandla, U. 1998. Predicting Disinfection Performance in Continuous Flow Systems from Batch Disnfection Kinetics. *Water Science and Technology*, 38 (6): 171–179.

He, X., Stanford, B.D., Adams, C., Rosenfeldt, E.J., Wert, E.C. 2017. Varied influence of microcystin structural difference on ELISA cross-reactivity and chlorination efficiency of congener mixtures. *Water Research*, 126 515–523.

Krasner, S.W., Mitch, W.A., McCurry, D.L., Hanigan, D., Westerhoff, P. 2013. Formation, precursors, control, and occurrence of nitrosamines in drinking water: A review. *Water Research*, 47 (13): 4433–4450.

Lawler, D.F., Singer, P.C. 1993. Analyzing Disinfection Kinetics and Reactor Desig : A Conceptual Approach Versus the SWTR. *Journal AWWA*, 85 (11): 67–76.

Levenspiel, O. 1999. Chemical Reaction Engineering, 3rd ed, Chemical Reaction Engineering. John Wiley & Sons, New York, NY.

Li, H., Finch, G.R., Smith, D.W., Belosevic, M. 2003. Sequential Disinfection Design Criteria for Inactivation of Cryptosporidium Oocysts in Drinking Water. Water Research Foundation, Denver, CO.

McGivney, W., Kawamura, S. 2008. Cost Estimating Manual for Water Treatment Facilities. John Wiley & Sons, Inc., Hoboken, NJ.

Najm, I., Patania Brown, N., Gramith, K., Hargy, T. 2009. Validating Disinfection in Ozone Contactors. Water Research Foundation, Denver, CO.

Olivieri, A., Crook, J., Anderson, M., Bull, R., Drewes, J., Haas, C., Jakubowski, W., Mccarty, P., Nelson, K., Rose, J., Sedlak, D., Wade, T. 2016. Evaluation of the Feasibility of Developing Uniform Water Recycling Criteria for Direct Potable Reuse. Fountain Valley, CA.

Onstad, G.D., Strauch, S., Meriluoto, J., Codd, G.A., Von Gunten, U. 2007. Selective oxidation of key functional groups in cyanotoxins during drinking water ozonation. *ES&T*, 41 (12): 4397–4404.

Oppenheimer, J.A., Aieta, M.E., Trussell, R.R., Jacangelo, J.G., Najm, I. 2000. Evaluation of Cryptosporidium Inactivation in Natural Waters. Water Research Foundation, Denver, CO.

Pecson, B.M., Triolo, S.C., Olivieri, S., Chen, E.C., Pisarenko, A.N., Yang, C.C., Olivieri, A., Haas, C.N., Trussell, R.S., Trussell, R.R. 2017. Reliability of pathogen control in direct potable reuse: Performance evaluation and QMRA of a full-scale 1 MGD advanced treatment train. *Water Research*, 122 258–268.

Pfeiffer, V., Barbeau, B. 2014. Validation of a simple method for predicting the disinfection performance in a flow-through contactor. *Water Research*, 49 144–156.

Porter, R.L., Stewart, K.P., Feagin, N., Perry, S. 2018. Baffling efficiency insights gained from tracer studies at 32 Washington treatment plants. *AWWA Water Science*, 1 (1): 1–11.

Rodríguez, E., Majado, M.E., Meriluoto, J., Acero, J.L. 2007a. Oxidation of microcystins by permanganate: Reaction kinetics and implications for water treatment. *Water Research*, 41 (1): 102–110.

Rodríguez, E., Onstad, G.D., Kull, T.P.J., Metcalf, J.S., Acero, J.L., von Gunten, U. 2007b. Oxidative elimination of cyanotoxins: Comparison of ozone, chlorine, chlorine dioxide and permanganate. *Water Research*, 41 (15): 3381–3393.

Rodríguez, E., Sordo, A., Metcalf, J.S., Acero, J.L., 2007c. Kinetics of the oxidation of cylindrospermopsin and anatoxin-a with chlorine, monochloramine and permanganate. *Water Research*, 41 (9): 2048–2056.

Sethi, V., Clark, R.M. 1998. Cost estimation models for drinking water treatment unit processes. *Indian Journal of Engineering and Materials Sciences*, 5 (8): 223–235.

Smeets, P.W.M.H., van der Helm, A.W.C., Dullemont, Y.J., Rietveld, L.C., van Dijk, J.C., Medema, G.J. 2006. Inactivation of Escherichia coli by ozone under bench-scale plug flow and full-scale hydraulic conditions. *Water Research*, 40 (17): 3239–3248.

Stanford, B.D., Adams, C., Rosenfeldt, E.J., Arevalo, E., Reinert, A. 2016. CyanoTOX: Tools for managing cyanotoxins in drinking water treatment with chemical oxidants. *Journal AWWA*, 108 (12): 41–46.

Tang, G., Adu-Sarkodie, K., Kim, D., Kim, J.H., Teefy, S., Shukairy, H.M., Mariñas, B.J. 2005. Modeling Cryptosporidium parvum oocyst inactivation and bromate formation in a full-scale ozone contactor. *ES&T*, 39 (23): 9343–9350.

Teefy, S. 1996. Tracer Studies in Water Treatment Facilities: A Protocol and Case Studies. Water Research Foundation, Denver, CO.

Texas Water Development Board (TWDB). 2015. Direct Potable Reuse Resource Document. Austin, TX.

USEPA. 2017. Potable Reuse Compendium. Washington, D.C.

USEPA. 2015. Drinking Water Health Advisory for the Cyanobacterial Toxin Cylindrospermopsin. Washington, D.C.

USEPA. 2010. Long Term 2 Enhanced Surface Water Treatment Rule Toolbox Guidance Manual. Washington, D.C.

USEPA. 2008. Ground Water Rule Corrective Actions Guidance Manual. Washington D.C.

USEPA. 1992. Use of Microbial Risk Assessment in Setting U.S. Drinking Water Standards. Washington, D.C.

USEPA. 1991. Guidance Manual for Compliance with the Filtration and Disinfection Requirements for Public Water Systems Using Surface Water Sources. Washington, D.C.

WateReuse Colorado. 2018. Advancing Direct Potable Reuse to Optimize Water Supplies and Meet Future Demands - Technical Memorandum 1 - Development of DPR Regulations in Colorado.

Westerhoff, P., Yoon, Y., Snyder, S., Wert, E. 2005. Fate of endocrine-disruptor, pharmaceutical, and personal care product chemicals during simulated drinking water treatment processes. *ES&T*, 39 (17): 6649–63.

Westrick, J.A., Szlag, D. 2018. A Cyanotoxin Primer for Drinking Water Professionals. *Journal AWWA*, 110 (8): E1–E16.

Wols, B.A., Hofman, J.A.M.H., Uijttewaal, W.S.J., Rietveld, L.C., van Dijk, J.C. 2010. Evaluation of different disinfection calculation methods using CFD. *Environ. Model. Softw.*, 25 (4): 573–582.

Zhang, J., Tejada-Martínez, A.E., Zhang, Q. 2014. Developments in computational fluid dynamics-based modeling for disinfection technologies over the last two decades: A review. *Environ. Model. Softw.*, 58 71–85.

CHAPTER 5 - CONCLUSIONS

The goal of this dissertation was to improve the prediction of contaminant degradation in water treatment reactors by accurately modeling reactor hydraulics. This goal was divided into three objectives. The first objective was to develop models for residence time distribution (RTD) that were more accurate than the plug flow reactor (PFR) t_{10} model while using fewer input parameters than alternative methods, such as the segregated flow (SF) model. The second objective was to assess whether flow segregation and earliness of mixing (i.e., micromixing) were significant in full-scale water treatment reactors. The final objective was to perform a quantitative evaluation of the effect of RTD model selection on predictions of contaminant degradation for a range of reactor types and sizes.

These three objectives progressed in order of dependence on modeling. The first objective required modeling RTD using a conservative, non-reactive tracer that could be directly observed at full scale. The second objective used chlorine and chloramine species as reactive tracers, and required modeling numerous simultaneous reactions. Modeled reactor outputs for this objective could be compared to full-scale observation. For the final objective, contaminant degradation was predicted using different reactor models without validation at full-scale. This objective depended on knowledge gained in objectives one and two to reach conclusions in the absence of full-scale validation.

From the research presented in this dissertation, the following major conclusions were reached:

1. Increasing the number of parallel, segregated flows in a reactor model (e.g., SF, certain reactor network (RN) models) produces more accurate models of RTD. Such parallel flows are appropriate for modeling a single first-order reaction, such as crediting disinfection using residual oxidant concentration. However, increasing the number of parallel, segregated flows may decrease the accuracy of micromixing representation. Therefore, when modeling conditions where micromixing is important, such as multiple simultaneous reactions or a single non-first-order reaction, caution should be used in creating models containing parallel, segregated flows.
2. Micromixing was found to be significant in both baffled and unbaffled clearwells at full scale. Micromixing was studied by observing chloramine breakpoint associated with temporal disinfectant switching.
3. The tanks-in-series (TIS) model provided significant improvement in RTD representation over the PFR t_{10} model and was capable of accurately representing observed micromixing in the reactors studied. For most reactors, the TIS model adequately balances accuracy and simplicity when modeling low log reductions (e.g., $\leq$ 3-log).
4. The SF model is not recommended for predicting contaminant degradation. For the reactors studied, the SF model required a large number of model inputs, poorly predicted micromixing conditions, likely overpredicted contaminant degradation in the presence of a decaying oxidant, and yielded errant predictions of contaminant degradation for non-monotonic tracer data.

5. The RN model accurately predicted RTD using fewer fitting parameters than the SF model. The RN model is best suited to conditions where accurately representing RTD is of high importance. Such situations include modeling high levels of inactivation (e.g., 6-log) in a single reactor or when designing for greater *Da* has adverse consequences (e.g., cost or formation of disinfection by-products). RN models may not accurately represent micromixing. Therefore, caution should be used when modeling multiple reactions.

The findings generated from this dissertation provide a fundamental basis for the rational design, operation, and regulation of water treatment processes. The TIS or RN models are recommended to be used for these purposes.

CHAPTER 6 - FUTURE WORK

Research presented in this dissertation provides a fundamental basis for improved prediction of contaminant degradation in water treatment reactors. This work also raises additional research questions:

1. **Could methods be developed to validate high log reductions at full scale in clearwells or ozone contactors?** This work compared predictions from different reactor models targeting 6-log reduction. Currently, there are no methods available to validate 6-log reduction at full-scale in clearwells and ozone contactors. The regulatory approach used by USEPA to compute pathogen log reduction in oxidation processes is based on the ratio CT achieved to CT required for a given log inactivation (USEPA 1991, USEPA 2010). Validation is not performed because pathogen concentrations in finished water are too low to be reliably measured (USEPA 1992). Conversely, methods exist for validating high log reductions in UV reactors using surrogates (USEPA 2006), with validation typically occurring at specialized testing facilities. There are also methods for validating log reduction in membrane filtration and assigning log removal credit (USEPA 2005, CDPH 2014). Developing methods for validating pathogen removal in full-scale clearwells and ozone contactors would provide greater assurance of public health protection, particularly in water reuse applications. Potential methods could include molecular

techniques or naturally occurring, non-pathogenic surrogates which have been used previously to demonstrate lower log reductions (Facile et al. 2000, Talbot et al. 2012).

2. **Could computational fluid dynamics (CFD) more accurately represent micromixing than the tanks-in-series (TIS) model?** The TIS model was observed to provide a reasonably accurate representation of micromixing in the reactors studied. Predictions from CFD could be compared to those from the TIS reactor. If CFD more accurately represented observed micromixing, CFD could provide more accurate predictions of contaminant degradation in multi-reaction systems (e.g., disinfection with a decaying oxidant). However, if the predictions are similar or less accurate than the TIS reactor, such findings would provide confidence that relatively simple methods such as the TIS model are sufficient for representing complex reaction and transport processes.
3. **Does the TIS reactor accurately represent micromixing in ozone contactors as well as clearwells?** This work indirectly observed micromixing in clearwells. The efficacy of the TIS reactor for representing micromixing should also be demonstrated in ozone contactors, where ozone injection is expected to affect reactor hydraulics.
4. **How could distribution system operations be modified to reduce the mixing of free chlorine and chloramine, and what would the effects be on disinfectant residual?** This work modeled temporal disinfectant switching in relatively simple systems: clearwells with single points of inflow and outflow. The methods presented here provided a reasonably accurate representation of breakpoint reactions in water treatment plants. However, distribution system hydraulics are considerably more complex. Distribution systems typically receive water from multiple entry points,

which may contain different concentrations of chlorine and/or ammonia. Distribution systems also have numerous storage reservoirs, which may not be flow-through reservoirs (i.e., common inlet and outlet) and are unlikely to have residence time distribution (RTD) characterized by tracer studies. Distribution system models such as EPANET are capable of performing source tracing (USEPA 2000), and recent advancements have allowed the simulation of multiple chemical species (EPA 2011). Modeling breakpoint chemistry in distribution systems would be expected to inform operations to reduce chlorine and chloramine mixing, improving stability of disinfectant residuals and reducing taste and odor complaints associated with di- and trichloramine species.

REFERENCES

California Department of Public Health (CDPH). 2014. Regulations Related to Recycled Water. California Code of Regulations Titles 22 and 17.

Facile, N., Barbeau, B., Prevost, M., & Koudjonou, B. 2000. Evaluating bacterial aerobic spores as a surrogate for Giardia and Cryptosporidium inactivation by ozone. *Water Research*, 34 (12): 3238-3246.

Talbot, P., Martinelli, L., Talvy, S., Chauveheid, E., & Haut, B. 2012. Ozone inactivation of resistant microorganisms: Laboratory analysis and evaluation of the efficiency of plants. *Water Research, 46* (18): 5893-5903.

United States Environmental Protection Agency (USEPA). 1991. Guidance Manual for Compliance with the Filtration and Disinfection Requirements for Public Water Systems Using Surface Water Sources. Washington, D.C.

United States Environmental Protection Agency (USEPA). 1992. Use of Microbial Risk Assessment in Setting U.S. Drinking Water Standards. Washington, D.C.

United States Environmental Protection Agency (USEPA). 2000. EPANET 2 Users Manual. EPA-600-R-00/57. Washington, DC.

United States Environmental Protection Agency (USEPA). 2005. Membrane Filtration Guidance Manual. Washington, D.C.

United States Environmental Protection Agency (USEPA). 2006. Ultraviolet Disinfection Guidance Manual for the Final Long Term 2 Enhanced Surface Water Treatment Rule. Washington, D.C.

United States Environmental Protection Agency (USEPA). 2010. Long Term 2 Enhanced Surface Water Treatment Rule Toolbox Guidance Manual. Washington, D.C.

United States Environmental Protection Agency (USEPA). 2011. EPANET Multi-Species Extension User's Manual. Cincinnat, OH.

APPENDIX A – SUPPORTING INFORMATION FOR CHAPTER 2

A.1. Example Code for Fitting Reactor Models to Tracer Data

```
##### Clear all existing R objects and plots
rm(list = ls()) # Clear workspace
dev.off(dev.list()["RStudioGD"]) # Clear plots


##### Install R packages
  # The following packages are required to run this code:  rJava, xlsx, nlstools, broom, ggplot2, and reshape2
  # Copy the following, and paste it into Tools > Install packages:  rJava, xlsx, nlstools, broom, ggplot2, reshape2
  # Note, you will need Java. Make sure the version of Java matches the version of R you are using (i.e., 32 vs 64 bit)
    # (https://www.java.com/en/download/manual.jsp)


##### Set Workspace, load packages and data

# Set workspace - Enter your filepath here - must use forward dashes
setwd("C:/Users/agorz/Desktop/RNM Demo/")

# Enter the name of the excel sheet containing your tracer data
DataFile <- "MyTracer.xlsx"

# Load ncessary R packages
require(xlsx) # For reading excel files
require(nlstools) # Has plotfit(), additional options with calculating confidence intervals
require(broom) # Has tidy(), which is used to make data frames out of fits
require(ggplot2) # Used in creating plots
require(reshape2) # Includes melt function required for ggplot

# Load tracer data from excel file (1 indicates first sheet)
dat <- read.xlsx(DataFile, sheetIndex = 1)
# Define shortlisted models A-I, which will later be fit to tracer data
  # See Figure 3 in Gorzalski et al. 2018 for model schematics (https://doi.org/10.1002/awwa.1071)
    # Full citation:  Gorzalski, A. S., Harrington, G. W., & Coronell, O. (2018). Modeling Water Treatment
    # Reactor Hydraulics Using Reactor Networks. Journal-American Water Works Association, 110(8), 13-29.

ModelA <- function(Theta,VF_TIS,n) {
  TIS(n,(Theta/VF_TIS) )}

ModelB <- function(Theta,VF_TIS1,VF_dead,Q1,n1,n2) {
  Q1*TIS(n1,(Theta/VF_TIS1*Q1) ) +
    (1-Q1)*TIS(n2,(Theta/(1-VF_TIS1-VF_dead)*(1-Q1)) )}

ModelC <- function(Theta,VF_TIS1,VF_TIS2,VF_dead,Q1,Q2,n1,n2,n3) {
  Q1*TIS(n1,(Theta/VF_TIS1*Q1) )+
    Q2*TIS(n2,(Theta/VF_TIS2*Q2) )+
    (1-Q1-Q2)*TIS(n3,(Theta/(1-VF_TIS1-VF_TIS2-VF_dead)*(1-Q1-Q2)) )}

ModelD <- function(Theta,VF_PFR,VF_dead) {
  ifelse(Theta<VF_PFR,0,1 - exp(-(Theta - VF_PFR)/ (1-VF_PFR-VF_dead) ))}

ModelE <- function(Theta,VF_PFR1,VF_TIS2,VF_dead,Q1,n) {
  Q1*TIS(n,ifelse(Theta<VF_PFR1/Q1,0, (Theta- (VF_PFR1/Q1) )/ (VF_TIS2/Q1) ) )+
    (1-Q1)*(1 - exp( -Theta/(1-VF_PFR1-VF_TIS2-VF_dead)*(1-Q1) ) )}

ModelF <- function(Theta,VF_PFR1,VF_TIS2,VF_dead,Q1,n2,n3) {
  Q1*TIS(n2,ifelse(Theta<VF_PFR1/Q1,0, (Theta- (VF_PFR1/Q1) )/ (VF_TIS2/Q1) ) )+
    (1-Q1)*TIS(n3,(Theta/(1-VF_PFR1-VF_TIS2-VF_dead)*(1-Q1)) )}

ModelG <- function(Theta,VF_CSTR1,VF_TIS2,VF_dead,Q1,Q2,n2,n3) {
  Q1*(1 - exp( -Theta/VF_CSTR1*Q1 ) )+
    Q2*TIS(n2,(Theta/VF_TIS2*Q2) )+
    (1-Q1-Q2)*TIS(n3,(Theta/(1-VF_CSTR1-VF_TIS2-VF_dead)*(1-Q1-Q2)) )}

ModelH <- function(Theta,VF_PFR1,VF_CSTR2,VF_PFR3,VF_dead,Q1) {
  Q1*ifelse(Theta<VF_PFR1/Q1,0,1 - exp(-(Theta - VF_PFR1/Q1)/ (VF_CSTR2/Q1) ))+
    (1-Q1)*ifelse(Theta<VF_PFR3/(1-Q1) ,0,1 - exp(-(Theta - VF_PFR3/(1-Q1) )/
                                                    ( (1-VF_PFR1-VF_CSTR2-VF_PFR3-VF_dead)/(1-Q1) ) ))}

ModelI <- function(Theta,VF_PFR1,VF_TIS2,VF_PFR3,VF_dead,Q1,n2,n4) {
  Q1*TIS(n2,ifelse(Theta<VF_PFR1/Q1,0, (Theta- (VF_PFR1/Q1) )/ (VF_TIS2/Q1) ) )+
    (1-Q1)*TIS(n4,ifelse(Theta<VF_PFR3/(1-Q1),0, (Theta- (VF_PFR3/(1-Q1)) )/ (
      (1-VF_PFR1-VF_TIS2-VF_PFR3-VF_dead)/(1-Q1)) ) )}
```

```
##### Perform Nonlinear Regression

# For each model conduct the fit, calculate MSE & RSE, & plot fit using nlstools' plotfit()

ModelAfit <- nls(CC0 ~ ModelA(Theta,VF_TIS1,n),data=dat,
                 algorithm = "port",
                 start = list(VF_TIS1 = 0.1, n = 5),
                 lower = list(VF_tis1 = 0.01, n = 1),
                 upper = list(VF_TIS1 = 2, n = 100),
                 trace = TRUE)
ModelAerr <- c(sum(residuals(ModelAfit)^2)/length(residuals(ModelAfit)),
  sqrt( sum(residuals(ModelAfit)^2)/(length(residuals(ModelAfit)) - length(coef(ModelAfit))) ))
ModelAerr <- data.frame(ModelAerr,row.names = c("MSE","RSE"))
plotfit(ModelAfit, smooth = TRUE)


ModelBfit <- nls(CC0 ~ ModelB(Theta,VF_TIS1,VF_dead,Q1,n1,n2),data=dat,
                 algorithm = "port",
                 start = list(VF_TIS1 = 0.3, VF_dead = 0.01, Q1 = 0.3, n1 = 10, n2 = 3),
                 lower = list(VF_TIS1 = 0.01, VF_dead = 0, Q1 = 0.01, n1 = 1, n2 = 1),
                 upper = list(VF_TIS1 = 2, VF_dead = 1, Q1 = 1, n1 = 100, n2 = 100),
                 trace = FALSE)
ModelBerr <- c(sum(residuals(ModelBfit)^2)/length(residuals(ModelBfit)),
               sqrt( sum(residuals(ModelBfit)^2)/(length(residuals(ModelBfit)) - length(coef(ModelBfit))) ))
ModelBerr <- data.frame(ModelBerr,row.names = c("MSE","RSE"))
plotfit(ModelBfit, smooth = TRUE)


ModelCfit <- nls(CC0 ~ ModelC(Theta,VF_TIS1,VF_TIS2,VF_dead,Q1,Q2,n1,n2,n3),data=dat,
                 algorithm = "port",
                 start = list(VF_TIS1 = 0.3, VF_TIS2 = 0.3, VF_dead = 0.001, Q1 = 0.2, Q2 = 0.6, n1 = 5, n2 = 5, n3 = 5),
                 lower = list(VF_TIS1 = 0.01, VF_TIS2 = 0.01, VF_dead = 0, Q1 = 0, Q2 = 0, n1 = 1, n2 = 1, n3 = 1),
                 upper = list(VF_TIS1 = 2, VF_TIS2 = 2, VF_dead = 1, Q1 = 1, Q2 = 1, n1 = 100, n2 = 100, n3 = 100),
                 trace = FALSE,
                 nls.control(maxiter = 100)) # Add more iterations for difficult fit
ModelCerr <- c(sum(residuals(ModelCfit)^2)/length(residuals(ModelCfit)),
               sqrt( sum(residuals(ModelCfit)^2)/(length(residuals(ModelCfit)) - length(coef(ModelCfit))) ))
ModelCerr <- data.frame(ModelCerr,row.names = c("MSE","RSE"))
plotfit(ModelCfit, smooth = TRUE)


ModelDfit <- nls(CC0 ~ ModelD(Theta,VF_PFR,VF_dead),data=dat,
                 algorithm = "port",
                 start = list(VF_PFR = 0.5, VF_dead = 0.1),
                 lower = list(VF_PFR = 0.01, VF_dead = -1),
                 upper = list(VF_PFR = 2, VF_dead = 1),
                 trace = FALSE)
ModelDerr <- c(sum(residuals(ModelDfit)^2)/length(residuals(ModelDfit)),
               sqrt( sum(residuals(ModelDfit)^2)/(length(residuals(ModelDfit)) - length(coef(ModelDfit))) ))
ModelDerr <- data.frame(ModelDerr,row.names = c("MSE","RSE"))
plotfit(ModelDfit, smooth = TRUE)
ModelEfit <- nls(CC0 ~ ModelE(Theta,VF_PFR1,VF_TIS2,VF_dead,Q1,n3),data=dat,
                 algorithm = "port",
                 start = list(VF_PFR1 = 0.1, VF_TIS2 = 0.6, VF_dead = 0.0, Q1 = 0.5, n3 = 2),
                 lower = list(VF_PFR1 = 0.01, VF_TIS2 = 0.01, VF_dead = -1, Q1 = 0.01, n3 = 1),
                 upper = list(VF_PFR1 = 2, VF_TIS2 = 2, VF_dead = 1, Q1 = 1, n3 = 100),
                 trace = FALSE,
                 nls.control(maxiter = 100)) # Add more iterations for difficult fit
ModelEerr <- c(sum(residuals(ModelEfit)^2)/length(residuals(ModelEfit)),
               sqrt( sum(residuals(ModelEfit)^2)/(length(residuals(ModelEfit)) - length(coef(ModelEfit))) ))
ModelEerr <- data.frame(ModelEerr,row.names = c("MSE","RSE"))
plotfit(ModelEfit, smooth = TRUE)


ModelFfit <- nls(CC0 ~ ModelF(Theta,VF_PFR1,VF_TIS2,VF_dead,Q1,n2, n3),data=dat,
                 algorithm = "port",
                 start = list(VF_PFR1 = 0.1, VF_TIS2 = 0.5, VF_dead = -0.1, Q1 = 0.6, n2 = 3, n3 = 3),
                 lower = list(VF_PFR1 = 0.01, VF_TIS2 = 0.01, VF_dead = -1, Q1 = 0.01, n2 = 1, n3 = 1),
                 upper = list(VF_PFR1 = 2, VF_TIS2 = 2, VF_dead = 1, Q1 = 1, n2 = 100, n3 = 100),
                 trace = FALSE)
ModelFerr <- c(sum(residuals(ModelFfit)^2)/length(residuals(ModelFfit)),
               sqrt( sum(residuals(ModelFfit)^2)/(length(residuals(ModelFfit)) - length(coef(ModelFfit))) ))
ModelFerr <- data.frame(ModelFerr,row.names = c("MSE","RSE"))
plotfit(ModelFfit, smooth = TRUE)


ModelGfit <- nls(CC0 ~ ModelG(Theta,VF_CSTR1,VF_TIS2,VF_dead,Q1,Q2,n2,n3),data=dat,
                 algorithm = "port",
                 start = list(VF_CSTR1 = 0.05, VF_TIS2 = 0.7, VF_dead = 0, Q1 = 0.05, Q2 = 0.8, n2 = 5, n3 = 5),
                 lower = list(VF_CSTR1 = 0.01, VF_TIS2 = 0.01, VF_dead = -1, Q1 = 0.01, Q2 = 0.01, n2 = 1, n3 = 1),
                 upper = list(VF_CSTR1 = 2, VF_TIS2 = 2, VF_dead = 1, Q1 = 1, Q2 = 1, n2 = 100, n3 = 100),
                 trace = FALSE)
ModelGerr <- c(sum(residuals(ModelGfit)^2)/length(residuals(ModelGfit)),
               sqrt( sum(residuals(ModelGfit)^2)/(length(residuals(ModelGfit)) - length(coef(ModelGfit))) ))
ModelGerr <- data.frame(ModelGerr,row.names = c("MSE","RSE"))
plotfit(ModelGfit, smooth = TRUE)
```

```
ModelHfit <- nls(CC0 ~ ModelH(Theta,VF_PFR1,VF_CSTR2,VF_PFR3,VF_dead,Q1),data=dat,
                 algorithm = "port",
                 start = list(VF_PFR1 = 0.2, VF_CSTR2 = 0.1, VF_PFR3 = 0.3, VF_dead = 0.01, Q1 = 0.5),
                 lower = list(VF_PFR1 = 0.01, VF_CSTR2 = 0.01, VF_PFR3 = 0.01, VF_dead = -1, Q1 = 0.01),
                 upper = list(VF_PFR1 = 2, VF_CSTR2 = 2, VF_PFR3 = 2, VF_dead = 1, Q1 = 1),
                 trace = FALSE)
ModelHerr <- c(sum(residuals(ModelHfit)^2)/length(residuals(ModelHfit)),
               sqrt( sum(residuals(ModelHfit)^2)/(length(residuals(ModelHfit)) - length(coef(ModelHfit))) ))
ModelHerr <- data.frame(ModelHerr,row.names = c("MSE","RSE"))
plotfit(ModelHfit, smooth = TRUE)


ModelIfit <- nls(CC0 ~ ModelI(Theta,VF_PFR1,VF_TIS2,VF_PFR3,VF_dead,Q1,n2,n4),data=dat,
                 algorithm = "port",
                 start = list(VF_PFR1 = 0.2, VF_TIS2 = 0.5, VF_PFR3 = 0.01, VF_dead = 0.01, Q1 = 0.5, n2 = 2, n4 = 3),
                 lower = list(VF_PFR1 = 0.01, VF_TIS2 = 0.01, VF_PFR3 = 0.01, VF_dead = -1, Q1 = 0.01, n2 = 1, n4 = 1),
                 upper = list(VF_PFR1 = 2, VF_TIS2 = 2, VF_PFR3 = 1, VF_dead = 1, Q1 = 1, n2 = 100, n4 = 100),
                 trace = FALSE)
ModelIerr <- c(sum(residuals(ModelIfit)^2)/length(residuals(ModelIfit)),
               sqrt( sum(residuals(ModelIfit)^2)/(length(residuals(ModelIfit)) - length(coef(ModelIfit))) ))
ModelIerr <- data.frame(ModelIerr,row.names = c("MSE","RSE"))
plotfit(ModelIfit, smooth = TRUE)


##### Write Model Fitting Parameters and Statistics to an Excel File

# Use confint2 to find 95% CI
# Use tidy() to convert results to data frame
# Use cbind to merge the two into 1 data frame
# Include 75, 85, 95% CI
CI1 = 0.75
CI2 = 0.85
CI3 = 0.95
# Using 'append=TRUE' tells write.xlsx to add this tab to the end
  # rather than creating a new sheet
fname <- "ParameterFits.xlsx"

# First tab will have MSE and RSE of all models that produced a fit
eNames <- cbind(ls(pattern="err")) # Find all variables that contain "err"
write.xlsx(do.call(cbind,apply(eNames,1,get)), # get() all elements of eNames, bind them together into a table
           file = fname, sheetName = "MSE_RSE")

# Write each fit to successive tabs. Information includes estimate, standard error, and CI for each variable
write.xlsx(cbind(tidy(ModelAfit), #
                 confint2(ModelAfit,level = CI1),
                 confint2(ModelAfit,level = CI2),
                 confint2(ModelAfit,level = CI3)   ),
           file = fname, append=TRUE, sheetName = "ModelA")

write.xlsx(cbind(tidy(ModelBfit),
                 confint2(ModelBfit,level = CI1),
                 confint2(ModelBfit,level = CI2),
                 confint2(ModelBfit,level = CI3)   ),
           file = fname, append=TRUE, sheetName = "ModelB")

write.xlsx(cbind(tidy(ModelCfit),
                 confint2(ModelCfit,level = CI1),
                 confint2(ModelCfit,level = CI2),
                 confint2(ModelCfit,level = CI3)   ),
           file = fname, append=TRUE, sheetName = "ModelC")

write.xlsx(cbind(tidy(ModelDfit),
                 confint2(ModelDfit,level = CI1),
                 confint2(ModelDfit,level = CI2),
                 confint2(ModelDfit,level = CI3)   ),
           file = fname, append=TRUE, sheetName = "ModelD")

write.xlsx(cbind(tidy(ModelEfit),
                 confint2(ModelEfit,level = CI1),
                 confint2(ModelEfit,level = CI2),
                 confint2(ModelEfit,level = CI3)   ),
           file = fname, append=TRUE, sheetName = "ModelE")

write.xlsx(cbind(tidy(ModelFfit),
                 confint2(ModelFfit,level = CI1),
                 confint2(ModelFfit,level = CI2),
                 confint2(ModelFfit,level = CI3)   ),
           file = fname, append=TRUE, sheetName = "ModelF")

write.xlsx(cbind(tidy(ModelGfit),
                 confint2(ModelGfit,level = CI1),
                 confint2(ModelGfit,level = CI2),
                 confint2(ModelGfit,level = CI3)   ),
           file = fname, append=TRUE, sheetName = "ModelG")

write.xlsx(cbind(tidy(ModelHfit),
                 confint2(ModelHfit,level = CI1),
                 confint2(ModelHfit,level = CI2),
                 confint2(ModelHfit,level = CI3)   ),
           file = fname, append=TRUE, sheetName = "ModelH")
```

```
write.xlsx(cbind(tidy(ModelIfit),
                 confint2(ModelIfit,level = CI1),
                 confint2(ModelIfit,level = CI2),
                 confint2(ModelIfit,level = CI3)   ),
           file = fname, append=TRUE, sheetName = "ModelI")


##### Export Model Fits to an Excel File

# Create a data frame with the outputs of all the models and the associated coefficients
# Create a set theta range (e.g., 0 to 3),
# create a variable with the model coeficients, then call them to evaluate the model
theta <- seq(0,3,0.01)
coefA <- coef(ModelAfit)
D_ModelA <- ModelA(theta,coefA[1],coefA[2])
coefB <- coef(ModelBfit)
D_ModelB <- ModelB(theta,coefB[1],coefB[2],coefB[3],coefB[4],coefB[5])
coefC <- coef(ModelCfit)
D_ModelC <- ModelC(theta,coefC[1],coefC[2],coefC[3],coefC[4],coefC[5],
                   coefC[6],coefC[7],coefC[8])
coefD <- coef(ModelDfit)
D_ModelD <- ModelD(theta,coefD[1],coefD[2])
coefE <- coef(ModelEfit)
D_ModelE <- ModelE(theta,coefE[1],coefE[2],coefE[3],coefE[4],coefE[5])
coefF <- coef(ModelFfit)
D_ModelF <- ModelF(theta,coefF[1],coefF[2],coefF[3],coefF[4],coefF[5],coefF[6])
coefG <- coef(ModelGfit)
D_ModelG <- ModelG(theta,coefG[1],coefG[2],coefG[3],coefG[4],coefG[5],
                   coefG[6],coefG[7])
coefH <- coef(ModelHfit)
D_ModelH <- ModelH(theta,coefH[1],coefH[2],coefH[3],coefH[4],coefH[5])
coefI <- coef(ModelIfit)
D_ModelI <- ModelI(theta,coefI[1],coefI[2],coefI[3],coefI[4],coefI[5],
                   coefI[6],coefI[7])


dNames <- cbind(ls(pattern="D_Model")) # Get filenames that contain "D_Model"
dNames <- c("theta",dNames) # Add theta to the above list
ModelTable <- apply(as.matrix(dNames),1,get) # get() all elements of eNames, bind them together into a table
colnames(ModelTable) <- c("Theta",substring(dNames[-1],3)) # Make table names theta and delete "D_" from model name

# Write table of theta and model outputs to excel
write.xlsx(ModelTable, file = "ModelOutput.xlsx", sheetName = "ModelOutput")


# Plot first 3 Model fits
ggplot(data=melt(D_df[,c(1,2,3,4)],id.vars="Theta"),aes(x=Theta,y=value,colour = variable)) +
  geom_point(data=dat,aes(x=Theta,y=CC0),colour = "black",size = 3, shape=21) +
  geom_line(size=1) +
  scale_colour_brewer(palette = "Set1") +
  xlim(0,3)+ylim(0,1) +
  labs(x=expression(theta),y="C/C0",color="Model")+
  theme_bw() +
  theme(legend.position=c(0.8,0.35),legend.key=element_rect(line="blank", size=1))

# Plot next 3 Model fits
ggplot(data=melt(D_df[,c(1,5,6,7)],id.vars="Theta"),aes(x=Theta,y=value,colour = variable)) +
  geom_point(data=dat,aes(x=Theta,y=CC0),colour = "black",size = 3, shape=21) +
  geom_line(size=1) +
  scale_colour_brewer(palette = "Set1") +
  xlim(0,3)+ylim(0,1) +
  labs(x=expression(theta),y="C/C0",color="Model")+
  theme_bw() +
  theme(legend.position=c(0.8,0.35),legend.key=element_rect(line="blank", size=1))

# Plot last 3 Model fits
ggplot(data=melt(D_df[,-(2:7)],id.vars="Theta"),aes(x=Theta,y=value,colour = variable)) +
  geom_point(data=dat,aes(x=Theta,y=CC0),colour = "black",size = 3, shape=21) +
  geom_line(size=1) +
  scale_colour_brewer(palette = "Set1") +
  xlim(0,3)+ylim(0,1) +
  labs(x=expression(theta),y="C/C0",color="Model")+
  theme_bw() +
  theme(legend.position=c(0.8,0.35),legend.key=element_rect(line="blank", size=1))
```

APPENDIX B – SUPPORTING INFORMATION FOR CHAPTER 3

B.1. Description of Clearwells And Mixing Conditions

As shown in Figure B.1, ammonia was injected upstream of Clearwell A. An 8 by 8.5-foot rectangular box conduit then carries the water 262 feet to Clearwell A. There was no mechanical or static mixing at the point of injection, but flow within the box conduit was turbulent (typical Reynolds number between 400,000 and 3,000,000 depending on temperature and flow). There was also active mixing where lime is injected into the clearwell (see Figure S4A) along with a static mixing chamber (see Figure B.4B). Clearwell A was baffled (see Figure B.1 and Figure B.4C), and all flow passed through a submerged overflow weir and through a second mixing chamber (see Figure B.3 and Figure B.4D) equipped with intermittently used chlorine and ammonia injection points. Water exited the clearwell to the adjacent pumping station. Online process monitoring equipment was fed by a sample tap located on a high-service main that receives continuous flow.

Ammonia was injected upstream of Clearwell B in an unmixed flow diversion chamber connected to a 78-inch diameter circular pipe that carries water 235 feet from the chamber to Clearwell B. The flow in the 78” pipe was turbulent with Reynolds Number between 300,000 to 4,000,000 depending on temperature and flow. Online process monitoring equipment was fed by a sample pump located near the clearwell effluent as shown in Figure B.2 (see picture in Figure B.5C).

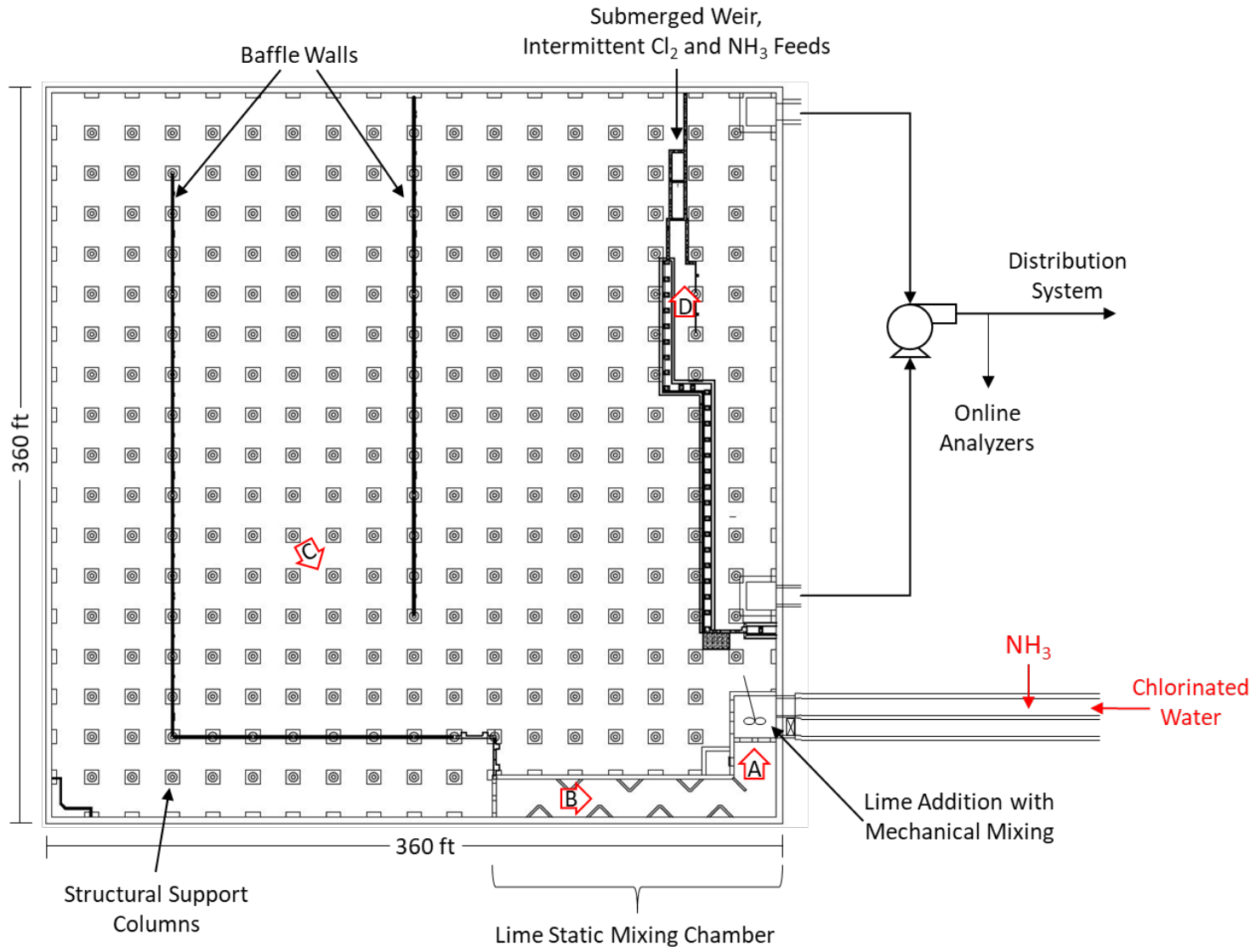

Figure B.1. Plan view of Clearwell A with schematic showing flow to distribution system and online analyzers. Views labeled A-D (red outlined arrows) are shown in Figure B.4. Intermittent feed lines are used when the upstream primary disinfection clearwell is out

of service, and ammonia is added to form chloramines leaving the second clearwell.

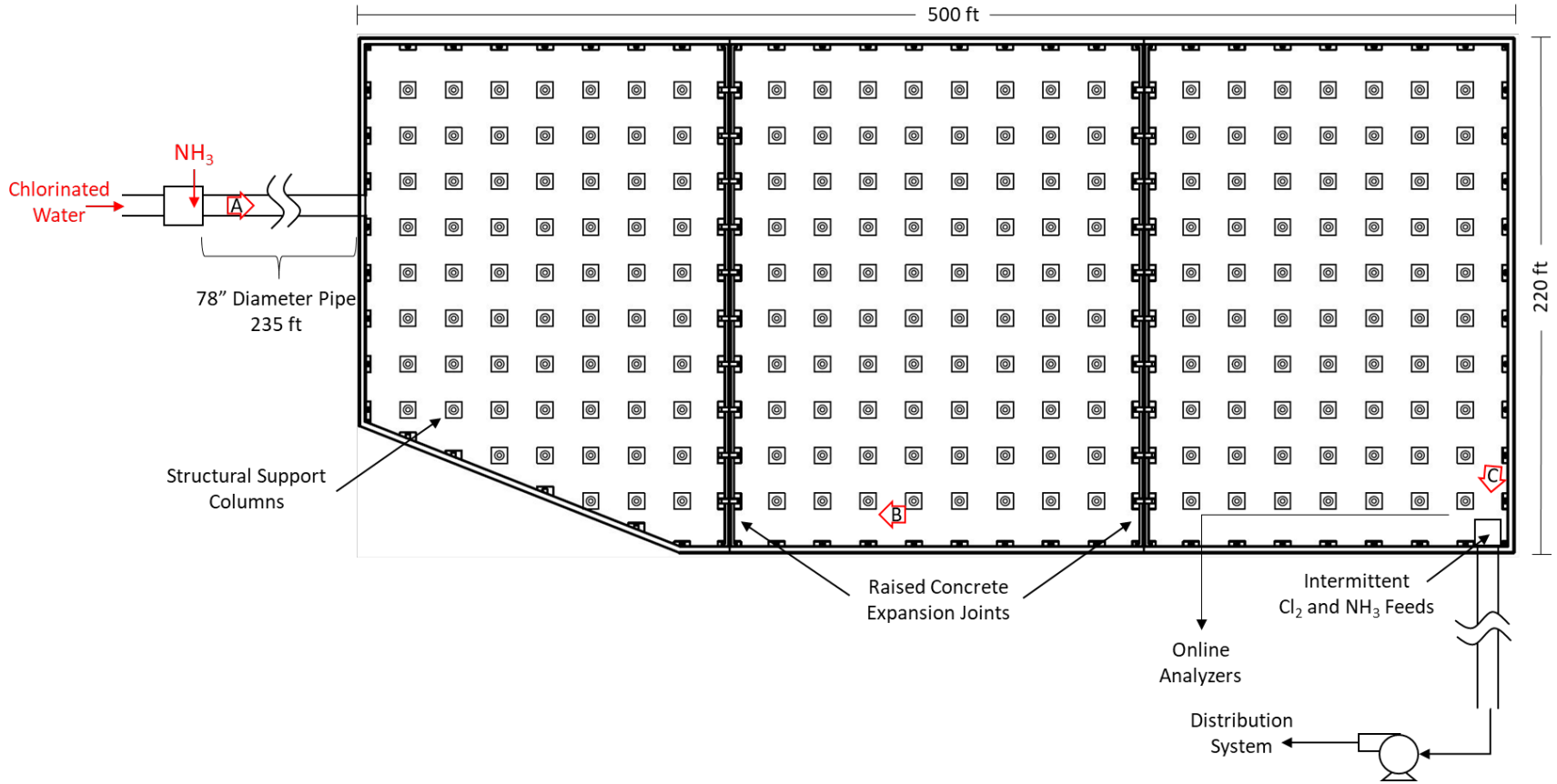

Figure B.2. Plan view of Clearwell B with schematic showing flow to distribution system and online analyzers. Views labeled A-C (red outlined arrows) are shown in Figure B.5. Intermittent feed lines are used when the upstream primary disinfection clearwell is out of service, and ammonia is added to form chloramines leaving the second clearwell.

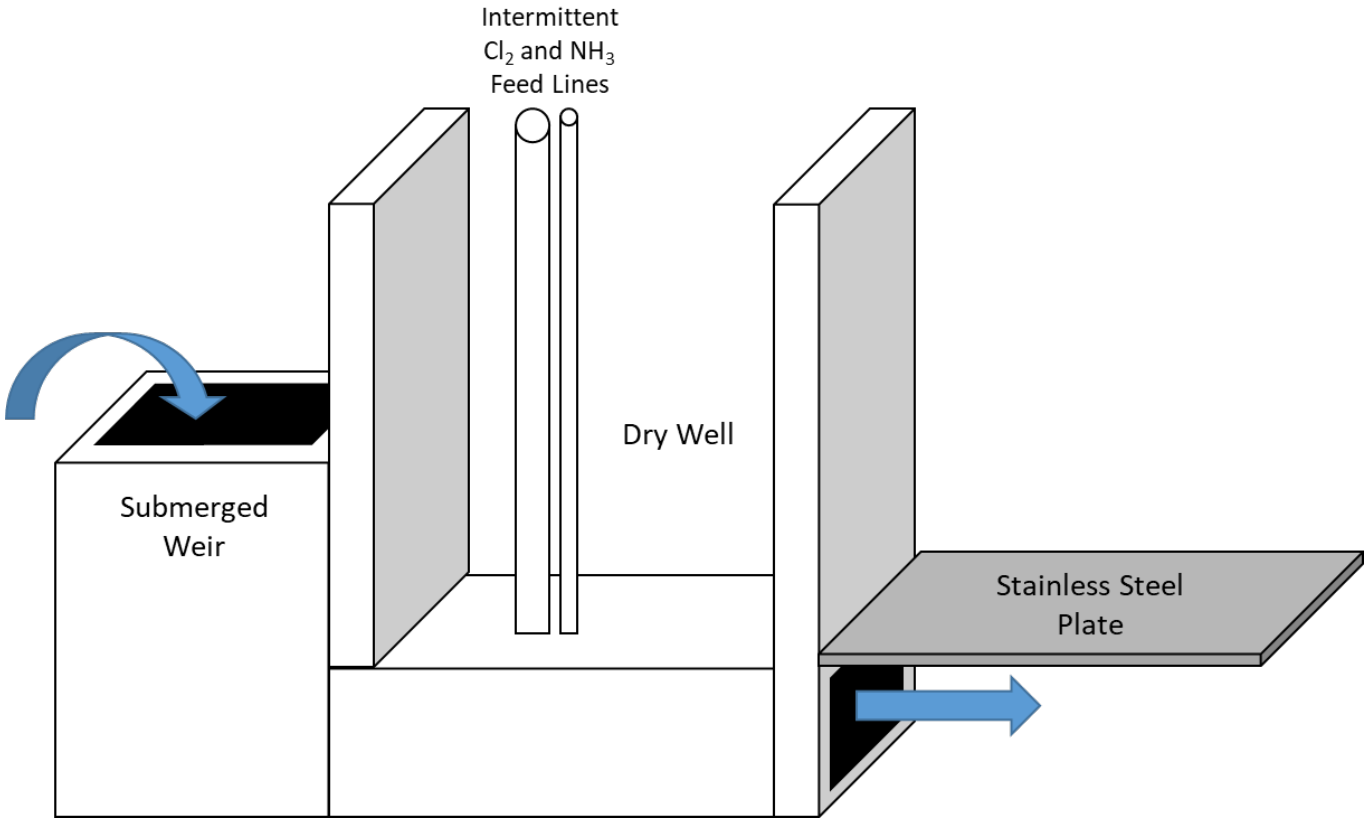

Figure B.3. Detail of the submerged weir and feed lines for chlorine and ammonia at the end of the clearwell. View D in Figure B.1 and Figure B.4 are taken looking upstream from the end of the stainless steel plate. This structure allows for the addition of chlorine and/or ammonia to potentially mitigate depressed chlorine residual associated with temporal disinfectant switching.

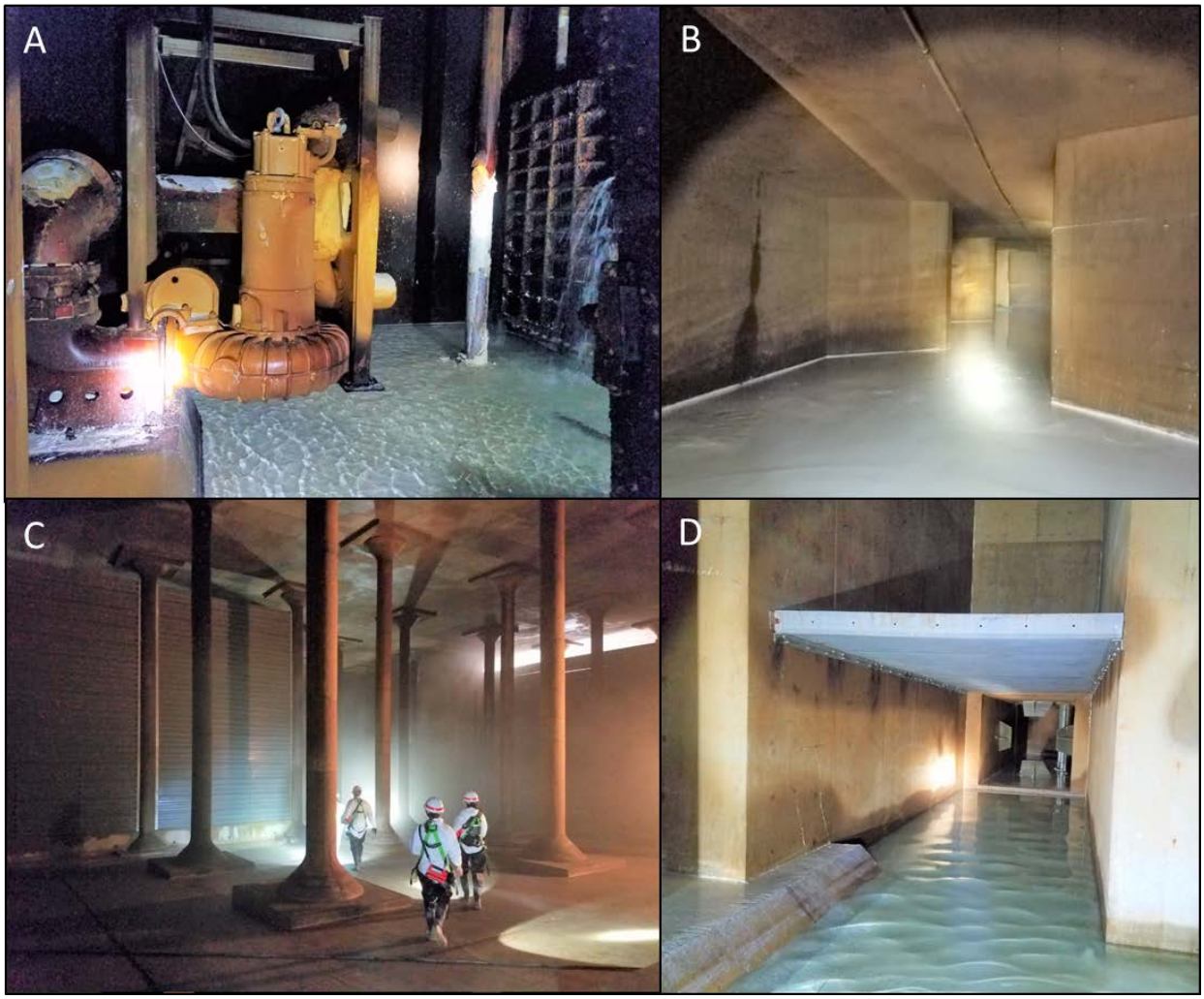

Figure B.4. Photographs of the interior of Clearwell A. Views A-D are indicated in Figure B.1, where photos correspond to (A) lime mixing pump, (B) lime mixing chamber, (C) mid clearwell at the end of one baffle wall, and (D) mixing chamber where chlorine and ammonia can be fed (see Figure B.2).

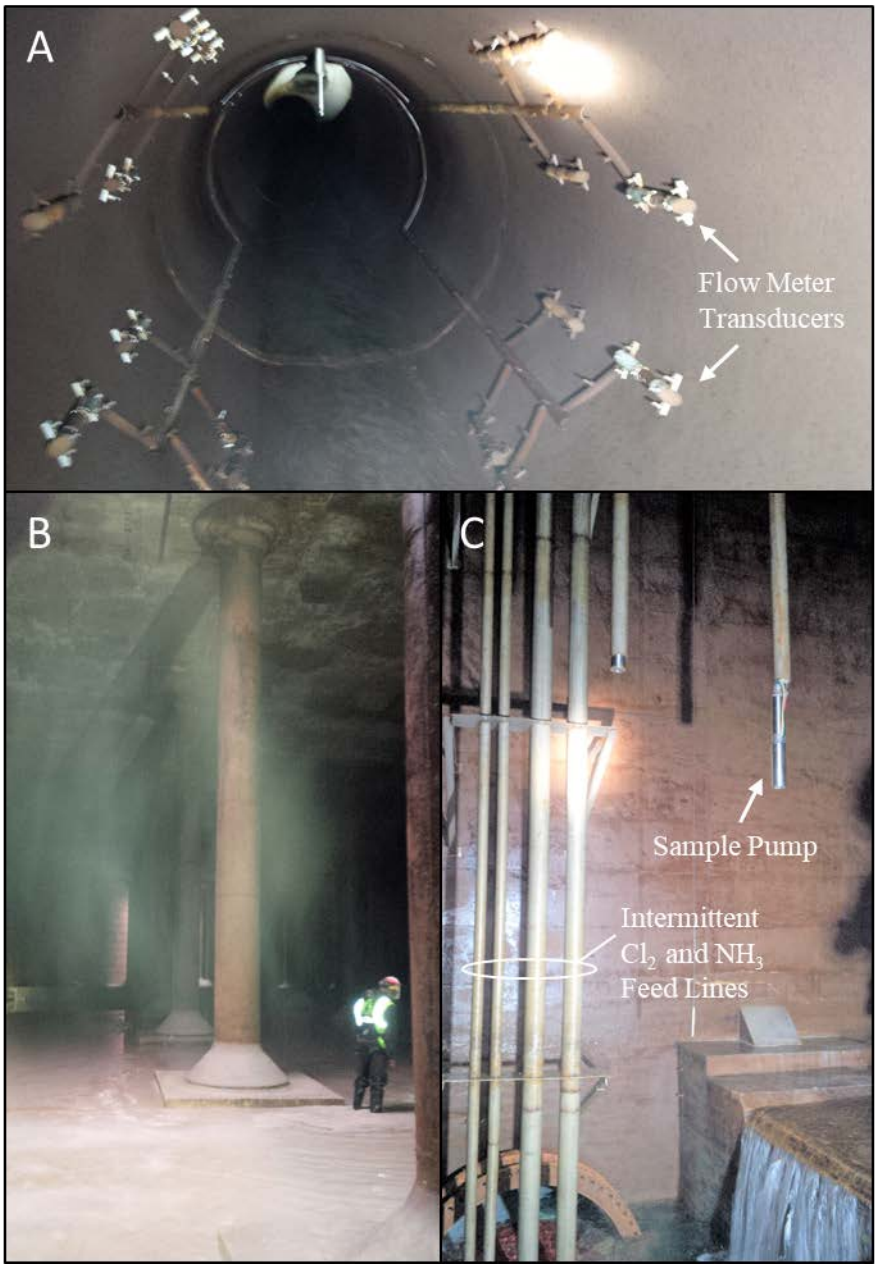

Figure B.5. Photographs of the interior of Clearwell B. Views A-C are indicated on Figure B.3, where photos correspond to (A) flow meter used for pacing ammonia feed, (B) mid clearwell, and (D) clearwell effluent with sample point and intermittent feed lines for chlorine and ammonia. Intermittent feed lines are used when the upstream primary disinfection clearwell is out of service, and ammonia is added to form chloramines leaving the second clearwell.

B.2. Model Calculations – Non-Steady State Calculation of Reactive Species in SF, TIS, and RN Models

Variable names used in R code are represented in this section by italicized text. Abbreviations such as $\Delta C/C_0$, Θ_i, and τ_j represent parameters from tracer data and operations data and are not variable names used in R code.

B.2.1 Model Inputs and Reaction Function Common to All Models

All models rely on the same inputs: date (*Date*), residence time (*HRT*) equal to volume divided by flow, free chlorine (*FreeCl*) molar concentration, and molar dose of ammonia (*NH3*). All of these inputs are stored in the variable *Influent*.

There is a function that constitutes the reaction model. This function calculates the speciation of chlorine and ammonia based on pH, calculates the rates of reaction based on pre-defined rate constants and current concentrations of associated species, and then calculates the rate of production or loss of a particular species based on the rates of reaction (see Table 3.2 in Chapter 3). This function returns the rate of production or loss for each species, which is used in the differential equation solving function *ode* in the *deSolve* package (Soetaert et al. 2010) in R (R Core Team 2016) to calculate changes in species concentrations over time. The *ode* function also requires initial species concentrations and durations of reaction as inputs.

B.2.2 Segregated Flow (SF) Model

For the SF model, the predicted effluent chemical species concentrations were calculated as the sum of individual PFR effluents weighted by $\Delta C/C_0$ (i.e., fraction of flow passing through each PFR). Each individual PFR effluent was predicted from influent species concentrations and reactions that would take place in the PFR (i.e., chloramine decay). Influent species were

selected by looking back in time $\Theta_i * \tau_j$ minutes, where Θ_i is the normalized run time of the associated tracer data point and τ_j is observed overall reactor τ at the time of interest. After solving for the PFR effluent concentrations using *ode*, the weighted concentrations can then be summed. This summary will be described in more detail in the following paragraphs.

At any single time point in the model (*CurDate*), the influent species concentrations will be different for each PFR because each PFR searches back a different period of time. To find the influent species for each PFR *i* at each point in time *j* in *CurDate*, the values of $\Theta_i * \tau_j$ (where τ_j = *HRT* at time *j*) are stored in a vector, *BackTime*. The target timestamps (*Tstamps*), are then found by subtracting *BackTime* from *CurDate*. Because *Tstamps* are unlikely to exactly match *Dates*, an *index* (vector equal to the length of tracer dataset) is found that minimizes the difference in the two date vectors (*Tstamps* and *Dates*).

A matrix of concentrations entering the overall reactor (*yLoop*) is then created. This matrix consists of *FreeCl*[*index*] and *NH3*[*index*], with all other species set to zero (i.e., NH_2Cl, $NHCl_2$, NCl_3, NO_3, intermediates). Concentrations of individual PFR effluents (*PFReffs*) are then calculated from the *yLoop* initial conditions at time $\Theta_i * \tau_j$ using the *ode* function in R. Each of the chemical species of interest is then calculated according the SF model: the summation of the product of $\Delta C/C_0$ and the average concentration output by successive PFRs.

The above then repeats for each time element of *Influent*.

B.2.3 Maximum Mixedness (MM) Model

The MM model used the same process for finding *yLoop* as was described above for the SF model. However, rather than using *yLoop* as the influent to *i* parallel PFRs, the MM model assumes a single reactor with flow injected at *i* locations throughout its length. Beginning with

the longest residence time *i* inject (Θ_i*τ_j), reaction products of *yLoop*[*i*] after (Θ_i - Θ_{i+1})*τ_j time were calculated using the *ode* function to find the bulk reactor concentration, *Cbulk*. Note that for the MM model, calculation begins with the longest residence time inject such that $\Theta_i > \Theta_{i+1}$ and $(C/C_0)_i > (C/C_0)_{i+1}$. At each successive injection point an initial *Cbulk* concentration, *CbulkInitial*, is calculated by from an assumed mixing of species from *Cbulk* at the previous time step with *yLoop* weighted by the proportion of flows represented (i.e., C/C_0 and $\Delta C/C_0$) as shown in the equation below.

$$CbulkInitial = \frac{Cbulk*\left(1-\left(\frac{C}{C_0}\right)_i\right) + yLoop[i+1]*\left(\left(\frac{C}{C_0}\right)_i - \left(\frac{C}{C_0}\right)_{i+1}\right)}{1-\left(\frac{C}{C_0}\right)_{i+1}}. \quad \text{B.1}$$

Reaction products of *CbulkInitial* after time (Θ_{i+1} - Θ_{i+2})*τ_j were computed using the *ode* function and became the new *Cbulk*. This process was then repeated for each *i* inject, and the overall process repeated for each time *j* in the model input time series.

B.2.4 Tanks-Series (TIS) Model

For the TIS model, predicted reactor effluent species concentrations were equal to the concentration in the last of a series of CSTRs. Concentrations in each CSTR were calculated from influent species concentration, flow displacement, and reactions that would take place in each CSTR. Unlike the retrospective selection of influent conditions used in the SF and MM models, the TIS model used influent flow to displace a volume in the CSTR. For example, if a TIS had τ = 300 minutes and n = 3, residence time in each CSTR would be 100 minutes. Using the five-minute time increment mentioned earlier, at each time step 5% of volume in each CSTR would be displaced, or $1.\overline{6}$% of the overall reactor volume. Species concentrations in each CSTR prior to reaction would be assumed to contain 95% of the previous time step plus 5% influent flow, with a reaction time in each CSTR equal to the time step divided by n (e.g., 5 min / 3 = $1.\overline{6}$

min). This summary will be described in more detail in the following paragraphs.

The fraction of reactor volume displaced by each time step (*step*) was calculated by dividing the duration of the timestep by the τ_j vector. The number of tanks, *n*, is specified. The residence time each CSTR, *TauTank*, is equal to τ_j/n. The size of step in each tank, *nstep*, is calculated as *n* times *step*.

The initial concentration of species throughout the TIS reactor (*Initial*) is assumed to be equal to the observed effluent conditions at the first point in the data set. Initial concentrations may include *FreeCl*, *NH3*, and combined chlorine, assumed to be in the form of monochloramine (*NH2Cl*). To eliminate background noise, *FreeCl*, *NH3*, and *NH2Cl* were assumed to be equal to zero if observed at concentrations of less than 10 µM, 20 µM, and 10 µM, respectively. These initial conditions are applied to the each CSTR (e.g., *C_1*, *C_2*, *C_3*) in the TIS reactor. A matrix of influent conditions (*C_inf*) is created, which consists of *FreeCl* and *NH3*, with all other species set to zero (i.e., NH_2Cl, $NHCl_2$, NCl_3, NO_3, intermediates).

After the initial conditions have been set at the first time step, for each subsequent time step the CSTR concentrations before (e.g., *C_1init*, *C_2init*, *C_3init*) and after (e.g., *C_1*, *C_2*, *C_3*) reaction are calculated. For the first CSTR, the initial concentration is calculated as

$$C\_1_{init,i} = C\_1_{i-1} * (1 - nstep) \; + \; C\_inf_{i-1} * nstep. \qquad \text{B.2}$$

For the second CSTR, the initial concentration is calculated as

$$C\_2_{init,i} = C\_2_{i-1} * (1 - nstep) \; + \; C\_1_{i-1} * nstep. \qquad \text{B.3}$$

This process continues for each CSTR in the TIS reactor. The post-reaction

concentrations (e.g., *C_1*, *C_2*, *C_3*) are calculated using the initial conditions (e.g., *C_1init*, *C_2init*, *C_3init*) after the reaction time $step_{i-1}*TauTank_{i-1}$ using the *ode* function in R. Species concentrations leaving the last CSTR in the series were equal to the reactor effluent concentrations.

B.2.5 Reactor Network (RN) Models

The RN models were calculated using the processes described above for each TIS reactor in the parallel TIS RN model and for the PFR and CSTRs in series, repeated in parallel RN model. There are a few differences to note. For the parallel TIS RN model (Clearwell A), *TauTank* and *nstep* vary for each TIS reactor.

For the first TIS, $Tau1Tank = \tau_j/n1tanks*V_{TIS1}/Q_{TIS1}$, $n1step = step*n1tanks*Q_{TIS1}/V_{TIS1}$, and reaction times are equal to $step_{i-1}*Tau1Tank_{i-1}$ where V_{TIS1} and Q_{TIS1} are volume and flow fractions. Similar calculations are made for the second TIS using *n1tanks*, V_{TIS1}, and Q_{TIS1}. Effluent species concentrations are then calculated as described above, and summed after weighting by Q_{TIS1} and Q_{TIS2}. The overall effluent concentration for Clearwell A then becomes

$$C_{effluent} = C\_13 * Q_{TIS1} + C\_9 * Q_{TIS2}. \quad \text{B.4}$$

For the PFR and CSTR in series, repeated in parallel RN model, residence time in each reactor is calculated as by taking τ_j times volume fraction over flow fraction. The process described above for SF is then used to calculate the effluent concentrations of each PFR. The concentrations in each CSTR are then calculated as described above for the TIS reactor. Effluent species concentrations are then summed after weighting by flow fractions as described for the first RN model. The effluent concentration was calculated as

$$C_{effluent} = C_{CSTR1} * Q_1 + C_{CSTR2} * Q_2. \quad \text{B.5}$$

B.3. Key Concepts – Detailed Discussion

B.3.1 Flow Segregation and Mixing

The concepts of flow segregation and earliness of mixing (i.e., micromixing) are both interrelated, and also intertwined with RTD (Levenspiel 1996). Degree of segregation describes to what extent flow within a reactor flows along separated paths, as opposed to mixed. Earliness of mixing describes whether flow entering a reactor mixes with the reactor contents when it enters, when it exits, or somewhere in between. To illustrate these concepts, Figure 3.3 (see Chapter 3) shows simple reactors where a yellow fluid and a blue fluid mix to form a green fluid. In a reactor with perfect segregation throughout (A), two flows would not mix until they leave the reactor; this is conceptually equivalent to having a zero residence time CSTR at the end of two PFRs, which produces the latest possible mixing. Conversely, with perfect mixing throughout (B), the reactor would function as a CSTR, immediately forming the green fluid. This would create the earliest possible mixing. If flow in the reactor was initially segregated and later mixed (C), the blue and yellow fluids would exist prior to forming the green fluid. Finally, if mixing occurred early in the reactor with subsequent segregation (D), the green fluid would be formed immediately before splitting into two separate flows of the green fluid.

B.3.2 Reactor Models

The tanks-in-series (TIS) reactor is made up of a finite number (*n*) of equal-volume, perfectly-mixed CSTRs arranged in series. Reactor network (RN) models are combinations of PFR, CSTR, and/or TIS reactors arranged in parallel and series combinations (see Chapter 2). The RN model sub-reactors are not assumed to have equal volume, volumes are instead determined by least squares regression. The reactor examples provided in Figure 3A, C, and D

are all examples of reactor networks. The segregated flow (SF) model represents a reactor as numerous parallel PFRs (Najm et al. 2009, Crittenden et al. 2005), and thus can be considered a special type of RN model that only uses PFRs. The SF model is similar to Figure 3A where the blue and yellow fluids have different residence times. The maximum mixedness (MM) model assumes that flow enters the reactor at multiple locations, perfectly mixing with reactor contents at the point of injection. This can conceptualized as a Figure 3C repeated in series for every entry point to the reactor.

The PFR, CSTR, TIS, and MM all assume only a single flow path, and thus have no flow segregation. Flow segregation is assumed to be perfect in SF model, and varies for RN model depending on whether the model splits flow into multiple paths. For earliness of mixing, the PFR and CSTR represent two extremes: flow entering a PFR is assumed to never mix with the original reactor contents, while in a CSTR influent flow is assumed to mix perfectly and instantaneously. The MM model assumes perfect mixing occurs as flows enter the reactor at multiple locations, but no longitudinal mixing. Mixing in a TIS reactor occurs in *n* stages. The SF model assumes that flow mixes at the latest possible time: when flow exits the reactor. Earliness of mixing will vary for a RN model depending on which reactor types are used and how these model types are arranged.

B.3.3 Predictions in Ideal Reactors: PFR and CSTR

Concentrations of relevant chemical species during $CombCl_2 \rightarrow FreeCl_2$ and $FreeCl_2 \rightarrow CombCl_2$ were predicted for two ideal reactors: the PFR and CSTR. The purpose of studying disinfectant switching in ideal reactors is twofold. The first reason is to introduce the reader to the building blocks of more complex models (i.e., TIS, SF, MM, RN). The second is to demonstrate what would happen if water treatment reactors were assumed to follow the two

extremes of plug and mixed flow.

The following water quality conditions were assumed for both reactors: pH 7.5, temperature 25ºC, 2 mM total inorganic carbon (TIC), 0 µM PO_4^{3-}, 50 µM influent monochloramine (NH_2Cl) or $FreeCl_2$, and 5 µM excess free ammonia when NH_2Cl was fed. A perfect step change in oxidant at time zero was assumed. Results from a CSTR and a PFR with nominal hydraulic residence time (τ) of 1 hour are shown in Figure B.6 and Figure B.7, respectively. These figures show both $CombCl_2 \rightarrow FreeCl_2$ and $FreeCl_2 \rightarrow CombCl_2$.

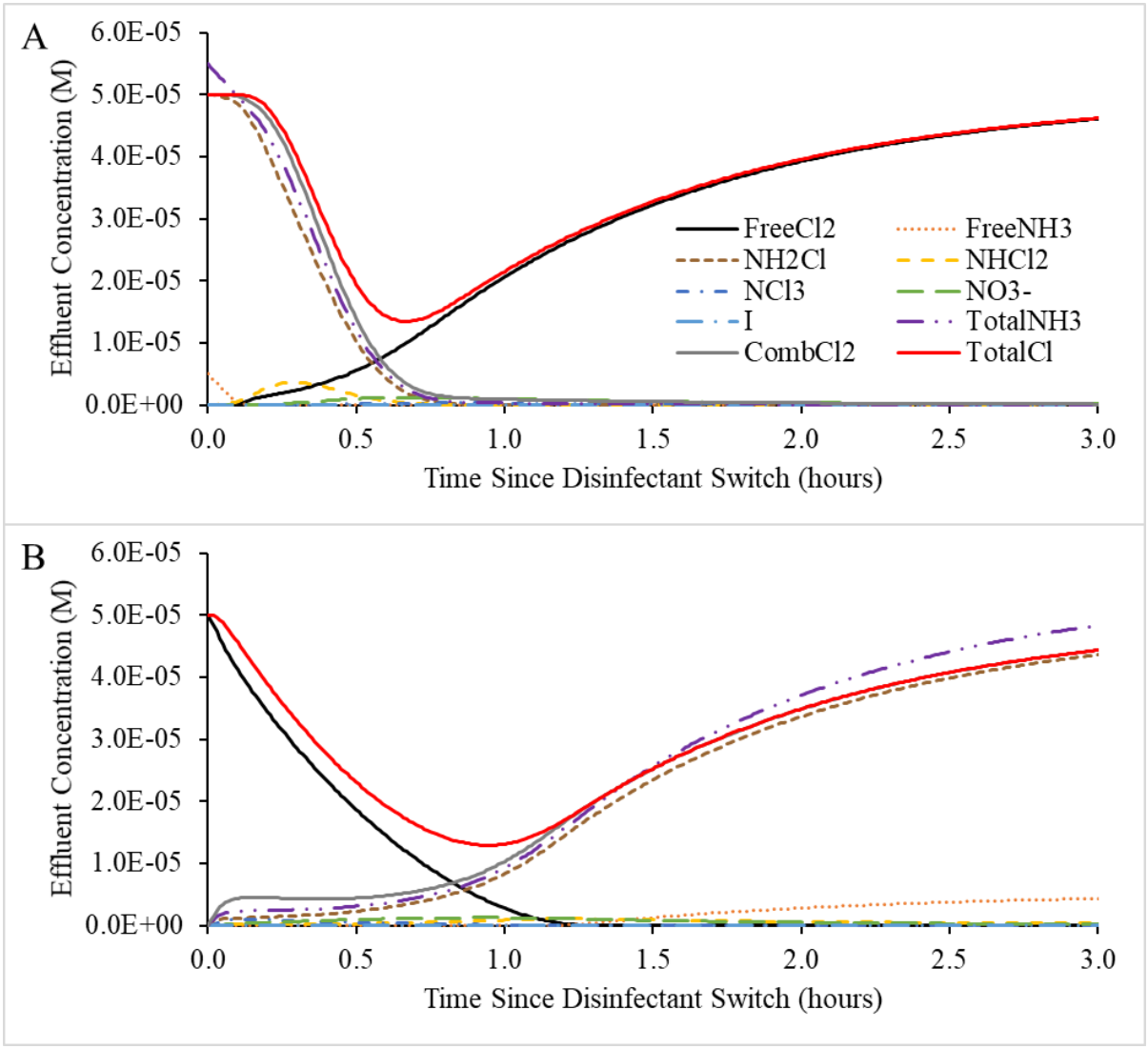

Figure B.6. Predicted effluent concentrations of species from a CSTR with τ = 1 hour for (A)

$CombCl_2 \rightarrow FreeCl_2$ and (B) $FreeCl_2 \rightarrow CombCl_2$. Species that remain near zero include NCl_3 and I.

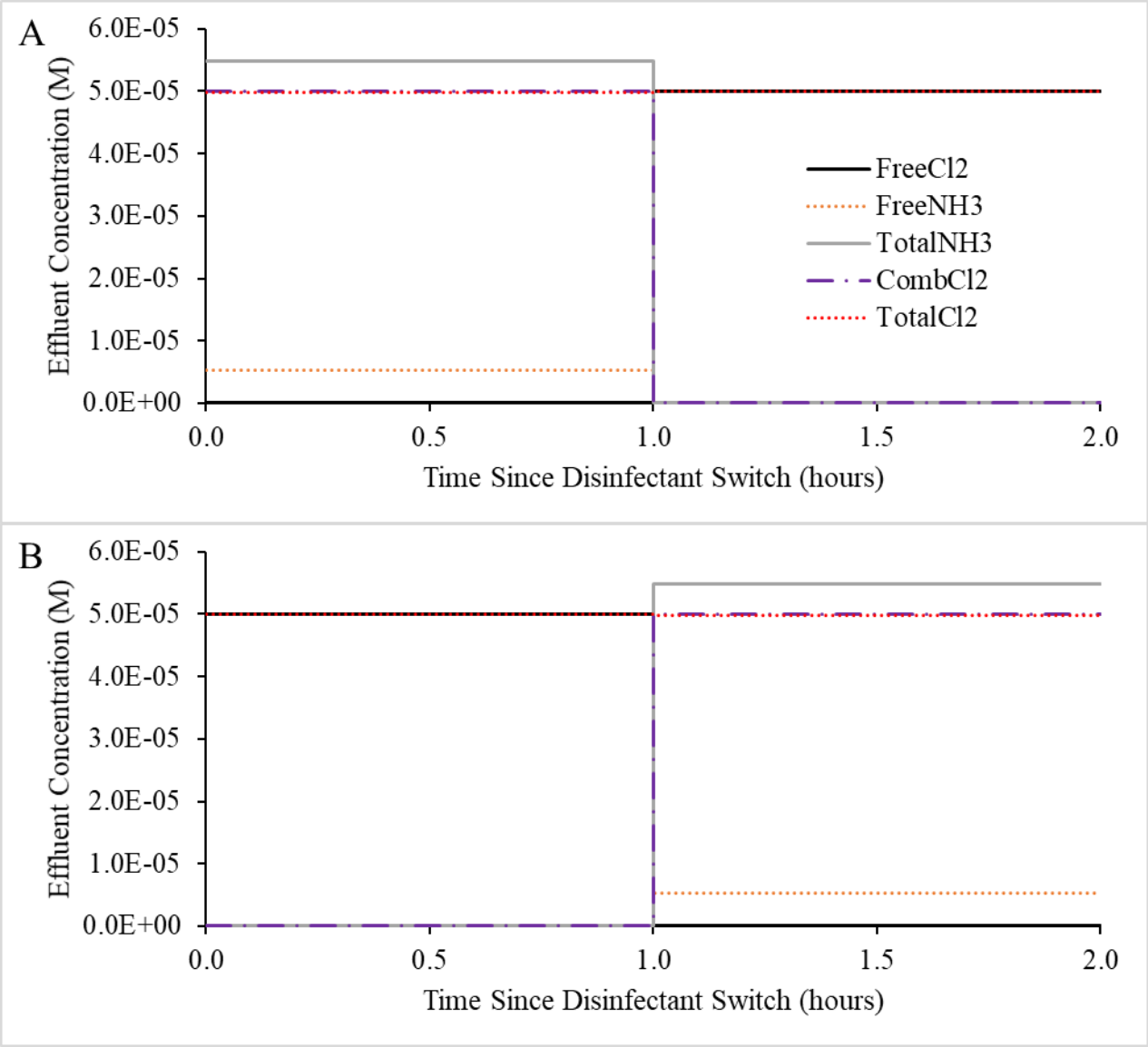

Figure B.7. Predicted effluent concentrations of species from a PFR with τ = 1 hour when (A) $CombCl_2 \rightarrow FreeCl_2$ and (B) $FreeCl_2 \rightarrow CombCl_2$.

The CSTR assumes complete internal mixing. For $CombCl_2 \rightarrow FreeCl_2$ and $FreeCl_2 \rightarrow CombCl_2$, $CombCl_2$ and $FreeCl_2$ species will react in the CSTR according to the reactions in Table 3.2 (see Chapter 3). This produces a predicted breakpoint phenomena. Reaction

predictions vary depending which disinfectant, $CombCl_2$ or $FreeCl_2$, was initially in the reactor. For $CombCl_2 \rightarrow FreeCl_2$, the minimum $TotalCl_2$ concentration predicted was 13.5 μM at 0.67 hours, while the minimum $TotalCl_2$ concentration predicted was 12.9 μM was 0.94 hours. Although the two minimum concentrations are similar, the breakpoint reaction proceeds more quickly for $CombCl_2 \rightarrow FreeCl_2$. For example, predicted effluent $TotalCl_2$ concentrations fell below 14.5 μM (1 mg/L) for 0.15 hours (from 0.60-0.75 hours) for $CombCl_2 \rightarrow FreeCl_2$, less than half as long as for $FreeCl_2 \rightarrow CombCl_2$ (0.31 hours, from 0.79-1.10 hours). Another difference to note is that $CombCl_2 \rightarrow FreeCl_2$ (panel A) produces more $NHCl_2$ than $FreeCl_2 \rightarrow CombCl_2$ (panel B). Since chloramine loss is primarily limited by the formation of $NHCl_2$ at circumneutral pH values (Jafvert and Valentine 1992, Vikesland et al. 2001), this may in part explain predictions of more rapid breakpoint in $CombCl_2 \rightarrow FreeCl_2$ than $FreeCl_2 \rightarrow CombCl_2$.

However, the period of $NHCl_2$ formation was brief and concentrations were low; NH_2Cl was the predominant chloramine species. For this reason, further results in this Key Concepts section report predictions for the sum of chloramine species (i.e., $CombCl_2$).

The PFR, unlike the CSTR, assumes no internal longitudinal mixing. There is no breakpoint in the absence of mixing as shown in Figure S7. This results in a predicted step change in species concentration at time $t = \tau$. Species exiting a PFR at time t are only dependent on the influent species at time t-τ. This will be important for the SF model, which assumes reactors behave as a set of parallel PFRs, none of which will individually predict breakpoint.

In summary, the CSTR predicted breakpoint phenomena, while the PFR did not. The predicted reactions in the CSTR were also different depending on whether free chlorine is added to NH_2Cl or NH_2Cl is added to free chlorine.

B.3.4 Predictions in SF and TIS Models

The next step in model development is to use the results from the previous section for PFRs and CSTRS to develop increasingly complex models: SF and TIS. This section presents results for hypothetical SF and TIS models. Reaction conditions are the same as those described in the preceding section, with only $CombCl_2 \rightarrow FreeCl_2$ results shown.

The conversion from $CombCl_2$ to $FreeCl_2$ was modeled for a TIS with $n = 3$ as shown in Figure B.8. Total reactor residence time was 1 hour, or 1/3 hour for each CSTR. Similar to Figure B.6, breakpoint was predicted for each CSTR in the TIS. Lower total chlorine residuals were predicted from each successive CSTR, with the overall reactor effluent (T3) being the lowest of the three. The TIS reactor with $n = 3$ predicted a higher minimum total chlorine residual than the single CSTR: 21.0 versus 13.5 μM. However, this may be due in part to insufficient time for breakpoint reactions in the reactor. Consider where the $CombCl_2$ and $FreeCl_2$ lines intersect for each of the three CSTRs. The model predicts that at this point, $CombCl_2$ and $FreeCl_2$ leave each CSTR at equal concentrations. Any such solution would be unstable, resulting in breakpoint reactions until only $CombCl_2$ or $FreeCl_2$ remain; which one remained would depend on free ammonia concentrations in the solution.

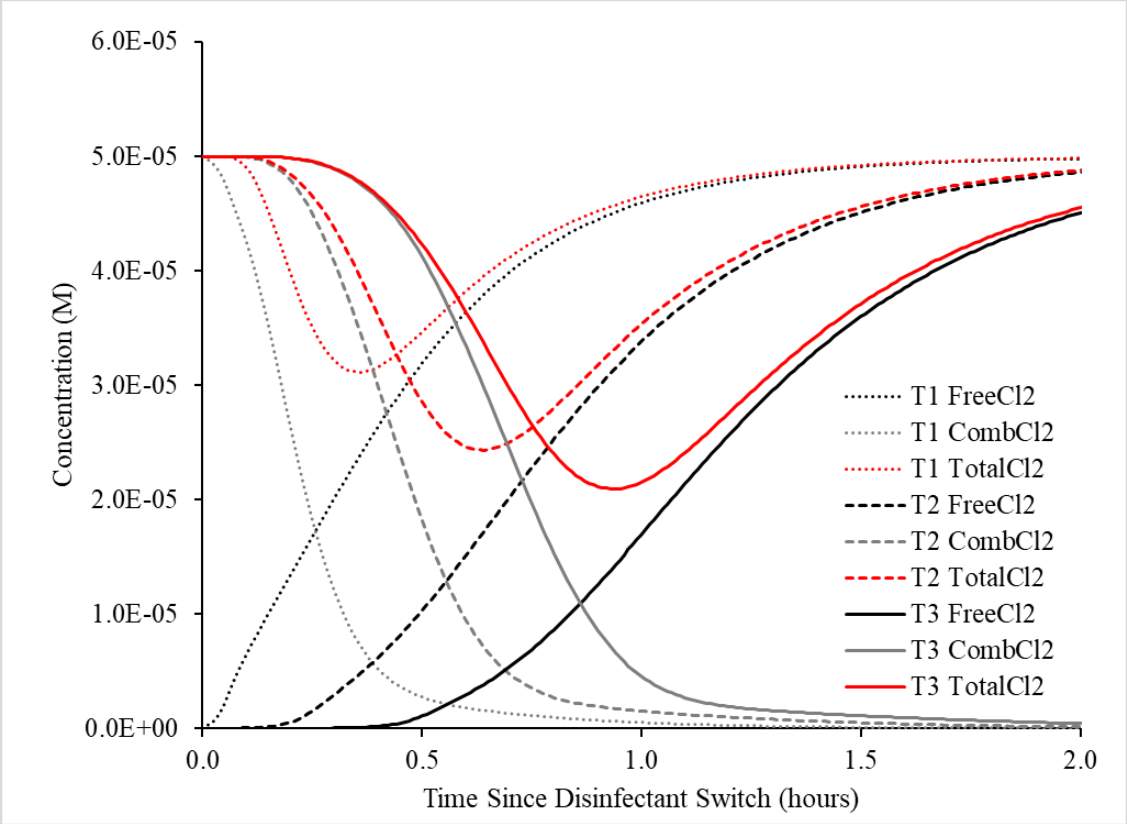

Figure B.8. Predicted effluent concentrations following $CombCl_2 \rightarrow FreeCl_2$ for each CSTR in a TIS reactor with n = 3. Total reactor τ = 1 hour, 1/3 hour per CSTR.

To study this issue further, an analysis was performed to predict how incomplete breakpoint reactions would proceed over time. Consider the predicted effluent concentrations of the third tank in Figure B.8. Figure B.9 shows how effluent concentrations of $FreeCl_2$, $CombCl_2$, and $TotalCl_2$ would change after 0, 5, and 60 minutes of additional reaction time. These "post-effluent" concentrations model what would happen downstream of the reactor, such as in a distribution system. Results show that for n = 3 and τ = 1 hour (panel A), breakpoint reactions would proceed after flow leaves the reactor, with predicted minimum $TotalCl_2$ residual reduced from 21.0 to 13.9 µM (7.1 µM difference, 34% reduction) after 5 minutes, and to 2.8 µM (18.2 µM difference, 87% reduction) after 60 minutes. If reactor residence time were increased from 1 hour to 10 hours, there would be more time for breakpoint reactions to occur, resulting in reduced effluent chlorine residuals as shown in Figure B.9B. The minimum $TotalCl_2$ residual in

the effluent flow (i.e., 0 min) would be reduced from 21.0 to 8.2 μM when residence time increased from 1 to 10 hours. The magnitude of change in post-effluent TotalCl_2 was reduced, however, from 7.1 to 1.2 μM after 5 minutes, and from 18.2 to 5.4 μM after 60 minutes, when residence time increased from 1 to 10 hours. This was because there was more time for breakpoint reactions to occur when τ = 10 hours. In summary, breakpoint reactions may be incomplete leaving TIS reactors, particularly when reactor residence time is short.

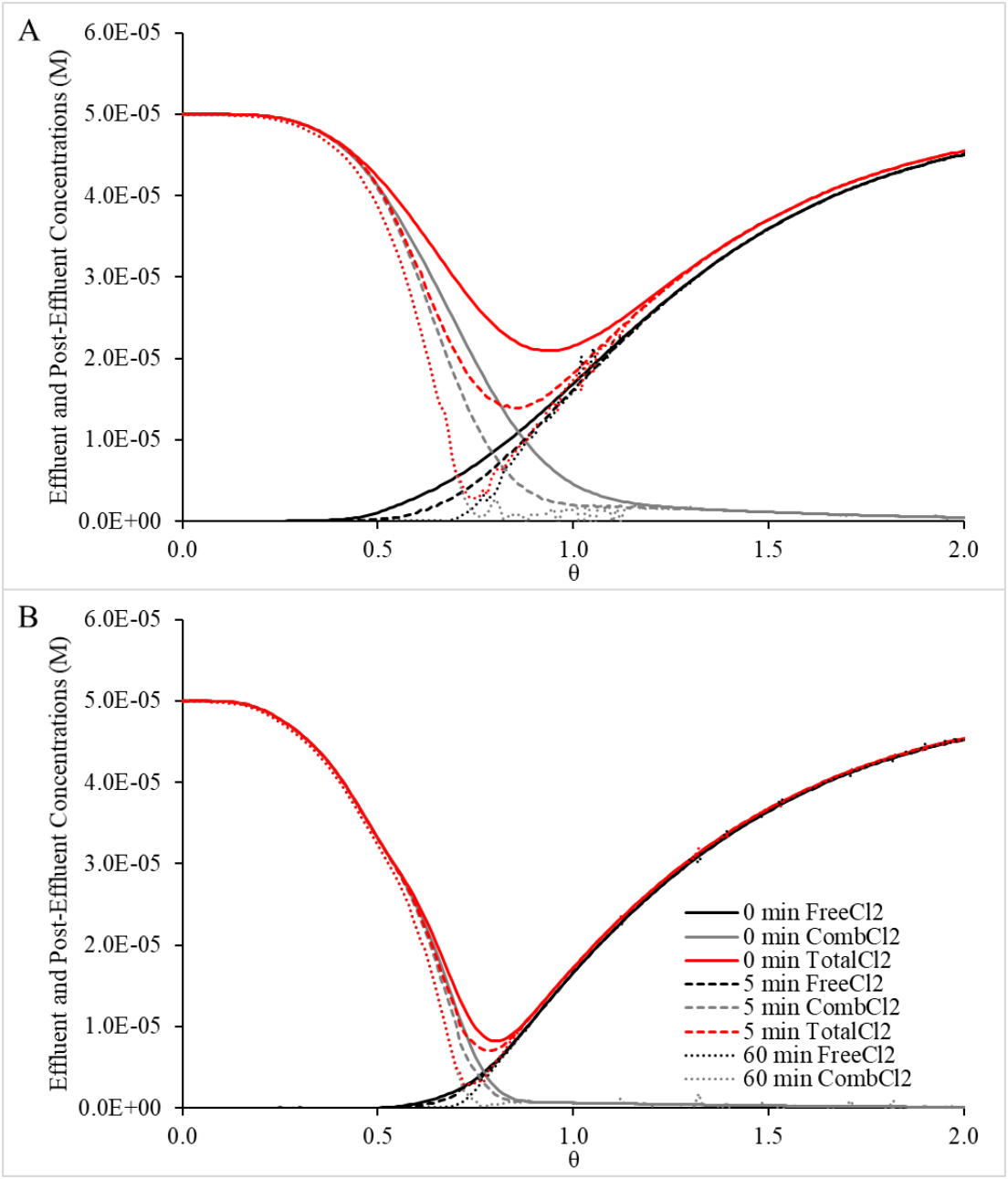

Figure B.9. Predicted effluent and post-effluent concentrations of $FreeCl_2$, $CombCl_2$, and $TotalCl_2$ following $CombCl_2 \rightarrow FreeCl_2$ for TIS reactors where n = 3 and (A) 1 hour residence time and (B) 10 hour residence time. Post-effluent concentrations show predictions of species concentration if a given sample of water was collected from the reactor effluent and held for some time in a batch reactor (i.e., 0, 5, or 60 minutes). Changes in post-effluent concentrations over time suggest that break point reactions are not yet complete in clearwell effluent, and model what would happen downstream of the clearwell, such as in a distribution system. Results indicate that breakpoint reactions in a TIS reactor (n = 3) would be much farther from completion in a reactor with a 1-hour residence time (panel A) than a 10-hour residence time (panel B).

An even more extreme example of breakpoint reactions not proceeding to completion is the SF model. There is no mixing in the SF model until flow leaves the reactor; at that time individual flows are assumed to be perfectly mixed but given zero time for reactions to take place. Consider a SF model consisting of three PFRs as shown in Figure B.10A. This hypothetical SF model has flow split evenly through the PFRs, each having τ equal to 0.5, 1.0, and 1.5 hours. It was assumed that $CombCl_2 \rightarrow FreeCl_2$ occurred at time zero. For time less than τ of the first PFR (i.e., $t < 0.5$ hr), all three reactors had $CombCl_2$ in their effluent (Figure B.10B). For time $0.5 < t < 1.0$ hr, the smallest PFR has $FreeCl_2$ in the effluent, while the other two have $CombCl_2$. Despite having both $CombCl_2$ and $FreeCl_2$ in the overall reactor effluent (see Figure B.10B), the SF model predicted no loss of $TotalCl_2$ residual because there was zero time for reactions to take place. As was discussed for the TIS reactor, the co-occurrence of $FreeCl_2$ and $CombCl_2$ in SF effluent would result in a loss of $TotalCl_2$ residual in post-effluent flow due to breakpoint reactions. Post-effluent breakpoint for time $0.5 < t < 1.0$ hr is shown in Figure B.10C. Breakpoint behavior would also be observed in post-effluent for time $0.5 < t < 1.0$ hr (see Figure B.10D), although this was predicted to produce a $FreeCl_2$ residual due to two of three PFRs having effluent free chlorine. Analysis of the SF model illustrated an important concept: reactor effluents from parallel flows have zero time for breakpoint reactions to occur, thus underestimating $TotalCl_2$ loss during temporal disinfectant switching. This finding is important not just for the SF model, but also for any RN model with parallel flows, including those selected for Clearwells A and B.

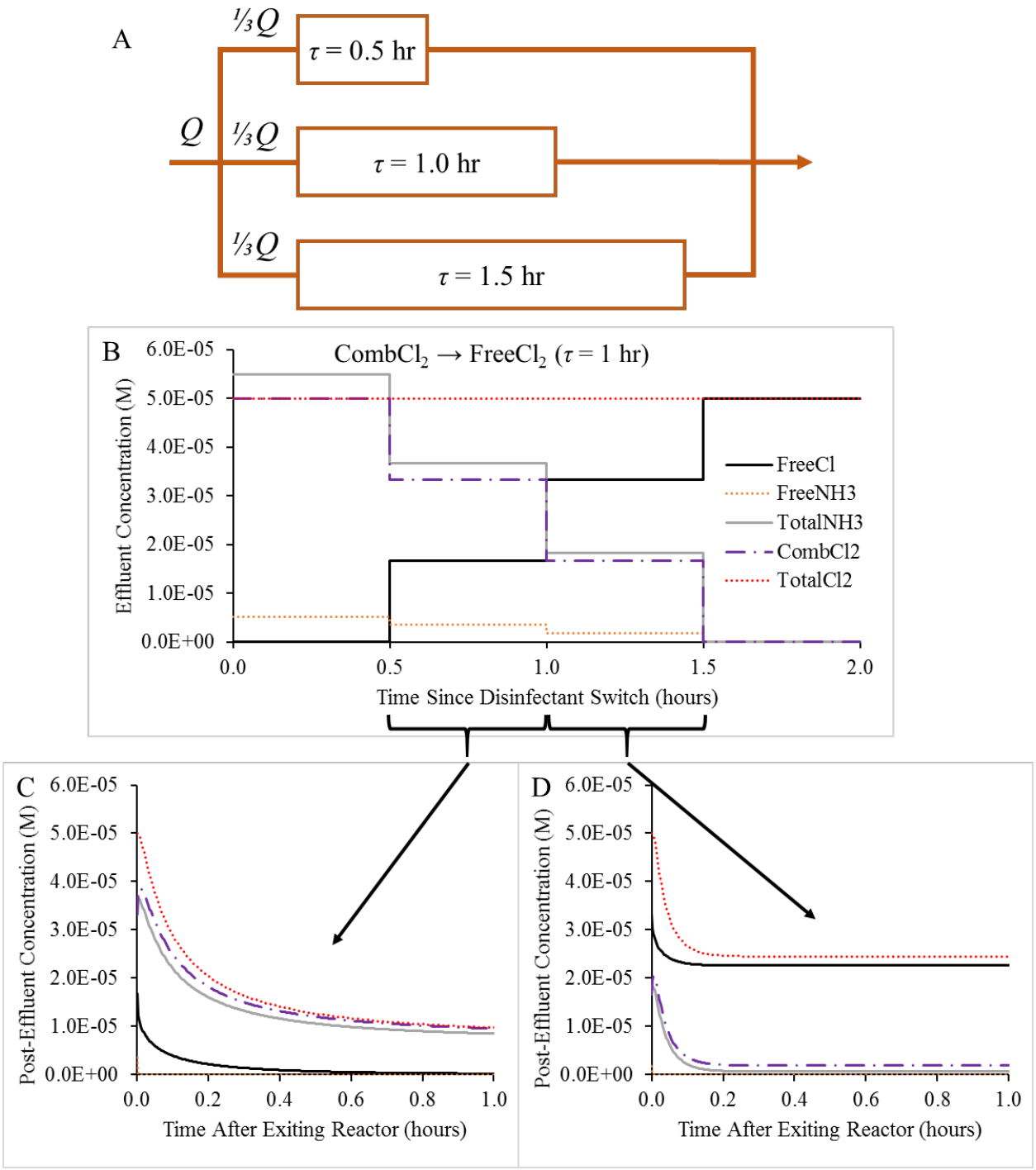

Figure B.10. (A) Schematic of a hypothetical segregated flow (SF) model, where PFRs in the SF model have τ = 0.5, 1.0, and 1.5 hours, with overall τ = 1.0 hour. (B) SF predictions of effluent species concentrations after $CombCl_2 \rightarrow FreeCl_2$. SF model assumes mixing leaving the reactor without time for reactions. After exiting the reactor, flow leaving the SF model between (C) 0.5 and 1.0 hours and (D) 1.0 and 1.5 hours would undergo reactions resulting in breakpoint from the mixing of $CombCl_2$ and $FreeCl_2$.

B.4. Representations of SF and MM at Steady State and Unsteady State

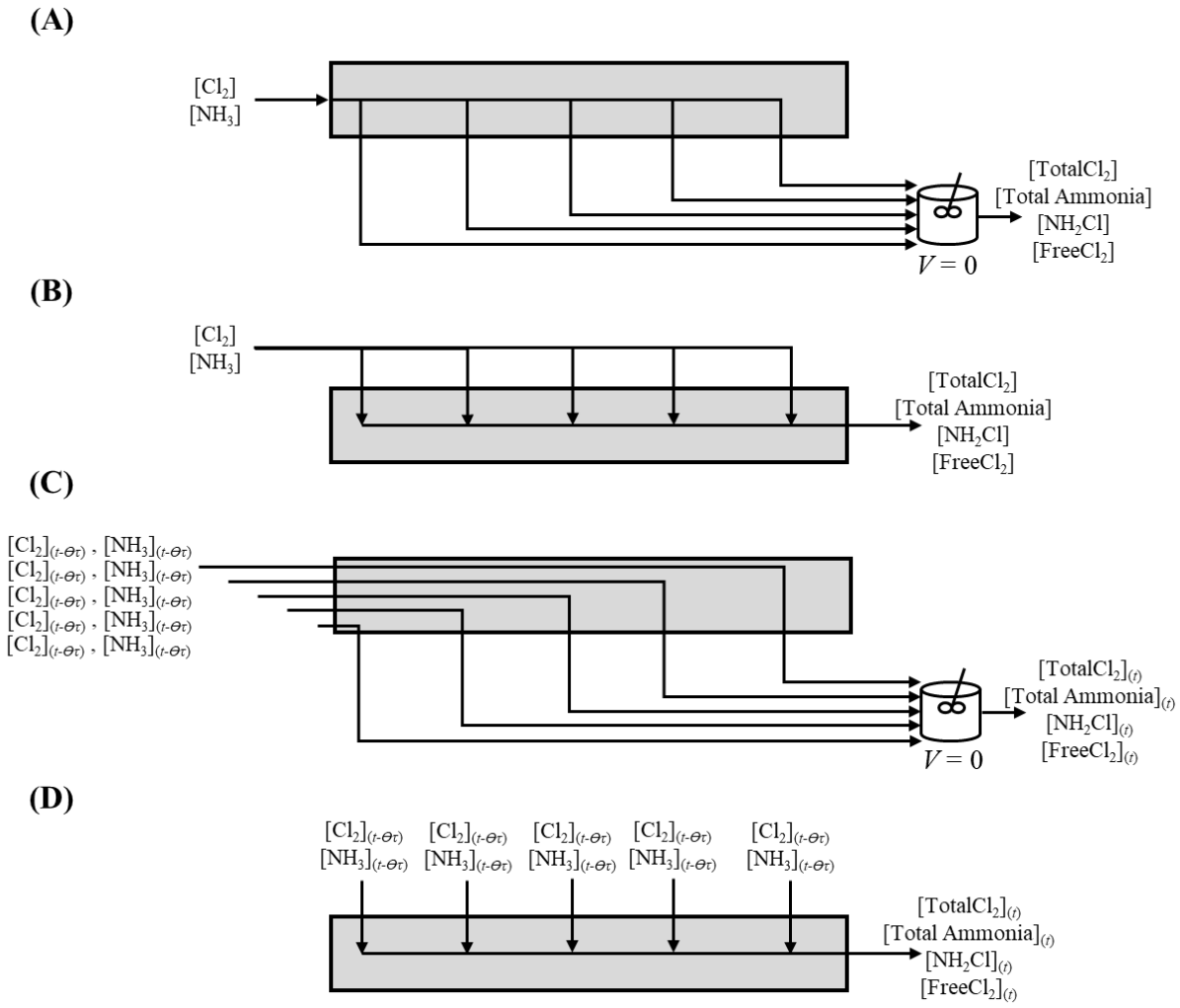

Figure B.11. Representations of the (A) segregated flow model at steady state, (B) maximum mixedness model at steady state, (C) segregated flow model with unsteady operation (i.e., used in this work), and (D) maximum mixedness model with unsteady operation (i.e., used in this work).

B.5. TIS Model Predictions When *n* is Varied

Reactor flows varied significantly throughout disinfectant conversion (see Figure 3.2 and Figure 3.9 in Chapter 3), unlike the conditions in which tracer studies were conducted (see in Figure 3.1 in Chapter 3). Therefore, it was of interest to test whether differences in RTD might produce better model fits. TIS models with *n* identified through least squares regression were compared with TIS models using *n*-2, *n*-1, *n*+1, and *n*+2 for Figure 3.4 – Figure 3.8 in Chapter 3.

The NRMSE for TotalCl$_2$ is shown in Figure B.12. For Clearwell A (see Figure 3.4 – Figure 3.6 in Chapter 3), the fitted value of *n* produced the best fit (i.e., had the lowest NRMSE). For Clearwell B (see Figure 3.7 and Figure 3.8 in Chapter 3), *n*-1 produced the best fit, with *n* performing the second best. These results indicate that the RTD model found by fitting *n* to tracer data was also the best *n* for predicting TotalCl$_2$ concentrations for Clearwell A, and second best for Clearwell B. This gives greater confidence that the RTD was not varying substantially with flow rate.

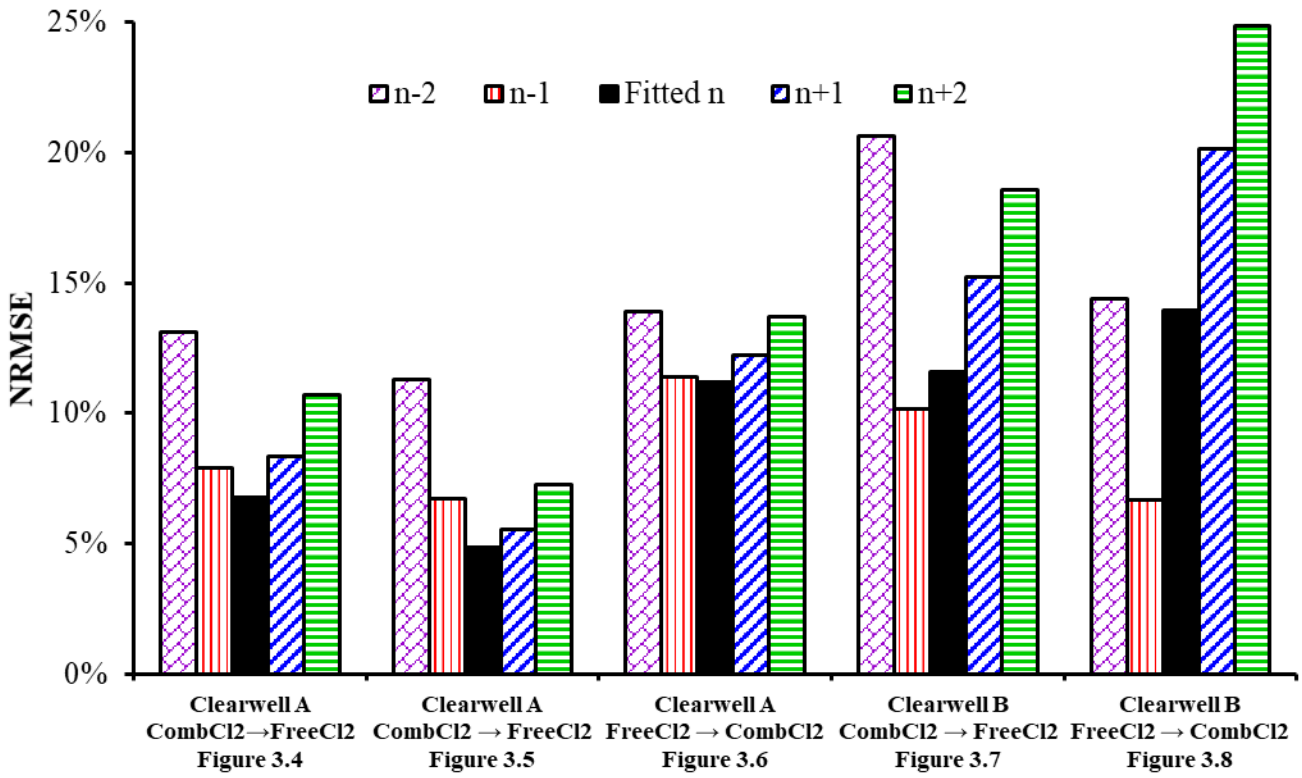

Figure B.12. TotalCl$_2$ NRMSE for TIS model predictions using *n* found by least squares regression (see Figure 3.1) as well as *n*-1, *n*-2, *n*+1, and *n*+2.

B.6. Example Code for Predicting Concentrations of Reactive Tracer Species

Code shown is for Clearwell A.

```
rm(list = ls()) # Clear workspace
dev.off(dev.list()["RStudioGD"]) # Clear plots

# This code will use the deSolve package by Soetaert et al. 2010
require(deSolve)

# Plotting package
require(ggplot2)
require(reshape2)
require(xlsx)

# Zoo for rollapply
require(zoo)

# svMisc to view progress of for loop
require(svMisc)

# Define important conditions
#chlorine:ammonia mass ratio
Cl_2_NH3 <- 4.6 # 4.5:1
pHi <- 7.7
PO4i <- 2.4 # mg/L as PO4
Temp <- 7 #degrees C, for modifying rate constants
TotC <- 0.766*2*10^-3 # Molar conc., 2x10^-3 approx. equal to 100 mg/L as CaCO3 at pH 7.7


### Load PI data - from SCADA historian
setwd("C:/Users/agorz/Documents/PhD Research/Paper 2/")
PIDataFile <- "CWA_Comb2Free_2018.xlsx"
deltaT <- 5 # PI data time intervals, in minutes
library(xlsx)
PIdata <- read.xlsx(PIDataFile, sheetIndex = 1) # load PI data



### Create tracer data from RN model fit
thetaStep <- 0.05 # Size of time step
thetaModel <- seq(0,3,thetaStep)

TIS <- function(n,theta){
  tisFuncI <- function(theta) {n*( (n*theta)^(n-1) ) / factorial(n-1) * exp(-n*theta)}
  sapply(theta,function(theta) integrate(tisFuncI,lower=0,upper=theta)$value)
}
parTT <- function(Theta,VF_TIS1,VF_dead,Q1,n1,n2) {
  Q1*TIS(n1,(Theta/VF_TIS1*Q1) ) +
    (1-Q1)*TIS(n2,(Theta/(1-VF_TIS1-VF_dead)*(1-Q1)) )}
CC0Model <- parTT(thetaModel,0.433,0.04098,0.61117,13,9)
ModeledTracerData <- cbind(thetaModel,CC0Model)
colnames(ModeledTracerData) <- c("Theta","CC0")

ModeledTracerData <- cbind(thetaModel,CC0Model)
colnames(ModeledTracerData) <- c("Theta","CC0")



# Convert Units from mg/L to mol/L
PIdata$AmmFeed <- PIdata$AmmFeed/14/10^3
PIdata$INF_FreeCl_DPD <- PIdata$INF_FreeCl_DPD/(35.453*2)/10^3
PIdata$EFF_FreeAm_CS <- PIdata$EFF_FreeAm_CS/14/10^3
PIdata$EFF_FreeCl_DPD <- PIdata$EFF_FreeCl_DPD/(35.453*2)/10^3
PIdata$EFF_TotCl_DPD <- PIdata$EFF_TotCl_DPD/(35.453*2)/10^3


# Calculate initial and influent conditions
Influent <- matrix( rep(NA, length(PIdata[,2])*4), ncol = 4)
Influent <- as.data.frame(Influent) # make matrix a data frame, necessary for melting later
colnames(Influent) <- c("Date","HRT","FreeCl","NH3")
Influent$HRT <- PIdata$HRT
Influent$Date <- PIdata$Date
Influent$FreeCl <- PIdata$INF_FreeCl_DPD
Influent$NH3 <- PIdata$AmmFeed

Initial <- matrix( rep(NA, 3), ncol = 3)
Initial <- as.data.frame(Initial) # make matrix a data frame, necessary for melting later
colnames(Initial) <- c("FreeCl","NH2Cl","NH3")
Initial$FreeCl <- ifelse(PIdata$EFF_FreeCl_DPD[1] < 1*10^-5,0, PIdata$EFF_FreeCl_DPD[1]) # To remove make zero if noise is present
Initial$NH2Cl  <- ifelse(PIdata$EFF_FreeCl_DPD[1] > 2*10^-5,0, PIdata$EFF_TotCl_DPD[1]) # Indicates free chlorine initially
Initial$NH3    <- ifelse(PIdata$EFF_FreeAm_CS[1] < 1*10^-5,0, PIdata$EFF_FreeAm_CS[1]) # To remove make zero if noise is present
```

```
### Set up Model and Initial Conditions

## Throw away initial conditions for model setup

# Define initial conditions in mg/L - need for calculating k's
FreeCli <- 4.0 # mg/L as Cl2
FreeNi <- 0.95 # mg/L as NH3-N
# Calc initial conditions in mol/L
H <- 10^-pHi
OH <- 10^-(14-pHi)
FreeCl <- 5*10^-5
FreeN <- FreeCl*(70.9 / (4.5*14) ) # Assumes excess ammonia - Cl2:NH3 ration of 4.5:1
TotP <- PO4i/94.97/10^3


## Model

# Define equlibrium speciation
Kw <- 10^-13.8
OH <- Kw/H

Ka1p <- 10^-1.90
Ka2p <- 10^-6.79
Ka3p <- 10^-11.62
Pdenom <- H^3 + (H^2)*Ka1p + H*Ka1p*Ka2p + Ka1p*Ka2p*Ka3p
H3PO4 <- TotP*(H^3)/Pdenom
H2PO4 <- TotP*(H^2)*Ka1p/Pdenom
HPO4  <- TotP*H*Ka1p*Ka2p/Pdenom
PO4   <- TotP*Ka1p*Ka2p*Ka3p/Pdenom

Kel <- 273 + Temp
kCO31 <- 10^-(1.48*(10^-4)*Kel^2 - 9.39*(10^-2)*Kel + 21.2) # See Vikeslund 2001
kCO32 <- 10^-(1.19*(10^-4)*Kel^2 - 7.99*(10^-2)*Kel + 23.6) # See Vikeslund 2001
Z <- H^2 + H*kCO31 + kCO31*kCO32# Demoninator in equilibrium expressions
H2CO3 <- TotC * H^2 / Z
HCO3 <- TotC * H * kCO31 / Z
CO3 <- TotC * kCO31 * kCO32 / Z

Knh3 <- 10^-(1.03*(10^-4)*Kel^2 - 9.21*(10^-2)*Kel + 27.6) # See Vikeslund 2001
NH4 <- FreeN*H/(H+Knh3)
NH3 <- FreeN*Knh3/(H+Knh3)

Khocl <- 10^-(1.18*(10^-4)*Kel^2 - 7.86*(10^-2)*Kel + 20.5) # See Vikeslund 2001
HOCl <- FreeCl*H/(Khocl+H)
OCl <- FreeCl*Khocl/(Khocl+H)

# Define rate constants - from Jafvert & Valentine
Kel <- Temp+273 #Temp in degrees K
k1 <- 2.37*(10^12)*exp(-1510/Kel) / 3600  # k HOCl+NH3->NH2Cl+H2O
k2 <- 6.7*(10^11)*exp(-8800/Kel) / 3600 # k NH2Cl+H2O->HOCl+NH3
k3 <- 1.08*(10^9)*exp(-2010/Kel) / 3600       # k HOCl+NH2Cl->NHCl2+H2O
k4 <- 2.3*10^-3 / 3600 # k NHCl2+H2O->HOCl+NH2Cl
k5 <- (3.78*(10^10)*exp(-2169/Kel)*H + 2.95*(10^10)*exp(-4026/Kel)*H2CO3 + 1.5*(10^35)*exp(-22144/Kel)*HCO3) / 3600  # k NH2Cl+NH2Cl->NHCl2+NH3
k6 <- 2.16*10^8 / 3600  # k NHCl2+NH3->NH2CL+NH2Cl
k7 <- 4*10^5 / 3600        # k NHCl2+H2O->I
k8 <- 1*10^8 / 3600  # k I+NHCl2->HOCl+products
k9 <- 3*10^7 / 3600  # k I+NH2Cl->products
k10 <- 55 / 3600    # k NH2Cl+NHCl2->products
k11 <- (5.72*(10^7)*HPO4 + 3.24*(10^8)*OCl + 1.18*(10^13)*OH + 2.16*(10^10)*CO3) / 3600 #k HOCl+NHCl2->NCl3+H2O
k12 <- 2*10^14 / 3600  # k NHCl2+NCl3+2H2O->2HOCl+products
k13 <- 5*10^12 / 3600   # k NH2Cl+NCl3+H2O->HOCl+products
k14 <- 8.3*10^5 / 3600        # k NHCl2+2HOCl+H2O->NO3+5H+4Cl
# Define chlorine/chloramine model
RxnFn <- function(Time,State,Pars){
  with(as.list(c(State,Pars)),{
    HOCl <- FreeCl*H/(Khocl+H)
    OCl <- FreeCl*Khocl/(Khocl+H)
    NH4 <- FreeN*H/(H+Knh3)
    NH3 <- FreeN*Knh3/(H+Knh3)
    r1 <- k1*HOCl*NH3
    r2 <- k2*NH2Cl
    r3 <- k3*HOCl*NH2Cl
    r4 <- k4*NHCl2
    r5 <- k5*(NH2Cl^2)
    r6 <- k6*NHCl2*NH3*H
    r7 <- k7*NHCl2*OH
    r8 <- k8*I*NHCl2
    r9 <- k9*I*NH2Cl
    r10 <- k10*NH2Cl*NHCl2
    r11 <- k11*NHCl2*HOCl
    r12 <- k12*NHCl2*NCl3*OH
    r13 <- k13*NH2Cl*NCl3*OH
    r14 <- k14*NHCl2*OCl

    dFreeCl <- -r1 + r2 - r3 + r4 + r8 - r11 + 2*r12 + r13 - 2*r14
    dFreeN <- -r1 + r2 + r4 + r5 - r6
    dNH2Cl <- r1 - r2 - r3 - 2*r5 + 2*r6 - r7 - r9 - r10 - r12
    dNHCl2 <- r3 - r4 + r5 - r6 - r8 - r10 - r11 - r12 + r14
    dNCl3 <- r11 - r12 - r13
    dNO3 <- r14 #+5H+5Cl
    dI <- r7 - r8 - r9

    return(list(c(dFreeCl,dFreeN,dNH2Cl,dNHCl2,dNCl3,dNO3,dI)))
  })
}
```

```
pars <- list(k1,k2,k3,k4,k5,k6,k7,k8,k9,k10,k11,k12,k13,k14,Khocl,Knh3,H,OH)



# Define copy.table function
# https://www.r-bloggers.com/using-the-windows-clipboard-or-passing-data-quickly-from-excel-to-r-and-back-again/
copy.table <- function(obj, size = 4096) {
  clip <- paste('clipboard-', size, sep = '')
  f <- file(description = clip, open = 'w')
  write.table(obj, f, row.names = FALSE, sep = '\t')
  close(f)
}
### SF Model

# Create empty data frame
SFA <- matrix( rep(NA, length(Influent[,1])*8), ncol = 8) #7 species plus time
SFA <- as.data.frame(SFA) # make matrix a data frame, necessary for melting later

#dat <- TracerData
dat <- ModeledTracerData

# Process for calculating effluent concentrations:
  # At each time in Influent, for each tracer data point:
    # Find time stamp looking back theta*HRT
    # Grab Cl2, NH3 at that time
    # Calculate species at time theta*HRT
  # Take mean of all tracer data points weighted by delta C/C0

for (i in 1:length(Influent[,1])){

  progress(i, max.value = length(Influent[,1]))

  # Find closest timestamp finding the minimum of the absolute value of the difference
  CurDate <- Influent$Date[i]
  BackDate <- dat[,1]*Influent$HRT[i]/24
  Tstamps <- CurDate - BackDate
  index <- rep(NA,length(Influent$Date[i]))
  for (z in 1:length(dat[,1])){
    index[z] <- which.min(abs(Influent$Date-Tstamps[z]))
  }

  # Find Influent Cl2, NH3 at index
  InfFreeCl <- Influent$FreeCl[index]
  InfNH3 <- Influent$NH3[index]

  # Create concentrations for downstream calculations
  yLoop <- cbind(FreeCl = InfFreeCl,
              FreeN = InfNH3,
              NH2Cl = rep(0,length(index)),
              #NH2Cl = Influent$NH2Cl[index], # use when assuming monochloramine formed upstream
              NHCl2 = rep(0,length(index)),
              NCl3 = rep(0,length(index)), NO3 = rep(0,length(index)), I = rep(0,length(index)) )

  # Calculate PFR effluents
  PFReffs <- matrix( rep(NA, length(dat[,1])*7), ncol = 7) #7 species
  PFReffs <- as.data.frame(PFReffs)
  for (z in 1:length(dat[,1])){
    tPFR <- c(0.1, max(10,dat[z,1]*Influent$HRT[i]*3600)) # Eq time = theta*HRT, if theta=0, use 10s
    val <- ode(func = RxnFn, y = yLoop[z,], parms = pars, times = tPFR, atol = 1e-10) # Set absolute tolerance; reduces output of errors
    PFReffs[z,1:7] <- val[2,2:8] # Extract values from solver output val
  }
  colnames(PFReffs) <- colnames(val[,2:8])

  # Take mean of all species
  SFA[i,1] <- Influent$Date[i]
  SFA[i,2] <- sum(rollmean(PFReffs$FreeCl,k=2)*(tail(dat[,2],-1)-head(dat[,2],-1)))*(1+(1-tail(dat[,2],1))) #Make larger when tracer doesn't go do C/C0=1
  SFA[i,3] <- sum(rollmean(PFReffs$FreeN,k=2)*(tail(dat[,2],-1)-head(dat[,2],-1)))*(1+(1-tail(dat[,2],1))) #Make larger when tracer doesn't go do C/C0=1
  SFA[i,4] <- sum(rollmean(PFReffs$NH2Cl,k=2)*(tail(dat[,2],-1)-head(dat[,2],-1)))*(1+(1-tail(dat[,2],1))) #Make larger when tracer doesn't go do C/C0=1
  SFA[i,5] <- sum(rollmean(PFReffs$NHCl2,k=2)*(tail(dat[,2],-1)-head(dat[,2],-1)))*(1+(1-tail(dat[,2],1))) #Make larger when tracer doesn't go do C/C0=1
  SFA[i,6] <- sum(rollmean(PFReffs$NCl3,k=2)*(tail(dat[,2],-1)-head(dat[,2],-1)))*(1+(1-tail(dat[,2],1))) #Make larger when tracer doesn't go do C/C0=1
  SFA[i,7] <- sum(rollmean(PFReffs$NO3,k=2)*(tail(dat[,2],-1)-head(dat[,2],-1)))*(1+(1-tail(dat[,2],1))) #Make larger when tracer doesn't go do C/C0=1
  SFA[i,8] <- sum(rollmean(PFReffs$I,k=2)*(tail(dat[,2],-1)-head(dat[,2],-1)))*(1+(1-tail(dat[,2],1))) #Make larger when tracer doesn't go do C/C0=1

}
colnames(SFA) <- colnames(val) #Define column names

# Calculate TotalCl and TotalN
SFA$TotalCl <- SFA$FreeCl+SFA$NH2Cl+2*SFA$NHCl2+3*SFA$NCl3
SFA$TotalN <- SFA$FreeN+SFA$NH2Cl+SFA$NHCl2+SFA$NCl3


copy.table(SFA)
```

```
### MM Model

# Create empty data frame
MMA <- matrix( rep(NA, length(Influent[,1])*8), ncol = 8) #7 species plus time
MMA <- as.data.frame(MMA) # make matrix a data frame, necessary for melting later
MMA[,1] <- Influent$Date

dat <- ModeledTracerData


for (i in 1:length(Influent[,1])){

  progress(i, max.value = length(Influent[,1]))

  # Find closest timestamp finding the minimum of the absolute value of the difference
  CurDate <- Influent$Date[i]
  BackDate <- dat[,1]*Influent$HRT[i]/24
  Tstamps <- CurDate - BackDate
  index <- rep(NA,length(Influent$Date[i]))
  for (z in 1:length(dat[,1])){
    index[z] <- which.min(abs(Influent$Date-Tstamps[z]))
  }

  # Find Influent Cl2, NH3 at index
  InfFreeCl <- Influent$FreeCl[index]
  InfNH3 <- Influent$NH3[index]

  # Create concentrations for downstream calculations
  yLoop <- cbind(FreeCl = InfFreeCl,
                 FreeN = InfNH3,
                 NH2Cl = rep(0,length(index)),
                 #NH2Cl = Influent$NH2Cl[index], # use when assuming monochloramine formed upstream
                 NHCl2 = rep(0,length(index)),
                 NCl3 = rep(0,length(index)), NO3 = rep(0,length(index)), I = rep(0,length(index)) )

  # Calculate Cbulk

  # Initial Cbulk
  tinit <- c(0.1, diff(tail(dat[,1],2)) * Influent$HRT[i] * 3600)
  val <- ode(func = RxnFn, y = yLoop[length(dat[,1]),], parms = pars, times = tinit, atol = 1e-10)
  Cbulk <- val[2,2:8]
  for (z in (length(dat[,1])-1) : 1){ # Note that order is reversed here to start at longest RTD tracer data
    #tPFR <- c(0.1, max(10,dat[z,1]*Influent$HRT[i]*3600)) # Eq time = theta*HRT, if theta=0, use 10s
    tStep <- c(0.1, ( dat[z+1,1]-dat[z,1]) * Influent$HRT[i]*3600 ) # Take difference in time of z and z+1
    Cbulk_init <- ( (1-dat[z+1,2])*Cbulk + (dat[z+1,2]-dat[z,2])*yLoop[z,] ) / (1-dat[z,2])# (Q1C1+Q2C2)/(Q1+Q2)
    val <- ode(func = RxnFn, y = Cbulk_init, parms = pars, times = tStep, atol = 1e-10) # Set absolute tolerance; reduces output of errors
    Cbulk <- val[2,2:8] # Extract values from solver output val
  }
  colnames(PFReffs) <- colnames(val[,2:8])

  # Fill MMA data frame with final output Cbulk
  MMA[i,2:8] <- Cbulk

}
colnames(MMA) <- colnames(val) #Define column names

# Calculate TotalCl and TotalN
MMA$TotalCl <- MMA$FreeCl+MMA$NH2Cl+2*MMA$NHCl2+3*MMA$NCl3
MMA$TotalN <- MMA$FreeN+MMA$NH2Cl+MMA$NHCl2+MMA$NCl3


copy.table(MMA)
```

```
### Single TIS where n=5

step <- deltaT/(PIdata$HRT*60)
time <- (PIdata$Date-PIdata$Date[1])*24 # in hours
Tau <- PIdata$HRT*3600 # seconds, Residence time

# Divide residence time among n tanks
n1tanks <- 5
Q1 <- 1
V1 <- 1
Tau1Tank <- Tau/n1tanks*V1/Q1
n1step <- step*n1tanks*Q1/V1 # Concentrations move through each tank n times as fast as step

# Define influent conditions

C_inf <- cbind(FreeCl = Influent$FreeCl,
               FreeN = Influent$NH3,
               NH2Cl = rep(0,length(time)),
               # NH2Cl = Influent$NH2Cl, # use this if assuming NH2Cl formed before entering
               NHCl2 = rep(0,length(time)), NCl3 = rep(0,length(time)),
               NO3 = rep(0,length(time)), I = rep(0,length(time)))
C_inf <- as.data.frame(C_inf) # make matrix a data frame

# Assume initial concentration in reactor is constant and equal to effluent conc.
C_0 <- c(FreeCl = Initial$FreeCl,
         FreeN = Initial$NH3,
         NH2Cl = Initial$NH2Cl,
         NHCl2 = 0, NCl3 = 0, NO3 = 0, I = 0)

C1_1 <- matrix( rep(NA, length(time)*8), ncol = 8) #7 species plus time
C1_1 <- as.data.frame(C1_1) # make matrix a data frame
C1_1[,1] <- time # Define time steps
C1_1[1,2:8] <- C_0 # Define initial conditions of concentration

# Make C2-C5 equal to C1 (initially)
C1_2 <- C1_1
C1_3 <- C1_1
C1_4 <- C1_1
C1_5 <- C1_1
for (i in 2:length(time)){

  progress(i, max.value = length(Influent[,1]))

  tcstr <- c(0.001,step[i-1]*Tau1Tank[i-1])

  C1_1i <- as.numeric(C1_1[i-1,2:8]*(1-n1step[i-1])+C_inf[i-1,]*n1step[i-1])
  C1_2i <- as.numeric(C1_2[i-1,2:8]*(1-n1step[i-1])+C1_1[i-1,2:8]*n1step[i-1])
  C1_3i <- as.numeric(C1_3[i-1,2:8]*(1-n1step[i-1])+C1_2[i-1,2:8]*n1step[i-1])
  C1_4i <- as.numeric(C1_4[i-1,2:8]*(1-n1step[i-1])+C1_3[i-1,2:8]*n1step[i-1])
  C1_5i <- as.numeric(C1_5[i-1,2:8]*(1-n1step[i-1])+C1_4[i-1,2:8]*n1step[i-1])

  names(C1_1i) <- names(C_0)
  names(C1_2i) <- names(C_0)
  names(C1_3i) <- names(C_0)
  names(C1_4i) <- names(C_0)
  names(C1_5i) <- names(C_0)

  val1 <- ode(func = RxnFn, y = C1_1i, parms = pars, times = tcstr)
  val2 <- ode(func = RxnFn, y = C1_2i, parms = pars, times = tcstr)
  val3 <- ode(func = RxnFn, y = C1_3i, parms = pars, times = tcstr)
  val4 <- ode(func = RxnFn, y = C1_4i, parms = pars, times = tcstr)
  val5 <- ode(func = RxnFn, y = C1_5i, parms = pars, times = tcstr)

  C1_1[i,2:8] <- val1[2,2:8] # for the second entry in val, the time of interest in teq
  C1_2[i,2:8] <- val2[2,2:8] # for the second entry in val, the time of interest in teq
  C1_3[i,2:8] <- val3[2,2:8] # for the second entry in val, the time of interest in teq
  C1_4[i,2:8] <- val4[2,2:8] # for the second entry in val, the time of interest in teq
  C1_5[i,2:8] <- val5[2,2:8] # for the second entry in val, the time of interest in teq

}


colnames(C1_1) <- colnames(val1) #Define column names
colnames(C1_2) <- colnames(val1) #Define column names
colnames(C1_3) <- colnames(val1) #Define column names
colnames(C1_4) <- colnames(val1) #Define column names
colnames(C1_5) <- colnames(val1) #Define column names
```

```r
# Calculate TotalCl and TotalN
C1_1$TotalCl <- C1_1$FreeCl+C1_1$NH2Cl+2*C1_1$NHCl2+3*C1_1$NCl3
C1_1$TotalN <- C1_1$FreeN+C1_1$NH2Cl+C1_1$NHCl2+C1_1$NCl3
C1_2$TotalCl <- C1_2$FreeCl+C1_2$NH2Cl+2*C1_2$NHCl2+3*C1_2$NCl3
C1_2$TotalN <- C1_2$FreeN+C1_2$NH2Cl+C1_2$NHCl2+C1_2$NCl3
C1_3$TotalCl <- C1_3$FreeCl+C1_3$NH2Cl+2*C1_3$NHCl2+3*C1_3$NCl3
C1_3$TotalN <- C1_3$FreeN+C1_3$NH2Cl+C1_3$NHCl2+C1_3$NCl3
C1_4$TotalCl <- C1_4$FreeCl+C1_4$NH2Cl+2*C1_4$NHCl2+3*C1_4$NCl3
C1_4$TotalN <- C1_4$FreeN+C1_4$NH2Cl+C1_4$NHCl2+C1_4$NCl3
C1_5$TotalCl <- C1_5$FreeCl+C1_5$NH2Cl+2*C1_5$NHCl2+3*C1_5$NCl3
C1_5$TotalN <- C1_5$FreeN+C1_5$NH2Cl+C1_5$NHCl2+C1_5$NCl3


plot_df <- melt(C1_5,id.vars="time")
ggplot(plot_df,aes(x=time, y=value, colour = variable))+
  geom_line(size=1)+
  scale_colour_brewer(palette = "Set1")+
  labs(x=expression(time),y="C/C0",color="variable")+
  theme_bw() + xlim(0,5*24)

# Write output to clipboard
copy.table(C1_5)
```

```
### RN Model
  # Create TISs with n=13 and n=9


# Theta = t/Tau, define a set of increasing thetas
step <- deltaT/(PIdata$HRT*60)
time <- (PIdata$Date-PIdata$Date[1])*24 # in hours
Tau <- PIdata$HRT*3600 # seconds, Residence time

# Divide residence time among n tanks
n1tanks <- 13
Q1 <- 0.61117
V1 <- 0.433
Tau1Tank <- Tau/n1tanks*V1/Q1
n1step <- step*n1tanks*Q1/V1 # Concentrations move through each tank n times as fast as step

n2tanks <- 9
Q2 <- 1-Q1
V2 <- 1-V1-0.04098
Tau2Tank <- Tau/n2tanks*V2/Q2
n2step <- step*n2tanks*Q2/V2

# Define influent conditions

C_inf <- cbind(FreeCl = Influent$FreeCl,
               FreeN = Influent$NH3,
               NH2Cl = rep(0,length(time)),
               # NH2Cl = Influent$NH2Cl, # use this if assuming NH2Cl formed before entering
               NHCl2 = rep(0,length(time)), NCl3 = rep(0,length(time)),
               NO3 = rep(0,length(time)), I = rep(0,length(time)))

C_inf <- as.data.frame(C_inf) # make matrix a data frame

# Assume initial concentration in reactor is constant and equal to effluent conc.
C_0 <- c(FreeCl = Initial$FreeCl,
         FreeN = Initial$NH3,
         NH2Cl = Initial$NH2Cl,
         NHCl2 = 0, NCl3 = 0, NO3 = 0, I = 0)

C1_1 <- matrix( rep(NA, length(time)*8), ncol = 8) #7 species plus time
C1_1 <- as.data.frame(C1_1) # make matrix a data frame
C1_1[,1] <- time # Define time steps
C1_1[1,2:8] <- C_0 # Define initial conditions of concentration

# Make C2-C5 equal to C1 (initially)
C1_2 <- C1_1
C1_3 <- C1_1
C1_4 <- C1_1
C1_5 <- C1_1
C1_6 <- C1_1
C1_7 <- C1_1
C1_8 <- C1_1
C1_9 <- C1_1
C1_10 <- C1_1
C1_11 <- C1_1
C1_12 <- C1_1
C1_13 <- C1_1

C2_1 <- C1_1
C2_2 <- C1_1
C2_3 <- C1_1
C2_4 <- C1_1
C2_5 <- C1_1
C2_6 <- C1_1
C2_7 <- C1_1
C2_8 <- C1_1
C2_9 <- C1_1
for (i in 2:length(time)){

  progress(i, max.value = length(Influent[,1]))

  tcstr1 <- c(0.001,step[i-1]*Tau1Tank[i-1])
  tcstr2 <- c(0.001,step[i-1]*Tau2Tank[i-1])

  C1_1i <- as.numeric(C1_1[i-1,2:8]*(1-n1step[i-1])+C_inf[i-1,]*n1step[i-1])
  C1_2i <- as.numeric(C1_2[i-1,2:8]*(1-n1step[i-1])+C1_1[i-1,2:8]*n1step[i-1])
  C1_3i <- as.numeric(C1_3[i-1,2:8]*(1-n1step[i-1])+C1_2[i-1,2:8]*n1step[i-1])
  C1_4i <- as.numeric(C1_4[i-1,2:8]*(1-n1step[i-1])+C1_3[i-1,2:8]*n1step[i-1])
  C1_5i <- as.numeric(C1_5[i-1,2:8]*(1-n1step[i-1])+C1_4[i-1,2:8]*n1step[i-1])
  C1_6i <- as.numeric(C1_6[i-1,2:8]*(1-n1step[i-1])+C1_5[i-1,2:8]*n1step[i-1])
  C1_7i <- as.numeric(C1_7[i-1,2:8]*(1-n1step[i-1])+C1_6[i-1,2:8]*n1step[i-1])
  C1_8i <- as.numeric(C1_8[i-1,2:8]*(1-n1step[i-1])+C1_7[i-1,2:8]*n1step[i-1])
  C1_9i <- as.numeric(C1_9[i-1,2:8]*(1-n1step[i-1])+C1_8[i-1,2:8]*n1step[i-1])
  C1_10i <- as.numeric(C1_10[i-1,2:8]*(1-n1step[i-1])+C1_9[i-1,2:8]*n1step[i-1])
  C1_11i <- as.numeric(C1_11[i-1,2:8]*(1-n1step[i-1])+C1_10[i-1,2:8]*n1step[i-1])
  C1_12i <- as.numeric(C1_12[i-1,2:8]*(1-n1step[i-1])+C1_11[i-1,2:8]*n1step[i-1])
  C1_13i <- as.numeric(C1_13[i-1,2:8]*(1-n1step[i-1])+C1_12[i-1,2:8]*n1step[i-1])
```

```
  C2_1i <- as.numeric(C2_1[i-1,2:8])*(1-n2step[i-1])+C_inf[i-1,]*n2step[i-1])
  C2_2i <- as.numeric(C2_2[i-1,2:8])*(1-n2step[i-1])+C2_1[i-1,2:8]*n2step[i-1])
  C2_3i <- as.numeric(C2_3[i-1,2:8])*(1-n2step[i-1])+C2_2[i-1,2:8]*n2step[i-1])
  C2_4i <- as.numeric(C2_4[i-1,2:8])*(1-n2step[i-1])+C2_3[i-1,2:8]*n2step[i-1])
  C2_5i <- as.numeric(C2_5[i-1,2:8])*(1-n2step[i-1])+C2_4[i-1,2:8]*n2step[i-1])
  C2_6i <- as.numeric(C2_6[i-1,2:8])*(1-n2step[i-1])+C2_5[i-1,2:8]*n2step[i-1])
  C2_7i <- as.numeric(C2_7[i-1,2:8])*(1-n2step[i-1])+C2_6[i-1,2:8]*n2step[i-1])
  C2_8i <- as.numeric(C2_8[i-1,2:8])*(1-n2step[i-1])+C2_7[i-1,2:8]*n2step[i-1])
  C2_9i <- as.numeric(C2_9[i-1,2:8])*(1-n2step[i-1])+C2_8[i-1,2:8]*n2step[i-1])

  names(C1_1i) <- names(C_0)
  names(C1_2i) <- names(C_0)
  names(C1_3i) <- names(C_0)
  names(C1_4i) <- names(C_0)
  names(C1_5i) <- names(C_0)
  names(C1_6i) <- names(C_0)
  names(C1_7i) <- names(C_0)
  names(C1_8i) <- names(C_0)
  names(C1_9i) <- names(C_0)
  names(C1_10i) <- names(C_0)
  names(C1_11i) <- names(C_0)
  names(C1_12i) <- names(C_0)
  names(C1_13i) <- names(C_0)

  names(C2_1i) <- names(C_0)
  names(C2_2i) <- names(C_0)
  names(C2_3i) <- names(C_0)
  names(C2_4i) <- names(C_0)
  names(C2_5i) <- names(C_0)
  names(C2_6i) <- names(C_0)
  names(C2_7i) <- names(C_0)
  names(C2_8i) <- names(C_0)
  names(C2_9i) <- names(C_0)
  val1_1 <- ode(func = RxnFn, y = C1_1i, parms = pars, times = tcstr1)
  val1_2 <- ode(func = RxnFn, y = C1_2i, parms = pars, times = tcstr1)
  val1_3 <- ode(func = RxnFn, y = C1_3i, parms = pars, times = tcstr1)
  val1_4 <- ode(func = RxnFn, y = C1_4i, parms = pars, times = tcstr1)
  val1_5 <- ode(func = RxnFn, y = C1_5i, parms = pars, times = tcstr1)
  val1_6 <- ode(func = RxnFn, y = C1_6i, parms = pars, times = tcstr1)
  val1_7 <- ode(func = RxnFn, y = C1_7i, parms = pars, times = tcstr1)
  val1_8 <- ode(func = RxnFn, y = C1_8i, parms = pars, times = tcstr1)
  val1_9 <- ode(func = RxnFn, y = C1_9i, parms = pars, times = tcstr1)
  val1_10 <- ode(func = RxnFn, y = C1_10i, parms = pars, times = tcstr1)
  val1_11 <- ode(func = RxnFn, y = C1_11i, parms = pars, times = tcstr1)
  val1_12 <- ode(func = RxnFn, y = C1_12i, parms = pars, times = tcstr1)
  val1_13 <- ode(func = RxnFn, y = C1_13i, parms = pars, times = tcstr1)

  val2_1 <- ode(func = RxnFn, y = C2_1i, parms = pars, times = tcstr2)
  val2_2 <- ode(func = RxnFn, y = C2_2i, parms = pars, times = tcstr2)
  val2_3 <- ode(func = RxnFn, y = C2_3i, parms = pars, times = tcstr2)
  val2_4 <- ode(func = RxnFn, y = C2_4i, parms = pars, times = tcstr2)
  val2_5 <- ode(func = RxnFn, y = C2_5i, parms = pars, times = tcstr2)
  val2_6 <- ode(func = RxnFn, y = C2_6i, parms = pars, times = tcstr2)
  val2_7 <- ode(func = RxnFn, y = C2_7i, parms = pars, times = tcstr2)
  val2_8 <- ode(func = RxnFn, y = C2_8i, parms = pars, times = tcstr2)
  val2_9 <- ode(func = RxnFn, y = C2_9i, parms = pars, times = tcstr2)

  C1_1[i,2:8] <- val1_1[2,2:8] # for the second entry in val1_, the time of interest in teq
  C1_2[i,2:8] <- val1_2[2,2:8] # for the second entry in val1_, the time of interest in teq
  C1_3[i,2:8] <- val1_3[2,2:8] # for the second entry in val1_, the time of interest in teq
  C1_4[i,2:8] <- val1_4[2,2:8] # for the second entry in val1_, the time of interest in teq
  C1_5[i,2:8] <- val1_5[2,2:8] # for the second entry in val1_, the time of interest in teq
  C1_6[i,2:8] <- val1_6[2,2:8] # for the second entry in val1_, the time of interest in teq
  C1_7[i,2:8] <- val1_7[2,2:8] # for the second entry in val1_, the time of interest in teq
  C1_8[i,2:8] <- val1_8[2,2:8] # for the second entry in val1_, the time of interest in teq
  C1_9[i,2:8] <- val1_9[2,2:8] # for the second entry in val1_, the time of interest in teq
  C1_10[i,2:8] <- val1_10[2,2:8] # for the second entry in val1_, the time of interest in teq
  C1_11[i,2:8] <- val1_11[2,2:8] # for the second entry in val1_, the time of interest in teq
  C1_12[i,2:8] <- val1_12[2,2:8] # for the second entry in val1_, the time of interest in teq
  C1_13[i,2:8] <- val1_13[2,2:8] # for the second entry in val, the time of interest in teq

  C2_1[i,2:8] <- val2_1[2,2:8] # for the second entry in val2_, the time of interest in teq
  C2_2[i,2:8] <- val2_2[2,2:8] # for the second entry in val2_, the time of interest in teq
  C2_3[i,2:8] <- val2_3[2,2:8] # for the second entry in val2_, the time of interest in teq
  C2_4[i,2:8] <- val2_4[2,2:8] # for the second entry in val2_, the time of interest in teq
  C2_5[i,2:8] <- val2_5[2,2:8] # for the second entry in val2_, the time of interest in teq
  C2_6[i,2:8] <- val2_6[2,2:8] # for the second entry in val2_, the time of interest in teq
  C2_7[i,2:8] <- val2_7[2,2:8] # for the second entry in val2_, the time of interest in teq
  C2_8[i,2:8] <- val2_8[2,2:8] # for the second entry in val2_, the time of interest in teq
  C2_9[i,2:8] <- val2_9[2,2:8] # for the second entry in val2_, the time of interest in teq
}
```

```r
colnames(C1_1) <- colnames(val1_1) #Define column names
colnames(C1_2) <- colnames(val1_1) #Define column names
colnames(C1_3) <- colnames(val1_1) #Define column names
colnames(C1_4) <- colnames(val1_1) #Define column names
colnames(C1_5) <- colnames(val1_1) #Define column names
colnames(C1_6) <- colnames(val1_1) #Define column names
colnames(C1_7) <- colnames(val1_1) #Define column names
colnames(C1_8) <- colnames(val1_1) #Define column names
colnames(C1_9) <- colnames(val1_1) #Define column names
colnames(C1_10) <- colnames(val1_1) #Define column names
colnames(C1_11) <- colnames(val1_1) #Define column names
colnames(C1_12) <- colnames(val1_1) #Define column names
colnames(C1_13) <- colnames(val1_1) #Define column names

colnames(C2_1) <- colnames(val1_1) #Define column names
colnames(C2_2) <- colnames(val1_1) #Define column names
colnames(C2_3) <- colnames(val1_1) #Define column names
colnames(C2_4) <- colnames(val1_1) #Define column names
colnames(C2_5) <- colnames(val1_1) #Define column names
colnames(C2_6) <- colnames(val1_1) #Define column names
colnames(C2_7) <- colnames(val1_1) #Define column names
colnames(C2_8) <- colnames(val1_1) #Define column names
colnames(C2_9) <- colnames(val1_1) #Define column names

# Calculate TotalCl and TotalN
C1_1$TotalCl <- C1_1$FreeCl+C1_1$NH2Cl+2*C1_1$NHCl2+3*C1_1$NCl3
C1_1$TotalN <- C1_1$FreeN+C1_1$NH2Cl+C1_1$NHCl2+C1_1$NCl3
C1_2$TotalCl <- C1_2$FreeCl+C1_2$NH2Cl+2*C1_2$NHCl2+3*C1_2$NCl3
C1_2$TotalN <- C1_2$FreeN+C1_2$NH2Cl+C1_2$NHCl2+C1_2$NCl3
C1_3$TotalCl <- C1_3$FreeCl+C1_3$NH2Cl+2*C1_3$NHCl2+3*C1_3$NCl3
C1_3$TotalN <- C1_3$FreeN+C1_3$NH2Cl+C1_3$NHCl2+C1_3$NCl3
C1_4$TotalCl <- C1_4$FreeCl+C1_4$NH2Cl+2*C1_4$NHCl2+3*C1_4$NCl3
C1_4$TotalN <- C1_4$FreeN+C1_4$NH2Cl+C1_4$NHCl2+C1_4$NCl3
C1_5$TotalCl <- C1_5$FreeCl+C1_5$NH2Cl+2*C1_5$NHCl2+3*C1_5$NCl3
C1_5$TotalN <- C1_5$FreeN+C1_5$NH2Cl+C1_5$NHCl2+C1_5$NCl3

C1_13$TotalCl <- C1_13$FreeCl+C1_13$NH2Cl+2*C1_13$NHCl2+3*C1_13$NCl3
C1_13$TotalN <- C1_13$FreeN+C1_13$NH2Cl+C1_13$NHCl2+C1_13$NCl3

C2_9$TotalCl <- C2_9$FreeCl+C2_9$NH2Cl+2*C2_9$NHCl2+3*C2_9$NCl3
C2_9$TotalN <- C2_9$FreeN+C2_9$NH2Cl+C2_9$NHCl2+C2_9$NCl3

C_eff <- cbind(time,C1_13[,2:10]*Q1+C2_9[,2:10]*Q2)


copy.table(C_eff)
```

REFERENCES

Crittenden, J. C., Trussell, R. R., Hand, D. W., Howe, K. J., & Tchobanoglous, G. 2005. MWH's water treatment: principles and design. 2nd Ed. Hoboken, NJ: John Wiley & Sons.

Gorzalski, A.S., Harrington, G.W., Coronell, O. 2018. Modeling water treatment reactor hydraulics using reactor networks. *Journal AWWA*, 110 (8): 13-29.

Jafvert, C. T., Valentine, R. L. 1992. Reaction scheme for the chlorination of ammoniacal water. *Environmental Science & Technology*, 26 (3): 577-586.

Levenspiel, O. 1999. *Chemical Reaction Engineering*. 3rd ed. New York: Wiley and Sons.
Oh, S. H., Cavendish, J. C. 1985. Mathematical modeling of catalytic converter lightoff. Part III: Prediction of vehicle exhaust emissions and parametric analysis. *AIChE Journal*, 31 (6): 943-949.

Najm, I.; Brown, N.P.; Gramith, K.; Hargy, T. 2009. Validating Disinfection in Ozone Contactors. Water Research Foundation. Denver, CO.

R Core Team. 2016. R: A language and environment for statistical computing. R Foundation for Statistical Computing, Vienna, Austria. URL https://www.R-project.org/.

Soetaert, K., Petzoldt, T., Setzer, R. W. 2010. Solving differential equations in R: package deSolve. *Journal of Statistical Software*, 33 (9): 1-25.

APPENDIX C – SUPPORTING INFORMATION FOR CHAPTER 4

Table C.1. Tracer data information.

ID	Plant Type	Contactor Type	Tracer Type	Volume (MG)	Flow (MGD)	τ (min)	t_{10}/τ	Reference
1A	Water	Clearwell	Step Dose	7.9	85	134	0.45	Chapter 2
1B	Water	Clearwell	Step Dose	11.9-12.4	68-104	165-252	0.45	Chapter 2
2A	Water	Clearwell	Step Dose	9.9	150	94.8	0.39	Teefy and Singer 1990
3A	Water	Filters (6)	Pulse Input	0.38	13.7	40	0.50 *	Teefy 1996
3B	Water	Chlorine Contact Basin	Step Dose	0.05	1.4	50	0.72-0.80	Teefy 1996
3C	Water	Chlorine Contact Basin	Step Dose	0.07	1.4	69	0.67	Teefy 1996
3D	Water	Ozone Contactor	Step Dose	0.02	1.4	23	0.61	Teefy 1996
3E	Wastewater	Secondary Clarifier	Pulse Input	1.9	10	270	0.19	Teefy 1996
3F	Wastewater	Chlorine Contact Chamber	Pulse Input	0.02	1.1	30	0.43	Teefy 1996
3G	Water	Clearwell	Step Dose	2.10	7.9	384	0.67	Teefy 1996
3H	Water	Clearwell (Circular)	Step Dose	1.32	6.1	312	0.57	Teefy 1996
4A	NR	NR	Step Dose	NR	NR	1.9	0.31 *	Carlson et al. 2001
5A	Water	Ozone Contactor	Step Dose	0.18	25.5	10	0.69 *	Najm et al. 2009
5B	Water	Ozone Contactor	Pulse Input	0.18	25.5	10	0.70 *	Najm et al. 2009
6A	Water	Clearwell	Step Dose	32.40	137	340	0.40	Chapter 3
6B	Water	Clearwell	Step Dose	19.61	104	272	0.40	Chapter 3
8A	Water	Clearwell	Step Dose	0.22	2.12	149.4	0.72	Porter et al. 2019
8B	Water	CT Basin	Step Dose	0.01	0.03	335.5	0.45	Porter et al. 2019
8C	Water	CT Basin	Step Dose	0.12	1.76	98.0	0.75	Porter et al. 2019
8D	Water	CT Basin & Clearwell in Series	Step Dose	0.06	0.49	177.3	0.69	Porter et al. 2019
8E	Water	Clearwell	Step Dose	0.01	0.05	200.3	0.35	Porter et al. 2019
8F	Water	Disinfection Wet well	Step Dose	0.01	1.08	15.0	0.9	Porter et al. 2019
8G	Water	Clearwell	Step Dose	0.01	0.43	39.0	0.72	Porter et al. 2019
8H	Water	Clearwell	Step Dose	0.27	3.36	117.0	0.91	Porter et al. 2019

8I	Water	Clearwell	Step Dose	0.04	0.57	96.9	0.65	Porter et al. 2019
8J	Water	Clearwell	Step Dose	0.18	2.17	118.2	0.53	Porter et al. 2019
8K	Water	Flocculatin Basin	Step Dose	0.001	0.114	13.3	0.46	Porter et al. 2019
8L	Water	Clearwell	Step Dose	0.08	1.30	83.8	0.66	Porter et al. 2019
8M	Water	Ozone Contactor	Step Dose	0.0002	0.0278	10.1	0.51	Porter et al. 2019
8N	Water	Chlorine Contact Basin	Step Dose	0.14	1.01	200.5	0.64	Porter et al. 2019
8O	Water	CT Basin	Step Dose	0.19	1.03	262.0	0.43	Porter et al. 2019
8P	Water	Clearwell	Step Dose	0.28	5.69	72.1	0.93	Porter et al. 2019
8Q	Water	Clearwell	Step Dose	0.05	0.83	91.2	0.75	Porter et al. 2019
8R	Water	Clearwell	Step Dose	0.04	0.46	129.2	0.76	Porter et al. 2019
8S	Water	Clearwell	Step Dose	0.17	1.79	138.1	0.59	Porter et al. 2019

NR - not reported

* Not reported, but calculated via linear interpolation from reported data

Plots of t_{10}/τ baffle factor versus V_{norm} before and after correction are shown in Figure C.1. Out of 35 uncorrected reactor data sets, 18 had $V_{norm} > 1.05$. For reactors with $t_{10}/\tau > 0.65$, nearly two-thirds had $V_{norm} > 1.2$. This suggests that many baffle factors may be overestimated due to inaccuracies in volume and/or flow metering. This further supports findings from Chapter 2 that volume and flow metering issues in tracer studies may be common.

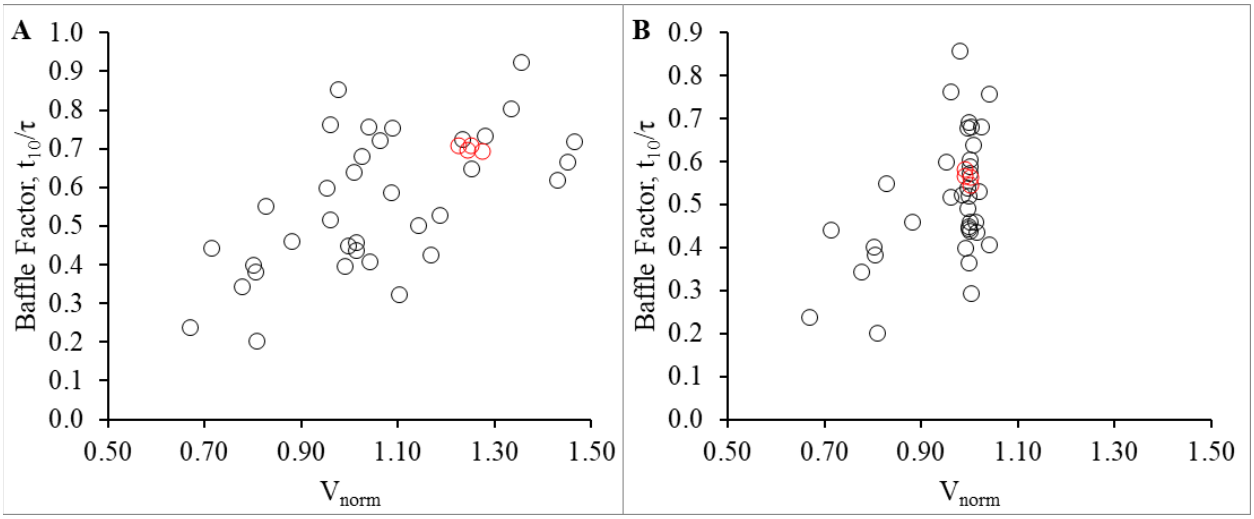

Figure C.1. Baffle factor (t_{10}/τ) versus normalized reactor volume (V_{norm}) before (A) and after data correction (B).

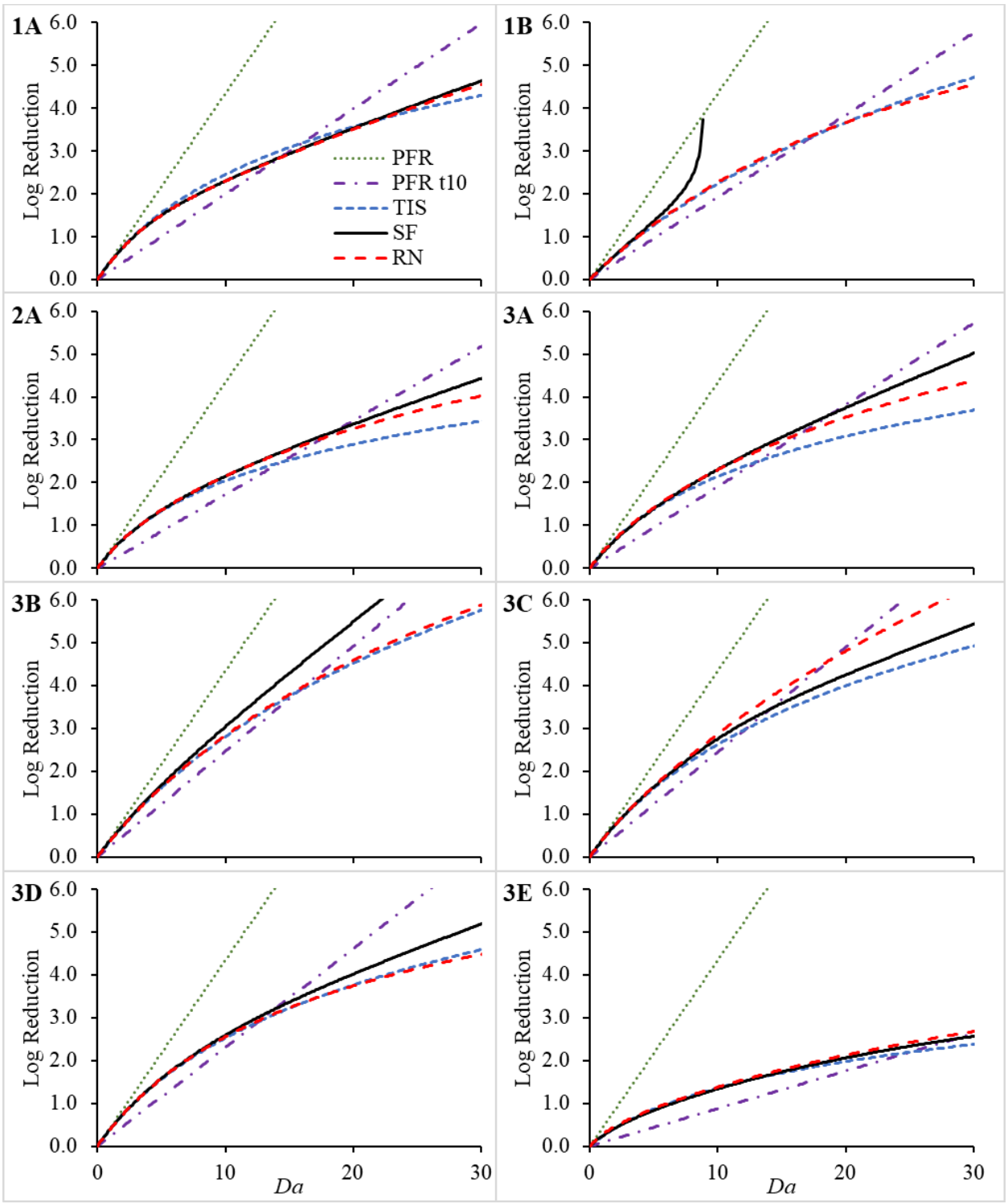

Figure C.2. Log reduction versus *Da* plots for reactors 1A through 3E.

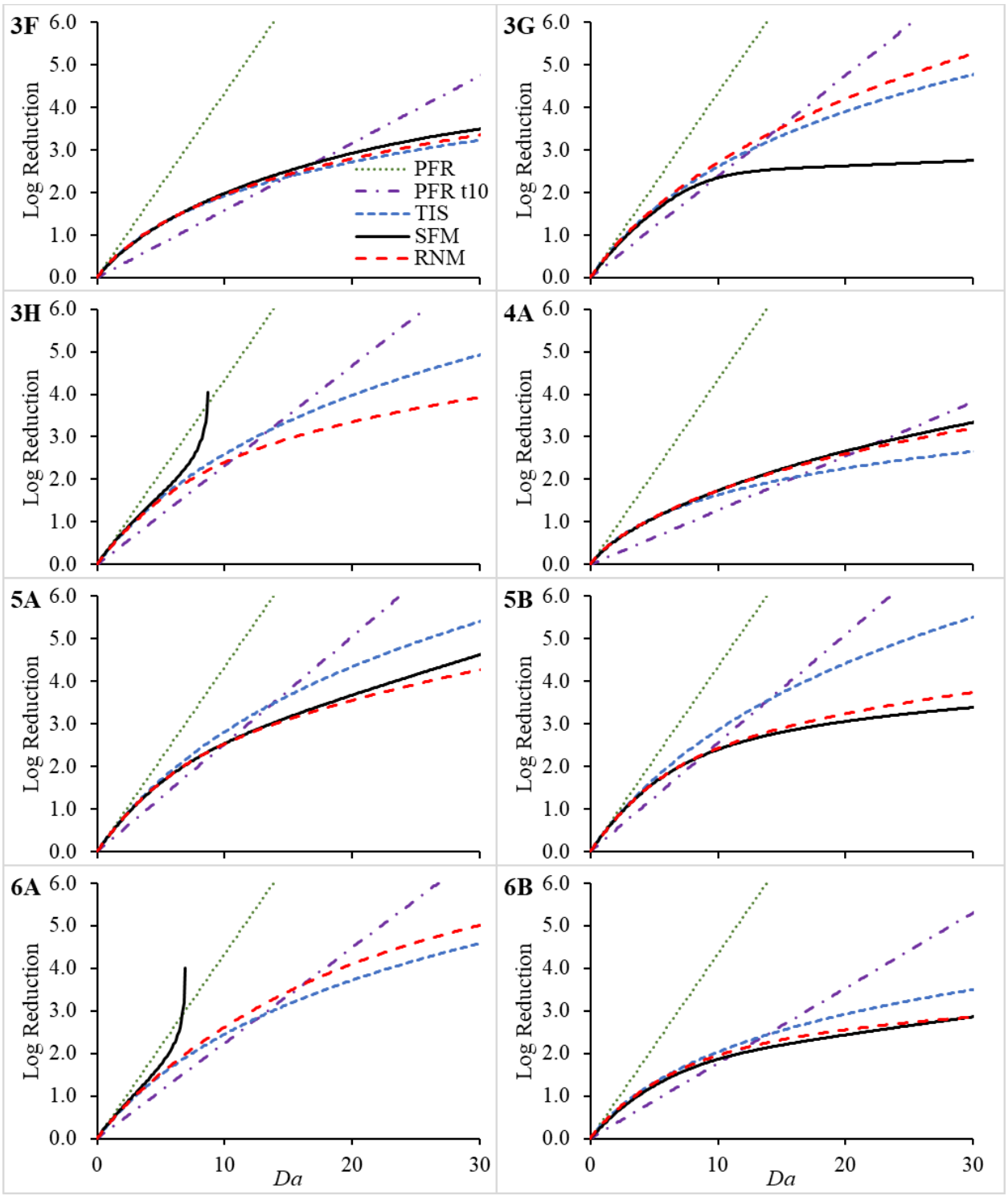

Figure C.3. Log reduction versus *Da* plots for reactors 3F through 6B.

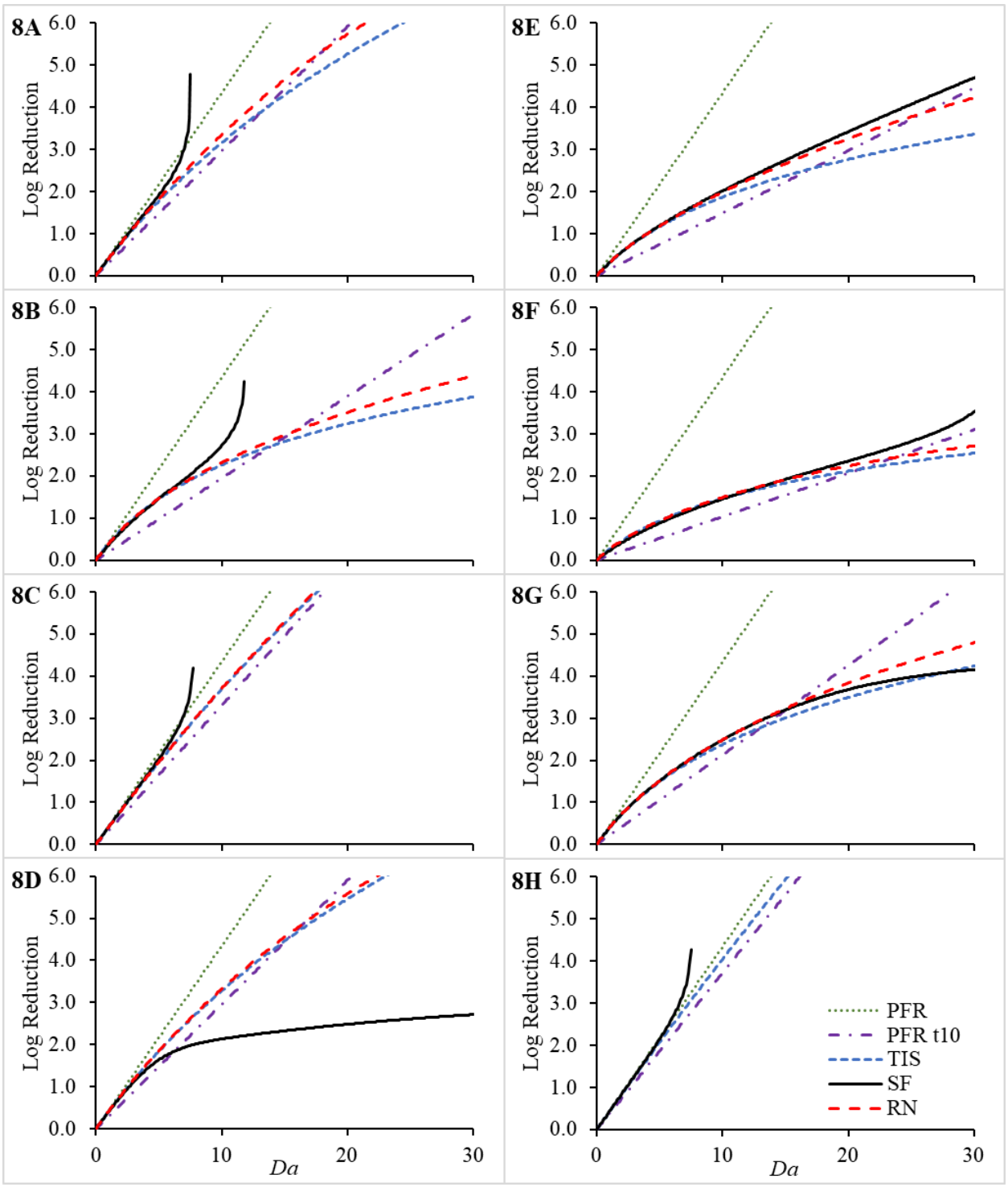

Figure C.4. Log reduction versus *Da* plots for reactors 8A through 8H.

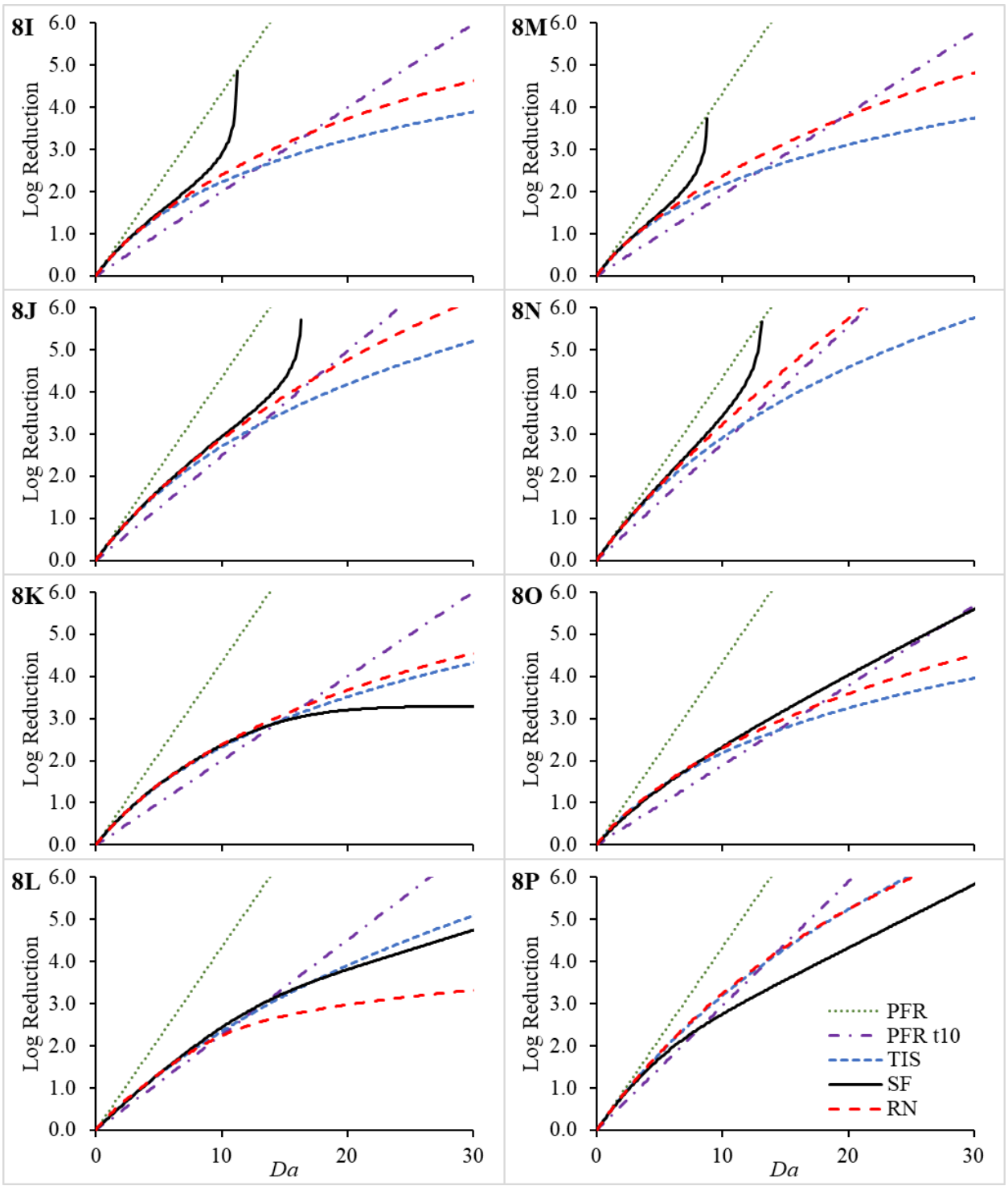

Figure C.5. Log reduction versus *Da* plots for reactors 8I through 8P.

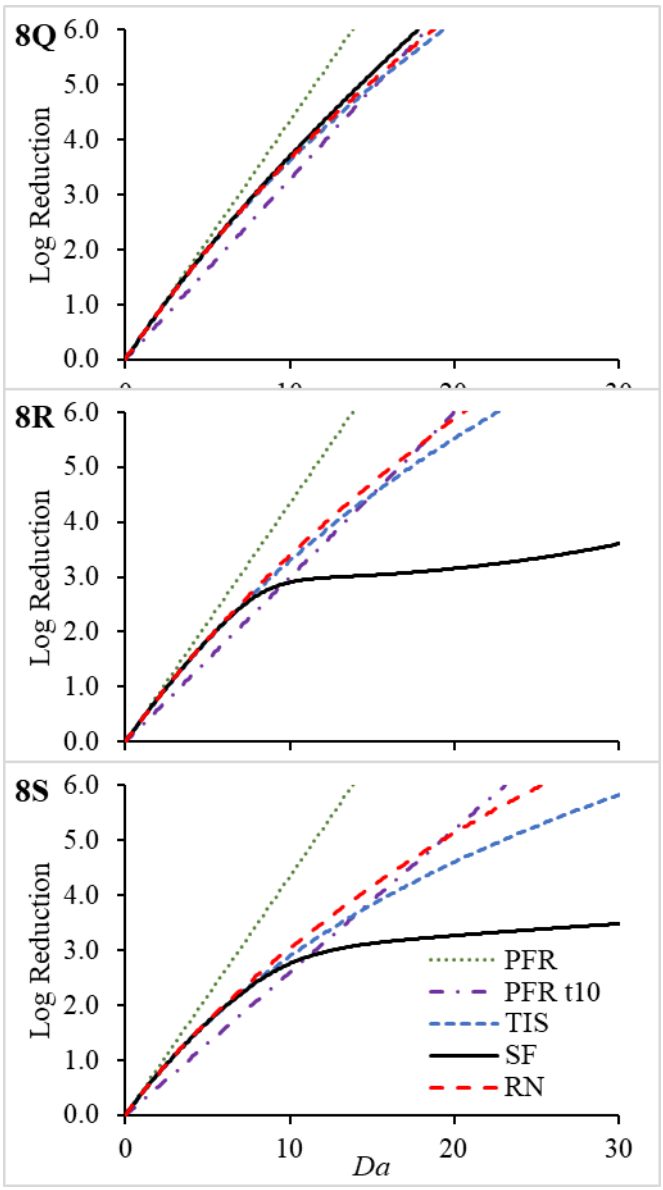

Figure C.6. Log reduction versus *Da* plots for reactors 8Q through 8S.

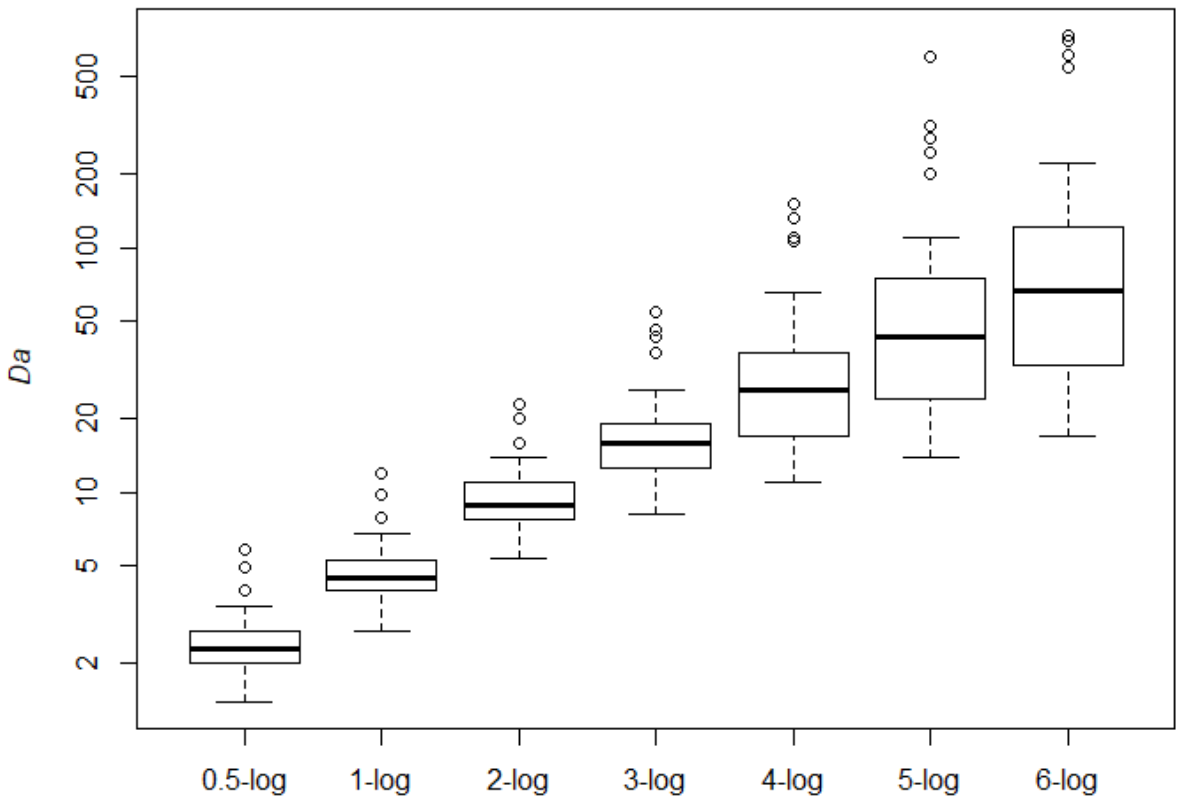

Figure C.7. Box and whisker plot of *Da* required to achieve different log reductions for each of the 35 reactors in Table C.1. Note that one observation for 6-log reduction is not included due to required *Da* > 1,000.